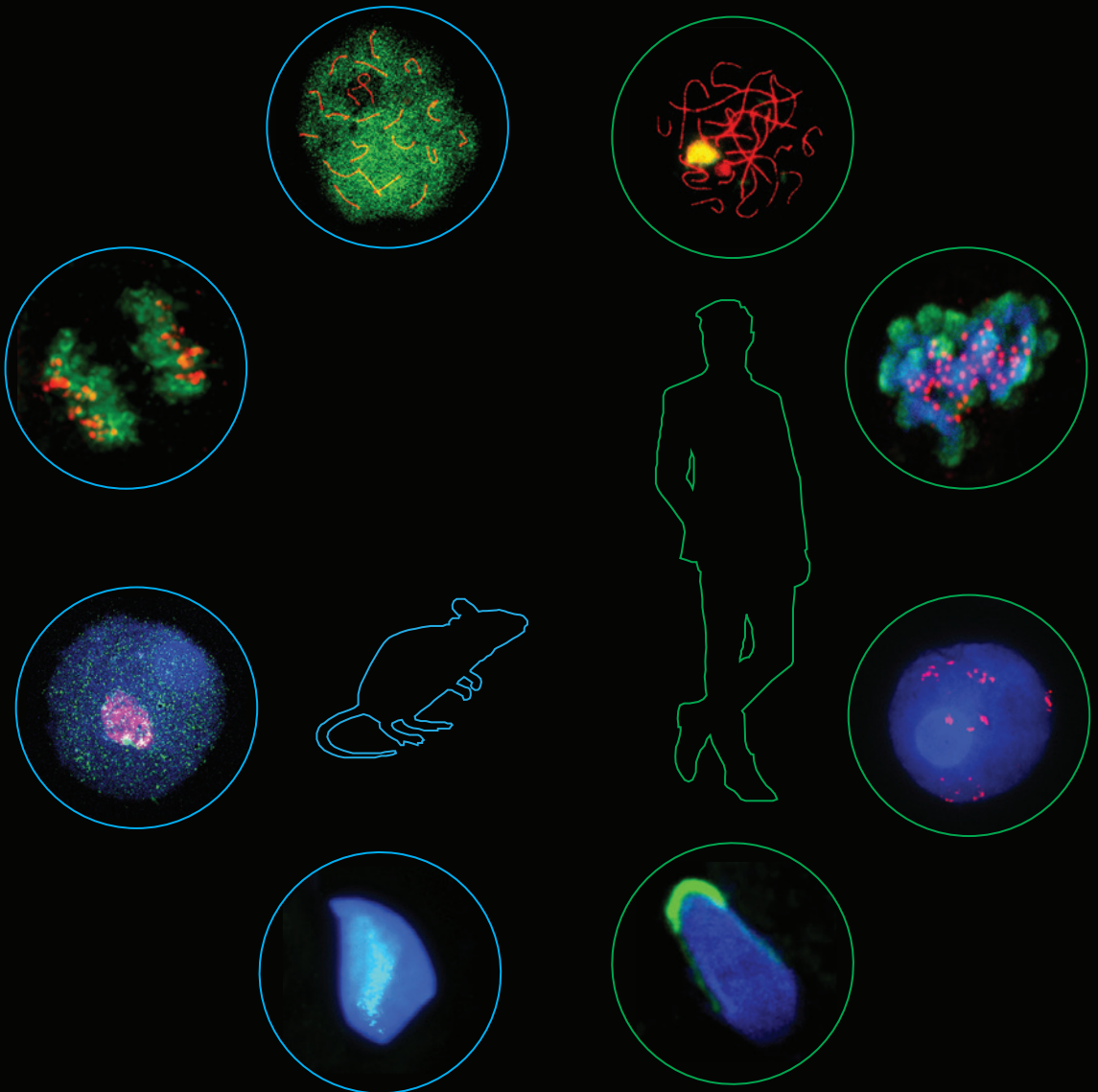# Dynamics of mouse and human gametogenesis

From microscopic analyses using immunohistochemical techniques to live cell imaging

Andrea Enguita-Marruedo

Dynamics of Mouse and Human Gametogenesis

From microscopic analyses using immunohistochemical techniques to live cell imaging

Andrea Enguita-Marruedo

Dynamics of Mouse and Human Gametogenesis

From microscopic analyses using immunohistochemical techniques to live cell imaging

Dynamiek van gametogenese bij muis en mens

Van microscopische analyse met immunohistochemische technieken tot het in beeld brengen van levende cellen

Thesis

to obtain the degree of Doctor from the Erasmus University Rotterdam

by command of the rector magnificus

Prof. dr. H.A.P. Pols

and in accordance with the decision of the Doctorate Board.

The public defence shall be held on

Tuesday 11 June 2019 at 13.30 hrs

by

Andrea Enguita-Marruedo

Born in Madrid, Spain

Erasmus University Rotterdam

DOCTORAL COMITTE

Promotor: Prof. dr. J.H. Gribnau

Other members: Prof. dr. A. Brehm
                         Prof. dr. A.B. Houtsmuller
                         Prof. dr. J.A. Grootegoed

Copromotors: Dr. ir. W.M. Baarends
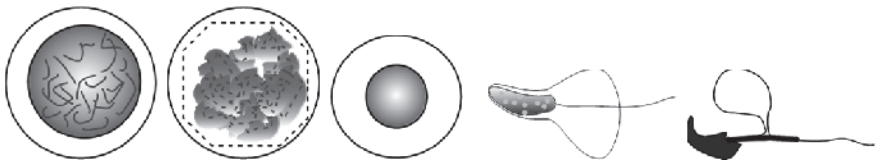   Dr. W.A. van Cappellen

TABLE OF CONTENTS

1

Introduction and scope of this thesis

INTRODUCTION

In sexually reproducing species, the formation of a new organism occurs by fusion of two specialized cells, called gametes. In mammals, species one gamete is the relatively large egg (maternal) and the other gamete is the smaller sperm cell (paternal). Gametes are haploid cells, meaning that they carry a single chromosome set (1n). Since sexually reproducing organisms are formed from diploid cells (each cell contains two sets of chromosomes), the fusion of the two gametes will restore the normal diploid chromosome number (2n). Gametes are formed during the processes of spermatogenesis in males and oogenesis in females. In both cases, diploid progenitor cells (spermatogonia or oogonia) will give rise to the haploid gametes (spermatozoa or egg). This thesis mainly focusses on different aspects of spermatogenesis, in both mouse and man.

ORGANIZATION OF THE SEMINIFEROUS TUBULES AND SPERMATOGENESIS

Spermatogenesis is a complex process which leads to the formation of four mature haploid gametes (spermatozoa) from only one diploid progenitor (spermatogonium) (Clermont 1972). Spermatogenesis occurs within the long seminiferous tubular structures of the testis (Hess 1999). The tunica propria, or outer layer of each seminiferous tubule, is mainly composed of testicular peritubular myoid cells (TMC), which are responsible for tubule contraction (Roosen-Runge 1951; Santiemma et al. 2001). These contractions, together with the fluid flow through the lumen, propel the nonmotile spermatozoa in the seminiferous tubule (Ellis et al. 1981). The inside of the tubule is formed by a seminiferous epithelium and a fluid-filled lumen, in which fully formed spermatozoa are released (Hess 1999; Ellis et al. 1981). The seminiferous epithelium contains both somatic and germ cells. The germ cells (spermatogonia, spermatocytes and round and elongating/elongated spermatids) are surrounded by cytoplasm of the somatic cell, the Sertoli cell (Hess 1999). The cytoplasm of the Sertoli cells extends the entire height of the epithelium, since these cells support and regulate all stages of spermatogenesis (Hess 1999). The Sertoli-Sertoli cell junctions, composed by tight junctions, gap junctions, desmosomes, and ectoplasmic specializations (a modified adherens junction-type found only in the testis), form the blood-testis barrier (BTB) (Mruk and Cheng 2015).

This barrier divides the seminiferous tubule into a basal and adluminal compartment. The spermatogonial stem cells and spermatogononia are located in the basal compartment. As cells enter meiotic prophase, they are transported across the barrier, and spermatocytes and later stages are thus developing in the adluminal compartment, whereby they gradually

move closer towards the lumen, as they develop (Mruk and Cheng 2015). The adluminal compartment constitutes a unique separated controllable (by the Sertoli cells) microenvironment in which germ cells can differentiate and mature, protected from the inside environment, and from possible autoinmume reactions (Pelletier and Byers 1992; Goossens and van Roy 2005; Mital et al. 2011; Pelletier 2011). Spermatogonia, spermatocytes and round spermatids attach to Sertoli cells via desmosomes and gap junctions, whereas elongating/elongated spermatids attach to Sertoli cells via ectoplasmic specializations (Mruk and Cheng 2015). Spermatogenesis in mice is organized in waves, and there is a strict timing of the different steps, which leads to an ordered and fixed association of cells. In mice, 12 different cellular associations or stages of the spermatogenic cycle can be distinguished (Oakberg 1956). In men, stages are not so clearly distinguishable, in a classical study (Clermont 1963), 6 stages were described, but more recently 12 stages could be discerned based on acrosome development (Muciaccia et al. 2013).

  Spermatogenesis can be divided in 3 stages: mitotic amplification of the progenitor cell (premeiotic phase), meiosis, and spermiogenesis (postmeiotic phase) (Fig. 1). During the first step, which occurs at regular intervals at each position in the seminiferous epithelium, spermatogenic stem cells give rise to a new generation of mitotically active spermatogonia (Gordon and Ruddle 1981). During the spermatogonial divisions, cytokinesis is not complete. Rather, the cells form a syncytium (which remains during the subsequent stages) whereby each cell communicates with the other via cytoplasmic bridges (Dym and Fawcett 1971). After a last round of DNA replication, these cells enter meiosis, and become primary spermatocytes. Meiosis is a specialized mechanism of cell division, which leads to a reduction of the chromosome number from diploid (2n) to haploid (n). This reduction is achieved via two consecutive divisions, frequently called meiosis I and meiosis II. During meiosis I, homologous chromosomes exchange genetic information and then segregate. Thus, the first meiotic division results in the formation of two haploid daughter cells, called secondary spermatocytes. During meiosis II, the sister chromatids segregate and two spermatids form from each secondary spermatocyte. As a result of the two meiotic divisions, each primary spermatocyte gives rise to four haploid spermatids.
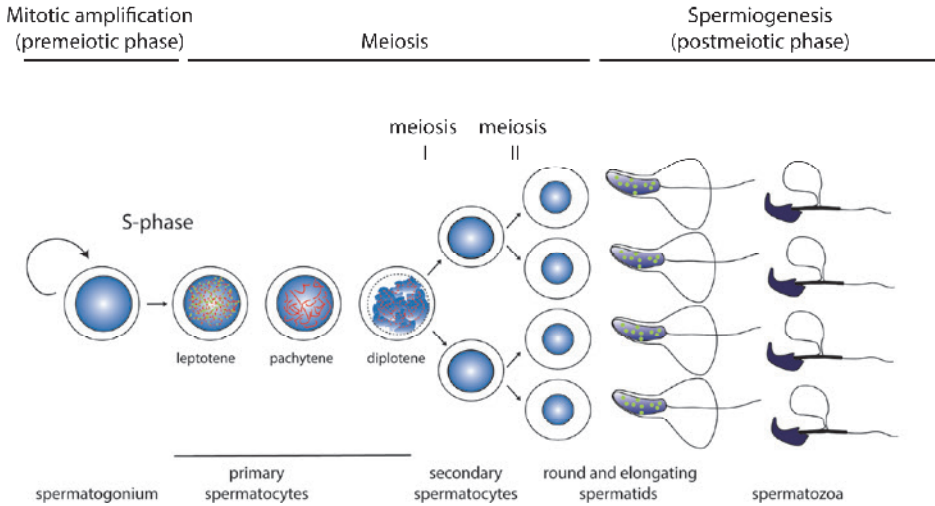
Fig. 1. Mammalian spermatogenesis.

During spermiogenesis, dramatic changes in cell shape occur; a tail is formed and the size of the nucleus dramatically decreases (Rathke et al. 2014). This is achieved by repackaging the DNA in a very compact form. In somatic cells, DNA is folded around nucleosomes, consisting of 8 histones (explained in more detail below). The DNA together with the nucleosomes and other regulatory proteins is called chromatin. During the enormous nuclear compaction that accompanies sperm formation, DNA is repackaged, mainly by small basic proteins called protamines, resulting in the formation of the mature spermatozoa with a very compact nucleus. However, chromatin changes are not an exclusive feature of this last step. During meiotic prophase, the genetic reshuffling that takes place is also accompanied by major chromatin changes. Chromatin structure regulation during meiosis and spermiogenesis will be discussed in more detail in the following sections

MEIOTIC PROPHASE I

Each meiotic division can be divided in the stages: prophase, metaphase, anaphase and telophase. The first meiotic prophase can be subdivided in: leptotene, zygotene, pachytene, diplotene and diakinesis. During these stages, a series of exclusive chromosomic events takes place: pairing (alignment of the homologous chromosomes), synapsis (formation of the synaptonemal complex) and recombination (DNA exchange between the homologous chromosomes) (Petronczki et al. 2003).

Homologous chromosome pairing

Homologous chromosomes must find and recognize each other in order to form pairs. Plants, animals and some fungi follow the so-called "canonical" program for pairing, meaning that genetic recombination plays a central mechanistic role. In contrast, other organisms (e.g fission yeast) have a somewhat different pairing program (non-canonical), which does not depend on genetic recombination (Zickler and Kleckner 2016). In the canonical program, recombination initiates with the formation of DNA double-strand breaks (DSBs) by the SPO11/TOPOVIBL complex and additional proteins at the beginning of meiosis (Baudat et al. 2000; Romanienko and Camerini-Otero 2000; Robert et al. 2016). The repair of meiotic DSBs somehow allows the homologs to specifically recognize each other and to come together in nuclear space, in an organized manner, by juxtaposition of their structural axes (Zickler and Kleckner 2016). Thus, the search for the homologous partner also requires global chromosome motions. The existence of such movements was initially revealed by light-microscopy studies of living meiotic cells from rat spermatocytes (Parvinen and Söderström 1976; Salonen et al. 1982). Since then, meiotic chromosome movements have been observed in vivo in a wide range of organisms, including mouse (Morimoto et al. 2012; Shibuya et al. 2014; Lee et al. 2015). Meiotic chromosome movements are led by the telomeric ends (Telomere-led rapid prophase movements, RPMs). RPMs start early in meiosis and require linkage of the telomeres to the cytoskeleton, through the nuclear membrane (Ding et al. 2007; Lee et al. 2012, 2015; Morimoto et al. 2012; Stewart and Burke 2014).

One of the most conspicuous features of meiotic prophase cells that has been observed in almost all analyzed sexually reproducing species to date (both organisms with canonical and non-canonical pairing programs) is the so-called bouquet stage, when telomeres cluster together in the nuclear periphery, and the thread-like chromosomes form a structure that is reminiscent of a bouquet of flowers (Scherthan 2007; Stewart and Burke 2014). The bouquet structure was originally described in 1921 (Gelei J 1921, reviewed in Zickler and Kleckner 2016) in flat-worm meiosis. This and subsequent studies in other species showed that homologs synapse during the bouquet stage, leading to the idea that the bouquet structure reduces the complexity of the homology search process required for pairing and synapsis. However, subsequent studies proposed that, in addition to the pairing process, formation of the bouquet has adopted new functions in concert with progressive evolution of the meiotic process (Zickler and Kleckner 2016). In organisms with recombination-mediated homolog pairing, like mouse and human, formation of the bouquet would also help to solve problems of resolution of entanglements or other DNA links like ectopic interactions between non-homologous chromosomes (Zickler and Kleckner 2016).

The synaptonemal complex

When mammalian cells enter prophase I, homologous chromosomes come together in a process that is known as pairing. During synapsis, homologous chromosomes become physically connected by the formation of a tripartite proteinaceous structure between them, called synaptonemal complex (SC). The SC is composed of two lateral elements (LEs, one per homolog) that associate with each other through the transverse filaments (TFs). These TFs overlap in the central region, forming the central element (CE) (Page and Hawley 2004). In mammals, the LEs and their precursors, the axial elements (AEs), are mainly composed of the proteins SYCP2 and SYCP3, while the TFs mainly consist of SYCP1 (Heyting 1996; Costa et al. 2005). The CE contains SYCP1 as well as other proteins like SYCE1, SYCE2, SYCE3 and TEX1 (Costa et al. 2005; Hamer et al. 2006; Schramm et al. 2011) (Fig. 2).
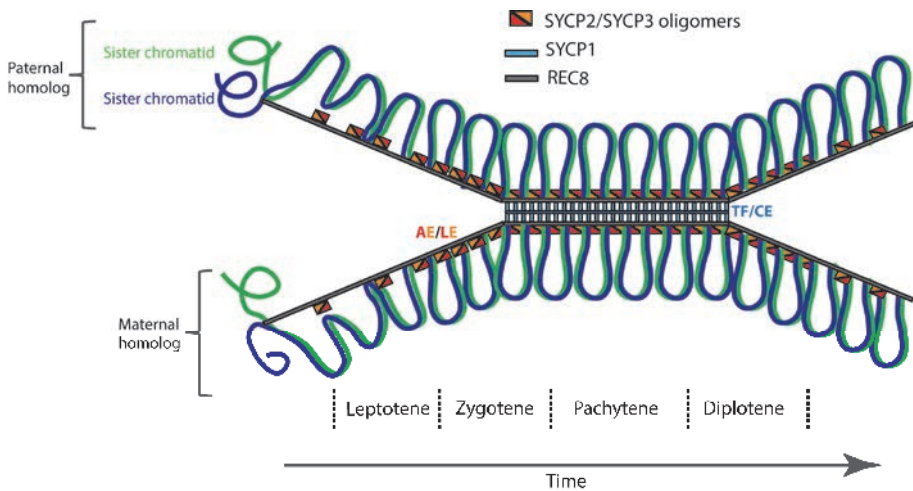
Fig. 2. Synaptonemal complex (SC) dynamics during the first meiotic prophase. The figure shows the SC at subsequent stages of meiotic prophase. Although the drawing is continuous, time progresses from left to right, and the vertical dotted lines represent the transition from one stage to the next: leptotene (formation of the axial elements), zygotene (initiation of synapsis), pachytene (complete synapsis) and diplotene (desynapsis). AE: axial element, LE: lateral element, TF: transverse element, CE: central element.

The assembly of the SC starts in leptotene with the formation of the AEs along the homologous chromosomes (Page and Hawley 2004; Heyting 2005). The beginning of the recombination process during this phase allows, in the majority of the species, the alignment of the homologous chromosomes (pairing) (Zickler and Kleckner 1999; Page and Hawley 2004). Synapsis is initiated during zygotene, with the assembly of the TFs along the AEs, which are called LEs in the synapsed configuration. The overlap between TFs from each

opposite LE in the central region produces the firm connection between the homologs, which is further strengthened by the central element proteins that also accumulate (Page and Hawley 2004). In pachytene, synapsis and recombination are complete. Recombination ends with the formation of crossovers (COs), and noncrossovers. These are the places where DNA exchange between homologous chromosomes has taken place, and in the case of a CO, whole arms of chromosomes are exchanged (Page and Hawley 2004). Crossover events can be visualized by the formation of chiasmata (Heyting 2005). At least 1 CO is needed per bivalent (obligatory CO), in order to ensure the proper orientation of the bivalents on the metaphase plate, and segregation of the homologous at the first meiotic division. In mouse, 1-3 COs are formed per bivalent (Anderson et al. 1999; Hassold et al. 2000; de Boer et al. 2006; Baudat and de Massy 2007). The sequential disassembly of the SC (desynapsis), which starts upon exit from pachytene and extends through late prophase (diplotene and diakinesis), is accompanied by changes in chromosome compaction and changes in the composition and localization of additional proteins required for the regulated loss of sister chromatid cohesion at metaphase I (MI). This process, termed chromosome remodeling, results in the characteristic cruciform configuration observed for bivalents by late diakinesis (Gao and Colaiácovo 2018). During this process in yeast and mice, the SC persists at centromeres where they have been proposed to promote proper centromere biorientation, leading to proper homolog segregation at MI (Gao and Colaiácovo 2018). True tripartite SC structure also remains at nascent chiasmata sites (Qiao et al. 2012). At the end of this process, the homologous chromosomes remain connected only by the chiasmata, the areas where the recombination took place (Page and Hawley 2004). The cohesion complex is then removed, only along the chromosome arms, so the homologous chromosomes can segregate to the daughter cells during the first meiotic metaphase to anaphase transition (Nasmyth and Haering 2005; Watanabe 2005).

Recombination

Recombination and synapsis are interdependent processes. Meiotic recombination is necessary to promote efficient SC formation in the majority of eukaryotes (Baudat et al. 2000; Romanienko and Camerini-Otero 2000). Conversely, mice with mutations in SC genes also display defects in recombination (de Vries et al. 2005; Wang and Höög 2006; Bolcun-Filas et al. 2007, 2009; Kouznetsova et al. 2011).

Meiotic homologous recombination (HR) is a special DNA DSB repair mechanism that is essential to ensure the correct chromosome segregation during the first meiotic division, and increases genetic diversity (Ehmsen and Heyer 2008; Krejci et al. 2012). It starts in leptotene with the formation of DSBs, mediated by the SPO11/TOPOVIBL complex (Vrielynck

et al. 2016; Robert et al. 2016) (Fig. 3). The removal of SPO11 by the MRN complex and CtIP (Hartsuiker et al. 2009; Mimitou and Symington 2009) exposes the DSBs. In addition, the interaction of MRN and ATM allows the phosphorylation of H2AX at serine 139 (γH2AX), which has a critical role in the regulation of the whole repair process (Mahadevaiah et al. 2001; Hamer et al. 2003; Chicheportiche et al. 2007; Kinner et al. 2008; Banerjee and Chakravarti 2011; Grabarz et al. 2012). When SPO11 is released, both DSBs ends are resected by EXO1, generating 3'single-stranded DNA (3'ssDNA). The ssDNA is recognized by replication protein A (RPA) complex (a heterotrimer of RPA1, RPA2 and RPA3), which protects ssDNA from degradation (Wold 1997). The meiosis-specific complex formed by the RPA1-homolog MEIOB (meiosis specific with OB domains) and SPATA22 (spermatogenesis associated 22) is also recruited to ssDNA and may interact with RPA complex in a collaborative manner (Souquet et al. 2013; Luo et al. 2013; Xu et al. 2017). These ssDNA binding proteins are then replaced by recombinases that form filaments, allowing the ssDNA to invade the double-stranded DNA of the homologous chromosome (Grabarz et al. 2012; Krejci et al. 2012). Two recombinases, named RAD51 and DMC1, are essential for this process in meiosis. RAD51 is expressed both in mitosis and meiosis, and most likely does not distinguish between the sister chromatid or the homologous chromosome as a template for repair, while DMC1, which is expressed exclusively during meiosis, is thought to be the critical component that promotes the election of the homologous chromosome as a template for DNA repair (Neale and Keeney 2006; La Volpe and Barchi 2012). The invasion of the homologous dsDNA results in the formation of a displacement loop (D loop) (Petukhova et al. 2000; Sehorn et al. 2004), which will result in the formation of a stable recombination molecule (joint molecule). Recombinases are now removed and DNA synthesis can take place. D loop stability will determine the next repair choice. If the newly synthetized strand dissociates from the D loop and reanneals to the parental strand, DNA will be repaired by synthesis-dependent strand annealing (SDSA), which results in the reformation of the original DNA molecule (McMahill et al. 2007). If the newly synthesized strand does not dissociate from the D loop and second end capture occurs, a double Holliday junction (dHJ) is formed The heterodimer formed by the proteins MSH4 and MSH5 (Mut S homolog 4 and 5) is involved in the stabilization of the D loop by adopting a clamp configuration (Youds and Boulton 2011; Kohl and Sekelsky 2013). Each dHJ can be resolved by either asymmetrical or symmetrical cleavage, which results in crossover (CO) or non-crossover (NCO) formation, respectively (Heyer et al. 2010). The vast majority of COs are obtained via resolution of the dHJ by the MLH1-MLH3 complex (Baker et al. 1996; Hunter and Borts 1997; Wang et al. 1999; Lipkin et al. 2002), while only a small number is processed via an alternative pathway involving the MUS81 protein (Holloway et al. 2008).
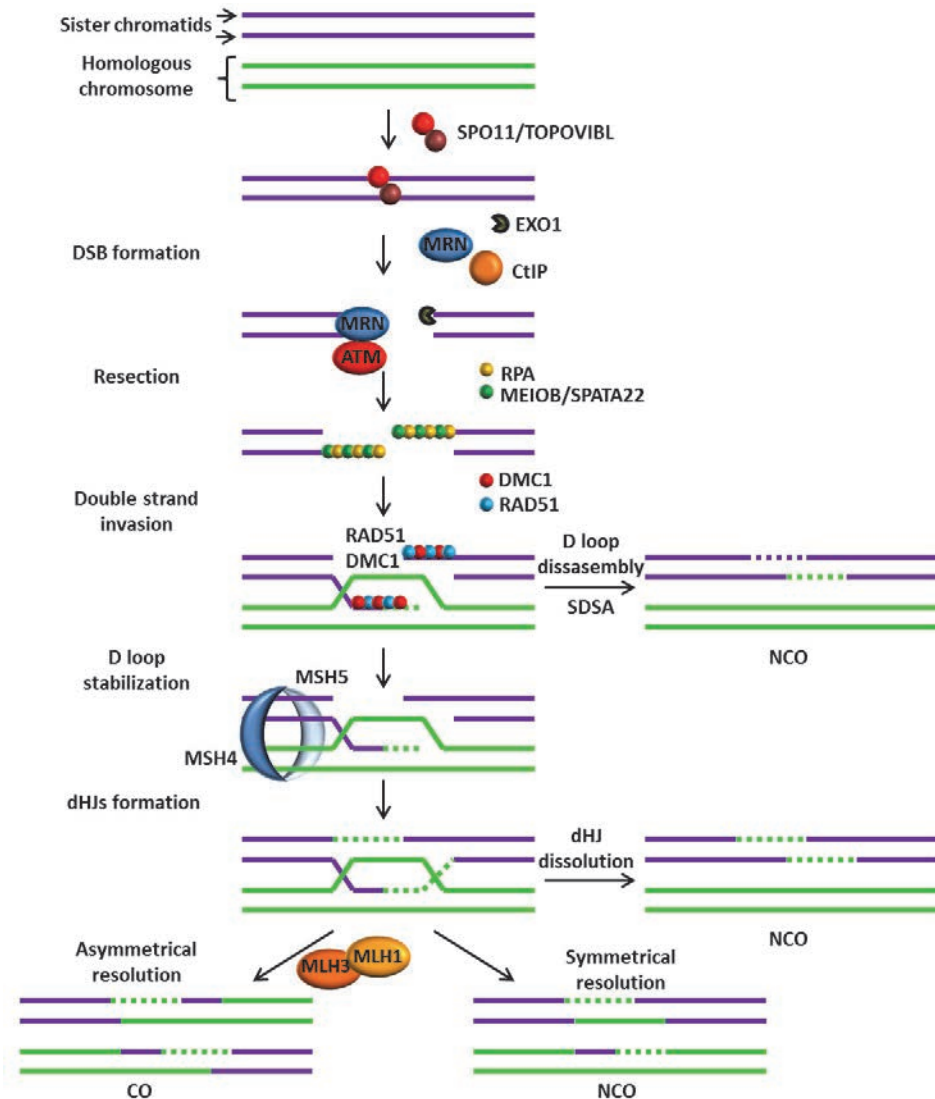
Fig. 3. DNA repair by homologous recombination (HR) and by synthesis-dependent strand annealing (SDSA). Meiotic nuclei contain pairs of homologous chromosomes (purple and green). Each homologous chromosome consists of two sister chromatids (two copies of the same dsDNA). Meiotic recombination is initiated by the formation of DSBs by the SPO11/TOPOVIBL heterotetramer. This complex (including a covalently bound DNA fragment) is later removed by the MRN complex and CtIP, leaving the DSBs exposed. Additionally, the interaction of MRN and ATM allows the phosphorylation of H2AX into γH2AX in the chromatin surronding the DSB. Once SPO11 is released, both DSBs ends are resected by EXO1, which generates 3'single-stranded DNA (3'ssDNA). This is recognized and bound by protein complexes including RPA and MEIOB/SPATA22, which protect it from degradation. These ssDNA binding proteins are replaced by the DMC1/RAD51 recombinases, allowing ssDNA to invade the double-stranded DNA of the homologous chromosome, which results in the

formation of a displacement loop (D loop). DMC1/RAD51 are then removed and DNA synthesis takes place. If the newly synthetized strand dissociates from the D loop and reanneals to the parental strand, DNA is repaired by synthesis-dependent strand annealing (SDSA). Loading of the MSH4/5 heterodimer, which adopts a clamp configuration, allows the stabilization of the D loop, facilitating the second end capture of the new synthetized strand, and the formation of a double Holliday junction (dHJ). Each dHJ can be resolved by either asymmetrical or symmetrical cleavage, which results in crossover (CO,) or non-crossover (NCO) formation. The vast majority of COs are obtained via resolution of the dHJ by the MLH1-MLH3 complex. See text for further details and references.

Meiotic checkpoints

The quality and integrity of the sperm genome depends on the proper execution of all the different steps during spermatogenesis, as well as on the activity of checkpoints mechanisms. These induce arrest or apoptosis of germ cells in which damage has been accumulated, or in which some developmental step was not properly completed. Two well-known checkpoints operate during the first meiotic division in mice, and are thought to operate also in human: the pachytene checkpoint and the Spindle Assembly Checkpoint (SAC). During prophase I, the processes of pairing, synapsis and recombination take place. However, the X and Y chromosomes differ both in size and content, meaning that pairing and synapsis occur only in a small homologous region, called the pseudo-autosomal region (PAR). The long non-homologous regions of the X and Y that remain unsynapsed become silenced during the first meiotic prophase, by a process that is called Meiotic Sex Chromosome Inactivation (MSCI), which leads to the formation of the so-called XY body (Turner et al. 2005, 2006; Turner 2007) (for more detailed information, see "Special features of the XY pair and its chromatin remodeling" section). Proper XY body formation relies on completion of chromosome pairing and DSB repair on the autosomes (Homolka et al. 2007). The pachytene checkpoint, which eliminates spermatocytes in which chromosomes have failed to complete synapsis, is functionally coupled to failure to form the XY body in male mice (Royo et al. 2010). Absence of proper transcriptional silencing of the sex chromosomes leads to aberrant activation of X- and/or Y-linked genes, which triggers the apoptotic process (Royo et al. 2010). In addition, a second, DNA damage-dependent, checkpoint operates, somewhat later during pachytene (Pacheco et al. 2015; Marcet-Ortega et al. 2017). In mouse, targeted mutation of genes important for meiotic DSB formation, DSB repair, or chromosome pairing almost invariably results in apoptotic elimination of virtually all spermatocytes at mid pachytene (de Rooij and de Boer 2003; Barchi et al. 2005; Hamer et al. 2008; Burgoyne et al. 2009).

When repair and chromosome pairing occur normally, the Spindle Assembly Checkpoint (SAC) comes into play, which assures the correct segregation of the chromosomes at the metaphase-to-anaphase transition. SAC, which acts in both mitosis and meiosis, is activated

prior to each cell division in mammalian cells and delays anaphase onset until all chromosomes are properly aligned on the metaphase plate, and correct tension is established between two poles (created by the attached microtubules) (Musacchio 2015). In meiosis I, pairs of homologous chromosomes, connected by chiasmata (the visible manifestation of crossovers) need to be separated. Therefore, sister kinetochores from one chromosome should attach to microtubules emanating from the same pole, while the two pairs of sister kinetochores from the homologous chromosome need to attach to the opposite pole. When this situation is achieved for all chromosome pairs, the SAC is inactivated, and transition to anaphase takes place. Lack of crossover formation is a well-known trigger of the SAC in mouse, which eventually leads to metaphase I arrest (Gorbsky 2015). During meiosis II (and mitosis) the situation differs. In this case, sister chromatids will separate, meaning that kinetochores of the same chromosome need to attach to opposite poles.

CHROMATIN REMODELLING DURING SPERMATOGENESIS

Epigenetics

In eukaryotic cells, genomic DNA is compacted by proteins called histones. The resulting complexes form the chromatin, together with additional proteins interacting with histones or DNA. The fundamental units of chromatin are the nucleosomes, which are octamers formed by two molecules of each of the canonical core histones H2A, H2B, H3, and H4. The major functions of the canonical histones are genome packaging and gene regulation. The linker histone H1 binds to the nucleosomal and linker DNA and contributes to a higher-order chromatin structure. Variants of all core and linker histones (histone variants) have been identified (Rathke et al. 2014). They play roles in a wide range of processes, such as transcription initiation or DNA repair, by establishing a distinct chromosomal domain to enable a specialized function (Rathke et al. 2014).

DNA wrapped around the histone octamer is generally inaccessible to DNA-binding proteins. This means that the access of transcription, replication, repair and recombination factors to the target DNA region is restricted by nucleosome formation. However, chromatin structure can be dynamically altered by modification of DNA, histones or both. Post-translational modifications (PTMs) of the histones result in conformational changes that may then facilitate access of factors to certain areas of the DNA, to allow proper execution of certain regulatory functions (Koyama and Kurumizaka 2018). The heritable non-genomic changes that determine gene expression patterns have been termed epigenetic changes.

Two important massive epigenetic changes accompany spermatogenesis in adults. The first involves the chromosome wide chromatin remodeling that occurs on the XY chromosomes during meiotic prophase. The second process is genome-wide and takes place during spermiogenesis, when the compaction of the nucleus requires a massive reorganization of the chromatin, from a nucleosomal histone-based structure to a structure largely based on protamines (Rathke et al. 2014). Before this, some of the histones are replaced by non-canonical equivalents, which prepare the chromatin for the process of histone-to-protamine transition (Rathke et al. 2014). During the following sections we will focus on each of these two extensive chromatin remodeling events.

Special features of the XY pair and its chromatin remodeling

In mouse and man, as in the vast majority of placental mammals, the male is the heterogametic sex, meaning that they carry two different sex chromosomes (X and Y). Females are generally homogametic, and carry two identical sex chromosomes (XX). In the same way as the autosomal chromosomes, the two X chromosomes of the females achieve complete synapsis during meiotic prophase. In males, X and Y differ both in size and gene content (Sutton et al. 2011). Pairing and synapsis occur only in a small homologous region, called the pseudo-autosomal region (PAR). The PAR in most mammals spans typically a few hundred kilobases (kb) to several megabases (Mb) in length, and constitutes only a small fraction of the X and Y chromosomes, imposing an extraordinary pressure on achieving recombination (obligatory crossover) in such a short genomic segment (Hinch et al. 2014). In mouse, this region is located at the end of the X and Y chromosomes, and spans only 700 kilobase (kb) in length (Perry et al. 2001). Humans have two PARs: PAR1, which is at the end of the short arm (Xp/Yp) of the sex chromosomes, and PAR2, which is at the end of the long arm (Xq/Yq) (Hinch et al. 2014). PAR1 is approximately 2.7 Mb long, and this is where the obligatory crossover takes place. In contrast, PAR2 is much smaller, approximately 330 kb, and the obligatory CO rarely occurs in this region (Hinch et al. 2014). The long non-homologous regions of the X and Y that remain unsynapsed become silenced during the first meiotic prophase, by a process that is called Meiotic Sex Chromosome Inactivation (MSCI) (Turner et al. 2005, 2006; Turner 2007). This process is considered a specific form of a more general silencing process that occurs in response to the presence of unpaired autosomal regions, named meiotic silencing of unsynapsed chromatin (MSUC) (Schimenti 2005; Turner et al. 2005; Baarends et al. 2005). MSCI is mediated by the localization of several proteins on the unsynapsed chromatin of the XY chromosomes. These factors belong to different pathways: DNA recombination/repair, synapsis and transcriptional silencing. The completion of this process involves epigenetics changes which result in the formation the so-called XY

body, from pachytene onwards. These chromatin modifications include phosphorylation of the histone H2A variant H2AX on serine 139 (γH2AX), which is a critical step in the inactivation of the sex chromosomes (Fernandez-Capetillo et al. 2003). After the accumulation of γH2AX, other events of chromatin remodeling occur on the XY body, like the substitution of the canonical histone H3.1 by H3.3 (van der Heijden et al. 2007), enrichment of macroH2A (mH2A) (Hoyer-Fender et al. 2000), and of repressive histone marks, like H3K9me3 (Page et al. 2012). Histone modifications known to mark transcriptional activity are absent from the XY body (van der Heijden et al. 2007), and no (phosphorylated) RNA pol II is observed in this area (Page et al. 2012). In mice, failure to form the XY body results in the apoptosis of the respective spermatocyte (see the section describing meiotic checkpoints).

Completion of meiosis leads to formation of four haploid round spermatids, which carry either an X or a Y chromosome. X and Y chromatin is still distinguishable, as they form a more dense DAPI-dense structure adjacent to the chromocenter, a DAPI dense area that contains the (peri)centromeric chromatin in the spermatids. Some of the repressive chromatin marks and chromatin-associated proteins observed on sex chromosomes during meiosis, like H3K9me2 and H3K9me3, are still visibly enriched on the post-meiotic chromatin (Turner et al. 2006; Namekawa et al. 2006; Greaves et al. 2006; Moretti et al. 2016). These heterochromatin-like features, together with microarray-type analysis, suggest that XY gene silencing persists in spermatids, with most genes repressed and only a few "escapees" (Turner et al. 2006; Namekawa et al. 2006; Greaves et al. 2006; Fallahi et al. 2010; Hu and Namekawa 2015). However, X-multicopy genes were not taken into account in these microarray studies, or all copies of a gene were considered as representing a single gene (Namekawa et al. 2006; Fallahi et al. 2010; Hu and Namekawa 2015). Indeed, recent studies have challenged these observations, and reported that after meiosis , the X chromosome encompasses a higher proportion of genes that are upregulated in round spermatids than autosomes, and also a higher proportion of genes with spermatid-specific expression (de novo expressed genes). Also the vast majority of Y-encoded expressed genes are exclusively expressed after meiosis (Moretti et al. 2016; Lukassen et al. 2018). These studies have concluded that the mouse sex chromosomes are no longer silenced after meiosis, but differently regulated compared to autosomes, accumulating different chromatin marks (Moretti et al. 2016).

Histone variants and the H2B-TH2B transition

While some non-canonical histones are ubiquitously expressed, others are restricted to a few tissues or specific cell functions (Rathke et al. 2014). In mouse and human, almost all the H2A, H2B, H3 and H1 variants are expressed in testis. The variants that are expressed in

post-meiotic germ cells are thought to have a role in loosening chromatin structure in preparation for the histone-to-protamine transition (Rathke et al. 2014). Here, we will focus on the testis-specific variant TH2B in mouse and man, which replaces most of the canonical H2B in early spermatocytes (Brock et al. 1980; Meistrich et al. 1985; Montellier et al. 2013). TH2B was first discovered in mammalian testes histone extracts in 1975 (Branson et al. 1975; Shires et al. 1975). Later studies in rat and mouse showed that TH2B is actively expressed in early primary spermatocytes (around preleptotene stage) until mid-late pachytene, and then remains the major form of H2B in round and elongating spermatids, gradually disappearing during condensation of the spermatid nucleus (Brock et al. 1980; Meistrich et al. 1985; Montellier et al. 2013). In humans, some TH2B is retained in mature sperm (van Roijen et al. 1998; Zalensky et al. 2002). Surprisingly, in the absence of TH2B in mice, H2B persists in spermatocytes, and spermatogenesis progresses normally, with no effect on fertility (Montellier et al. 2013; Hoghoughi et al. 2018). The data showed that nucleosomes in TH2B-deficient cells undergo specific epigenetic adaptation, involving placement of histone post-translational modifications that enhance nucleosome instability. Therefore, the primary function of TH2B could be to generate less stable nucleosomes, which would lower the energy necessary for the cells to undergo genome-wide histone exchanges in later stages. In accordance with this, Li et al. (2005) reported that a histone octamer containing TH2B presents an increased instability compared to a canonical octamer.

Chromatin modifications preceding the histone-to-protamine transition

In addition to the incorporation of histone variants, certain histones PTMs that occur before the histone-to-protamine transition, are thought to also facilitate the eviction of nucleosomes by affecting the higher-order chromatin structure (Rathke et al. 2014). Hyperacetylation of histone H4 appears just prior to histone removal and disappears in condensing spermatids prior to protamine incorporation. It is thought that its presence leads to an open chromatin structure that facilitates and induces histone replacement (Boskovic and Torres-Padilla 2013; Rathke et al. 2014). In the mouse, histone hyperacetylation starts while a general transcription shutdown is observed. Therefore, elongating spermatids heavily acetylate their histones in the total absence of DNA transcription (Gaucher et al. 2010). In mouse and human, reduced levels of histone H4 hyperacetylation in sperm correlates with impaired fertility (Rathke et al. 2014). Histone hyperacetylation is known to play an essential role in driving stage-specific male germ cell gene expression. Two of the acetyltransferases involved in this process, CBP and P300, have been reported to regulate the expression of genes involved in metabolic remodeling and chromatin reorganization. Both type of genes are repressed during meiosis, and whilst genes involved in chromatin

reorganization reactivate in early round spermatids, genes involved in cell metabolism reactivate in elongating spermatids, just previous to the transcription shut-down. Thus, this indicates the existence of a stage-specific tightly regulated gene expression program (Boussouar et al. 2014).

Besides acetylation, histone methylation of H3 at different residues has also been observed in elongating spermatids (Godmann et al. 2007). While some of these methylations would assist in achieving a more-open chromatin configuration, others would be expected to assist in promoting the opposite situation. The existence of both might be important to maintain the balance between sites with "opened" and "closed" chromatin (Rathke et al. 2014). Increased histone ubiquitination of histone H2A and H2B has also been observed during meiosis and in elongating spermatids in mice (Chen et al. 1998; Baarends et al. 1999; Rathke et al. 2014). However, if it has a function in histone eviction is still unclear. Additionally, a wave of hypercrotonylation accompanies spermatid elongation, suggesting that this modification might also be relevant for chromatin remodeling during spermiogenesis (Tan et al. 2011; Rathke et al. 2014).

Histone removal during spermiogenesis

At the end of spermatogenesis, the nucleosomal histone-based structure is substituted by a structure based on protamines (PRMs), with an intermediate step involving transition proteins (TPs). Transient appearance of DNA breaks is associated with this process (Rathke et al. 2014). In mammalian species, two types of transition proteins can be found, TP1 and TP2, encoded by *Tnp1* and *Tnp2* genes. TP1 is only 55 amino acids residues in size, and it is highly conserved across mammalian species. TP2, in contrast, exhibits a high degree of sequence divergence across mammals, and only about 50% amino acid homology between mouse and human (Bao and Bedford 2016). *Tnp1* knockout mice are mostly sterile (around 60% of the males) and present severely reduced sperm motility and increased levels of TP2 and some protamine 2 precursors in spermatid nuclei (Yu et al. 2000). *Tnp2* knockout mice are fertile and display only mild abnormalities. Mice lacking both TP1 and TP2 are sterile, showing irregular chromatin condensation in all spermatids (Zhao et al. 2004; Rathke et al. 2014). Mammalian protamines are proteins with a low molecular mass, enriched in arginine and cysteine (Doenecke et al. 1997; Govin et al. 2004; Rathke et al. 2014). They allow an enormous condensation of the nucleus, which enhances sperm motility and protects DNA from damage (Oliva 2006). Most mammals have one protamine gene. However, both the human and mouse genomes contain two; Protamine 1 (*PRM1/Prm1*) and 2 (*PRM2/Prm2*) clustered on the same chromosome (Rathke et al. 2014; Bao and Bedford 2016). Cho et al. (2001) reported that deletion of one allele of either *Prm1* or *Prm2* results in severely

aberrant spermatogenesis and sterility of the mouse (haploinsufficiency). In contrast, a most recent study reported that *Prm2*^{+/-} mice were fertile and produced normal sperm, while complete lack of *Prm2* caused infertility with severe defects in sperm head morphology and sperm motility (Schneider et al. 2016).

The classic view on the histone-to-protamine transition proposed that histones (canonical and non-canonical) are substituted first by transition proteins (TPs) (Meistrich et al. 2003) and finally by protamines (Lewis et al. 2003; Rathke et al. 2014). In a recent study, Barral et al. (2017) have proposed an additional step involving a function of the histone H2A variant H2A.L.2, which is expressed concomitant with TPs. H2A.L.2 dimerizes with TH2B and creates nucleosomes, which display an open structure with flexible DNA ends that allows TPs to be loaded onto the chromatin. TP loading does not directly lead to histone replacement but rather facilitates the recruitment of Prms and their processing. Prms are then the true mediators of histone replacement. Incorporation of protamine results in a higher degree of compaction of the chromatin (6-20 fold higher compared to histone-mediated packaging) (Ward and Coffey 1991; Balhorn et al. 2000). Despite the massive replacement of histones by protamines, a certain fraction of histones (canonical and non-canonical) persist in the sperm (10-15% in humans and 1 % in mouse) (Steger 1999; Van Der Heijden et al. 2005; Carrell et al. 2007; De Vries et al. 2012). These remaining histones may influence the development of the early embryo and epigenetic inheritance (Rathke et al. 2014).

IN VITRO LIVE IMAGING TECHNIQUES/gametogenesis in vitro

Gametogenesis can be viewed as one of the most complex cellular differentiation processes in the body. Researches have struggled to find the optimal conditions to support these processes in vitro for a long time, and these efforts continue nowadays. One of the key moments for the development of oogenesis in vitro occurred in 1996, when Eppig and O'Brien (1996) applied a two-step culture method with isolated newborn mouse ovaries. The initial step involved ovarian organ culture to produce preantral follicles. During the second step, oocyte–granulosa cell complexes were isolated from the ovarian organ and further cultured to complete oocyte growth and development. Live offspring was generated after using this oocytes for In Vitro Fertilization (IVF) (Eppig and O'Brien 1996; Wang et al. 2017). However, it was not till 2016 when two studies reported reconstitution of the entire process of mammalian oogenesis from embryo to adult in vitro using a multistep culture procedure (Morohaku et al. 2016; Hikabe et al. 2016). Morohaku et al. (2016) significantly improved the method to obtain secondary follicles from intact embryonic ovary cultures, and to produce oocytes able to complete meiotic maturation and support embryo development from

cultured oocyte-granulosa cell complexes. Hikabe et al. (2016) following Morohaku et al. (2016) added two steps to the procedure consisting of producing primordial germ cells (PGCs)-like cells derived from epiblast like cells (EpiLCs) and reconstructing embryonic ovaries by aggregating these cells with somatic cells. In this way the authors were able to reconstitute in vitro the entire cycle of the mouse female germ line from embryo to adult, starting from embryonic stem cells (Wang et al. 2017).

Obtaining a method for in vitro spermatogenesis appears to be more challenging than oogenesis, although the first attempts to develop complete spermatogenesis in vitro were performed already nearly one century ago, when Champy et al. (1920) cultured small parts of testis from adult rabbits in blood plasma. In 1937, it was reported that spermatogenesis proceeded up to the pachytene stage of meiosis in male gonads of newborn mice and rat placed on a clot (Martinovitch 1937). Although the organ culture methods and conditions evolved in the following years, it was not till 2011 when Sato et al developed a method to induce complete spermatogenesis in cultured neonatal mouse testis, and achieved the production of functional sperm and normal offspring (Sato et al. 2011). In these experiments, testis tissue fragments of about 1-3 mm in diameter were placed on agarose gel half-soaked in medium, according to the traditional gas-liquid interphase method (Trowell 1959). The addition of Knockout Replacement Serum (KRS) to the medium proved to be essential to induce spermatogenesis, which could be maintained for more than two months. However, this was still far from comparable to the overall efficiency and duration of spermatogenesis in vivo. Next steps in in vitro spermatogenesis systems seem to involve the development of circulatory mechanisms. This would imitate blood capillaries function, which continuously supply nutrients and oxygen to the tissue, and remove waste products, promoting the homeostasis of the tissue. Recently, Komeya et al. (2016) developed a microfluidics (MF) device which incorporated a porous membrane that separate the cultured tissue from a slowly flowing medium. Using this kind of system, spermatogenesis in testis tissue has been maintained up to 6 months, from which healthy offspring was obtained (using assisted reproduction technology) (Komeya et al. 2016).

SCOPE OF THIS THESIS

During spermatogenesis and oogenesis, germ cells go through a long and complex journey, at the end of which they will become mature gametes. Defects that may occur during this process can lead to infertility or genetic abnormalities in the offspring. Two main genomic events need to be achieved during spermatogenesis in mammals. First, haploid cells need to be generated through meiosis, and secondly, the genome needs to be repackaged to fit the aerodynamic sperm head, and to protect the genome during its journey towards the egg.

To understand basic aspects of chromosome behaviour during these processes and to apply this knowledge in order to better understand causes of male infertility in man, this thesis has focused on development of new tools to be able to study aspects of chromosome pairing, meiotic division and postmeiotic chromatin reorganization in living mouse spermatogenic cells, as well as on development of better methods to asses which defects occur most frequently in relation to meiotic checkpoint activation in fixed material from human testis biopsies.

In **Chapters 2** and **3**, we describe a system to follow and study different aspects of mouse gametogenesis in living cells, in the natural environment of the seminiferous tubule or the embryonic ovary. In these chapters, we have focused on the in vivo study of meiosis, which is at the heart of gametogenesis, and required to generate haploid cells from diploid precursors. For this, we have used mice expressing N- or C-terminal fluorescent-tagged SYCP3 (mCherry-SYCP3 (CSYCP) and SYCP3-mCherry (SYCPC)), alone (**Chapter 2**), or in combination with GFP-tagged histone H2B (H2B-GFP) (**Chapter 3**). SYCP3 is a component of the synaptonemal complex, a transient protein structure that connects homologous chromosomes during meiotic prophase. This allowed us to perform detailed analyses of the synaptonemal complex, and chromosome and nuclear dynamics during meiotic prophase I in oocytes and spermatocytes. Later stages of male meiosis, from diplotene up to the formation of secondary spermatocytes, were analyzed in **Chapter 3.** We paid special attention to the metaphase-to-anaphase I transition. We observed that the cultured spermatocytes remained in the first meiotic metaphase for more then 11 hours, indicating that the satisfaction of the SAC takes a very long time during meiosis I, in comparison to what is known about the metaphase-to-anaphase transition in different mammalian mitotic cell types. Interestingly, activation of the SAC followed by cell death appeared to be a frequent event in human males suffering from azoospermia caused by spermatogenic impairment (**Chapter 4A**). In this chapter we describe the development and optimization of an immunofluorescent staining method to analyze human surplus paraffin-embedded testis

biopsy samples of non-obstructive azoospermia patients. Next (**Chapter 4B**), we applied this method to characterize the spermatogenic impairment of two brothers in which a homozygous mutation in the *RNF212* gene was identified, and in a patient with compound heterozygosity at the *STAG3* gene. RNF212 in mouse is required for crossover formation, and mouse *Stag3* knockouts fail to form the synaptonemal complex. Our immunohistochemical analyses provided support for a causative role of the identified mutations in the male infertility phenotype, but also pointed to possible mouse/human differences in the function of RNF212. Finally, we applied and adapted the method described in **Chapter 2** to analyses of the dynamics of the histone-to-protamine transition during spermiogenesis, as part of a study to define the function of the chromatin-helicase-DNA 5 (CHD5) protein, expressed in round spermatids, and known to be required for fertility (**Chapter 5**). In this chapter, we have also assessed if CHD5 (and additionally CHD3 and/or CHD3/4, which are expressed earlier in spermatocytes) may function as part of the NuRD remodeling complex in male germ cells. Since an enrichment of CHD5 is observed on part of the Y chromosome, we have also analysed if CHD5 regulates Y chromosomal gene expression. Our preliminary experiments indicate that CHD5 is not required for Y-chromosomal gene expression in spermatids, but does affect global chromatin structure, although when compared to wild type, loss of histones during nuclear elongation in spermatids appeared to occur with similar overall dynamics. In **Chapter 6** we discuss the findings presented in the previous chapters and address possible further directions of the research work we have presented in this thesis.

REFERENCES

Anderson LK, Reeves A, Webb LM, Ashley T (1999) Distribution of crossing over on mouse synaptonemal complexes using immunofluorescent localization of MLH1 protein. Genetics 151:1569–79

Baarends WM, Hoogerbrugge JW, Roest HP, et al (1999) Histone ubiquitination and chromatin remodeling in mouse spermatogenesis. Dev Biol 207:322–33. doi: 10.1006/dbio.1998.9155

Baarends WM, Wassenaar E, van der Laan R, et al (2005) Silencing of Unpaired Chromatin and Histone H2A Ubiquitination in Mammalian Meiosis. Mol Cell Biol 25:1041–1053. doi: 10.1128/MCB.25.3.1041-1053.2005

Baker SM, Plug AW, Prolla TA, et al (1996) Involvement of mouse Mlh1 in DNA mismatch repair and meiotic crossing over. Nat Genet 13:336–42. doi: 10.1038/ng0796-336

Balhorn R, Brewer L, Corzett M (2000) DNA condensation by protamine and arginine-rich peptides: analysis of toroid stability using single DNA molecules. Mol Reprod Dev 56:230–4. doi: 10.1002/(SICI)1098-2795(200006)56:2+<230::AID-MRD3>3.0.CO;2-V

Banerjee T, Chakravarti D (2011) A peek into the complex realm of histone phosphorylation. Mol Cell Biol 31:4858–73. doi: 10.1128/MCB.05631-11

Bao J, Bedford MT (2016) Epigenetic regulation of the histone-to-protamine transition during spermiogenesis. Reproduction 151:R55–R70. doi: 10.1530/REP-15-0562

Barchi M, Mahadevaiah S, Di Giacomo M, et al (2005) Surveillance of different recombination defects in mouse spermatocytes yields distinct responses despite elimination at an identical developmental stage. Mol Cell Biol 25:7203–15. doi: 10.1128/MCB.25.16.7203-7215.2005

Barral S, Morozumi Y, Tanaka H, et al (2017) Histone Variant H2A.L.2 Guides Transition Protein-Dependent Protamine Assembly in Male Germ Cells. Mol Cell 66:89–101.e8. doi: 10.1016/j.molcel.2017.02.025

Baudat F, de Massy B (2007) Regulating double-stranded DNA break repair towards crossover or non-crossover during mammalian meiosis. Chromosom Res 15:565–577. doi: 10.1007/s10577-007-1140-3

Baudat F, Manova K, Yuen JP, et al (2000) Chromosome synapsis defects and sexually dimorphic meiotic progression in mice lacking Spo11. Mol Cell 6:989–98

Bolcun-Filas E, Costa Y, Speed R, et al (2007) SYCE2 is required for synaptonemal complex assembly, double strand break repair, and homologous recombination. J Cell Biol 176:741–7. doi: 10.1083/jcb.200610027

Bolcun-Filas E, Hall E, Speed R, et al (2009) Mutation of the mouse Syce1 gene disrupts synapsis and suggests a link between synaptonemal complex structural components and DNA repair. PLoS Genet 5:e1000393. doi: 10.1371/journal.pgen.1000393

Boskovic A, Torres-Padilla M-E (2013) How mammals pack their sperm: a variant matter. Genes Dev 27:1635–9. doi: 10.1101/gad.226167.113

Boussouar F, Goudarzi A, Buchou T, et al (2014) A specific CBP/p300-dependent gene expression programme drives the metabolic remodelling in late stages of spermatogenesis. Andrology 2:351–9. doi: 10.1111/j.2047-2927.2014.00184.x

Branson RE, Grimes SR, Yonuschot G, Irvin JL (1975) The histones of rat testis. Arch Biochem Biophys 168:403–12

Brock W a, Trostle PK, Meistrich ML (1980) Meiotic synthesis of testis histones in the rat. Proc Natl Acad Sci U S A 77:371–5. doi: 10.1073/pnas.77.1.371

Burgoyne PS, Mahadevaiah SK, Turner JMA (2009) The consequences of asynapsis for mammalian meiosis. Nat Rev Genet 10:207–16. doi: 10.1038/nrg2505

Carrell DT, Emery BR, Hammoud S (2007) Altered protamine expression and diminished spermatogenesis: What is the link? Hum Reprod Update 13:313–327. doi: 10.1093/humupd/dml057

Champy C (1920) Quelques resultats de la methode de culture des tissus. Arch Zool Exp Gen.60:461–500

Chen HY, Sun JM, Zhang Y, et al (1998) Ubiquitination of histone H3 in elongating spermatids of rat testes. J Biol Chem 273:13165–9

Chicheportiche A, Bernardino-Sgherri J, de Massy B, Dutrillaux B (2007) Characterization of Spo11-

dependent and independent phospho-H2AX foci during meiotic prophase I in the male mouse. J Cell Sci 120:1733–42. doi: 10.1242/jcs.004945

Cho C, Willis WD, Goulding EH, et al (2001) Haploinsufficiency of protamine-1 or -2 causes infertility in mice. Nat Genet 28:82–86. doi: 10.1038/88313

Clermont Y (1972) Kinetics of spermatogenesis in mammals: seminiferous epithelium cycle and spermatogonial renewal. Physiol Rev 52:198–236. doi: 10.1152/physrev.1972.52.1.198

Clermont Y (1963) The cycle of the seminiferous epithelium in man. Am J Anat 112:35–51. doi: 10.1002/aja.1001120103

Costa Y, Speed R, Ollinger R, et al (2005) Two novel proteins recruited by synaptonemal complex protein 1 (SYCP1) are at the centre of meiosis. J Cell Sci 118:2755–62. doi: 10.1242/jcs.02402

de Boer E, Stam P, Dietrich AJJ, et al (2006) Two levels of interference in mouse meiotic recombination. Proc Natl Acad Sci U S A 103:9607–12. doi: 10.1073/pnas.0600418103

de Rooij DG, de Boer P (2003) Specific arrests of spermatogenesis in genetically modified and mutant mice. Cytogenet Genome Res 103:267–76. doi: 10.1159/000076812

de Vries FAT, de Boer E, van den Bosch M, et al (2005) Mouse Sycp1 functions in synaptonemal complex assembly, meiotic recombination, and XY body formation. Genes Dev 19:1376–89. doi: 10.1101/gad.329705

de Vries M, Ramos L, Housein Z, De Boer P (2012) Chromatin remodelling initiation during human spermiogenesis. Biol Open 1:446–457. doi: 10.1242/bio.2012844

Ding X, Xu R, Yu J, et al (2007) SUN1 is required for telomere attachment to nuclear envelope and gametogenesis in mice. Dev Cell 12:863–72. doi: 10.1016/j.devcel.2007.03.018

Doenecke D, Drabent B, Bode C, et al (1997) Histone gene expression and chromatin structure during spermatogenesis. Adv Exp Med Biol 424:37–48

Dym M, Fawcett DW (1971) Further observations on the numbers of spermatogonia, spermatocytes, and spermatids connected by intercellular bridges in the mammalian testis. Biol Reprod 4:195–215

Ehmsen KT, Heyer W-D (2008) Biochemistry of Meiotic Recombination: Formation, Processing, and Resolution of Recombination Intermediates. In: Recombination and Meiosis. Springer Berlin Heidelberg, Berlin, Heidelberg, pp 91–164

Ellis LC, Groesbeck MD, Farr CH, Tesi RJ (1981) Contractility of seminiferous tubules as related to sperm transport in the male. Arch Androl 6:283–94

Eppig JJ, O'Brien MJ (1996) Development in vitro of mouse oocytes from primordial follicles. Biol Reprod 54:197–207

Fallahi M, Getun I V, Wu ZK, Bois PRJ (2010) A Global Expression Switch Marks Pachytene Initiation during Mouse Male Meiosis. Genes (Basel) 1:469–83. doi: 10.3390/genes1030469

Fernandez-Capetillo O, Mahadevaiah SK, Celeste A, et al (2003) H2AX is required for chromatin remodeling and inactivation of sex chromosomes in male mouse meiosis. Dev Cell 4:497–508

Gao J, Colaiácovo MP (2018) Zipping and Unzipping: Protein Modifications Regulating Synaptonemal Complex Dynamics. Trends Genet 34:232–245. doi: 10.1016/j.tig.2017.12.001

Gaucher J, Reynoird N, Montellier E, et al (2010) From meiosis to postmeiotic events: The secrets of histone disappearance. FEBS J. 277:599–604

Godmann M, Auger V, Ferraroni-Aguiar V, et al (2007) Dynamic regulation of histone H3 methylation at lysine 4 in mammalian spermatogenesis. Biol Reprod 77:754–64. doi: 10.1095/biolreprod.107.062265

Goossens S, van Roy F (2005) Cadherin-mediated cell-cell adhesion in the testis. Front Biosci 10:398–419

Gorbsky GJ (2015) The spindle checkpoint and chromosome segregation in meiosis. FEBS J 282:2471–87. doi: 10.1111/febs.13166

Gordon JW, Ruddle FH (1981) Mammalian gonadal determination and gametogenesis. Science 211:1265–71

Govin J, Caron C, Lestrat C, et al (2004) The role of histones in chromatin remodelling during mammalian spermiogenesis. Eur J Biochem 271:3459–3469. doi: 10.1111/j.1432-1033.2004.04266.x

Grabarz A, Barascu A, Guirouilh-Barbat J, Lopez BS (2012) Initiation of DNA double strand break repair: signaling and single-stranded resection

dictate the choice between homologous recombination, non-homologous end-joining and alternative end-joining. Am J Cancer Res 2:249–68

Greaves IK, Rangasamy D, Devoy M, et al (2006) The X and Y chromosomes assemble into H2A.Z-containing [corrected] facultative heterochromatin [corrected] following meiosis. Mol Cell Biol 26:5394–405. doi: 10.1128/MCB.00519-06

Hamer G, Gell K, Kouznetsova A, et al (2006) Characterization of a novel meiosis-specific protein within the central element of the synaptonemal complex. J Cell Sci 119:4025–32. doi: 10.1242/jcs.03182

Hamer G, Novak I, Kouznetsova A, Höög C (2008) Disruption of pairing and synapsis of chromosomes causes stage-specific apoptosis of male meiotic cells. Theriogenology 69:333–9. doi: 10.1016/j.theriogenology.2007.09.029

Hamer G, Roepers-Gajadien HL, van Duyn-Goedhart A, et al (2003) DNA double-strand breaks and gamma-H2AX signaling in the testis. Biol Reprod 68:628–34

Hartsuiker E, Mizuno K, Molnar M, et al (2009) Ctp1CtIP and Rad32Mre11 Nuclease Activity Are Required for Rec12Spo11 Removal, but Rec12Spo11 Removal Is Dispensable for Other MRN-Dependent Meiotic Functions. Mol Cell Biol 29:1671–1681. doi: 10.1128/MCB.01182-08

Hassold T, Sherman S, Hunt P (2000) Counting cross-overs: characterizing meiotic recombination in mammals. Hum Mol Genet 9:2409–19

Hess RA(1999).Spermatogenesis, Overview.Encyclopedia Reprod 45: 39-545.

Heyer W-D, Ehmsen KT, Liu J (2010) Regulation of homologous recombination in eukaryotes. Annu Rev Genet 44:113–39. doi: 10.1146/annurev-genet-051710-150955

Heyting C (1996) Synaptonemal complexes: structure and function. Curr Opin Cell Biol 8:389–96

Heyting C (2005) Meiotic transverse filament proteins: essential for crossing over. Transgenic Res 14:547–50. doi: 10.1007/s11248-005-8925-y

Hikabe O, Hamazaki N, Nagamatsu G, et al (2016) Reconstitution in vitro of the entire cycle of the mouse female germ line. Nature 539:299–303. doi: 10.1038/nature20104

Hinch AG, Altemose N, Noor N, et al (2014) Recombination in the human Pseudoautosomal region PAR1. PLoS Genet 10:e1004503. doi: 10.1371/journal.pgen.1004503

Hoghoughi N, Barral S, Vargas A, et al (2018) Histone variants: essential actors in male genome programming. J Biochem 163:97–103. doi: 10.1093/jb/mvx079

Holloway JK, Booth J, Edelmann W, et al (2008) MUS81 Generates a Subset of MLH1-MLH3–Independent Crossovers in Mammalian Meiosis. PLoS Genet 4:e1000186. doi: 10.1371/journal.pgen.1000186

Homolka D, Ivanek R, Capkova J, et al (2007) Chromosomal rearrangement interferes with meiotic X chromosome inactivation. Genome Res 17:1431–1437. doi: 10.1101/gr.6520107

Hoyer-Fender S, Costanzi C, Pehrson JR (2000) Histone macroH2A1.2 is concentrated in the XY-body by the early pachytene stage of spermatogenesis. Exp Cell Res 258:254–60. doi: 10.1006/excr.2000.4951

Hu YC, Namekawa SH (2015) Functional significance of the sex chromosomes during spermatogenesis. Reproduction 149:R265–R277. doi: 10.1530/REP-14-0613

Hunter N, Borts RH (1997) Mlh1 is unique among mismatch repair proteins in its ability to promote crossing-over during meiosis. Genes Dev 11:1573–82

Kinner A, Wu W, Staudt C, Iliakis G (2008) Gamma-H2AX in recognition and signaling of DNA double-strand breaks in the context of chromatin. Nucleic Acids Res 36:5678–94. doi: 10.1093/nar/gkn550

Kohl KP, Sekelsky J (2013) Meiotic and mitotic recombination in meiosis. Genetics 194:327–34. doi: 10.1534/genetics.113.150581

Komeya M, Kimura H, Nakamura H, et al (2016) Long-term ex vivo maintenance of testis tissues producing fertile sperm in a microfluidic device. Sci Rep 6:21472. doi: 10.1038/srep21472

Kouznetsova A, Benavente R, Pastink A, Höög C (2011) Meiosis in Mice without a Synaptonemal Complex. PLoS One 6:e28255. doi: 10.1371/journal.pone.0028255

Koyama M, Kurumizaka H (2018) Structural diversity of the nucleosome. J Biochem 163:85–95. doi: 10.1093/jb/mvx081

Krejci L, Altmannova V, Spirek M, Zhao X (2012) Homologous recombination and its regulation. Nucleic Acids Res 40:5795–5818. doi: 10.1093/nar/gks270

La Volpe A, Barchi M (2012) Meiotic double strand breaks repair in sexually reproducing eukaryotes: We are not all equal. Exp Cell Res 318:1333–1339. doi: 10.1016/j.yexcr.2012.03.014

Lee C-Y, Conrad MN, Dresser ME (2012) Meiotic chromosome pairing is promoted by telomere-led chromosome movements independent of bouquet formation. PLoS Genet 8:e1002730. doi: 10.1371/journal.pgen.1002730

Lee CY, Horn HF, Stewart CL, et al (2015) Mechanism and Regulation of Rapid Telomere Prophase Movements in Mouse Meiotic Chromosomes. Cell Rep 11:551–563. doi: 10.1016/j.celrep.2015.03.045

Lewis JD, Song Y, De Jong ME, et al (2003) A walk though vertebrate and invertebrate protamines. Chromosoma 111:473–482

Li A, Maffey AH, Abbott WD, et al (2005) Characterization of nucleosomes consisting of the human testis/sperm-specific histone H2B variant (hTSH2B). Biochemistry 44:2529–35. doi: 10.1021/bi048061n

Lipkin SM, Moens PB, Wang V, et al (2002) Meiotic arrest and aneuploidy in MLH3-deficient mice. Nat Genet 31:385–90. doi: 10.1038/ng931

Lukassen S, Bosch E, Ekici AB, Winterpacht A (2018) Characterization of germ cell differentiation in the male mouse through single-cell RNA sequencing. Sci Rep 8:6521. doi: 10.1038/s41598-018-24725-0

Luo M, Yang F, Leu NA, et al (2013) MEIOB exhibits single-stranded DNA-binding and exonuclease activities and is essential for meiotic recombination. Nat Commun 4:2788. doi: 10.1038/ncomms3788

Mahadevaiah SK, Turner JM, Baudat F, et al (2001) Recombinational DNA double-strand breaks in mice precede synapsis. Nat Genet 27:271–6. doi: 10.1038/85830

Marcet-Ortega M, Pacheco S, Martínez-Marchal A, et al (2017) p53 and TAp63 participate in the recombination-dependent pachytene arrest in mouse spermatocytes. PLoS Genet 13:e1006845. doi: 10.1371/journal.pgen.1006845

Martinovitch PN (1937) Development in vitro of the Mammalian Gonad. Nature 139:413–413. doi: 10.1038/139413a0

McMahill MS, Sham CW, Bishop DK (2007) Synthesis-dependent strand annealing in meiosis. PLoS Biol 5:2589–2601. doi: 10.1371/journal.pbio.0050299

Meistrich ML, Bucci LR, Trostle-Weige PK, Brock WA (1985) Histone variants in rat spermatogonia and primary spermatocytes. Dev Biol 112:230–240. doi: 10.1016/0012-1606(85)90137-X

Meistrich ML, Mohapatra B, Shirley CR, Zhao M (2003) Roles of transition nuclear proteins in spermiogenesis. Chromosoma 111:483–488

Mimitou EP, Symington LS (2009) DNA end resection: Many nucleases make light work. DNA Repair (Amst). 8:983–995

Mital P, Hinton BT, Dufour JM (2011) The blood-testis and blood-epididymis barriers are more than just their tight junctions. Biol Reprod 84:851–8. doi: 10.1095/biolreprod.110.087452

Montellier E, Boussouar F, Rousseaux S, et al (2013) Chromatin-to-nucleoprotamine transition is controlled by the histone H2B variant TH2B. Genes Dev 27:1680–1692. doi: 10.1101/gad.220095.113

Moretti C, Vaiman D, Tores F, Cocquet J (2016) Expression and epigenomic landscape of the sex chromosomes in mouse post-meiotic male germ cells. Epigenetics Chromatin 9:47. doi: 10.1186/s13072-016-0099-8

Morimoto A, Shibuya H, Zhu X, et al (2012) A conserved KASH domain protein associates with telomeres, SUN1, and dynactin during mammalian meiosis. J Cell Biol 198:165–72. doi: 10.1083/jcb.201204085

Morohaku K, Tanimoto R, Sasaki K, et al (2016) Complete in vitro generation of fertile oocytes from mouse primordial germ cells. Proc Natl Acad Sci 113:9021–9026. doi: 10.1073/pnas.1603817113

Mruk DD, Cheng CY (2015) The Mammalian Blood-Testis Barrier: Its Biology and Regulation. Endocr Rev 36:564–91. doi: 10.1210/er.2014-1101

Muciaccia B, Boitani C, Berloco BP, et al (2013) Novel stage classification of human spermatogenesis based on acrosome development. Biol Reprod 89:60. doi: 10.1095/biolreprod.113.111682

Musacchio A (2015) The Molecular Biology of Spindle Assembly Checkpoint Signaling Dynamics. Curr Biol 25:R1002–R1018. doi: 10.1016/j.cub.2015.08.051

Namekawa SH, Park PJ, Zhang L-F, et al (2006) Postmeiotic Sex Chromatin in the Male Germline of Mice. Curr Biol 16:660–667. doi: 10.1016/j.cub.2006.01.066

Nasmyth K, Haering CH (2005) The structure and function of smc and kleisin complexes. Annu Rev Biochem 74:595–648. doi: 10.1146/annurev.biochem.74.082803.133219

Neale MJ, Keeney S (2006) Clarifying the mechanics of DNA strand exchange in meiotic recombination. Nature 442:153–8. doi: 10.1038/nature04885

Oakberg EF (1956) Duration of spermatogenesis in the mouse and timing of stages of the cycle of the seminiferous epithelium. Am J Anat 99:507–516. doi: 10.1002/aja.1000990307

Oliva R (2006) Protamines and male infertility. Hum. Reprod. Update 12:417–435

Pacheco S, Marcet-Ortega M, Lange J, et al (2015) The ATM signaling cascade promotes recombination-dependent pachytene arrest in mouse spermatocytes. PLoS Genet 11:e1005017. doi: 10.1371/journal.pgen.1005017

Page J, de la Fuente R, Manterola M, et al (2012) Inactivation or non-reactivation: what accounts better for the silence of sex chromosomes during mammalian male meiosis? Chromosoma 121:307–326. doi: 10.1007/s00412-012-0364-y

Page SL, Hawley RS (2004) The genetics and molecular biology of the synaptonemal complex. Annu Rev Cell Dev Biol 20:525–558. doi: 10.1146/annurev.cellbio.19.111301.155141

Parvinen M, Söderström KO (1976) Chromosome rotation and formation of synapsis. Nature 260:534–535. doi: 10.1038/260534a0

Pelletier R-M (2011) The blood-testis barrier: the junctional permeability, the proteins and the lipids. Prog Histochem Cytochem 46:49–127. doi: 10.1016/j.proghi.2011.05.001

Pelletier RM, Byers SW (1992) The blood-testis barrier and Sertoli cell junctions: structural considerations. Microsc Res Tech 20:3–33. doi: 10.1002/jemt.1070200104

Perry J, Palmer S, Gabriel A, Ashworth A (2001) A short pseudoautosomal region in laboratory mice. Genome Res 11:1826–32. doi: 10.1101/gr.203001

Petronczki M, Siomos MF, Nasmyth K (2003) Un ménage à quatre: the molecular biology of chromosome segregation in meiosis. Cell 112:423–40

Petukhova G, Sung P, Klein H (2000) Promotion of Rad51-dependent D-loop formation by yeast recombination factor Rdh54/Tid1. Genes Dev 14:2206–2215. doi: 10.1101/gad.826100

Qiao H, Chen JK, Reynolds A, et al (2012) Interplay between Synaptonemal Complex, Homologous Recombination, and Centromeres during Mammalian Meiosis. PLoS Genet 8:e1002790. doi: 10.1371/journal.pgen.1002790

Rathke C, Baarends WM, Awe S, Renkawitz-Pohl R (2014) Chromatin dynamics during spermiogenesis. Biochim. Biophys. Acta - Gene Regul. Mech. 1839:155–168

Robert T, Nore A, Brun C, et al (2016) The TopoVIB-Like protein family is required for meiotic DNA double-strand break formation. Science 351:943–9. doi: 10.1126/science.aad5309

Romanienko PJ, Camerini-Otero RD (2000) The mouse Spo11 gene is required for meiotic chromosome synapsis. Mol Cell 6:975–87

Roosen-Runge EC (1951) Motions of the seminiferous tubule of rat and dog. Anat Rec 133(supl): 109

Royo H, Polikiewicz G, Mahadevaiah SK, et al (2010) Evidence that meiotic sex chromosome inactivation is essential for male fertility. Curr Biol 20:2117–23. doi: 10.1016/j.cub.2010.11.010

Salonen K, Paranko J, Parvinen M (1982) A colcemid-sensitive mechanism involved in regulation of chromosome movements during meiotic pairing. Chromosoma 85:611–618. doi: 10.1007/BF00330775

Santiemma V, Rossi F, Guerrini L, et al (2001) Adrenomedullin inhibits the contraction of cultured rat testicular peritubular myoid cells induced by endothelin-1. Biol Reprod 64:619–24

Sato T, Katagiri K, Gohbara A, et al (2011) In vitro production of functional sperm in cultured neonatal mouse testes. Nature 471:504–507. doi: 10.1038/nature09850

Scherthan H (2007) Telomeres and meiosis in health and disease. Cell Mol Life Sci 64:117–124. doi: 10.1007/s00018-006-6463-2

Schimenti J (2005) Synapsis or silence. Nat Genet 37:11–13. doi: 10.1038/ng0105-11

Schneider S, Balbach M, Jan F Jikeli JFJJF, et al (2016) Re-visiting the Protamine-2 locus: deletion, but not haploinsufficiency, renders male mice infertile. Sci Rep 6:36764. doi: 10.1038/srep36764

Schramm S, Fraune J, Naumann R, et al (2011) A novel mouse synaptonemal complex protein is essential for loading of central element proteins, recombination, and fertility. PLoS Genet 7:e1002088. doi: 10.1371/journal.pgen.1002088

Sehorn MG, Sigurdsson S, Bussen W, et al (2004) Human meiotic recombinase Dmc1 promotes ATP-dependent homologous DNA strand exchange. Nature 429:433–437. doi: 10.1038/nature02563

Shibuya H, Morimoto A, Watanabe Y (2014) The Dissection of Meiotic Chromosome Movement in Mice Using an In Vivo Electroporation Technique. PLoS Genet 10:. doi: 10.1371/journal.pgen.1004821

Shires A, Carpenter MP, Chalkley R (1975) New histones found in mature mammalian testes. Proc Natl Acad Sci U S A 72:2714–8

Souquet B, Abby E, Hervé R, et al (2013) MEIOB targets single-strand DNA and is necessary for meiotic recombination. PLoS Genet 9:e1003784. doi: 10.1371/journal.pgen.1003784

Steger K (1999) Transcriptional and translational regulation of gene expression in haploid spermatids. Anat Embryol (Berl) 199:471–487

Stewart CL, Burke B (2014) The missing LINC: a mammalian KASH-domain protein coupling meiotic chromosomes to the cytoskeleton. Nucleus 5:3–10. doi: 10.4161/nucl.27819

Sutton E, Hughes J, White S, et al (2011) Identification of SOX3 as an XX male sex reversal gene in mice and humans. J Clin Invest 121:328–41. doi: 10.1172/JCI42580

Tan M, Luo H, Lee S, et al (2011) Identification of 67 histone marks and histone lysine crotonylation as a new type of histone modification. Cell 146:1016–28. doi: 10.1016/j.cell.2011.08.008

TROWELL OA (1959) The culture of mature organs in a synthetic medium. Exp Cell Res 16:118–47

Turner JMA (2007) Meiotic sex chromosome inactivation. Development 134:1823–1831. doi: 10.1242/dev.000018

Turner JMA, Mahadevaiah SK, Ellis PJI, et al (2006) Pachytene asynapsis drives meiotic sex chromosome inactivation and leads to substantial postmeiotic repression in spermatids. Dev Cell 10:521–9. doi: 10.1016/j.devcel.2006.02.009

Turner JMA, Mahadevaiah SK, Fernandez-Capetillo O, et al (2005) Silencing of unsynapsed meiotic chromosomes in the mouse. Nat Genet 37:41–47. doi: 10.1038/ng1484

van der Heijden GW, Derijck AAHA, Pósfai E, et al (2007) Chromosome-wide nucleosome replacement and H3.3 incorporation during mammalian meiotic sex chromosome inactivation. Nat Genet 39:251–8. doi: 10.1038/ng1949

van Der Heijden GW, Dieker JW, Derijck AAHA, et al (2005) Asymmetry in Histone H3 variants and lysine methylation between paternal and maternal chromatin of the early mouse zygote. Mech Dev 122:1008–1022. doi: 10.1016/j.mod.2005.04.009

van Roijen HJ, Ooms MP, Spaargaren MC, et al (1998) Immunoexpression of testis-specific histone 2B in human spermatozoa and testis tissue. Hum Reprod 13:1559–66

Vrielynck N, Chambon A, Vezon D, et al (2016) A DNA topoisomerase VI-like complex initiates meiotic recombination. Science (80-) 351:939–943. doi: 10.1126/science.aad5196

Wang H, Höög C (2006) Structural damage to meiotic chromosomes impairs DNA recombination and checkpoint control in mammalian oocytes. J Cell Biol 173:485–95. doi: 10.1083/jcb.200512077

Wang J-J, Ge W, Liu J-C, et al (2017) Complete in vitro oogenesis: retrospects and prospects. Cell Death Differ 24:1845–1852. doi: 10.1038/cdd.2017.134

Wang TF, Kleckner N, Hunter N (1999) Functional specificity of MutL homologs in yeast: evidence for three Mlh1-based heterocomplexes with distinct roles during meiosis in recombination and mismatch correction. Proc Natl Acad Sci U S A 96:13914–9

Ward WS, Coffey DS (1991) DNA packaging and organization in mammalian spermatozoa: comparison with somatic cells. Biol Reprod 44:569–74

Watanabe Y (2005) Shugoshin: guardian spirit at the centromere. Curr Opin Cell Biol 17:590–595. doi: 10.1016/j.ceb.2005.10.003

Wold MS (1997) REPLICATION PROTEIN A:A Heterotrimeric, Single-Stranded DNA-Binding

1

Protein Required for Eukaryotic DNA Metabolism. Annu Rev Biochem 66:61–92. doi: 10.1146/annurev.biochem.66.1.61

Xu Y, Greenberg RA, Schonbrunn E, Wang PJ (2017) Meiosis-specific proteins MEIOB and SPATA22 cooperatively associate with the single-stranded DNA-binding replication protein A complex and DNA double-strand breaks†. Biol Reprod 96:1096–1104. doi: 10.1093/biolre/iox040

Youds JL, Boulton SJ (2011) The choice in meiosis - defining the factors that influence crossover or non-crossover formation. J Cell Sci 124:501–513. doi: 10.1242/jcs.074427

Yu YE, Zhang Y, Unni E, et al (2000) Abnormal spermatogenesis and reduced fertility in transition nuclear protein 1-deficient mice. Proc Natl Acad Sci U S A 97:4683–4688. doi: 10.1073/pnas.97.9.4683

Zalensky AO, Siino JS, Gineitis AA, et al (2002) Human testis/sperm-specific histone H2B (hTSH2B). Molecular cloning and characterization. J Biol Chem 277:43474–80. doi: 10.1074/jbc.M206065200

Zhao M, Shirley CR, Mounsey S, Meistrich ML (2004) Nucleoprotein transitions during spermiogenesis in mice with transition nuclear protein Tnp1 and Tnp2 mutations. Biol Reprod 71:1016–25. doi: 10.1095/biolreprod.104.028191

Zickler D, Kleckner N (1999) Meiotic chromosomes: integrating structure and function. Annu Rev Genet 33:603–754. doi: 10.1146/annurev.genet.33.1.603

Zickler D, Kleckner N (2016) A few of our favorite things: Pairing, the bouquet, crossover interference and evolution of meiosis. Semin. Cell Dev. Biol. 54:135–148

2
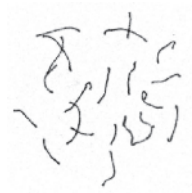
Live cell analyses of synaptonemal complex dynamics and chromosome movements in cultured mouse testis tubules and embryonic ovaries

Live cell analyses of synaptonemal complex dynamics and chromosome movements in cultured mouse testis tubules and embryonic ovaries

Andrea Enguita-Marruedo[1], Wiggert A. Van Cappellen[2], Jos W. Hoogerbrugge[1], Fabrizia Carofiglio[1], Evelyne Wassenaar[1], Johan A. Slotman[2], Adriaan Houtsmuller[2], and Willy M. Baarends[1*]

1) Department of Developmental Biology

2) Department of Pathology/Erasmus Optical Imaging Centre, Erasmus MC, Rotterdam, The Netherlands

*Corresponding author: Willy M. Baarends w.baarends@erasmusmc.nl

Short title: Mouse synaptonemal complex dynamics

Keywords: meiotic prophase; SYCP3; in vitro culture; spermatocyte; oocyte; synaptonemal complex

ABSTRACT

During mammalian meiotic prophase, homologous chromosomes connect through the formation of the Synaptonemal Complex (SC). SYCP3 is a component of the lateral elements of the SC. We have generated transgenic mice expressing N- or C-terminal fluorescent-tagged SYCP3 (mCherry-SYCP3 (CSYCP) and SYCP3-mCherry (SYCPC)) to study SC dynamics and chromosome movements in vivo. Neither transgene rescued meiotic aberrations in *Sycp3* knockouts, but CSYCP could form short axial element-like structures in the absence of endogenous SYCP3. On the wild type background, both fusion proteins localized to the axes of the SC together with endogenous SYCP3, albeit with delayed initiation (from pachytene) in spermatocytes. Around 40% of CSYCP and SYCPC that accumulated on the SC was rapidly exchanging with other tagged proteins, as analysed by fluorescent recovery after photobleaching (FRAP) assay. We used the CSYCP transgenic mice for further live cell analyses and observed synchronized bouquet configurations in living cysts of two or three zygotene oocyte nuclei expressing CSYCP, which presented cycles of telomere clustering and dissolution. Rapid chromosome movements were observed in both zygotene oocytes and pachytene spermatocytes, but rotational movements of the nucleus were more clear in oocytes. In diplotene spermatocytes, desynapsis was found to proceed in a discontinuous manner, whereby even brief chromosome re-association events were observed. Thus, this live imaging approach can be used to follow changes in the dynamic behaviour of the nucleus and chromatin, in normal mice and different infertile mouse models.

INTRODUCTION

In all sexually reproducing diploid species, homologous chromosomes must separate faithfully during the first meiotic division, to generate two haploid cells. Leading up to this event, homologs must form pairs. This requires dynamic movements of chromosomes inside the nucleus, as has been visualized in living rodent spermatocytes using transillumination microscopy already several decades ago (Parvinen and Soderstrom 1976; Salonen et al. 1982). One of the most conspicuous features of meiotic prophase cells that has been observed in almost all analyzed sexually reproducing species to date is the so-called bouquet stage, when telomeres cluster together in the nuclear periphery, and the thread-like chromosomes form a structure that is reminiscent of a bouquet of flowers (Scherthan 2007; Stewart and Burke 2014). In addition, rapid telomere movements occur in both yeast and mouse, and both processes require linkage of the telomeres to the cytoskeleton, through the nuclear membrane (Lee et al. 2012; Lee et al. 2015). These dynamic processes occur hand-in-hand with the initiation of homologous chromosome pairing. Correct chromosome pairing also requires the formation and repair of DNA double-strand breaks, mediated by the SPO11/TOPOVIBL complex (Baudat et al. 2000; Robert et al. 2016; Romanienko and Camerini-Otero 2000), together with additional meiosis-specific proteins. In addition, a DSB independent role of SPO11 in early homologous chromosome interactions has been described (Boateng et al. 2013). Pairing results in synapsis, defined as the formation of a physical proteinaceous connection between the chromosomes, in a zipper-like fashion along the chromosomal arms. This connecting protein structure is called the synaptonemal complex (SC) and is composed of two lateral elements (LEs, one per homolog) that associate with each other through the transverse filaments (TFs). They overlap in the central region, forming the central element (CE) (Page and Hawley 2004). In mammals, the LEs and their precursors, the axial elements (AEs), are mainly composed of the proteins SYCP2 and SYCP3, while the TFs mainly consist of SYCP1 (Costa et al. 2005; Heyting 1996). The CE contains SYCP1 as well as other proteins like SYCE1, SYCE2, SYCE3, and TEX1 (Costa et al. 2005; Hamer et al. 2006; Schramm et al. 2011).

With the advent of technologies to express fluorescent tagged proteins, and the means to analyze their expression in living cells using confocal fluorescent microscopy, more possibilities to investigate chromosome movement in detail have arisen. In mice carrying a SYCP3-EYFP transgene driven by a *Pgk2*-promoter, labeled SCs were analyzed in cultured pachytene spermatocytes embedded in a fibrinogen clot for periods of up to 6 h (Morelli et al. 2008). In these nuclei, only subtle movements were detected. More recently (Shibuya et al. 2014) used in vivo DNA electroporation to express fluorescent-tagged SYCP3 and TRF1 in

mouse spermatocytes. Cultured cells were analyzed for periods no longer than 10 min. The analysis of the SYCP3 behavior showed rapid movements of chromosomes within the nuclei throughout meiotic prophase. A recent study (Rog and Dernburg 2015) developed in the model organism *C. elegans*, involved analyses of the behavior of the SC in the worms in vivo.

We aimed to study the dynamics of chromosomes and the SC in living mouse spermatocytes or oocytes, in their natural environment (inside the seminiferous tubule or the ovary). We have generated transgenic mice expressing N- or C-terminal fluorescent-tagged SYCP3-mCherry, and developed a method that allows us to culture seminiferous tubules or ovaries during short-term (minutes) and long-term overnight cell imaging experiments. SYCP3 is an important functional component of the axial/lateral elements of the SC. Disruption of *Sycp3* leads to aberrant chromosome pairing and synapsis, and spermatocytes do not progress further than a zygotene-like stage (Hamer et al. 2008; Royo et al. 2010). Female $Sycp3^{-/-}$ knockouts show milder defects, and they are subfertile, showing a reduction in litter size (Yuan et al. 2002).

Here, we show that both N-terminal and C-terminal tagging of SYCP3 precludes formation of functional SYCP3 filaments in the absence of endogenous, untagged SYCP3. However, when untagged SYCP3 is also expressed, the tagged proteins can accumulate on the axial elements, exchange dynamically, and do not interfere with normal progression of oogenesis and spermatogenesis. This allowed us to perform detailed analyses of chromosome and nuclear movements during early and late meiotic prophase in oocytes and spermatocytes, respectively. Thereby, this study provides novel insight in nuclear rotation speed, dynamics of bouquet formation, and progression of desynapsis in living mouse meiocytes in a tissue context.

RESULTS

Transgenic expression of fluorescent-tagged SYCP3

To drive expression of the transgenes encoding SYCP3 tagged with mCherry at either the N- or C-terminal end of the protein, we used a promoter fragment of *Smc1b*, previously reported to drive specific expression in spermatocytes from leptotene onwards (Fig. S1a) (Adelfalk et al. 2009). We confirmed expression of the tagged protein first on Western blot, using total testis protein extracts from mice of different age. A single band was observed for N-terminally tagged SYCP3 (CSYCP), but C-terminal-tagged SYCP3 (SYCPC) was expressed in two forms, most likely as a result of the presence of two possible start codons in the first exon, as previously reported (Alsheimer et al. 2010). The levels of the two tagged proteins were lower compared to the level of endogenous SYCP3, and expression initiated later
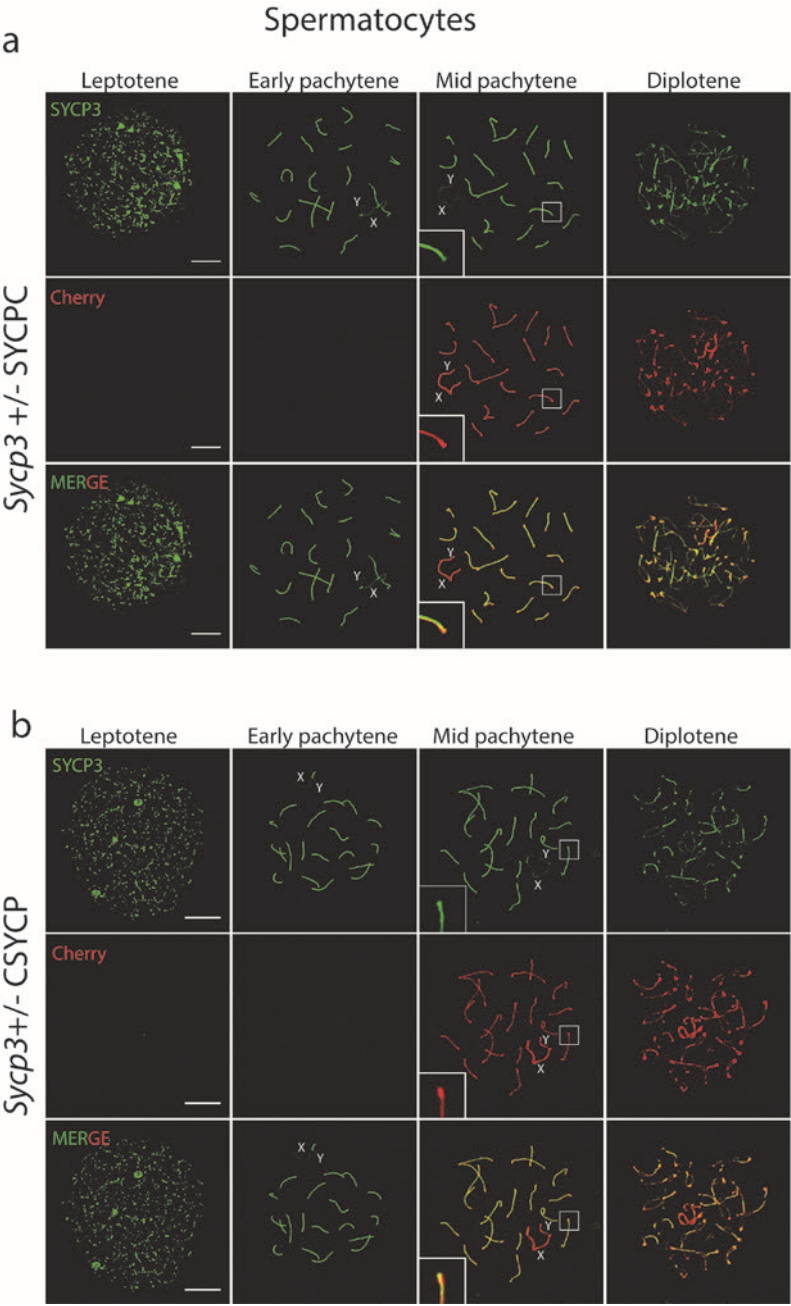
during postnatal development (Fig. S1b). Thus, although endogenous SMC1B and SYCP3 are known to display very similar expression patterns in spermatocytes (Dobson et al. 1994; Revenkova et al. 2001), the *Smc1b* promoter fragment used here resulted in reduced and delayed expression of fluorescent-tagged SYCP3 compared to endogenous SYCP3.

SYCPC and CSYCP locate on the axis of the fully formed SC in spermatocytes, and also on axial elements in oocytes on a wild-type background
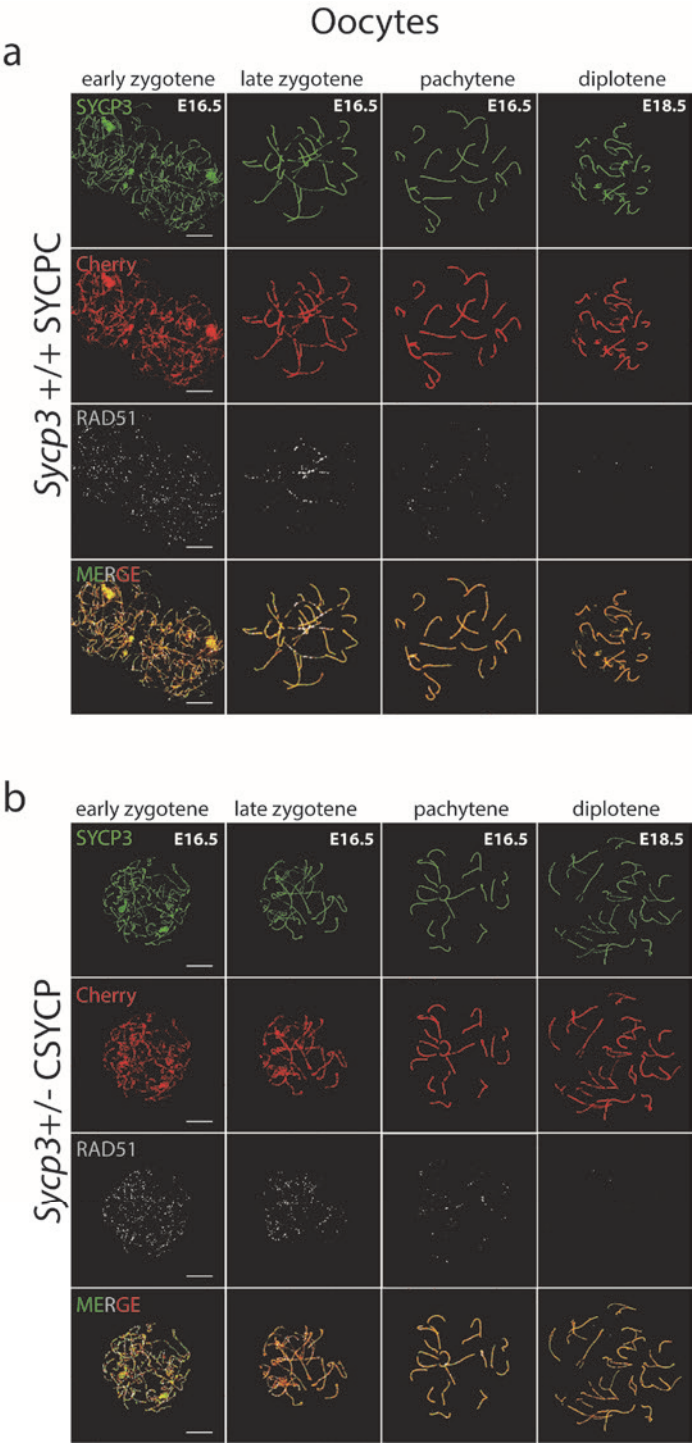
Next, we analyzed the localization of both fusion proteins in nuclear spread preparations of spermatocytes and oocytes, whereby the transgene was expressed either on a wild-type or *Sycp3*^{+/−} background. We detected both endogenous and transgenic SYCP3, making use of anti-SYCP3 antibody, and could selectively analyze the tagged protein by detecting the fluorescent signal from the mCherry moiety.

In males, SYCPC as well as CSYPC were detected from pachytene onwards, along the lateral elements of the SC, colocalizing with endogenous SYCP3 (Fig. 1). Interestingly, both fusion proteins displayed a signal of higher intensity at telomeric ends of the SC of the autosomes (Fig. 1a, b, enlargements in mid pachytene) and also along the axial elements of the X and Y chromosomes (Fig. 1a, b, mCherry signal in mid pachytene). Enrichment of fusion protein on the XY pair was most evident for CSYCP (Fig. 1b, mCherry signal in mid pachytene). In contrast, the overall SYCP3 signal (Fig. 1a,b, SYCP3 in mid pachytene, consisting of endogenous as well as tagged protein) was lower along the non-synapsed XY axes, compared to the synapsed autosomes, and no thickening was observed at the SC ends.

In embryonic ovaries, CSYCP and SYCPC were detected in oocyte nuclei from leptotene (embryonic day 16.5 (E16.5) until diplotene (E18.5) stages (Fig. 2a, b, staging of oocytes is described in the "Materials and methods"section). Also here, the tagged proteins colocalized with endogenous SYCP3. We did not detect either fusion protein in ovaries isolated from embryos younger than E16.5. No differences were observed between the patterns of the two fusion proteins, and also not between the overall SYCP3 signal and that of the mCherry-tagged protein only. The fact that both SYCPC and CSYCP localize to axial elements in leptotene and zygotene oocytes, but not in such early spermatocyte nuclei, is most likely due to the fact that the *Smc1b* promoter fragment used in our transgene constructs is not yet active in leptotene and zygotene spermatocytes in our models (see the "Discussion" section).

Fig. 1. Expression of SYCPC andCSYCP in wild-type spermatocytes. Immunostaining of SYCP3 (green) on *Sycp3*$^{+/-}$ SYCPC **(a)** and *Sycp3*$^{+/-}$ CSYCP **(b)** spermatocyte nuclei at different stagesof meiotic prophase. The red signal represents the mCherry signal (no antibody detection). Scale bar 10 μm

2

◄ **Fig. 2. Expression of SYCPC and CSYCP in wild-type oocytes**. Immunostaining of SYCP3 (green) and RAD51 (white, pseudo-color from infrared) on *Sycp3* $^{+/+}$ SYCPC **(a)** and *Sycp3* $^{+/-}$ CSYCP **(b)** oocyte nuclei from embryonic ovaries isolated at E16.5 (early and late zygotene and pachytene) and E18.5 (diplotene). mCherry (red) is visualized directly (no antibody detection). Scale bar 10 µm.

mCherry-tagged SYCP3 does not interfere with normal meiotic progression but cannot rescue the *Sycp3* knockout phenotype

Tagging a protein in vivo may interfere with its normal function. In addition, regulation of expression of our transgene differs from that of endogenous SYCP3, which may also influence its degree of functionality. To assess whether the expression of the two SYCP3 fusion proteins interfered with normal progression of meiosis, we assessed overall fertility (Fig. S2a), crossover frequency (Fig. S2b), and persistence of DSBs in late meiotic prophase (Fig. S2c) in males carrying the transgene in addition to one or two wild-type *Sycp3* alleles. None of these parameters were affected. To investigate to what extent the SYCPC and CSYCP proteins were capable of functionally replacing endogenous SYCP3, we analyzed the meiotic phenotype of *Sycp3* $^{-/-}$ male and female mice, in the presence or absence of SYCPC and CSYCP. Prophase substages were determined using the known stage-specific localization pattern of the meiosis-specific cohesin component REC8, which mostly colocalizes with SYCP3 in wild-type spermatocytes and oocytes (Lee et al. 2003). In male *Sycp3* $^{-/-}$, *Sycp3* $^{-/-}$ SYCPC, and *Sycp3* $^{-/-}$ CSYCP spreads, we observed leptotene and zygotene-like stages (Fig. 3a–c), but no cells in which complete synapsis was achieved. In addition, no SYCPC protein was detected in *Sycp3* $^{-/-}$ SYCPC males, upon staining with anti-SYCP3 (Fig. 3b). In contrast, CSYCP could be detected as small patches along the axial elements (Fig. 3c) in 67% of the nuclei analyzed (n = 52 nuclei, 2 mice). When CSYCP was present, it mostly colocalized with REC8 (Fig. 3c,enlargements). Immunodetection of SYCP1 (marker of synapsis) revealed that the degree of synapsis *in Sycp3* $^{-/-}$ CSYCP, *Sycp3* $^{-/-}$, and *Sycp3* $^{-/-}$ SYCPC spermatocytes was similar (Fig. 3d–f). Interestingly, CSYCP accumulation was less apparent on (heterologously) synapsed SC fragments compared to unsynapsed axial elements (Fig. 3f, enlargements). To further evaluate functionality of SYCPC and CSYCP, we analyzed if our tagged SYCP3 proteins would alter the pattern of SYCP2 accumulation on the knockout background, since it has been reported that SYCP2 fails to localize to the axes upon knockout of *Sycp3* (Pelttari et al. 2001), and vice versa (Yang et al. 2006). However, in contrast to the published results, we observed that SYCP2 was still present on the axes of *Sycp3* $^{-/-}$ spermatocytes, and also of *Sycp3* $^{-/-}$ SYCPC and *Sycp3* $^{-/-}$ CSYCP spermatocytes (Fig. S3a,b). Identical results were obtained with two different antibodies targeting SYCP2. Thus, it appears that SYCP2 localization does not depend on SYCP3 expression and is not influenced by the presence of

mCherry-tagged SYCP3. Together, the data indicate that the *Sycp3$^{-/-}$* phenotype is not rescued by either transgene in males.
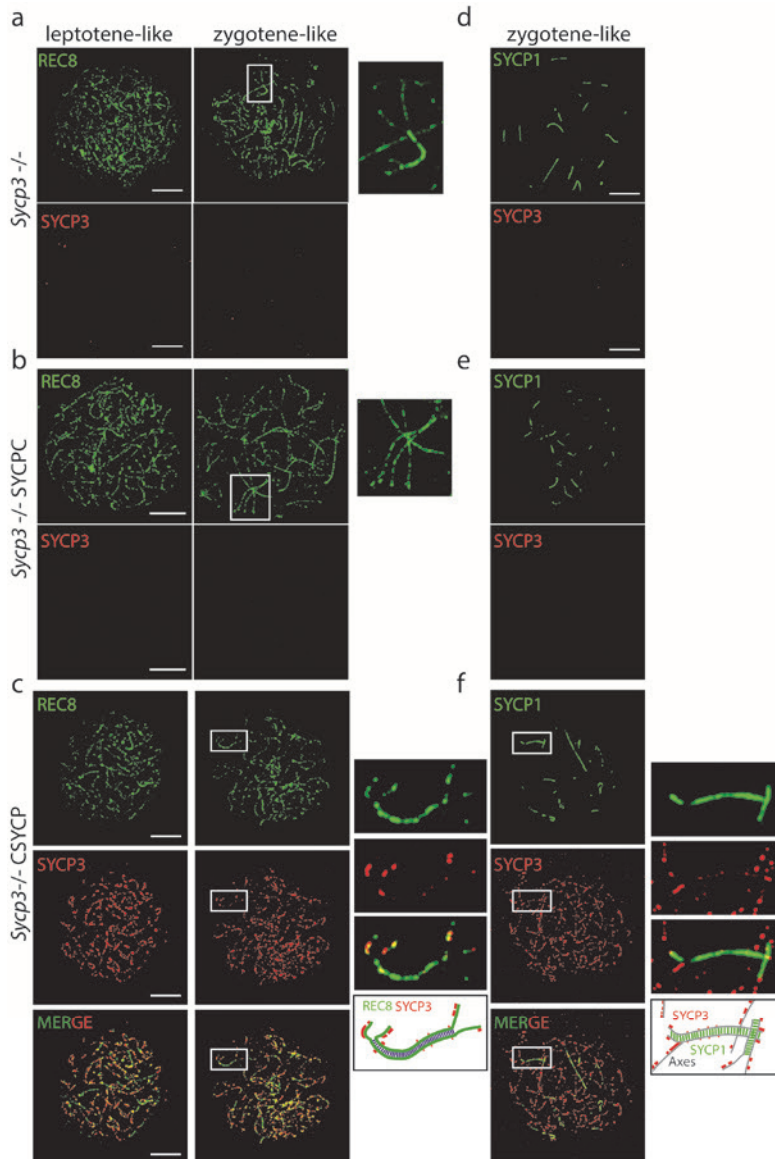
Fig. 3. Expression of SYCPC and CSYCP in *Sycp3$^{-/-}$* spermatocytes. Immunostaining of REC8 (green) and SYCP3 (red) **(a–c)** or SYCP1 (green) and SYCP3 (red) **(d–f)** on *Sycp3$^{-/-}$* **(a, d)**, *Sycp3$^{-/-}$* SYCPC **(b,e)**, and *Sycp3$^{-/-}$* CSYCP **(c, f)** spermatocyte spreads. Enlarged regions (indicated by white boxes) are shown on the right **(a–c, f)**. Below the enlargements in **c** and **f**, a schematic drawing clarifies the merged image. Scale bar 10 μm

We then determined if SYCPC and CSYCP proteins could functionally replace SYCP3 in females. Similar to what was observed in males, SYCPC did not localize to axial elements in the absence of endogenous SYCP3 in E16.5 leptotene and zygotene oocytes (Fig. S4a) but showed focal accumulation on chromatin (not in association with axial elements) at later stages, in late pachytene/diplotene-like oocytes at E18.5 (Fig. 4b). CSYCP already accumulated on the chromatin at leptotene and zygotene in E16.5 $Sycp3^{-/-}$ CSYCP oocytes (Fig. S4b) and clearly displayed axial localization when cells reached a pachytene-like stage (E16.5, Fig. 4a and S4b; E18.5, Fig. 4b). However, the protein covered only part of the axes visualized by anti-REC8. During normal meiotic prophase progression, RAD51 foci numbers (indicative of DSB repair sites) gradually decrease and disappear in diplotene. In contrast, RAD51 foci are retained in $Sycp3^{-/-}$ pachytene and diplotene oocytes (Wang and Hoog 2006). The presence of SYCPC or CSYCP did not reduce the number of persisting RAD51 foci in $Sycp3^{-/-}$ pachytene and diplotene oocytes at E18.5 (Fig. S5a-c). In addition, MLH1 foci numbers (indicative of crossover sites (Kolas and Cohen 2004; Moens et al. 2002)) did not differ between the genotypes (Fig. 4b). Thus, the tagged proteins do not rescue the $Sycp3^{-/-}$ oocyte phenotype either.

Identification of prophase substages in living spermatocytes and oocytes expressing CSYCP

We setup a method to allow time-lapse analyses of oocytes and spermatocytes in cultured embryonic ovaries and tubule fragments, respectively. We used females (E16.5) and males carrying the CSYCP transgene on the wild-type background. The organs or tubule fragments were cultured in a gelatinous protein mixture (basement membrane extract, BME) to maintain three-dimensional structures (see the "Material and methods" section for more details). Stages from leptotene to pachytene were observed in oocytes (Fig. 5a, upper panel) and identified as follows: leptotene nuclei displayed thin axes, and their telomeres were dispersed in the nucleus (Fig. 5a, upper panel, leptotene). Clustering of telomeres in the periphery of the nucleus was observed during the bouquet stage (Fig. 5a, upper panel, zygotene/bouquet). Subsequently, the thickness of the axes varied upon synapsis progression. In pachytene oocytes, all the axes were synapsed (Fig. 5a, upper panel, early pachytene). In the same way, completely synapsed axes were observed in pachytene spermatocytes in $Sycp3^{+/-}$ CSYCP males (Fig. 5a, lower panel). In late pachytene, thicker chromosome ends and brighter XY axes were observed (Fig. 5a, lower panel, late pachytene). Finally, partially desynapsed axes were observed in diplotene spermatocytes (Fig. 5a, lower panel, diplotene). Although we mainly focused on CSYCP for our time-lapse experiments, similar in vivo observations were made in cultured ovaries and testis tubules

from mice expressing SYCPC (see for example Fig. 5b, SYCPC and CSYCP patterns in spermatocytes (imaged at somewhat lower resolution compared to Fig. 5a)).
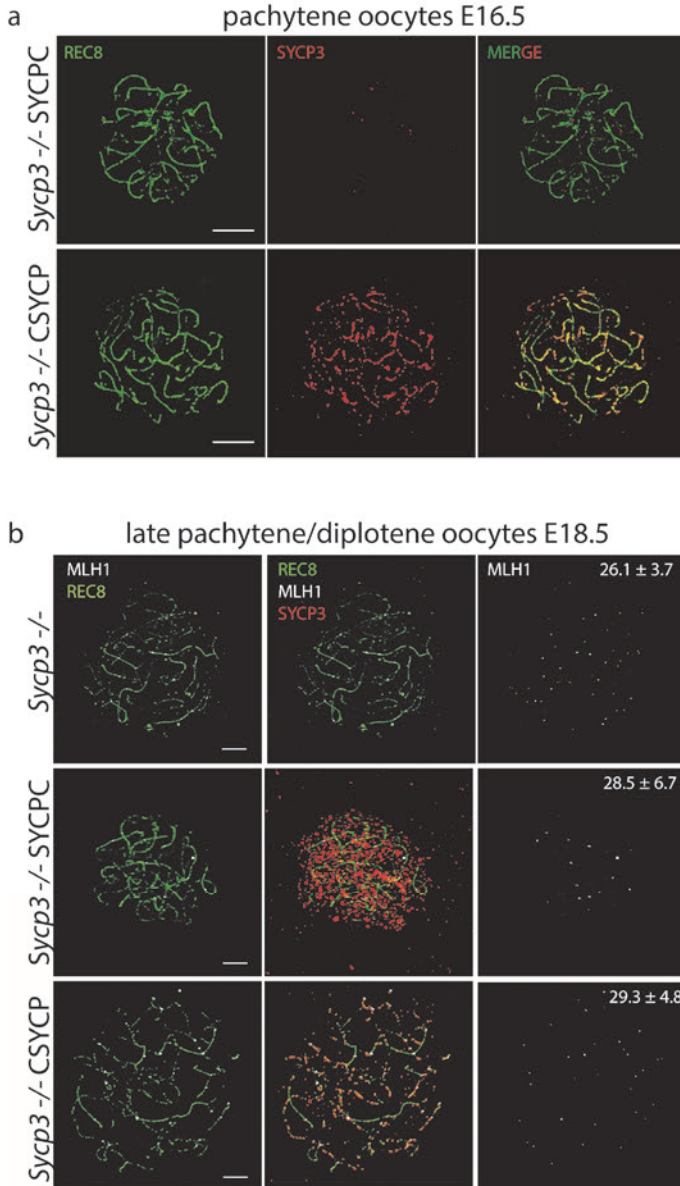

Fig. 4 Expression of SYCPC and CSYCP in Sycp3−/− oocytes. Immunostaining of REC8 (green) and SYCP3 (red) on *Sycp3*$^{-/-}$ SYCPC and *Sycp3*$^{-/-}$ CSYCP pachytene oocyte nuclei at E16.5 **(a)**. Immunostaining of REC8 (green), SYCP3 (red), and MLH1 (white, pseudo-color from infrared) on *Sycp3*$^{-/-}$, *Sycp3*$^{-/-}$ SYCPC, and *Sycp3*$^{-/-}$ CSYCP oocyte nuclei at E18.5 **(b)**. Mean of MLH1 foci ± SD are displayed in the images, n = 7 nuclei for *Sycp3*$^{-/-}$ and *Sycp3*$^{-/-}$CSYCP, n = 6 nuclei for *Sycp3*$^{-/-}$SYCPC.
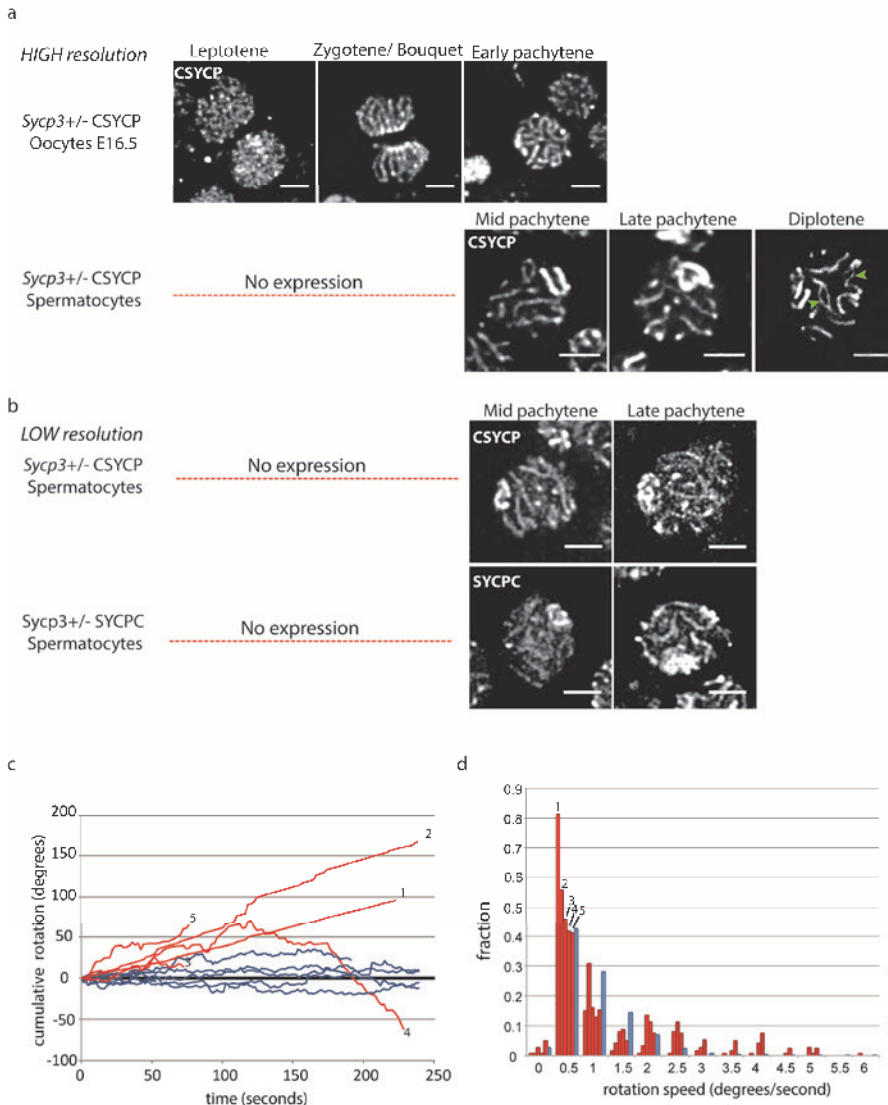
Fig. 5 Live imaging: CSYCP in oocytes and spermatocytes (a) and CSYCP and SYCPC in spermatocytes (b). High-resolution images are depicted in **a** (obtained using the SP5 confocal microscope, except for the diplotene spermatocyte (lower panel), which was generated using the Airy-scan detector). Green arrowheads in the diplotene spermatocyte indicate desynapsed regions. Low-resolution images are shown in **b** (SP5 confocal microscope). The low-resolution images display more background and less clear axes. No expression indicates absence of fusion protein expression during leptotene and zygotene stages in spermatocytes. Scale bar 5 µm. **c** Cumulative rotations of oocytes (red) and spermatocytes (blue) plotted against time (seconds). Clockwise rotations are added as positive values (Y axis), while counterclockwise rotations are negative values. **d** Relative frequencies of rotation speeds of each oocyte (red) and all analyzed spermatocytes (all speeds included, distributions of individual spermatocytes were similar, blue). Same oocyte in **c** and **d** is indicated with the same number. N = 5 oocytes and 6 spermatocytes

Synaptonemal complex movements are rapid during prophase

Movements were highly dynamic during the entire meiotic prophase, in both male and female meiocytes. Two types of movements were observed: rotation of the nucleus itself and movement of the SC inside the nucleus. The rapid movements prompted us to perform an experiment whereby we recorded a single plane with a time lapse of only 1.5–2 s (this short time frame in between recordings precluded imaging multiple planes). To estimate nuclear rotation speed, we then selected single zygotene oocyte and pachytene spermatocyte nuclei that could be traced in time and calculated rotation angles between two consecutive time points as described in the "Materials and methods"section. We then plotted the cumulative rotation angle against time, whereby rotations in clockwise direction were considered as positive angles and counterclockwise rotations as negative angles (Fig. 5c). Interestingly, oocytes rotated for long time periods in a single direction, whereas spermatocytes presented a kind of "wiggling" movement. However, the oocytes displayed more variability in rotational speed frequency distribution (Fig. 5d), in contrast to the spermatocytes, for which the majority of measured rotation speeds were relatively small (71% of speeds between 0.5 and 1.5 degrees/s).

The extensive rotation of the nucleus itself, together with the SC movements, increased complexity to such an extent that we could not follow movement of individual autosomal SCs in oocytes and spermatocytes. The XY axis in pachytene and diplotene spermatocytes was more easily traceable because of its high mCherry signal. Taking the center of the XY axis as reference, we found that it moved with a speed of 24 ± 15 nm/s (n = 10 nuclei). This displacement is the combined result of nuclear rotation and independent movement of the XY within the nucleus.

Meiotic prophase progression, including bouquet formation, is synchronized between oocytes in the same cyst

The fast movements of chromatin and nuclei in early prophase oocytes precluded detailed analyses of the progression of synapsis of individual chromosomes in time. Nevertheless, we could study some other general features in these oocytes. Frequently, we observed two, or sometimes even three, oocytes that moved together as a single unit during the whole recording (from several minutes until a maximum of 10 h in the overnight experiments). The two or three connected oocytes were always found in the same meiotic stage, indicating synchronized progression through meiosis (videos 1, 2 and 3). The telomeres could be distinguished because of their higher fluorescent signal compared to the rest of the axes, allowing us to observe events of clustering/dissolution of telomeres during the zygotene stage. Clustering and dissolution events sometimes followed each other in rapid succession,

even within a few seconds of each other (video 4, bouquet formation can be clearly observed at t = 6 s in the upper nucleus. Dissolution occurs immediately thereafter). These brief clustering events could be unstable or random events, and we expected that a real functional bouquet event would be maintained for a longer time period. For this reason, we also analyzed bouquet progression in our overnight experiments. In order to prevent problems of bleaching during the long experiment, but to be able to follow nuclei despite the high movement frequency, an interval of 10 min was chosen for these time-lapse 3D recordings. The fast movements of the chromosomes and nuclei, together with the low resolution in Z, prevented us from obtaining a high-resolution 3D image of the stacks. Still, we could identify bouquet stages using two criteria: clear linear organization of several telomeres next to each other in one of the planes of the z-stack and the continuation of this situation during at least two consecutive time points. This second criterion was also applied to the non-bouquet situation. The observations on different groups of nuclei (N) (N1 and N4, experiment 1; N2, N3 and N5, experiment 2) are summarized in Fig. 6. The nuclei were ordered according to their degree of meiotic progression, whereby N1 and N2 were at the earliest stages of prophase, followed by N3, N4, and N5, which represented more and more advanced stages of zygotene development.

The duration of bouquet configuration varied among these nuclei, ranging from 20 min (by definition the shortest duration possible) to 2 h and 10 min. The behavior of the nuclei within one cyst also varied. In N2 and N5, we observed bouquet formation in only one of the two nuclei. In N1, one bouquet is dissolved earlier than the other, but in N3 and N4, the nuclei in the cyst behaved synchronously and the bouquet configuration appeared and disappeared approximately at the same time. Some cysts (nucleus B of N3, and nucleus B of N4) exhibited two cycles of telomere clustering, dissolution, and reclustering. Single time point observations of dissolution or clustering could also frequently be observed. As an example, the complete sequence of images for N3 is shown in Fig. S6. Interestingly, when bouquets of two nuclei were present in the same syncytium, they always appeared as if facing each other.

Axis separation starts in interstitial regions and progresses towards the telomeres of the chromosomes

In diplotene spermatocytes, it was possible to follow the process of axis separation (further referred to as desynapsis) for single chromosome pairs in five bivalents. Desynapsis initiated in the interstitial region of the chromosomes and progressed towards the telomeres (Fig. 7a–e, videos 5-9, representing bivalent a–e, respectively).
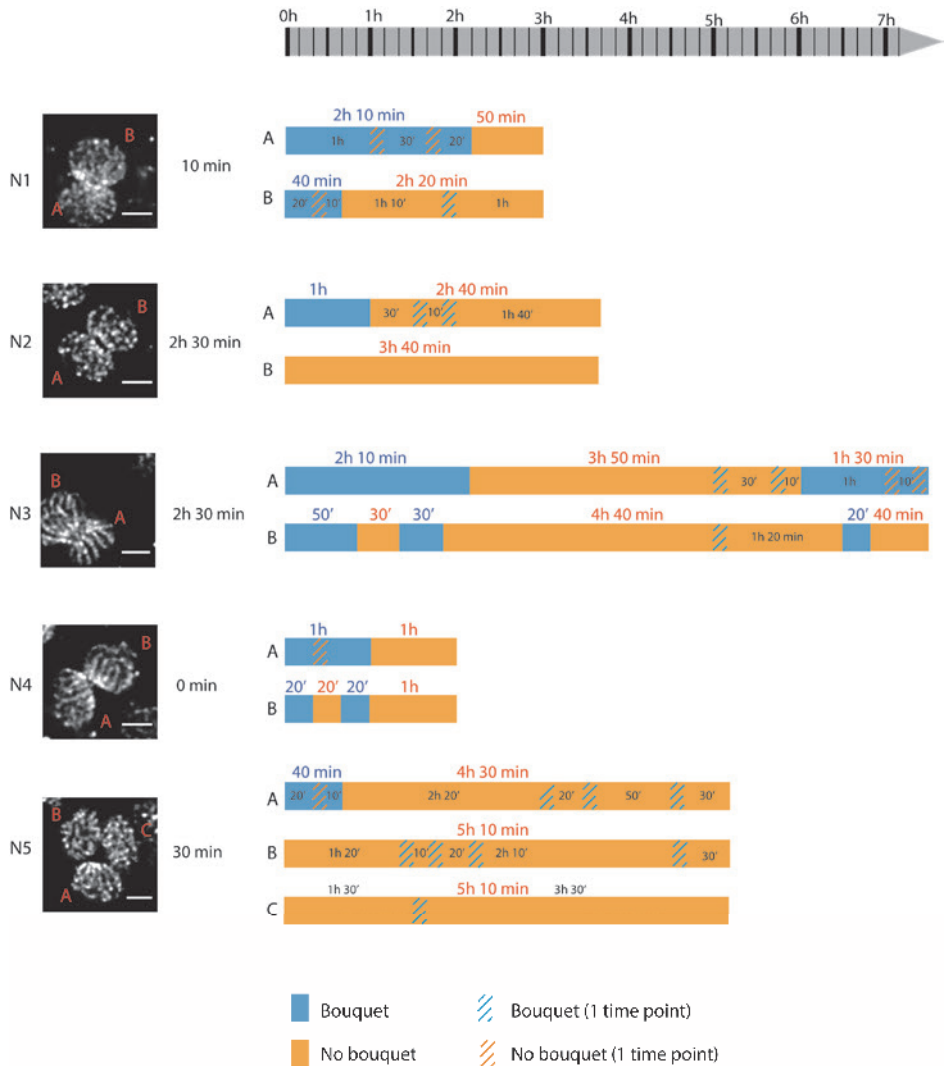
Fig. 6. Bouquet progression in oocytes. Five groups of zygotene nuclei of two different experiments (experiment 1: N1 and N4; experiment 2: N2, N3 and N5) were analyzed. Nuclei are ordered from early to late zygotene, from top to bottom of the figure. An image at t0 is showed for N1-N4. For N5, t5 was chosen, to be able to show the three nuclei in the same plane. Scale bar 5 μm. The amount of time passed up to the first observed bouquet is indicated before each time bar. Blue bars indicate periods during which a bouquet stage was observed; orange bars indicate periods in which no bouquet was observed for longer than 10 min. Orange diagonal lines indicate loss of clear bouquet configuration at only a single time point; blue diagonal bars indicate apparent bouquet organization of chromosomes at only a single time point

In the bivalent shown in Fig. 7a and video 5, desynapsis progressed from the desynapsis initiation point indicated with a green arrowhead, while there was no progression of desynapsis from the area indicated with the red arrowhead, indicating that desynapsis does

not proceed in a similar fashion from each initiation point on a single bivalent. In all nuclei, desynapsis was discontinuous and even resynapsis was observed for two bivalents (Fig. 7f, nucleus b and e, videos 6 and 9). This can also be inferred from the desynapsis length plotted against time for each individual bivalent that was traced (Fig. 7f). In addition, the frequency distribution of the measured speeds visualizes the variability of the velocity (Fig. 7g: desynapsis (positive values) and resynapsis (negative values)). Around 60% of the measured velocities were included in the interval between - 0.5 and 0.5 µm/min, indicating that most of the time period during which the measurements took place was taken up by only minute changes in the degree of axis separation. When visible desynapsis/resynapsis took place, the most frequently measured speed was around 1 µm/min for both situations (11 and 13%, respectively). Faster velocities were rare during resynapsis, but relatively frequent during desynapsis (16% of the values were between 1.5 and 3.5 µm/min). In addition, desynapsis events occurred more frequently (27% of the measured speeds) than resynapsis (16%), explaining the overall increase in desynapsis over time for all analyzed bivalents.

CSYCP and SYCPC can be recruited to the lateral elements of the SC

To determine if CSYCP and SYCPC were stably bound to the lateral elements in spermatocytes, fluorescence recovery after photobleaching (FRAP) was performed. The recovery of at least 10 individual spermatocytes was analyzed per transgenic mouse, expressing either SYCPC or CSYCP in the presence of untagged protein. A single strip that spanned the middle part of the nucleus was photobleached. To reduce technical artifacts due to the high frequency of nucleus and chromosome movement, the nucleus was imaged with a small interval of 0.020 s, and a total time of 1 min, and the XY was never included inside the bleached strip. The average and normalized fluorescence recovery of CSYCP and SYCPC was plotted against time (Fig. 8). A final recovery of 40% was observed within 1 min for both CSYCP and SYCPC in the two experiments.

▶ **Fig. 7. Analyses of axis separation in diplotene spermatocytes**. **(a–e)** Desynapsis progression in five different bivalents of *Sycp3*$^{+/-}$ CSYCP diplotene spermatocytes. CSYCP is visualized in gray. An overview of the whole field of view at T0 is shown in the upper panels (scale bar 5 µm). Below each image, enlargements of the bivalent that desynapses (indicated by a boxed area) are shown at T0 and at T8 or T9 (4 or 4. 5 min later). Scale bar 2 µm. **(f)** Progression of desynapsis in time for each bivalent. Note that bivalent **e** (light green) could not be measured at t = 1 min and t = 2 min, because it moved outside the field of view (see video 9). **(g)** Frequency distribution of the desynapsis (positive)/resynapsis (negative) speeds of the five bivalents. Speeds were measured as described in the "Materials and methods" section. All speeds of all bivalents were analyzed together
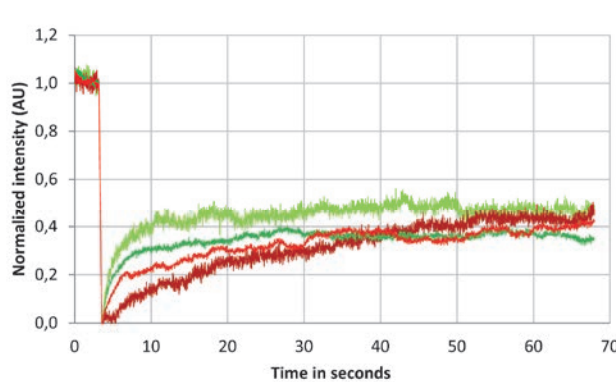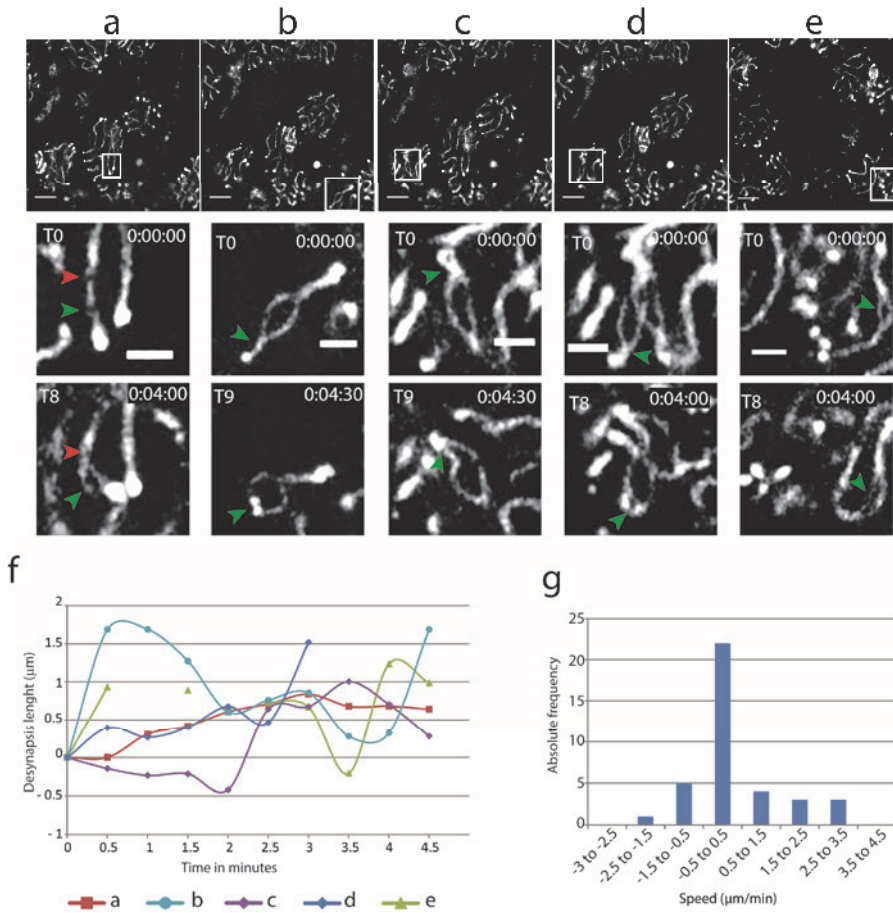
Fig. 8 Fluorescence recovery after photobleaching of SYCPC and CSYCP in autosomes of pachytene spermatocytes. Each line represents the averaged and normalized fluorescent recovery of at least ten spermatocyte nuclei of one mouse testis. The results obtained of two *Sycp3*^{+/−} SYCPC (green) and two *Sycp3*^{+/−} CSYCP (red) males are plotted against time. Total time recording after bleaching 1 min. Time lapse 0.020 s.

DISCUSSION

Both N- and C-terminal fusion of mCherry to SYCP3 affects filament formation

Neither transgene could rescue the aberrant chromosome pairing and frequent asynapsis that is observed upon knockout of *Sycp3* in the male mice (Yuan et al. 2000). However, while no SYCPC was detected on the axes of spermatocytes and oocytes on a *Sycp3* knockout background, CSYCP could form small patches. Recent results from in vitro analyses have indicated that SYCP3 may assemble in tetramers (Syrjanen et al. 2014). Self-interactions among these tetramers (self-assembly), depending on the last six amino acids of the C-terminal of SYCP3, mediate SYCP3 filament formation in vitro. In these in vitro experiments, the N-terminus appeared to be more important for DNA binding (Syrjanen et al. 2014). We assume that tagging the C-terminus of SYCP3 (SYCPC) precludes de novo assembly of the protein on chromosomal axes but still allows it to associate with DNA at random sites in the chromatin, in the absence of endogenous SYCP3. On the other hand, the intact C-terminus of CSYCP allows it to properly localize to the axes where oligomers can assemble with each other. However, because the N-terminal tag interferes with higher order structures and/or because the DNA-binding capacity is affected, only small filaments can be formed. Although we cannot exclude that the added mCherry tags affect overall protein folding, we think that this is unlikely, given the fact that both proteins are recruited properly to the SC on the wild-type background. The aberrant chromatin localization pattern of both SCYCP and SYCPC in the absence of endogenous SYCP3 already explains their lack of functionality. However, in addition, the aberrant timing of transgene activation during meiotic prophase, as revealed on the wildtype background (see below), may also contribute to the lack of rescue of the *Sycp3* knockout phenotype.

SYCPC and CSYCP can accumulate on the axes of the SC and their expression does not interfere with fertility

We observed that, on the wild-type background, both CSYCP and SYCPC localize to the axes of the SC, together with endogenous SYCP3, from pachytene onwards in male mice, and from leptotene onwards in embryonic ovaries at E16.5 or later. The lack of SYCPC and CSYCP accumulation on axial elements in wild-type early spermatocytes was unexpected, since the *Smc1b* promoter fragment that we used has been reported to drive expression from leptotene onwards (Adelfalk et al. 2009). The expression pattern for both transgenes in our mouse models follows the overall pattern of transcriptional activity that has been reported for male meiotic prophase: a general transcriptional inactivation occurs in early stages of male meiosis (leptotene, zygotene and early pachytene), followed be reactivation from mid

pachytene onwards (Kierszenbaum and Tres 1974; Monesi 1964; Page et al. 2012). Thus, it is possible that the transgenes are situated in regions that are subject to this global inactivation mechanism, and therefore can only be transcribed from pachytene onwards in males, when global transcription is reactivated. However, we cannot exclude that the observed expression patterns are inherent to the promoter fragment used. In females, expression of the fusion protein was also observed later than expected, and while endogenous SYCP3 can be detected from E13.5 onwards, the tagged proteins were only expressed from E16.5 onwards, when leptotene oocytes still form. Since the tagged proteins are expressed (and incorporated into the LEs) only from pachytene onwards in males, and FRAP analyses showed a final recovery of 40% for both SYCPC and CSYCP during pachytene, we can conclude that tagged SYCP3 can be recruited to already synapsed axes and exchange there. These data might suggest that a mixed filament of endogenous and tagged SYCP3 forms, whereby endogenous SYCP3 protein also exchanges. However, we cannot exclude that the tagged proteins are loosely associated and do not exchange with endogenous SYCP3.

Remarkably, both $Sycp3^{+/-}$ SYCPC and $Sycp3^{+/-}$ CSYCP spermatocytes presented a stronger mCherry signal on the (largely) unsynapsed XY compared to the synapsed autosomes. Also, the telomeric regions of the chromosomal axes are enriched for the fusion proteins. Using antibody staining, to detect both endogenous and tagged SYCP3, we observed a dimmer signal on the XY due to the single axes, and no enrichment at the telomeres in mid pachytene, similar to the wild-type pattern. This difference might be explained by increased exchange between endogenous SYCP3 and SYCPC/CSYCP in these regions, if this type of exchange occurs. In this situation, possible differences in the turnover of tagged SYCP3 and endogenous SYCP3 would be relevant. As pachytene progresses, the relative amount of tagged SYCP3 compared to endogenous SYCP3 may increase, allowing an increase in the amount of tagged protein in regions that somehow are exchanging more SYCP3. In the absence of exchange of tagged SYCP3 with endogenous SYCP3, the data can also be explained by the presence of more binding sites for the fusion protein, in the unsynapsed XY and telomeric regions, compared to the rest of the SC, in combination with an overall (much) lower expression of the fusion protein compared to endogenous protein, masking this effect in the immunostainings. The extra accumulation of SYCPC and CSYCP on the axial/lateral elements of the XY pair adds another interesting feature to the structural properties the XY pair, in addition to the described relatively short chromatin loops and long lateral elements of the pseudoautosomal region of the XY pair (Kauppi et al. 2011), which is the part that actually displays stable synapsis.

Wild-type males and females expressing either transgene displayed normal progression through meiotic prophase, and overall fertility was not affected. In addition, we observed no detrimental effects of the long-term and short imaging experiments, since the overall morphology of the nuclei and the SC had not changed, and cellular movements kept occurring within the ovaries and tubule fragments that were cultured for short or long (overnight) periods. In the tubule cultures, contractions of the tubules also still occurred after overnight imaging. Thus, despite the fact that the proteins cannot fully replace endogenous SYCP3, our system provides a tool to study meiosis in living cells, in the natural context of the seminiferous tubule or the embryonic ovary.

Nuclear rotations and chromosome movements

We have observed two types of movements inside the cultured seminiferous tubules and the ovaries of our transgenic mouse models: the rotation of the nucleus itself and movement of the SC inside the nucleus. The analysis of the movement of the SC inside the nucleus revealed an average speed of the SC of the XY of 24 ± 15 nm/s. Other groups measured telomere velocity in mouse pachytene cells and observed 130 nm/s (Shibuya et al. 2014) or 36 ± 14.8 nm/s (Lee et al. 2015). The latter result nicely fits our data; a somewhat faster movement of the telomeres compared to the rest of the chromosome is to be expected, since the movement of the telomeres along the nuclear envelope may displace also the rest of the chromosome, but to a lesser extent. Related to this, in maize pachytene cells, it has also been observed that chromosome ends travel faster than interstitial regions of the same chromosomes (Sheehan and Pawlowski 2009). Whether the chromosome movements that we observed in late meiotic prophase have any function is unknown. However, it seems to be an evolutionary conserved feature, since it has also been described for budding yeast, where telomere speed was similar in paired and non-paired configurations (Scherthan et al. 2007; Conrad et al. 2008; Koszul et al. 2008). For budding yeast, it has been suggested that chromosome movements after chromosome pairing could be required to help to prevent topological entanglements or to eliminate them if they persist up to the pachytene stage (Koszul et al. 2008). Alternatively, late telomere movements could have a role in late steps of recombination like Holliday junction formation and resolution in pachytene (Scherthan et al. 2007).

Existence of nuclear rotation was also mentioned in previous studies in rat spermatocytes (Parvinen and Soderstrom 1976), but not further characterized. We have analyzed the rotation of the nuclei in zygotene oocytes and pachytene spermatocytes, and we have observed longer time periods of rotation in a single direction in oocytes in early meiotic prophase, compared to pachytene spermatocytes. This observation is consistent with the

fact that rotational movements accompany chromosome pairing, and the idea that perhaps concerted movements of telomeres to the same site on the nuclear envelope induce rotations of the entire nucleus (Scherthan et al. 1996). Indeed, the function of the rotational movements in promoting pairing seems to be conserved in evolution. However, the pattern of these movements appears to vary among organisms. In maize meiocytes, oscillations back and forth are the most common type of nuclear rotational movement, although rotations in a single direction (small and large) have also been observed (Sheehan and Pawlowski 2009). In fission yeast, oscillations of the entire nucleus between the two poles (horsetail movements) start just after bouquet formation. The impairment of these movements results in reduced pairing of the homologous chromosomes (Yamamoto and Hiraoka 2001; Saito et al. 2005; Chacon et al. 2016). Interestingly, horsetail movements continue after pairing has been achieved. Their inhibition after pairing produces mis-segregation of the chromosomes during the first meiotic division. Such late oscillations may prevent prolonged associations of the homologous chromosomes once pairing has been achieved, which may lead to irresolvable recombination intermediates and segregation failure (Chacon et al. 2016). The "wiggling" of late spermatocyte nuclei could assist in a similar process, also in combination with the movement of the chromosomes.

The bouquet stage in mouse oocytes is dynamic

It is known that primordial germ cells form cysts connected by intercellular bridges in the ovaries of E11.5 to E17.5 mice (Pepling 2006; Pepling and Spradling 1998). Accordingly, we have observed that E16.5 oocytes frequently formed groups of two, and occasionally three, nuclei that localized in a single cytoplasm. Bouquet formation within such syncytia was frequently synchronized and the opposite localization of the telomere clusters gave such nuclei a "kissing" appearance. The intercellular bridges could be involved in this synchronization, since bundles of microtubules have been shown to traverse intercellular bridges (Pepling and Spradling 1998). These microtubules are implicated in cellular transport among cells in a cyst (Pepling and Spradling 1998), but they could also play an important role in the synchronization of bouquet formation and connect the cytoplasmic components of the proteins that mediate the clustering of telomeres in association with the nuclear membrane.

In female mice, bouquet formation has been reported to peak at mid to late zygotene and to persist in a substantial proportion of pachytene oocytes (Tankimanova et al. 2004). In accordance with this observation on fixed samples, the living nuclei in which we observed a bouquet were most often in a mid-late zygotene stage. Because of the limitations of our imaging system, we cannot exclude that we underestimate the duration of the bouquet

stage. However, what is clear is that the bouquet stage is highly dynamic. During the recordings, some nuclei exhibited two cycles of telomere clustering, dissolution, and reclustering. In some nuclei within a syncytium, the bouquet of one nucleus dissolved while in the other it remained, followed by reclustering of the telomeres in the nucleus that had previously lost its bouquet configuration. In other syncytia, clustering and dissolution cycles occurred more synchronously and sometimes a dissolution/reclustering cycle could be very rapid (around 20 min). Maybe some events of dissolution occur when not all the chromosomes are synapsed or when (partial) nonhomologous associations are present that activate a feedback mechanism that triggers reformation of the bouquet, to allow complete synapsis of the remaining unsynapsed axes. Alternatively, or in addition, telomere declustering and reclustering events could be important to solve whole chromosome entanglements, known as "interlocks" that are present during synapsis but absent by the end of pachytene (and therefore resolved) (Zickler and Kleckner 2015; Zickler and Kleckner 2016).

Desynapsis

Finally, we were also able to follow axis separation, representing desynapsis in male diplotene spermatocytes. In these cases, we observed initiation of desynapsis in the interstitial region of the chromosomes and progression of desynapsis towards the telomeres. Since we could only follow five bivalents, we cannot exclude that desynapsis events might also start from the telomeres. The speed of desynapsis varied; we observed discontinuous progression, and even brief events of resynapsis, indicating that desynapsis occurs in bursts and may also halt for a certain time period. Given the overall normal development of spermatocytes even during overnight imaging experiments, and the observation that multiple desynapsis or resynapsis proceedings could be traced for a single bivalent, we infer that our settings do not interfere with overall chromosome behavior during meiotic prophase. If we estimate the total length of the SC to be around 200 μm (Baarends et al. 2003), it might be expected that desynapsis would not take much longer than 200 min, since multiple bivalents are usually observed to desynapse simultaneously. However, analyses of fixed samples has indicated that in mouse, diplotene lasts around 3 days (Oud et al. 1979). Thus, it can be concluded that the duration of desynapsis is limited by factors other than the actual constraints of the desynapsis process itself.

In summary, we have used the mCherry SYCP3 and SYCP3 mCherry male and female mice to study synaptonemal complex and chromosome dynamics in vivo, for the first time in the natural context of the seminiferous tubule or the ovary, during an imaging time frame of several hours. We have focused on bouquet formation, nuclear rotation, and desynapsis

events. In addition to providing new insights in the dynamics of chromosome behavior in wild-type meiocytes, our method can be used as a tool to study alterations in the chromosome dynamics of meiocytes in gonads of infertile mouse models.

Materials and methods

Ethics statement

All animal experiments were approved by the local animal experiments committee DEC Consult and animals were maintained under supervision of the Animal Welfare Officer.

Generation of SYCPC and CSYCP mice

In order to study the dynamics of the SC, we have generated transgenic mice expressing N- or C- terminal fusions of SYCP3 with the mCherry protein. To this end, we first cloned the coding region of the mouse *Sycp3* gene into the mCherry C1 or N1 vector. The mouse *Sycp3* coding region was amplified using forward primer 5' CCGCTCGAGTGCTTCGAGGGTGTG3' and reversed primer 5'CGCGGATCCAGACTCATCAGAATAACATG 3' to generate CSYCP and forward primer CCGCTCGAGTCAGATGCTTCGAGGGTG and reversed primer 5'CGCGGATCCCAGAATAACATGGATTGAAGAG 3' to generate SYCPC. Both fragments were cut with XhoI and BamH1 and cloned into the multiple cloning site of the C1 and N1 vector, respectively. Subsequently, we amplified a 295 bp fragment of the *Smc1β*-promoter previously described to drive expression from leptotene onwards (Adelfalk et al., 2009) using PCR primers SMC1bFo r : 5' CCGCTATTAATCACGGCAAGAAAAGCCC 3' and SMC1bRev: 5' CTAGCTAGCGACCGGTGCCTCAGCC 3' followed by digestion of the fragment with AseI and NheI and cloning into the two vectors containing the SYCPC and CSYCP constructs by replacing the CMV promoter in these plasmids. Finally, the constructs were digested with EciI, purified and injected in the pronuclei of FVB zygotes using standard methods. Transgenic mice were tested for expression of the transgenes in the testes, and the SYCP3 open reading frame was sequenced to exclude point mutations. Mice carrying the transgenes could be bred to homozygosity without affecting overall health. Animals were genotyped using standard DNA isolation (DNA isolated from tail or toe tips) and PCR procedures using the following primer sets: forward primer 5'CACCATCGTGGAACAGTACG3' and reverse primer 5'GGGAGGTGTGGGAGGTTTT3' for CSYCP and forward primer 5'GCAAGGGCGAGGAGGATAAC 3' and reverse primer 5'TTGCCGATTTCGGCCTATTG 3' for SYCPC.

Mice

Sycp3 knockout mice were described previously (Yuan et al. 2000) and crossed with SYCPC or CSYCP mice. Testes were isolated from immature and adult male mice. To obtain ovaries containing oocytes at different stages of meiotic prophase, $Sycp3^{+/-}$ (or occasionally $Sycp3^{-/-}$ in case of females) with or without the CSYCP or SYCPC transgene were mated and ovaries were isolated from embryos at E.15.5, 16.5, or E18.5. (the day at which a plug was observed was considered as day 0.5 of embryonic development, E0.5). Meiotic progression in females differs in terms of timing and stage appearance compared to the male. The more or less synchronous development of oocytes in the embryonic ovary allowed us to predict in which stage the majority of the cells would be depending on the embryonic day of development. In this way, the majority of the oocytes will be at leptotene or zygotene at E15.5 and E16.5 and at pachytene or diplotene at E18.5 (Ashley 2004; Dietrich and Mulder 1983).

Western blotting

Testes were isolated from SYCPC and CSYCP mice of different ages (SYCPC 11, 16, and 19 days old, CSYCP 12, 15, and 22 days old). Total testis protein isolation and Western blotting of 12% SDS-PAGE gels were performed as described previously (Mulugeta Achame et al. 2010). Rabbit polyclonal anti-SYCP3 (Lammers et al. 1994) was diluted 1:5000. Peroxidase-labeled secondary antibody (Sigma) was used, and antigen-antibody complexes were detected using a chemoluminescence kit (Du Pont/NEN,Bad Homburg, Germany) according to the instructions provided by the manufacturer.

Immunocytochemistry

Spread nuclei of spermatocytes and oocytes were prepared from isolated gonads as described by Peters et al. (1997) and stored at - 80C. Thawed slides were washed in PBS (3 × 10 min), and non-specific sites were blocked with 0.5% w/v BSA and 0.5% w/v milk powder in PBS. Primary antibodies were diluted in 10% w/v BSA in PBS, and incubations were performed overnight at room temperature in a humid chamber. Subsequently, slides were washed (3 × 10 min) in PBS, blocked in 10% v/v normal goat serum (Sigma) in blocking buffer (supernatant of 5% w/v milk powder in PBS centrifuged at 14,000 rpm for 10 min), and incubated with secondary antibodies in 10% normal goat serum in blocking buffer at room temperature for 2 h. Finally, slides were washed (3 × 10 min) in PBS and embedded in Prolong Gold with DAPI (Invitrogen). For stainings involving two primary antibodies generated in the same species, the immunostaining was performed sequentially. After adding one of the two primary antibodies, and its detection on the next day with a secondary antibody, the other primary antibody was added and detected the day thereafter

with a secondary antibody of a different color. Note that the protein detected by the antibody added on the first day would be visible in the colors of each of the two secondary antibodies, while the protein detected by the primary antibody that was added on the second day would be visible only in the color of the last secondary antibody.

Primary antibodies: mouse monoclonal anti-SYCP3 (ABCAM:ab97672) at 1:200, rabbit polyclonal anti-SYCP3 (Lammers et al. 1994) at 1:10000, guinea pig polyclonal anti- SYCP2 (Yang et al. 2006) at 1:100, rabbit polyclonal anti- SYCP2 (Offenberg et al. 1998) at 1:400, rabbit polyclonal anti-RAD51 (Essers et al. 2002) at 1:500, rabbit polyclonal anti-REC8 (N-terminus, affinity purified) at 1:50 (Eijpe et al. 2003), rabbit polyclonal anti-SYCP1 (Meuwissen et al. 1992) at 1:5000, mouse monoclonal anti-MLH1 (cat. 551,091, BD Pharmigen) at 1:25. For secondary antibodies, we used a goat anti-rabbit alexa 488 IgG, goat anti-rabbit alexa 633 IgG, goat anti-mouse alexa 488, and goat anti-mouse alexa 546 IgG, all at 1:500 dilution.

Fluorescent images were obtained using a fluorescence microscope (Axioplan 2; Carl Zeiss) equipped with a digital camera (Coolsnap-Pro; Photometrics). Confocal images were taken using a Zeiss LSM700 confocal, equipped with a digital camera (Axiocam MRm Rev.3 1388X1040 monochrome camera for epi-fluorescence). Foci were counted using ImageJ software (FIJI); we counted foci using the find maxima function and set the noise tolerance manually.

Staging of spermatocytes and oocytes

Staging of wild-type spermatocytes and oocytes was based on the pattern of the SYCP3 or REC8 (*Sycp3*$^{-/-}$ spermatocytes and oocytes). In addition, RAD51 was used in order to distinguish between zygotene (250–100 foci, as the number of foci decreases as synapsis progresses) and diplotene oocytes (< 10 foci (Moens et al. 1997). Alternatively, the presence of MLH1 foci was used as marker of pachytene and diplotene oocytes.

Isolation of testis tubules and embryonic ovaries for culture

Adult mouse testes from transgenic mice carrying the CSYCP or SYCPC transgene were isolated and dissected following a previously described protocol (van der Laan et al. 2004) with some modifications. Decapsulated testes were immersed in 20 ml Dulbecco's phosphate-buffered saline (Invitrogen, Carlsbad, CA, USA) containing 1.1 mM Ca^{2+}, 0.52 mM Mg^{2+}, 6 mM DL-lactic acid, and 5.6 mM glucose (PBS^{+}), in the presence of collagenase (1 µg/µl, type 1 Worthington) and hyaluronidase (0.5 µg/µl, H3884 Sigma) in a 50-ml falcon tube. The testes were then incubated in a water bath at 33 °C and shaken at 90 cycles/min, amplitude of 20 mm, for 5 min. The incubation was stopped when the enzymatic digestion

had resulted in dissociation of the interstitial tissue and disengagement of testis tubules. Tubules were separated from interstitial cells by washing in PBS$^+$ twice. Next, tubules were placed in a 30-mm BSA-coated Petri dish, where the tubules were separated from each other using dissection tweezers (Nr. 5). After cutting small fragments, these were carefully transferred to a 15-mm BSA-coated Petri dish. After collecting a pool of fragments, we used dissection tweezers (Nr. 5) to place 4–5 of these fragments into a 50-µl drop containing 1:4 v/v (RPMI + 10% KRS culture medium)/Cultrex® Basement Membrane Extract (BME), type 2; Trevigen pipetted onto a 24-mm laminin-coated cover slip in each live cell chamber. The chambers with the tubules were centrifuged 5 min at 500 rpm and 4 °C. Next, the chambers were incubated for 30 min at 33 °C to allow the BME to jellify. Finally, 2 ml of RPMI + 10% KRS culture medium was added. For embryonic ovary culture, pregnant females were killed at different time points after timed matings. Embryos were collected and ovaries were isolated and placed temporarily in PBS$^+$ (without DL-lactic acid). Once all the ovaries had been collected, they were transferred to the live cell chamber, prepared as described for the tubules. The rest of the protocol was also identical, with the exception of the medium (αMEM, Gibco) and the temperature (37 °C instead of 33).

Confocal and time-lapse microscopy

For the time-lapse imaging, we used a Leica SP5 confocal microscope. To specifically follow desynapsis in diplotene spermatocytes, we used a Zeiss LSM880 microscope with airy-scan detector. Chamber and objective (40 × 1.25 NA, oil immersion) were kept at 33 °C for seminiferous tubules and 37 °C for ovaries. The chambers with the tubules or ovaries were also maintained at 5% CO2. Red fluorescent images were obtained after excitation with a 594-nm laser and detection through a 600–680 band pass filter.

For the FRAP analysis, we bleached a single strip of 16 pixels high (pixel size 0.11 µm XY) that spanned the middle part of the nucleus, for five iterations at high laser intensity (100% of the 594 and 561 nm laser). The recovery of fluorescence in the strips was monitored during 1 min at intervals of 0.020 s at 6–12% of the laser intensity applied for bleaching (12% for the mice carrying the SYCPC transgene and 6% for the mouse carrying the CSYCP transgene, due to its higher signal intensity).Samples of two mice, one carrying CSYCP and the other carrying SYCPC, were processed together and analyzed the same day. Another set of two mice carrying each variant of the transgene was used to confirm the results.

For the overnight time-lapse experiments, we selected 5–10 different positions along each tubule or ovary, and for each position, a stack of approximately 30 slices of 1 µm was made. The lapse between images was 10 min. For the short videos time-lapse experiments, total time and lapse varied between experiments.

Analysis of the rotation, chromosome movements, and axis separation

Time-lapse videos of one plane per time point and a time lapse of 1.5–2 s were recorded for this analysis. For the rotation in X-Y analysis, single oocytes or spermatocytes were selected. The rotation angle of the time point t + 1 with respect to t was calculated. For this, the nucleus at t + 1 was translated (X,Y) and rotated until the correlation between t and t + 1 was the highest. From the rotation angle, we calculated the rotation speeds (degrees/s).

To measure the speed of the XY chromosome in pachytene spermatocytes, we measured the distance from the center of the XY at time t + 1 to the center at time t and divided this value by the time in seconds.

To measure the speed of desynapsis, the length of the remaining synapsed (bivalent b, d) or desynapsed (bivalent a,c, e) fragment was measured at each analyzed time point, in one single XY plane. The length difference between the two time points was measured and used to calculate the speed. Speeds were determined for each 30-s interval during the time period for which the bivalents could be traced.

Compliance with ethical standards:

Conflict of interest. The authors declare that they have no conflict of interest.

Ethical approval. All applicable international, national, and/or institutional guidelines for the care and use of animals were followed. All procedures performed in studies involving animals were in accordance with the ethical standards of the institution or practice at which the studies were conducted.

REFERENCES

Adelfalk C et al. (2009) Cohesin SMC1beta protects telomeres in meiocytes J Cell Biol 187:185-199 doi:10.1083/jcb.200808016

Alsheimer M, Baier A, Schramm S, Schutz W, Benavente R (2010) Synaptonemal complex protein SYCP3 exists in two isoforms showing different conservation in mammalian evolution Cytogenet Genome Res 128:162-168 doi:10.1159/000303341

Ashley T (2004) The mouse "tool box" for meiotic studies Cytogenet Genome Res 105:166-171 doi:10.1159/000078186

Baarends WM et al. (2003) Loss of HR6B ubiquitin-conjugating activity results in damaged synaptonemal complex structure and increased crossing-over frequency during the male meiotic prophase Mol Cell Biol 23:1151-1162

Baudat F, Manova K, Yuen JP, Jasin M, Keeney S (2000) Chromosome synapsis defects and sexually dimorphic meiotic progression in mice lacking spo11 Mol Cell 6:989-998

Boateng KA, Bellani MA, Gregoretti IV, Pratto F, Camerini-Otero RD (2013) Homologous pairing preceding SPO11-mediated double-strand breaks in mice Developmental cell 24:196-205 doi:10.1016/j.devcel.2012.12.002

Chacon MR, Delivani P, Tolic IM (2016) Meiotic Nuclear Oscillations Are Necessary to Avoid Excessive Chromosome Associations Cell Rep 17:1632-1645 doi:10.1016/j.celrep.2016.10.014

Conrad MN et al. (2008) Rapid telomere movement in meiotic prophase is promoted by NDJ1, MPS3, and CSM4 and is modulated by recombination Cell 133:1175-1187

Costa Y et al. (2005) Two novel proteins recruited by synaptonemal complex protein 1 (SYCP1) are at the centre of meiosis J Cell Sci 118:2755-2762 doi:10.1242/jcs.02402

Dietrich AJ, Mulder RJ (1983) A light- and electron microscopic analysis of meiotic prophase in female mice Chromosoma 88:377-385

Dobson MJ, Pearlman RE, Karaiskakis A, Spyropoulos B, Moens PB (1994) Synaptonemal complex proteins: occurrence, epitope mapping and chromosome disjunction Journal of cell science 107 (Pt 10):2749-2760

Eijpe M, Offenberg H, Jessberger R, Revenkova E, Heyting C (2003) Meiotic cohesin REC8 marks the axial elements of rat synaptonemal complexes before cohesins SMC1beta and SMC3 J Cell Biol 160:657-670 doi:10.1083/jcb.200212080

Essers J et al. (2002) Analysis of mouse Rad54 expression and its implications for homologous recombination DNA Repair (Amst) 1:779-793 doi:S1568786402001106

Hamer G, Gell K, Kouznetsova A, Novak I, Benavente R, Hoog C (2006) Characterization of a novel meiosis-specific protein within the central element of the synaptonemal complex J Cell Sci 119:4025-4032 doi:10.1242/jcs.03182

Hamer G, Novak I, Kouznetsova A, Hoog C (2008) Disruption of pairing and synapsis of chromosomes causes stage-specific apoptosis

of male meiotic cells Theriogenology 69:333-339 doi:10.1016/j.theriogenology.2007.09.029

Heyting C (1996) Synaptonemal complexes: structure and function Curr Opin Cell Biol 8:389-396

Kauppi L, Barchi M, Baudat F, Romanienko PJ, Keeney S, Jasin M (2011) Distinct properties of the XY pseudoautosomal region crucial for male meiosis Science 331:916-920 doi:10.1126/science.1195774

Kierszenbaum AL, Tres LL (1974) Nucleolar and perichromosomal RNA synthesis during meiotic prophase in the mouse testis J Cell Biol 60:39-53

Kolas NK, Cohen PE (2004) Novel and diverse functions of the DNA mismatch repair family in mammalian meiosis and recombination Cytogenet Genome Res 107:216-231 doi:10.1159/000080600

Koszul R, Kim KP, Prentiss M, Kleckner N, Kameoka S (2008) Actin-mediated motion of meiotic chromosomes Cell 133:1188-1201 doi:10.1016/j.cell.2008.04.050

Lammers JH, Offenberg HH, van Aalderen M, Vink AC, Dietrich AJ, Heyting C (1994) The gene encoding a major component of the lateral elements of synaptonemal complexes of the rat is related to X-linked lymphocyte-regulated genes Mol Cell Biol 14:1137-1146

Lee CY, Conrad MN, Dresser ME (2012) Meiotic chromosome pairing is promoted by telomere-led chromosome movements independent of bouquet formation PLoS genetics 8:e1002730 doi:10.1371/journal.pgen.1002730

Lee CY et al. (2015) Mechanism and regulation of rapid telomere prophase movements in mouse meiotic chromosomes Cell Rep 11:551-563 doi:10.1016/j.celrep.2015.03.045

Lee J, Iwai T, Yokota T, Yamashita M (2003) Temporally and spatially selective loss of Rec8 protein from meiotic chromosomes during mammalian meiosis J Cell Sci 116:2781-2790 doi:10.1242/jcs.00495

Meuwissen RL, Offenberg HH, Dietrich AJ, Riesewijk A, van Iersel M, Heyting C (1992) A coiled-coil related protein specific for synapsed regions of meiotic prophase chromosomes EMBO J 11:5091-5100

Moens PB, Kolas NK, Tarsounas M, Marcon E, Cohen PE, Spyropoulos B (2002) The time course and chromosomal localization of recombination-related proteins at meiosis in the mouse are compatible with models that can resolve the early DNA-DNA interactions without reciprocal recombination J Cell Sci 115:1611-1622

Moens PB, Chen DJ, Shen Z, Kolas N, Tarsounas M, Heng HH, Spyropoulos B (1997) Rad51 immunocytology in rat and mouse spermatocytes and oocytes Chromosoma 106:207-215

Monesi V (1964) Ribonucleic Acid Synthesis during Mitosis and Meiosis in the Mouse Testis J Cell Biol 22:521-532

Morelli MA, Werling U, Edelmann W, Roberson MS, Cohen PE (2008) Analysis of meiotic prophase I in live mouse spermatocytes Chromosome Res 16:743-760 doi:10.1007/s10577-008-1224-8

Mulugeta Achame E et al. (2010) The ubiquitin-conjugating enzyme HR6B is required for maintenance of X chromosome silencing in mouse spermatocytes and spermatids BMC Genomics 11:367

Offenberg HH, Schalk JA, Meuwissen RL, van Aalderen M, Kester HA, Dietrich AJ, Heyting C (1998) SCP2: a major protein component of the axial elements of synaptonemal complexes of the rat Nucleic Acids Res 26:2572-2579

Oud JL, de Jong JH, de Rooij DG (1979) A sequential analysis of meiosis in the male mouse using a restricted spermatocyte population obtained by a hydroxyurea/triaziquone treatment Chromosoma 71:237-248

Page J et al. (2012) Inactivation or non-reactivation: what accounts better for the silence of sex chromosomes during mammalian male meiosis? Chromosoma 121:307-326 doi:10.1007/s00412-012-0364-y

Page SL, Hawley RS (2004) The genetics and molecular biology of the synaptonemal complex Annu Rev Cell Dev Biol 20:525-558 doi:10.1146/annurev.cellbio.19.111301.155141

Parvinen M, Soderstrom KO (1976) Chromosome rotation and formation of synapsis Nature 260:534-535

Pelttari J et al. (2001) A meiotic chromosomal core consisting of cohesin complex proteins recruits DNA recombination proteins and promotes synapsis in the absence of an axial element in mammalian meiotic cells Mol Cell

Biol 21:5667-5677 doi:10.1128/MCB.21.16.5667-5677.2001

Pepling ME (2006) From primordial germ cell to primordial follicle: mammalian female germ cell development Genesis 44:622-632 doi:10.1002/dvg.20258

Pepling ME, Spradling AC (1998) Female mouse germ cells form synchronously dividing cysts Development 125:3323-3328

Roest HP et al. (1996) Inactivation of the HR6B ubiquitin-conjugating DNA repair enzyme in mice causes male sterility associated with chromatin modification Cell 86:799-810

Revenkova E, Eijpe M, Heyting C, Gross B, Jessberger R (2001) Novel meiosis-specific isoform of mammalian SMC1 Mol Cell Biol 21:6984-6998

Robert T, Nore A, Brun C, Maffre C, Crimi B, Bourbon HM, de Massy B (2016) The TopoVIB-Like protein family is required for meiotic DNA double-strand break formation Science 351:943-949 doi:10.1126/science.aad5309

Rog O, Dernburg AF (2015) Direct Visualization Reveals Kinetics of Meiotic Chromosome Synapsis Cell Rep doi:10.1016/j.celrep.2015.02.032

Romanienko PJ, Camerini-Otero RD (2000) The mouse spo11 gene is required for meiotic chromosome synapsis Mol Cell 6:975-987

Royo H et al. (2010) Evidence that meiotic sex chromosome inactivation is essential for male fertility Curr Biol 20:2117-2123 doi: 10.1016/j.cub.2010.11.010

Saito TT, Tougan T, Okuzaki D, Kasama T, Nojima H (2005) Mcp6, a meiosis-specific

coiled-coil protein of Schizosaccharomyces pombe, localizes to the spindle pole body and is required for horsetail movement and recombination J Cell Sci 118:447-459 doi:10.1242/jcs.01629

Salonen K, Paranko J, Parvinen M (1982) A colcemid-sensitive mechanism involved in regulation of chromosome movements during meiotic pairing Chromosoma 85:611-618

Scherthan H, Wang H, Adelfalk C, White EJ, Cowan C, Cande WZ, Kaback DB (2007) Chromosome mobility during meiotic prophase in Saccharomyces cerevisiae Proc Natl Acad Sci U S A 104:16934-16939

Scherthan H (2007) Telomere attachment and clustering during meiosis Cell Mol Life Sci 64:117-124 doi:10.1007/s00018-006-6463-2

Scherthan H, Weich S, Schwegler H, Heyting C, Harle M, Cremer T (1996) Centromere and telomere movements during early meiotic prophase of mouse and man are associated with the onset of chromosome pairing J Cell Biol 134:1109-1125

Schramm S et al. (2011) A novel mouse synaptonemal complex protein is essential for loading of central element proteins, recombination, and fertility PLoS Genet 7:e1002088
doi:10.1371/journal.pgen.1002088

Sheehan MJ, Pawlowski WP (2009) Live imaging of rapid chromosome movements in meiotic prophase I in maize Proc Natl Acad Sci U S A 106:20989-20994
doi:10.1073/pnas.0906498106

Shibuya H, Morimoto A, Watanabe Y (2014) The dissection of meiotic chromosome movement in mice using an in vivo electroporation technique PLoS Genet 10:e1004821 doi:10.1371/journal.pgen.1004821

Stewart CL, Burke B (2014) The missing LINC: a mammalian KASH-domain protein coupling meiotic chromosomes to the cytoskeleton Nucleus 5:3-10 doi:10.4161/nucl.27819

Syrjanen JL, Pellegrini L, Davies OR (2014) A molecular model for the role of SYCP3 in meiotic chromosome organisation Elife 3 doi:10.7554/eLife.02963

Tankimanova M, Hulten MA, Tease C (2004) The initiation of homologous chromosome synapsis in mouse fetal oocytes is not directly driven by centromere and telomere clustering in the bouquet Cytogenet Genome Res 105:172-181 doi:10.1159/000078187

van der Laan R et al. (2004) Ubiquitin ligase Rad18Sc localizes to the XY body and to other chromosomal regions that are unpaired and transcriptionally silenced during male meiotic prophase J Cell Sci 117:5023-5033 doi:10.1242/jcs.01368

Wang H, Hoog C (2006) Structural damage to meiotic chromosomes impairs DNA recombination and checkpoint control in mammalian oocytes J Cell Biol 173:485-495 doi:10.1083/jcb.200512077

Yamamoto A, Hiraoka Y (2001) How do meiotic chromosomes meet their homologous partners?: lessons from fission yeast Bioessays 23:526-533 doi:10.1002/bies.1072

Yang F, De La Fuente R, Leu NA, Baumann C, McLaughlin KJ, Wang PJ (2006) Mouse SYCP2 is required for synaptonemal complex assembly and chromosomal synapsis during

male meiosis J Cell Biol 173:497-507 doi:10.1083/jcb.200603063

Yuan L, Liu JG, Hoja MR, Wilbertz J, Nordqvist K, Hoog C (2002) Female germ cell aneuploidy and embryo death in mice lacking the meiosis-specific protein SCP3 Science 296:1115-1118 doi:10.1126/science.1070594

Yuan L, Liu JG, Zhao J, Brundell E, Daneholt B, Hoog C (2000) The murine SCP3 gene is required for synaptonemal complex assembly, chromosome synapsis, and male fertility Mol Cell 5:73-83

Zickler D, Kleckner N (2015) Recombination, Pairing, and Synapsis of Homologs during Meiosis Cold Spring Harb Perspect Biol 7 doi:10.1101/cshperspect.a016626

Zickler D, Kleckner N (2016) A few of our favorite things: Pairing, the bouquet, crossover interference and evolution of meiosis Semin Cell Dev Biol 54:135-148 doi:10.1016/j.semcdb.2016.02.024

SUPPLEMENTAL FIGURES

a

b
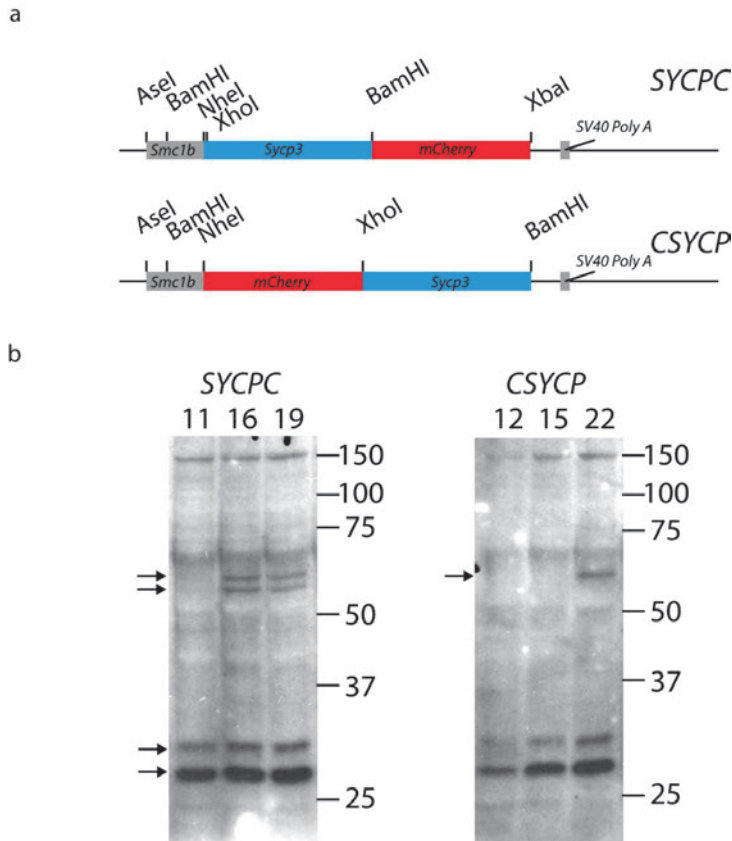
Fig. S1 Generation of transgenic mice expressing N- and C-terminal fusions of SYCP3 to mCherry. **(a)** Schematic drawing of SYCPC and CSYCP constructs. See Materials and Methods for details. **(b)** Western blot of total testis protein extracts isolated from mice of different age, stained with anti-SYCP3 antibody. Testis extracts were prepared from SYCPC mice of 11, 16 and 19 days-old, and of CSYCP mice of 12, 15 and 22 days-old. Two bands of around 30 K, representing the endogenous SYCP3 protein are detected at all ages. Expression of both fusion proteins (around 60 K) is initiated later, and the overall expression level is lower than that of endogenous SYCP3
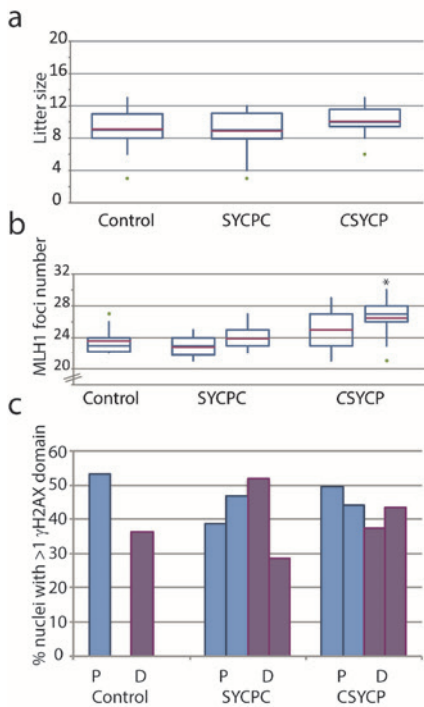
Fig. S2. SYCPC and CSYCP expression does not interfere with meiotic progression and fertility in males and females. (a) Box plots of litter sizes from backcrosses of control mice (*Ube2b*^{+/−} mice (Roest et al. 1996) (9.1 ± 2.4, SD; n = 18 breedings)), and SCYCP (10.1 ± 2.0, SD; n = 16 breedings) and CSYCP (8.9 ± 2.7, SD; n = 26 breedings) mice to FVB mice. All breedings took place in the same period in our animal facility (period 2009–2012). No significant differences between genotypes were observed (Mann-Whitney U test). Median values are indicated by the horizontal blue lines within each box, mean values are shown in red. The upper and lower whiskers indicate the upper and lower quartiles of the values, respectively. Outliers are shown as green dots. **(b)** Box plots of MLH1 foci numbers in late pachytene/early diplotene nuclei of control (*Sycp3*^{+/−} (23.6 ± 1.7,SD; n = 10 nuclei)), two *Sycp3*^{+/−} SYCPC (22.8 ± 1.3,SD and 23.9 ± 1.6,SD; n = 12 and 11, respectively),and two *Sycp3*^{+/−} CSYCP (25 ± 2.8,SD and 26.4 ± 2.5, SD; n = 11 and 13, respectively) male mice. Only a single *Sycp3*^{+/−} CSYCP mouse displayed a slight increase in MLH1 foci number compared to the *Sycp3*^{+/−} and *Sycp3*^{+/−} SYCPC mice (p = 0.009, Mann-Whitney U test). **(c)** Percentage of late pachytene/diplotene nuclei displaying one or more H2AX domains in addition to the XY body in one control (*Sycp3*^{+/−}), two *Sycp3*^{+/−} SYCPC and two *Sycp3*^{+/−} CSYCP mice. We observed no statistically significant effect of the transgenes on the persistence of DNA damage (Mann Whitney U test, n = 100 nuclei for each mouse).
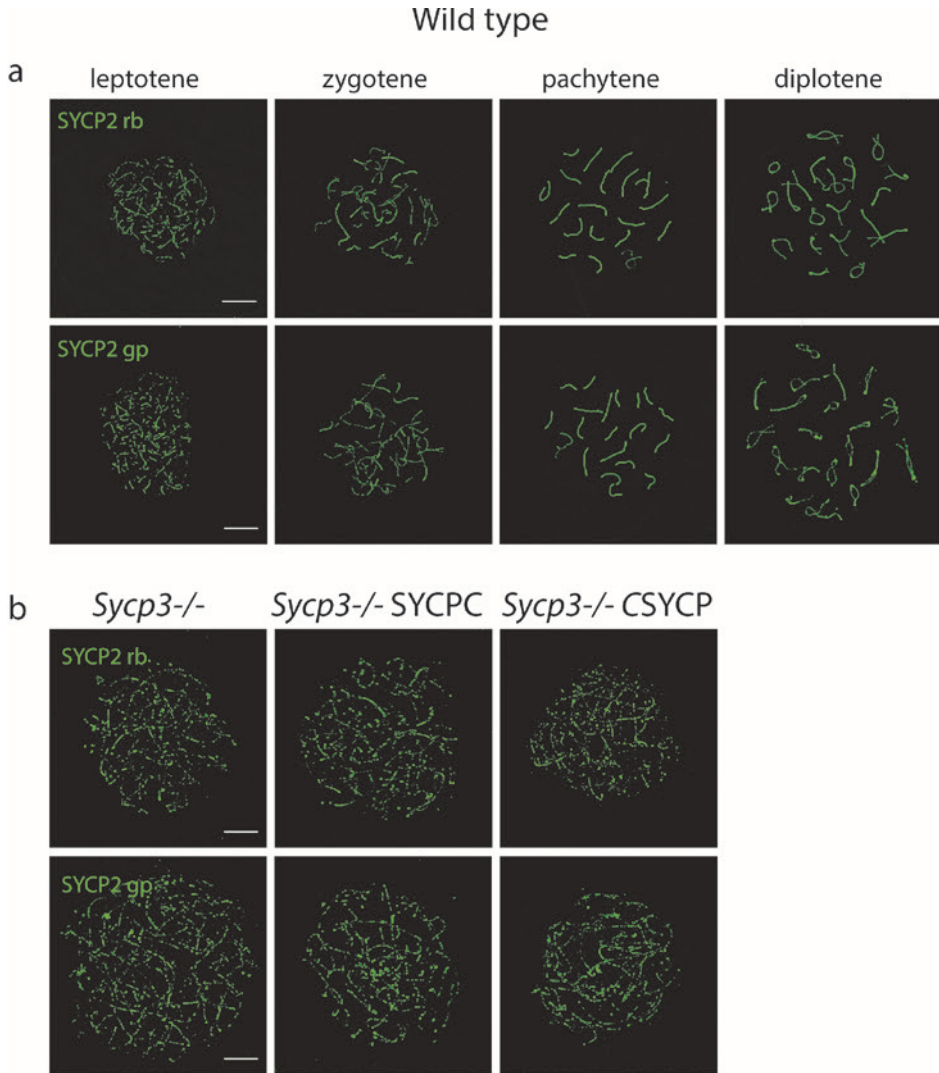
Fig. S3. SYCP2 is expressed as axial element component in *Sycp3^{-/-}* spermatocyte nuclei. Immunostaining of SYCP2 (green) on spermatocyte nuclei using two different antibodies: rabbit anti-SYCP2 (SYCP2 rb) and guinea pig anti-SYCP2 (SYCP2 gp) . **(a)** Wild type nuclei at indicated prophase stages **(b)** Zygotene-like nuclei of *Sycp3^{-/-}*, *Sycp3^{-/-}* SYCPC, and *Sycp3^{-/-}* CSYCP mice. Scale bar 10 μm.
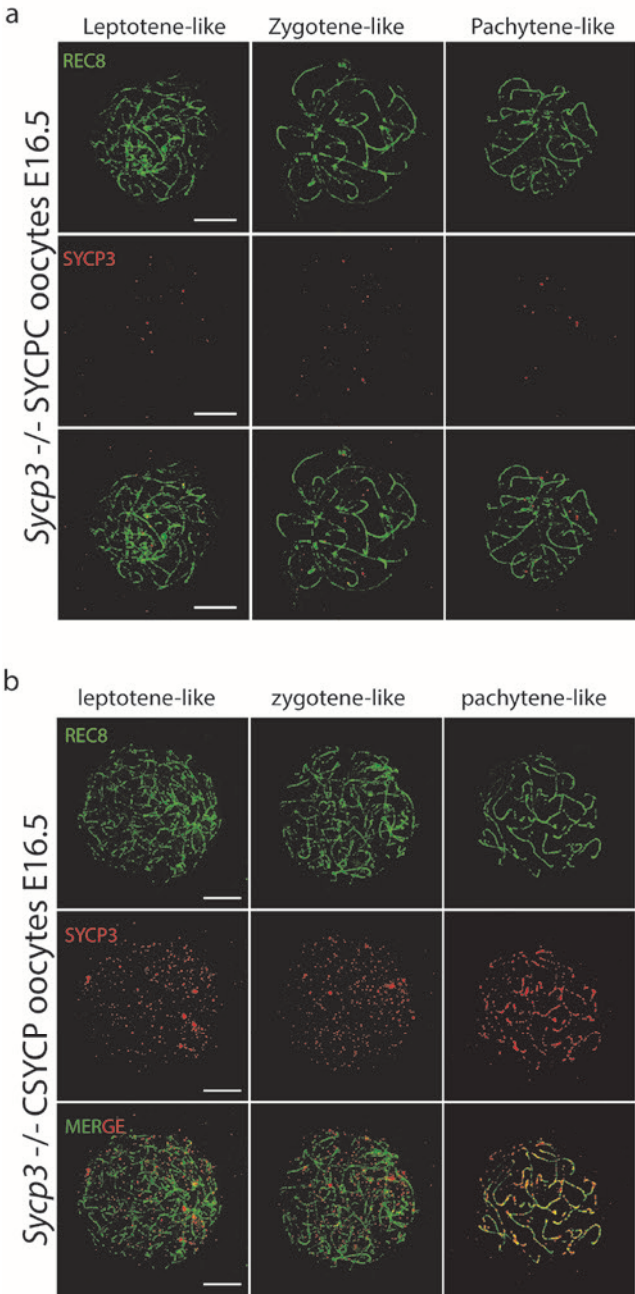
Fig. S4 Localisation pattern of tagged SYCP3 in E16.5 oocytes. **(a)** $Sycp3^{-/-}$ ^{S}YCPC **(b)** $Sycp3^{-/-}$ CSYCP. Immunostaining of REC8 (green) and SYCP3 (red). Scale bar 10 μm
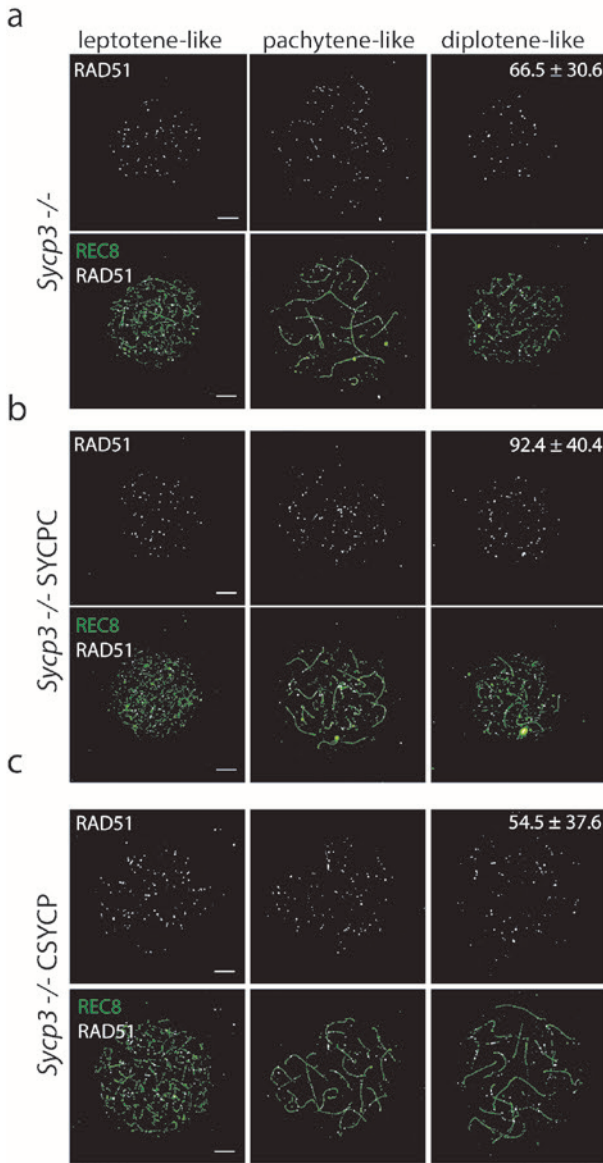
Fig. S5. Immunostaining of REC8 (green) and RAD51 (white) on *Sycp3*^{-/-} (a), *Sycp3*^{-/-} SYCPC **(b)** and *Sycp3*^{-/-} CSYCP (c) oocyte nuclei at E18.5. Means of RAD51 foci number ± SD in diplotene-like stage are displayed in the images (*N* = 6 nuclei for *Sycp3*^{+/-} SYCPC and *Sycp3*^{+/-} CSYCP; *n* = 8 nuclei for *Sycp3*^{-/-} and *Sycp3*^{-/-} SYCPC; n = 11 nuclei for *Sycp3*^{-/-} CSYCP). Scale bar 10 µm
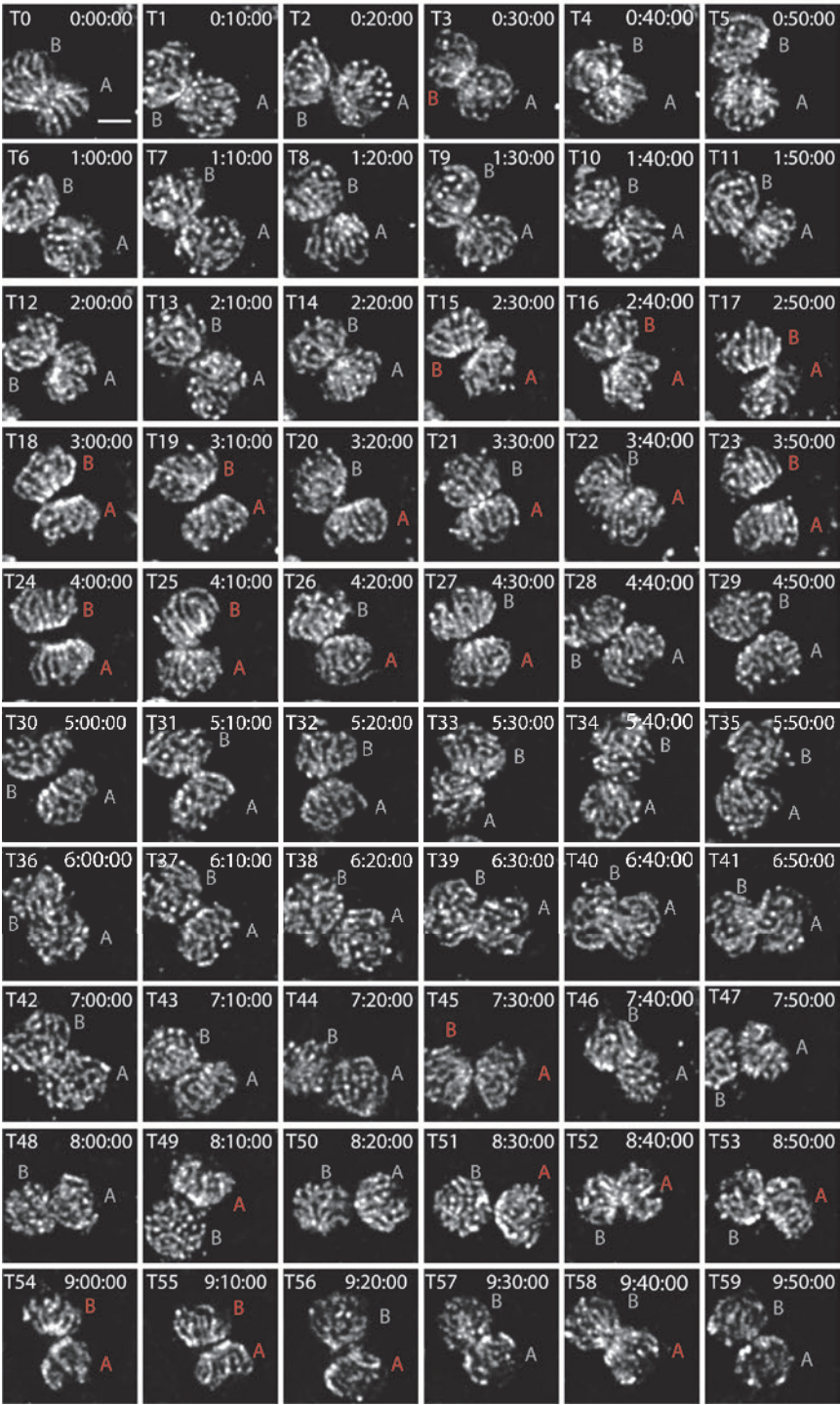
◀ **Fig. S6. Bouquet progression of the N3 cyst**. Each image represents the single plane of each nucleus that showed the clearest telomere organization. At some time points this required displaying each nucleus from a separate plane; these were then merged in one image for a better visualization (T1-T7, T9, T10, T13, T21, T25, T34, T37, T38 and T44). Scale bar 5 μm. Nuclei are labeled A and B. If a bouquet configuration is observed, these letters are red. (T0- T14) time previous to the formation of the bouquet. A one-time point clustering can be observed at T3 in nucleus B. (T15-T27) Bouquet in A. (T15-T19 and T23-T25). Bouquet in B. One time point clustering for both of the nuclei at T45 and for A at T49. Reclustering of nucleus A at T51 till T59, for nucleus B at T54 till T55. Some 1-time point dissolutions of nucleus A at T57 and T59

VIDEOS

Video 1. Two leptotene oocytes at E16.5 sharing the same cyst. 1 plane, 2 s interval. Total recording time 2 min.

Video 2. Two late zygotenes oocytes at E16.5 sharing the same cyst. 1 plane, 2 s interval. Total recording time 2 min.

Video 3. Three zygotenes oocytes at E16.5 sharing the same cyst. Stack, 5 s interval. Total recording 2 min.

Video 4. Two zygotenes oocytes at E16.5 sharing the same cyst. At $t = 6$ s, a bouquet configuration can be clearly observed. 1 plane, 3 s interval. Total recording 12 s.

Video 5. Desynapsis progression in a *Sycp3*$^{+/-}$ CSYCP diplotene spermatocyte ((a) in Fig. 7). Arrow heads indicate desynapsed sites, the position indicated with a green arrow was followed. No desynapsis progression was observed from the position indicated with a red arrow. 1 plane, 30 s interval, total recording 4 min 30 s.

Video 6. Desynapsis progression in a *Sycp3*$^{+/-}$ CSYCP diplotene spermatocyte ((b) in Fig. 7). The green arrow heads indicate the position where desynapsis/resynapsis take place. 1 plane, 30 s interval, total recording 4 min 30 s.

Video 7. Desynapsis progression in a *Sycp3*$^{+/-}$ CSYCP diplotene spermatocyte ((c) in Fig. 7). Green arrow head indicates the last synapsed part of the bivalent where the desynapsis occurs. 1 plane, 30 s interval, total recording 4 min 30 s.

Video 8 Desynapsis progression in a *Sycp3*$^{+/-}$ CSYCP diplotene spermatocyte ((d) in Fig. 7). The green arrow heads indicate the position where desynapsis occurs. 1 plane, 30 s interval, total recording 4 min 30 s.

Video 9 Desynapsis progression in a *Sycp3*$^{+/-}$ CSYCP diplotene spermatocyte ((e) in Fig. 7). The green arrow heads indicate the position where desynapsis/resynapsis take place. 1 plane, 30 s interval, total recording 4 min 30 s

Videos can be seen at the online version of this article: https://doi.org/10.1007/s00412-018-0668-7

3
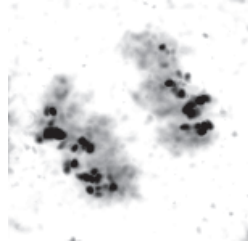
Unraveling the dynamics of the first meiotic division in cultured mouse testis tubules

Work in progress

Unraveling the dynamics of the first meiotic division in cultured mouse testis tubules

Andrea Enguita-Marruedo[1], Wiggert A. Van Cappellen[2], Johan A. Slotman[2], Adriaan Houtsmuller[2], and Willy M. Baarends[1]

1) Department of Developmental Biology

2) Department of Pathology/Erasmus Optical Imaging Centre, Erasmus MC, Rotterdam, The Netherlands.

3

Keywords: spermatogenesis, meiosis, live cell imaging, spindle assembly checkpoint, metaphase arrest

ABSTRACT

Following a lenghty prophase, meiotic divisions are of short duration, and substages are rarely observed in fixed samples of mammalian testes. Here we have used transgenic mice expressing mCherry-tagged SYCP3 (component of the synaptonemal complex, which connects homologous chromosomes during meiotic prophase), and GFP-tagged histone H2B to follow meiotic progression and visualize chromatin. In order to unravel the dynamics of the first meiotic division, we focussed on the development from diplotene up to the formation of secondary spermatocytes. Insight in the dynamics of meiotic cell behaviour in the context of the tubular structure can shed light on the possible role of the syncytium of spermatogenic cells in synchronization of events, and provide information on the molecular processes that ensure fidelity of this division. We observed that transition from diplotene to prometaphase was complete within 20 minutes. Metaphase started with a period of 20-120 minutes during which chromosome oscillations with large amplitude occurred. Subsequently, all chromosomes clustered together in a single group, and only oscillations with small amplitude took place. This latter period lasted extremely long (more than 12 hours). Metaphase-to-anaphase transitions were rapid (<10 minutes), and formation of secondary spermatocytes occurred between 10 and 50 minutes after chromosome division, whereby the two daughter cells behaved synchronously. Although grouped cells appeared to enter diakinesis more or less simultaneously, timing of further progression differed between cells, indicating cell-autonomous regulation. We observed aberrations that led to collapse and reinitiation of metaphase, or to a kind of telophase arrest. These data indicate that in mouse, male meiotic metaphase I chromosomes require an extremely lengthy period to satisfy the spindle assembly checkpoint, and this may contribute to the extreme high fidelity of male mouse meiosis.

INTRODUCTION

The concept of cell division as the mechanism by which new cells are formed was developed in the first half of the 19th century (reviewed in Mazzarello 1999). This concept (part of the cell theory) has been modernized as chromosomes, chromosome duplication and DNA were discovered. The distinction between mitotic and meiotic cell divisions, and the observation that meiosis involved ploidy reduction was first made by Eduard van Beneden in 1883, using a nematode (Ascaris megalocephala) with a very low chromosome number (van Beneden 1883, reviewed in Hamoir 1992). This allowed accurate drawings of the different substages of meiosis, but the actual dynamics of the meiotic divisions could not be assessed, since fixed material was used. Since then, researchers have attempted to study the dynamics of mitosis and meiosis in living cells. For example, oscillatory movements of chromosomes before alignment at the metaphase plate were observed using chick tissue culture 70 years ago (Hughes and Swann 1948). Subsequent advances in microscopy, cell culture methods and the development of techniques to fluorescently tag proteins, have facilitated analyses of these processes at high resolution in living organisms. 3D live imaging in HeLa cells stably expressing the kinetochore protein CENP-A fused to EGFP, has served to describe oscillatory movements and kinetochore alignment within the mitotic metaphase plate in more detail (Jaqaman et al. 2010). Also the activation of the mitotic checkpoint in response to lagging chromosomes has been studied in human Ptk1 cells and primary fibroblasts expressing H2B-GFP (Cimini et al. 2001, 2002). In mouse meiosis, oocytes coexpressing H2B-RFP and β-Tubulin-GFP have been used to study age-related meiotic segregation errors in mammals (Lister et al. 2010). Some aspects of chromosome organization are of course profoundly different between a mitotic division and the first meiotic division. Meiotic prophase usually lasts much longer than mitotic prophase because homologous chromosomes have to pair, synapse (physical proteinaceous connection along chromosomal axes), and recombine. Then, as cells enter metaphase (M-phase), the kinetochores of the homologous chromosomes (meiosis I) or of the sister chromatids (mitosis) must be attached to opposite spindle poles (bipolar orientation). As meiotic cells undergo the metaphase-to-anaphase I transition, sister chromatid cohesion is removed along chromosome arms, but protected at centromeres. In contrast, in mitosis, chromosome arm cohesion is mostly lost during prophase, and loss of centromere cohesion actually heralds the transition to anaphase. To what extent these differences would also affect the dynamics of the M-phase is not known. The so-called Spindle Assembly Checkpoint (SAC) controls the transition from metaphase to anaphase during both meiosis and mitosis. Microtubules attach to the kinetochores, creating tension between opposite spindles if the chromosomes are correctly bi-oriented, and cells can progress to anaphase (Rieder and

Salmon 1998). Lack of tension leads to the activation of SAC, and eventually to apoptosis of the cell. However, the fidelity of chromosome segregation is not absolute, and errors lead to aneuploidy in somatic cells (mitosis) or in sperm cells and oocytes (meiosis) (Sun and Kim 2012; Musacchio 2015; Faisal and Kauppi 2016; Marston and Wassmann 2017) .

Here, we aimed to extend the knowledge we have about the dynamics of the first meiotic division in vivo, using mouse male meiosis as a model, and through analyses of spermatocytes in the natural context of the seminiferous tubule. For this, we used mice co-expressing mCherry-tagged SYCP3 (CSYCP) and GFP-tagged histone H2B (H2B-GFP). This has resulted in a complete analysis of the first meiotic division, which we have followed from diplotene up to the formation of secondary spermatocytes. Progression of the cells from one stage to the other appeared to depend on both a syncytium-dependent regulation , as well as a cell autonomous regulation. The time required for spermatocytes to develop from metaphase to anaphase was very long (>12 hours), probably because of the activation of the Spindle Assembly Checkpoint. In rare cases, when cells progressed to anaphase after a much shorter time interval, chromosome aberrations were observed, suggesting that this long period is indeed necessary for correct alignment and segregation of the chromosomes. This study provides a complete description of the dynamics and chromatin features of the first meiotic M-phase in mouse spermatocytes in the natural context of the seminiferous tubule, and the data indicate tight regulation of the first meiotic division.

RESULTS

Transgenic expression of fluorescent tagged SYCP3 and H2B

In this study, mice expressing transgenes encoding SYCP3 tagged with mCherry at the N-terminus (CSYCP) and H2B tagged with GFP (H2B-GFP) were used. CSYCP expression (driven by a promoter fragment of *Smc1b*) initiates in pachytene, and colocalizes with endogenous SYCP3 from that point onwards (Enguita-Marruedo et al. 2018). SYCP3 is a component of the axial elements which form protein axes along the chromosomal axes in early meiotic prophase cells (leptotene and zygotene). As the chromosome pairs connect, these axial structures form the lateral elements of the synaptonemal complex, which physically connects the chromosomes during later meiotic prophase (pachytene) (Page and Hawley 2004). The *H2b-Gfp* transgene is driven by a CAG promoter and ubiquitously expressed (Hadjantonakis and Papaioannou 2004). Using spermatocyte spread preparations of mice carrying the H2B-GFP transgene (Fig. 1A) and wild type mice (Fig. 1 B), we observed that the tagged H2B protein was normally incorporated in nucleosomes of spermatogonia, and highly expressed in these cells. However, a dramatic reduction in the level of expression was already observed in the transition from spermatogonia B to spermatocytes, although a low

level of H2B-GFP remained. When spermatid elongation and condensation occurred, this remaining signal was gradually lost, similar to what was observed for endogenous H3.1 although the patterns do not fully overlap (Fig. 1A). Loss of a large fraction of H2B-GFP at meiotic entry may be caused by nucleosomal reorganization that is known to occur early in spermatogenesis, when part of the canonical histones is replaced by (testis-specific) variants. One of these is the testis-specific H2B isoform, TH2B, which replaces most of H2B during the transition from spermatogonia to spermatocytes (Montellier et al. 2013). It is highly likely that H2B-GFP is also partially replaced by TH2B, as suggested by the coincident drastic decrease of H2B-GFP signal and the appearance of TH2B that we observed in spermatocytes (Fig. 2). Still, the remaining amount of H2B-GFP signal allows visualization of chromatin during the subsequent steps. This signal, in combination with the stage-specific pattern of CSYCP expression, allowed us to characterize meiotic divisions and different aspects of chromatin remodelling in male mice in vivo.

Identification of stages in the cultured mouse seminiferous tubules based on H2B-GFP and CSYCP patterns

Spermatogenesis in mice is organized in waves, and there is a strict timing of the different steps, which leads to an ordered and fixed association of cells at a given position in the seminiferous tubules. In mice, 12 different cellular associations or stages can be distinguished, which follow each other in time at a specific position, and also along the length of the seminiferous tubule (Oakberg 1956). In our three dimensional tubule culture system (see Materials and Methods for details), we could also distinguish each of these 12 different cellular associations or stages. We focused on stage XI (where diplotene spermatocytes are present, which will progress to metaphase I in the next step), and stage XII (where meiotic divisions take place) (Fig. 3). At this stage, we observed spermatogonia or very early primary spermatocytes displaying the highest signal of H2B-GFP in comparison to later stages, and no CSYCP signal. Pachytene (chromosomes fully paired and connected via the synaptonemal complex) and diplotene (synaptonemal complex is gradually removed) spermatocytes displayed H2B-GFP (lower compared to earlier cell types) as well as CSYCP (present at chromosomes axes and at centromeres), in agreement with our earlier observations using mice carrying only the *CSYCP* transgene (Enguita-Marruedo et al. 2018). (Pro)metaphase I stages displayed also H2B signal and CSYCP (at the centromeres and freely diffusing in the cytoplasm). Metaphase II stages were not identified, probably because they display a less clear SYCP3 pattern and dimmer H2B-GFP signal, which may have made it difficult to distinguish them from the other types of cells. A much shorther duration of metaphase II compared to metaphase I would also explain the lack of detection.

The layer closest to the lumen contained round and elongating spermatids, and in these cells H2B-GFP signal was even lower compared to what was observed in spermatocytes, and it decreased further as spermiogenesis progressed (Fig. 3, arrow).
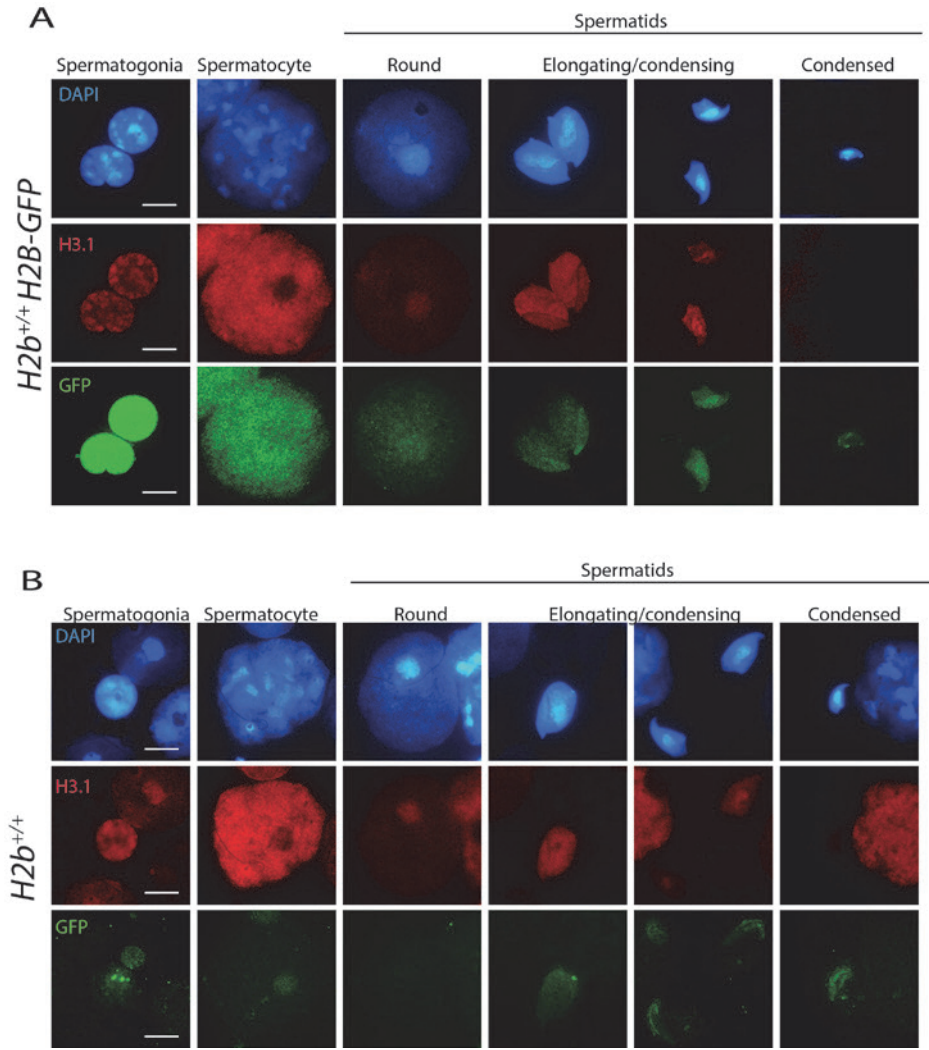
Fig. 1. Expression of H3.1 and H2B-GFP during spermatogenesis. Immunostaining of H3.1 (red) and GFP (green) in $H2b^{+/+}$ H2B-GFP mouse **(a)** and $H2b^{+/+}$ mouse **(b)** germ cells. Scale bar 10 μm.
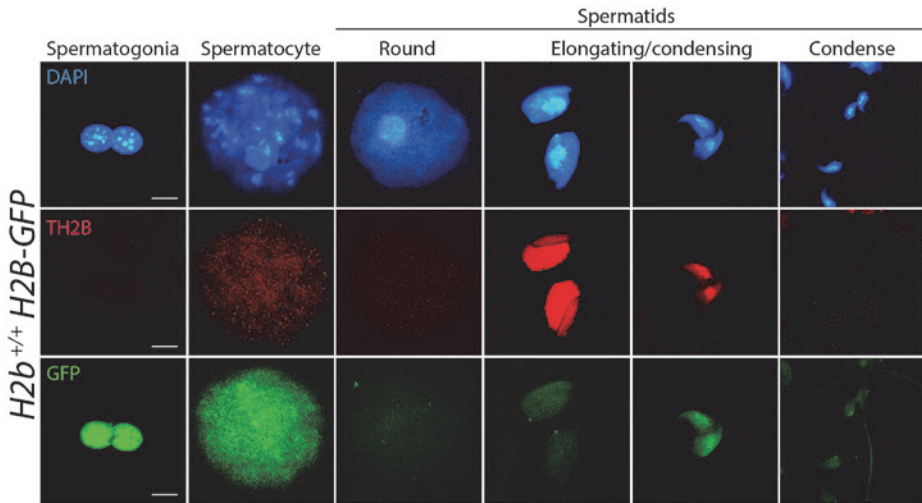
Fig. 2. Expression of H2B and TH2B during spermatogenesis. Immunostaining of TH2B (red) and H2B-GFP (green) in $H2b^{+/+}$ H2B-GFP mouse germ cells. Scale bar 10 μm.
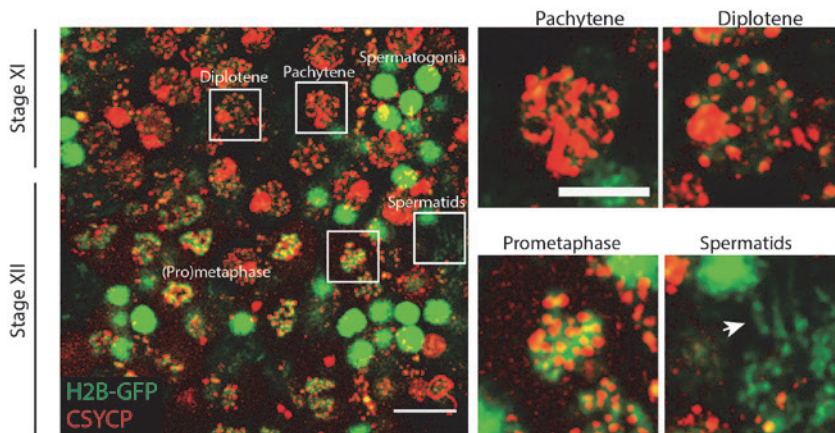
Fig. 3. Stages XI and XII of the spermatogenic cycle. H2B-GFP is visualized in green, while CSYCP is visualized in red. Maximum projection (9 slices). Scale bar 20 μm (overview image), scale bar 10 μm (zoom-in images).

Metaphase-to-anaphase transition in mitosis and meiosis

We performed short video recordings (time lapse of 1 minute and total duration of 15-20 minutes) of tubule positions that contained mitotic and/or meiotic metaphases. Mitotic metaphases were situated in the outer layers of the tubule while meiosis I metaphases were found in the inner layers, at stage XII of the cycle of the seminiferous tubules. Several mitotic cells divided at the same time or in rapid succession in the same position. Dividing

meiotic cells were more difficult to find, and frequently none or just one metaphase cell progressed to anaphase during the recording. Meiotic metaphases displayed dimmer H2B signal than mitotic metaphases, and Cherry signal at the centromeres (Video 1, the starting time-points of division have been synchronized between the meiotic and the upper mitotic cells). Before segregation, two rows of centromeres (visualized in meiotic cells only through CSYCP persisting at these sites) were visible at opposite sides of the meiotic metaphase plate (in accordance with biorientation of the homologous chromosomes) (Videos 1 and 2, biorientation of the centromeres can be observed at t=0 and t= 16 minutes, respectively). For both meiotic and mitotic divisions, the time between metaphase and anaphase A (two chromatin sets clearly separated) was approximately 3 minutes. Further separation of the poles occurred at later time points, which probably corresponds to anaphase B (elongation of the spindle). This lasted about 5-7 minutes in the mitotic divisions, and 8 minutes in the only meiotic division for which this process could be followed. After completion of the first meiotic division, chromatin of the daughter cells started to decondense, acquiring a rounder shape in time. Centromeres lost their distal position and distributed uniformly within the cell (Video 3, which corresponds to the complete recording of the meiotic cell of Video 1), indication that the daughter cells were further progressing to telophase and eventually developed into secondary spermatocytes.

First meiotic division during overnight experiments

Since short video recordings (15-20 minutes) were not long enough to follow the progression from prometaphase to secondary spermatocyte or later stages in meiosis, we decided to analyse this process in overnight experiments. An interval of 10 min was chosen for these time-lapse recordings, in order to prevent problems of bleaching and cell damage during the long experiment. The observations are summarized in Fig. 4. Diplotene spermatocytes displayed bright cherry signal at XY chromosomes and the telomeres (Fig. 4, diplotene image, arrow), while the rest of the autosomal axes presented a much dimmer signal (in Fig. 4, the time elapsed until each traced diplotene nucleus reached diakinesis is displayed at the left side of the green bars). Diakinesis itself was brief (≤ 10 minutes) (Fig 4, green bars). In the transition from diplotene to diakinesis, mCherry signal was rapidly lost from the chromosome arms (but not from the centromeres and telomeres), and freely diffused into the cytoplasm. CSYCP remained in the cytoplasm in subsequent stages, also in early round spermatids. A considerable condensation of the chromatin was visible during the diakinesis to prometaphase transition. Interestingly, diplotene cells that were close to each other had a tendency to progress to metaphase in a consecutive manner (video 4, cells in

diplotene stage appear at t= 9 (C10), t=12 (C2) and t=16 (C4)), and progress up to prometaphase at t=17, t = 17 and t= 18, respectively).
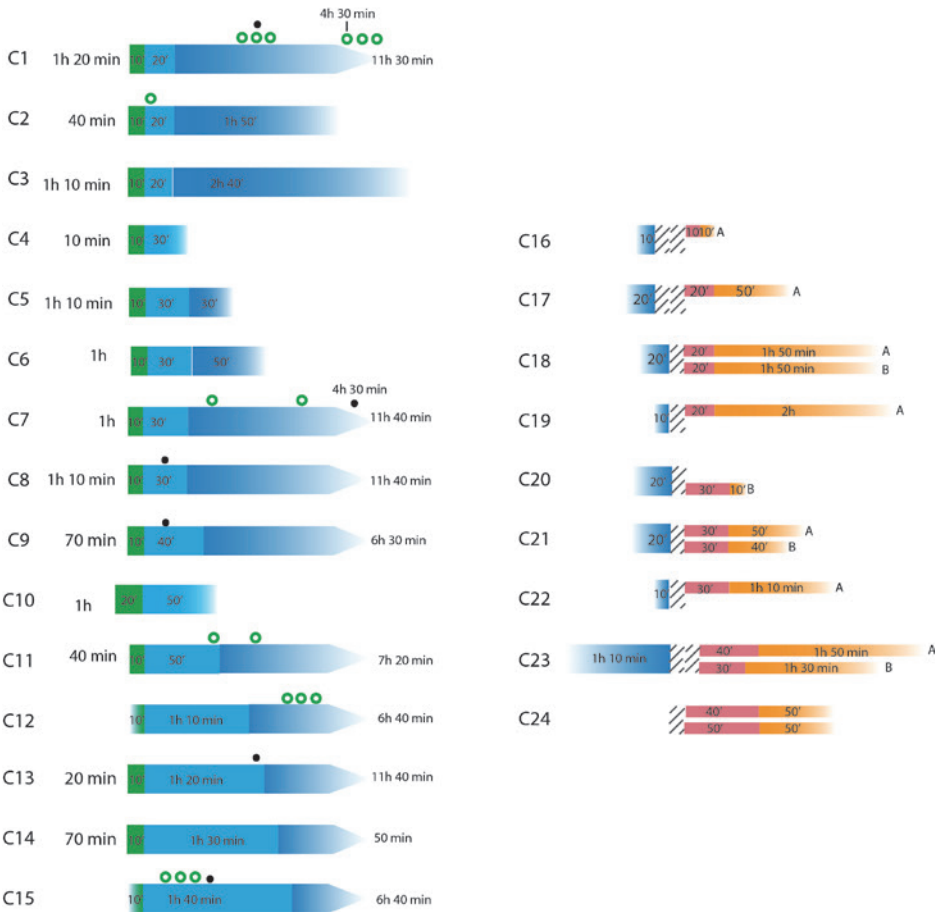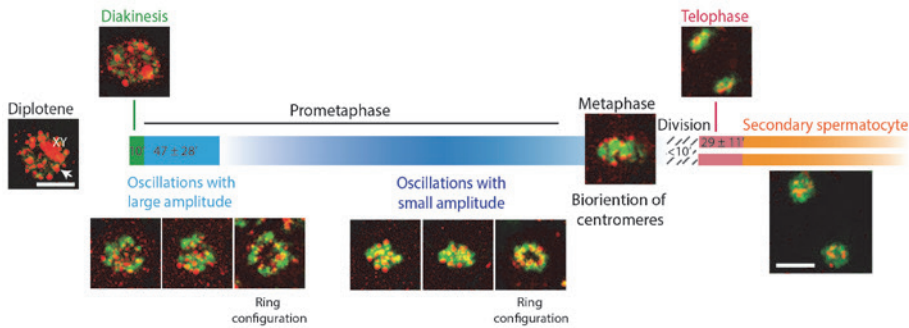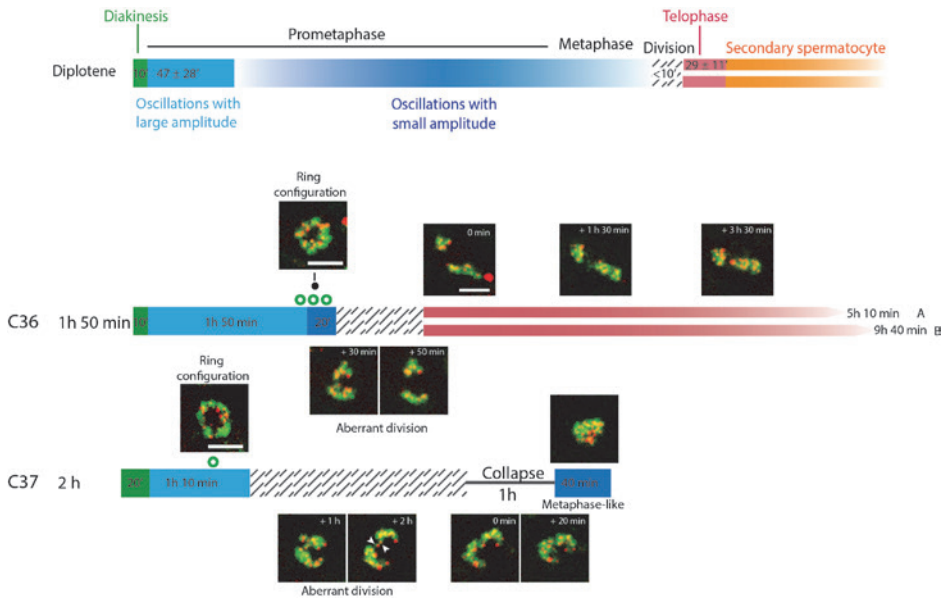
◀ **Fig. 4. Progression of meiosis**. Timeline with the different meiotic stages (upper part), including the mean duration (± SD) of the phases we could completely cover during the experiments. Representative photomicrographs of each stage are also shown. The arrow points to one of the centromere/telomere at diplotene stage. Below, the observations for each cell (C number refers to individual cells) are displayed: cells followed from diplotene till premetaphase stage (left), cells from the metaphase/anaphase stage till secondary spermatocyte (right). The amount of time between the beginning of the recording till cells reached diakinesis are shown at the left side. Bars indicate periods in which the cell is at the stage of: diakinesis (green bars), (pro)metaphase (period of oscillations with large amplitude, light blue bars; period of oscillations with small amplitude, dark blue bars), telophase (red bars), secondary spermatocyte (orange bars). Black diagonal lines indicate metaphase to-anaphase transition. Clear chromatin condensation (black point), ring configuration of chromosomes (green ring).

Subsequently, chromosomes oscillated to finally align at the metaphase plate. We could distinguish two types of oscillations. First, large amplitude oscillations (light blue bars) appeared, involving highly variable movements of groups of chromosomes through the cytoplasm (47 ± 28 min). Next, smaller amplitude oscillations followed (these occurred when all chromosomes were together in a single group), indicating that only small movements or adjustments took place. In a separate short recording experiment we also observed this type of oscillation (video 5, 1 min lapse), in this particular cell, a "chromatin unit" (probably a univalent) went in and out of the metaphase plate multiple times during the recording. At some time-points in this video, we could distinguish one or two cherry-positive signals (arrows), which would correspond to the centromeres of the univalent. Most of the other centromeres seem to be already bioriented, suggesting that the cell is arrested by the spindle attachment checkpoint. After 56 minutes, the chromatin unit was still not aligned in the equatorial plate. Indeed, from our overnight experiments we observed that these oscillations appeared to take a long time, and none of the cells we followed from diakinesis progressed to anaphase during the overnight experiments (covering 12 hours in metaphase for some cells). Even in cells that were in prometaphase stage already since the beginning of the recording, no progression to anaphase was observed (summarized in Fig. S1), reinforcing the idea that the period of small amplitude oscillations is long. Two of the cells represented in this figure (C31 and C32) displayed a sudden increase of red (C31) or green (32) signal after 5h and 10 min and 7h 20 min of the recording, respectively, suggesting that these cells died, possibly through apoptosis (Fig. S1, red cross). The other cells in Fig. 4 or Fig. S1 did not show these features, suggesting that they were still viable. Additionally, we observed two cells (out of 37 tracked cells) (C36 and C37, Fig. 5) of which one (C36) displayed a period of small oscillations of only 20 minutes, and the other (C37) completely lacked this type of oscillation. Both these cells displayed metaphase-to-anaphase transition failure, possibly illustrating the importance of a long period of oscillations with small amplitude. For the first cell (C36) an unbalanced distribution of the chromatin between the two poles was evident at anaphase I, suggesting a difference in ploidy of the daughter cells. 10 hours after division,

the daughter cells had still not progressed to form clear secondary spermatocytes. The second cell (C37) displayed a clear bridge during the metaphase-to-anaphase transition, which lasted 2 hours and 30 minutes. Subsequently, the two sets of chromosomes repositioned and formed a single mass again (anaphase collapse). In general, we observed a gradual condensation of chromatin as prometaphase progressed, but at some time points, a brief, more pronounced chromatin condensation was apparent (Fig. 4, 5 and Fig S1, black points).

Fig. 5. Cells displaying metaphase-to-anaphase transition failure. Timeline with the different stages (upper part), including the mean duration (± SD) of the phases (no apoptotic) we could completely cover during the experiments. The amount of time between the beginning of the recording till cells reached diakinesis are shown at the left side. Ring configuration of chromosomes (green ring). White arrowheads in C37 indicate the presence of two centromeres signals in the chromosome bridge.

It has been described for mitotic cells that shortly after nuclear envelope breakdown (early prometaphase), the chromosomes adopt a ring configuration, with the arms pointing outwards and the centromeres inwards. Since the microtubules are situated in the central part of the ring, this configuration facilitates the kinetochore-spindle interactions (Magidson et al. 2011). Such a ring configuration was observed for some of the meiotic metaphase cells, during both oscillation with large and small amplitude (Figs. 4, 5 and S1, ring configuration

image and green ring), although not all the centromeres were so clearly pointing outwards. This configuration may be overlooked if the orientation in the field of view through the cell is perpendicular to that of the ring.

Metaphase-to-anaphase I transition and formation of secondary spermatocytes

The long duration of the period of small oscillations prevented us from following cells during the entire transition from diakinesis to secondary spermatocytes. However, we could follow cells from the metaphase/anaphase stage onwards (Fig. 4, right side). We observed a clear metaphase plate (visualized by H2B-GFP), with the centromeres positioned at opposite sides (biorientation of the homologous chromosomes) before division. Metaphase-to-anaphase transition was complete in about 10 minutes. Some metaphase cells that were close to each other progressed to anaphase in a consecutive manner, but others showed asynchrony in this transition (video 4, C24 was at anaphase stage at t=1, C16 and C20 were in metaphase stage and progressed to anaphase at t=2 and t=3, respectively. C25, in contrast, remained in metaphase stage during the whole recording). After telophase, chromatin of the daughter cells gradually decondensed, and the cells recovered the round shape. These cells, containing nuclei again, were considered as having entered the secondary spermatocyte stage. The moment of clear formation of secondary spermatocytes varied among different cells, and was observed between 10 and 50 minutes after chromosome division. However, this progression appeared to be synchronized between the two daughter cells. Decondensation of the chromatin continued for some time after nuclei had acquired a round shape.

Because we selected positions already in late stage XII (Positions 1, 2 and 3, in which alignment of the chromosomes and biorientation of the centromeres were (almost) complete at T1), events of metaphase-to-anaphase transition and progression to secondary spermatocyte were observed only during the first four hours of the experiment (Fig. S2, green bars). Still, some of the prometaphase cells in the same region were not observed to progress to anaphase but moved to other layers during later time points (C25, 27 and 30), or remained in prometaphase stage for the rest of the recording (C34). Interestingly, we generally observed a continuous lateral flow of cells in the adluminal compartment (most likely as a consequence of the contractions of the tubule) in these positions. Cells that came into view as a result of this flow belonged to stage XI (diplotenes, red bars) (Video 4, diplotene cells came into view at t= 9 (C10), t=12 (C2) and t=16 (C4)). So apparently, cells at an earlier stage moved in the field of view, while the later cells could no longer be tracked.

This phenomenon may explain the lack of metaphase-to-anaphase transitions observed at later time points in these positions. Two of the selected positions displayed stage XI (positions 4 and 5) and early stage XII (position 4), and therefore no metaphase-to-anaphase transition were expected for these locations. Metaphase-to-anaphase transition was observed in two cells (C36 and C37, orange bars) at position 5 (Stage XI), but these were aberrant.

DISCUSSION

Transition from prophase I to metaphase I is not completely synchronized among cells

During our overnight time lapse experiments, we observed that progression from diplotene to metaphase and later stages did not occur in all cells at the same time. Two factors seem to play a role in the progression to the next stage. First, a certain spatio-temporal relation appears to exist, and cells that are close to each other showed a tendency to progress to the next stage in a consecutive manner, in particular when cells underwent the diplotene-to-metaphase transition. Cytokinesis is not complete during spermatogonial divisions, and cells form a syncytium (which remains during the subsequent stages) whereby each cells communicates with the others via cytoplasmic bridges (Dym and Fawcett 1971). Since spermatocytes develop in a syncytium it might be that stochastic differences in nuclear levels of critical cell cycle regulators such as cyclin A1(Liu et al. 1998), may propel one cell into prometaphase, and the positive feedback-mechanisms that are usually associated with cell cycle phase transitions then spread in a wave-like manner through the syncytium. We also observed asynchrony in the transition from metaphase-to-anaphase among the different cells. Since the correct attachment to the spindle of each homologous is a matter of "trial and error", different cells may need different times until all chromosomes are correctly bioriented. Besides the external factors the cell may receive, progression to anaphase will not to occur until the SAC is satisfied for each chromosome, and the signaling machinery that allows metaphase-to-anaphase transition in one cell can apparently act independent from inhibitory signaling at incorrectly aligned chromosomes in neighboring cells. The live analyses thus allow us to suggest that cohorts of late spermatocytes (most likely connected through cytoplasmic bridges) might be pushed into M-phase by signals that travel through the different connected cells, whereas the spindle assembly checkpoint may act locally and therefore cell-autonomously, creating more asynchrony within one syncytium.

Another interesting feature we have observed during our overnight experiments is the lateral flow of cells belonging to the adluminal compartment, when contractions of the

tubule occur. Cells in the basal layer remained more stably at their position. During spermatogenesis, differentiating germ cells migrate from the basal to the adluminal compartment by going through the blood testis barrier, while maintaining close contact with the surrounding Sertoli cells via specialized ectoplasmic specializations and desmosome-like junctions (Goossens and van Roy 2005; Xiao et al. 2013). Since these cells can move from a more basal location towards the lumen, it could be expected that they might also move in lateral or transversal directions in certain circumstances. The blood-testis barrier's strength is achieved by the combination of several co-existing junction types (tight junction, ectoplasmic specializations, gap junctions and desmosomes) (Pelletier and Byers 1992; Goossens and van Roy 2005; Mital et al. 2011; Pelletier 2011; Xiao et al. 2013). Interestingly, these junctions undergo extensive restructuring at Stages VIII–IX to facilitate the transit of preleptotene spermatocytes from the basal to the adluminal compartment. At the same time, spermiation takes place at late Stage VIII to release the mature spermatozoa into the tubule lumen, with the sperm late-stage apical ectoplasmic specializations undergoing disintegration (Xiao et al. 2013). Adluminal germ cell-Sertoli interactions could become more "loose "during this restructuring period. This, in combination with the increase of the contractile movements once sperm has been released (Harris and Nicholson 1998, and own observations) could explain the creation of the flow of cells in some positions. It should also be taken into account that the in vitro culture conditions, and the fragmentation of the tubules may affect the dynamic properties of the contraction-induced flow of cells.

Prolonged arrest in meiotic metaphase I in cultured mouse spermatocytes

During both mitotic and meiotic prometaphase, activities of microtubules and associated motor proteins lead to oscillatory movements of chromosomes inside the cell to finally align at the metaphase plate. The spatial organization of chromosomes during prometaphase facilitates spindle assembly and biorientation (Magidson et al. 2011; Itoh et al. 2018). In mitosis, the process of chromosome alignment has been divided into distinct phases after the Nuclear Envelope Breakdown (NEBD): prometaphase rosette (appears only in half of the analysed M-phases), congression, equatorial ring, and bi-orientation. End-on microtubule attachments are observed only during bi-orientation, while lateral attachments are present in the previous phases (Itoh et al. 2018). Congression, or the movement of chromosomes to the metaphase plate, would correspond to the period of oscillations with large amplitude. In early prometaphase spermatocytes, we also observed first large-amplitude oscillations (duration 20-100 min), followed by more subtle oscillations when chromosomes had localised in a smaller area in the center of the cell. Using 3D live cell imaging, Jaqaman et al. (2010) described oscillations and chromosome movements in HeLa cells at metaphase,

whereby the metaphase plate became thinner as the amplitude of the oscillations was gradually reduced. Similar to their observations, our meiotic metaphase plates also appeared to become thinner as cells progressed towards anaphase. While we did not observe rosette-like structures in our metaphase spermatocytes, as described for mitotic metaphases, we did observe a ring configuration in some cells, and this then occurred either during the period of large or small amplitude oscillations. In the mitotic ring, the chromosome arms point outwards and the centromeres inwards, where the microtubules are situated in the central part of the ring, facilitating in this way the kinetochores-spindle interactions (Magidson et al. 2011). The meiotic ring may have a similar function. During the period of oscillations with small amplitude, small-scale adjustments could take place (e.g. solve incorrect attachments to the spindle), until all the chromosomes are correctly bi-oriented. The metaphase checkpoint would also act at this point, preventing the cell to progress to anaphase till this requirement is satisfied.

Interestingly, although the above described typical features of chromosome movement during mitotic metaphase were also observed in meiotic spermatocyte metaphases, metaphase I in mouse spermatocytes in our culture system lasted more than 10 hours. This long metaphase I duration is striking, and has not been described for normal mitotic cells. M-phase in somatic cells usually takes less than 1h (Mazia 1961; Fry et al. 1961; Odartchenko et al. 1964), although in specific type of cells it can take longer, like in isthmal cells, where M-phase has been described to take up to 8.3 hours in mice (el-Alfy and Leblond 1987). However, even in this case, metaphase lasted only 0.2 hours, and anaphase 0.06 hours, and a lengthy prophase and telophase caused the long M-phase (el-Alfy and Leblond 1987). In fission yeast meiosis, meiosis I takes only about 0.6 hours (Nachman et al. 2007). Nevertheless, this may be different in more complex organisms, such as mammals. A comparison between young and old female mice showed that the time between the breakdown of the germinal vesicle (GVB) and chromosome congression (corresponding to the herein described large amplitude oscillations) had a duration between 2 and 6.5 hours for both cases. The time between chromosome congression and anaphase onset (corresponding to the herein described small amplitude movements) had a duration between 2 and 6.5 hours for the young female mice, and between 2 and 15.8 hours for the old female mice (Lister et al. 2010). This indicates that in mammals, meiotic metaphase may indeed take much more time compared to a mitotic metaphase. The whole period between diakinesis/prometaphase and round spermatid formation (stage XII) has been estimated to last 20.8 hours in mouse (Oakberg 1956) and it has not been established how long each of the substages, such as metaphase I lasts. According to our observations, the period between diakinesis and formation of secondary spermatocytes could take about 14 hours to be

complete (Fig. 4). Unfortunately, we could not follow the second meiotic division further than the early secondary spermatocytes after telophase I, probably because of the less clear Cherry pattern and dimmer H2B-GFP signal, which made them difficult to identify. However, we inferred that if the transition from diakinesis to early secondary spermatocytes takes about 14 hours, second meiotic division should be complete in about 6 hours (total time of stage XII is 20.8 hours). If we take into account that the second meiotic division is more similar to mitosis (Ashley 2004), we expect indeed that it would take much less time than the first meiotic division.

Aberrant metaphases may be caused in part by erroneous attachment of microtubules to kinetochores

It has been proposed that meiotic or mitotic malsegregation may occur when incorrect microtubule attachments and/or kinetochore orientation are not corrected before anaphase (Nicklas and Koch 1969; Ault and Rieder 1992). This may occur in the two cells displayed in Fig. 5. The short (only 20 minutes, first cell) or absent (second cell) period of oscillations with small amplitude may indicate incomplete or absent activation of the SAC (and therefore absence of arrest until all chromosomes are properly aligned). Missegregation of chromosomes during metaphase I may occur when the two homologs are pulled towards the same pole (mono-orientation of the two kinetochore doublets). Alternatively merotelic kinetochore orientation, whereby a single kinetochore, or the doublet of kinetochores of a single chromosome, are pulled towards opposite poles, may eventually also lead to aneuploid meiotic products. In mitotic cells, live imaging of H2B histone-GFP transfected cells showed that cells with mono-oriented chromosomes are efficiently detected by the SAC and never enter anaphase. Merotelic kinetochore orientation was not so frequently detected by the checkpoint, and viewed as a potential mechanism of aneuploidy in human cells (Cimini et al. 2002). A merotelic orientation of the bivalent may have occurred in C37, resulting in a formation of a clear chromosome bridge between the two poles. It is interesting to note that these incorrect meiotic divisions occurred in wild-type cells. It will be interesting to analyse the frequency of these aberrations in more detail, and assess if the frequency of their occurence increases in certain infertile mouse models (e.g. mouse models displaying metaphase arrest or anaphase segregation errors), or upon treatment with spindle destabilizing agents.

In mitosis, anaphase correction has been described as a mechanism to prevent mis-segregation of merotelically oriented chromosomes (Cimini et al. 2004). The experiments showed that during anaphase, the bundle of microtubules attached to the incorrect pole

lengthened, pushing the chromosome to the correct pole , resulting in correct segregation of the merotelically oriented chromosome. This may explain the final inclusion of some lagging chromosomes we have observed in mitotic divisions (e.g. video 1, arrow, mitotic divisions). More studies are necessary to unravel if this mechanism is acting in these cases, and if it could be also present during the meiotic divisions.

In summary, we have used male mice expressing mCherry-tagged SYCP3 (CSYCP) and GFP-tagged histone H2B (H2B-GFP) to follow meiosis I (from diplotene up to the formation of secondary spermatocytes) in vivo, in the natural context of cultured seminiferous tubule fragments. In this context, progression from one stage to the other seems to depend on signals coming from the syncytium, but also from each individual cell. Interestingly, transition from metaphase to anaphase seems to depend almost exclusively on internal signals, probably involving the Spindle Assembly Checkpoint (SAC), which delays the onset of anaphase until all chromosomes are correctly aligned.

MATERIALS AND METHODS

Ethics statement

All animal experiments were approved by the local animal experiments committee DEC Consult and animals were maintained under supervision of the Animal Welfare Officer.

Breeding and genotyping of H2B-GFP/CSYCP mice

CSYCP mice were described previously (Enguita-Marruedo et al. 2018).These were originally generated on an FVB background. *H2B-GFP* mice, officially named B6.Cg-Tg(HIST1H2BB/EGFP)1Pa/J (Hadjantonakis and Papaioannou 2004) were obtained from the Jackson Laboratory (https://www.jax.org/strain/006069). Both transgenes were combined in one mouse line by crossing the two lines, and mice containing both transgenes were identified by PCR on tail tip or toe tip DNA using forward primers 5'CACCATCGTGGAACAGTACG3' for CSYCP AND 5'GGCCACAAGTTCAGCGTGTC3' for H2B-GFP and reversed primers 5'GGGAGGTGTGGGAGGTTTT3' for *CSYCP* and 5'ATGCGGTTCACCAGGTGTC3' for *H2B-GFP*. PCR was carried out using standard protocols and the following conditions for *CSYCP*: Initial hold at for 5 minutes at 94°C, followed by 35 cycles of 94°C for 45 seconds,54°C for 1 minute, 72°C for 1 minute, and finally 72°C for 10 minutes. This generated a fragment of 947bp, specific for the presence of the transgene. For *H2B-GFP* the conditions were: Initial hold at for 5 minutes at 94°C, followed by 35 cycles of 94°C for 30 seconds, 60°C for 1 minute, 72°C for 1 minute, and finally 72°C for 10 minutes.

This generated a fragment of 300bp. This mouse line, carrying the two transgenes, was kept through backcrossing to C57Bl6.

Immunocytochemistry

Spread nuclei of spermatocytes were prepared from isolated gonads as described by Peters et al. 1997, and stored at −80C. Thawed slides were washed in PBS (3×10 min), and non-specific sites were blocked with 0.5% w/v BSA and 0.5% w/v milk powder in PBS. Primary antibodies were diluted in 10% w/v BSA in PBS, and incubations were performed overnight at room temperature in a humid chamber. Subsequently, slides were washed (3×10 min) in PBS, blocked in 10% v/v normal goat serum (Sigma) in blocking buffer (supernatant of 5% w/v milk powder in PBS centrifuged at 14,000 rpm for 10 min), and incubated with secondary antibodies in 10% normal goat serum in blocking buffer at room temperature for 2 hours. Finally, slides were washed (3×10 min) in PBS and embedded in Prolong Gold with DAPI (Invitrogen).

Primary antibodies: rabbit polyclonal anti-SYCP3 (Lammers et al. 1994) at 1:10000, mouse polyclonal anti- H3.1/3.2 (van der Heijden et al. 2005) at 1:5000,mouse monoclonal anti-TH2B (MAB5208 Millipore) at 1:1000, rabbit polyclonal anti-GFP (ABCAM:ab290 anti-GFP). For secondary antibodies, we used a goat anti-rabbit alexa 488 IgG, goat anti-mouse alexa 488, goat anti-rabbit 546 IgG, donkey anti-goat alexa 488, donkey anti-rabbit alexa 546, donkey anti-mouse alexa 633 IgG, all at 1:500 dilution

Isolation of testis tubules for culture

Adult mouse testes from transgenic mice carrying the *Csycp* and *H2b-gfp* transgene were isolated and dissected following a previously described protocol(van der Laan et al. 2004) with some modifications. Decapsulated testes were immersed in 20 ml Dulbecco's phosphate buffered saline (Invitrogen, Carlsbad, CA, USA) containing 1.1 mM Ca^{2+}, 0.52 mM $Mg2^{+}$, 6mM DL-lactic acid and 5.6 mM glucose (PBS^{+}), in the presence of collagenase (1μg/μl; type 1 Worthington) and hyaluronidase (0.5 μg/μl; H3884 Sigma) in a 50 ml falcon tube. The testes were then incubated in a waterbath at 33C and shaken at 90 cycles/min, amplitude of 20 mm, for 5 minutes. The incubation was stopped when the enzymatic digestion had resulted in dissociation of the interstitial tissue and disengagement of testis tubules. Tubules were separated from interstitial cells by washing in PBS^{+} twice. Next, tubules were placed in a 30 mm BSA-coated Petri dish, where the tubules were separated from each other using dissection tweezers (Nr. 5). We staged the tubules using the transillumination technique (Kotaja, Kimmins et al. 2004). Small tubule fragments (of about 1

cm) staged between stages VI-XII (containing spermatocytes in late pachytene, diplotene or metaphase/anaphase stage) were selected and carefully transferred to a 15 mm BSA-coated Petri dish. Please note that testicular myoid cells, the main component of the outer layer of the seminiferous tubules, were present in the fragments used during the experiments, indicating that this method keeps the tubule wall intact.   After collecting a pool of fragments, we used dissection tweezers (Nr. 5) to place 4-5 of these fragments into a 50 µl drop containing 1:4 v/v (RPMI + 10% KRS culture medium)/ Cultrex® Basement Membrane Extract (BME), type 2; Trevigen pipetted onto a 24 mm laminin-coated cover slip in each live cell chamber. The chambers with the tubules were centrifuged 5 minutes at 500 rpm and $4^{o}C$, so the seminiferous tubules went close enough to the coverslip in order to allow the imaging. Next, the chambers were incubated for 30 minutes at $33^{o}C$ to allow the BME to jellify. Finally, 2 ml of RPMI + 10% KRS culture medium was added.

Fluorescent and time lapse microscopy

Fluorescent images from immunostained samples were obtained using a fluorescent microscope (Axioplan 2; Carl Zeiss) equipped with a digital camera (Coolsnap-Pro; Photometrics).

For the time lapse imaging, we used a Leica SP5 confocal microscope. Chamber and objective (40 x 1.25 NA, oil immersion) were kept at 33 ^{o}C and 5% CO_2 in air. Red fluorescent images were obtained with a 594-mm laser and detection through a 600-680 band pass filter. Green fluorescent images were obtained after excitation with a 488-nm laser and detection through a 500-550 band pass filter. For the short video recordings, stacks of 7 slices of 1 µm were made (zoom 4). The time lapse between images was 10 minutes and a total duration of 15-20 minutes. For the overnight time lapse experiment, 9 positions in the same tubule were selected (this selection excluded the cut ends of the tubules, where high levels of cell death/loss were present). For each position a stack of around 30 slices of 1 µm was made (512 x 512 pixel size). The time lapse between images was 10 minutes.

Cells were selected manually by visual inspection. To track the selected cell, a Maximum projection was created (which included 3 layers below and 3 layers above the cell). Additionally, the complete stack was also used to check each of the observations per time point.

REFERENCES

Ashley T (2004) The mouse "tool box" for meiotic studies. Cytogenet Genome Res 105:166–71. doi: 10.1159/000078186

Ault JG, Rieder CL (1992) Chromosome mal-orientation and reorientation during mitosis. Cell Motil Cytoskeleton 22:155–9. doi: 10.1002/cm.970220302

Cimini D, Cameron LA, Salmon ED (2004) Anaphase spindle mechanics prevent mis-segregation of merotelically oriented chromosomes. Curr Biol 14:2149–55. doi: 10.1016/j.cub.2004.11.029

Cimini D, Fioravanti D, Salmon ED, Degrassi F (2002) Merotelic kinetochore orientation versus chromosome mono-orientation in the origin of lagging chromosomes in human primary cells. J Cell Sci 115:507–15

Cimini D, Howell B, Maddox P, et al (2001) Merotelic kinetochore orientation is a major mechanism of aneuploidy in mitotic mammalian tissue cells. J Cell Biol 153:517–27

Dym M, Fawcett DW (1971) Further observations on the numbers of spermatogonia, spermatocytes, and spermatids connected by intercellular bridges in the mammalian testis. Biol Reprod 4:195–215

el-Alfy M, Leblond CP (1987) Long duration of mitosis and consequences for the cell cycle concept, as seen in the isthmal cells of the mouse pyloric antrum. II. Duration of mitotic phases and cycle stages, and their relation to one another. Cell Tissue Kinet 20:215–26

Enguita-Marruedo A, Van Cappellen WA, Hoogerbrugge JW, et al (2018) Live cell analyses of synaptonemal complex dynamics and chromosome movements in cultured mouse testis tubules and embryonic ovaries. Chromosoma. doi: 10.1007/s00412-018-0668-7

Faisal I, Kauppi L (2016) Sex chromosome recombination failure, apoptosis, and fertility in male mice. Chromosoma 125:227–35. doi: 10.1007/s00412-015-0542-9

Fry RJ, Lesher S, Kohn HI (1961) A method for determining mitotic time. Exp Cell Res 25:469–71

Goossens S, van Roy F (2005) Cadherin-mediated cell-cell adhesion in the testis. Front Biosci 10:398–419

Hadjantonakis A-K, Papaioannou VE (2004) Dynamic in vivo imaging and cell tracking using a histone fluorescent protein fusion in mice. BMC Biotechnol 4:33. doi: 10.1186/1472-6750-4-33

Hamoir G (1992) The discovery of meiosis by E. Van Beneden, a breakthrough in the morphological phase of heredity. Int J Dev Biol 36:9–15

Harris GC, Nicholson HD (1998) Stage-related differences in rat seminiferous tubule contractility in vitro and their response to oxytocin. J Endocrinol 157:251–7

Hughes AF, Swann MM (1948) Anaphase Movements in the Living Cell. J Exp Biol 25:

Itoh G, Ikeda M, Iemura K, et al (2018) Lateral attachment of kinetochores to microtubules is enriched in prometaphase rosette and facilitates chromosome alignment and bi-orientation establishment. Sci Rep. doi: 10.1038/s41598-018-22164-5

Jaqaman K, King EM, Amaro AC, et al (2010) Kinetochore alignment within the metaphase plate is regulated by centromere stiffness and microtubule depolymerases. J Cell Biol 188:665–679. doi: 10.1083/jcb.200909005

Lammers JH, Offenberg HH, van Aalderen M, Vink AC, Dietrich AJ, Heyting C (1994) The gene encoding a major component of the lateral elements of synaptonemal complexes of the rat is related to X-linked lymphocyte-regulated genes Mol Cell Biol 14:1137-1146

Lister LM, Kouznetsova A, Hyslop LA, et al (2010) Age-related meiotic segregation errors in mammalian oocytes are preceded by depletion of cohesin and Sgo2. Curr Biol 20:1511–21. doi: 10.1016/j.cub.2010.08.023

Liu D, Matzuk MM, Sung WK, et al (1998) Cyclin A1 is required for meiosis in the male mouse. Nat Genet 20:377–80. doi: 10.1038/3855

Magidson V, O'Connell CB, Lončarek J, et al (2011) The Spatial Arrangement of Chromosomes during Prometaphase Facilitates Spindle Assembly. Cell 146:555–567. doi: 10.1016/J.CELL.2011.07.012

Marston AL, Wassmann K (2017) Multiple Duties for Spindle Assembly Checkpoint Kinases in Meiosis. Front cell Dev Biol 5:109. doi: 10.3389/fcell.2017.00109

Mazia D (1961) Mitosis and the Physiology of Cell Division. Cell 77–412. doi: 10.1016/B978-0-12-123303-7.50008-9

Mazzarello P (1999) A unifying concept: the history of cell theory. Nat Cell Biol 1:E13–E15. doi: 10.1038/8964

Mital P, Hinton BT, Dufour JM (2011) The blood-testis and blood-epididymis barriers are more than just their tight junctions. Biol Reprod 84:851–8. doi: 10.1095/biolreprod.110.087452

Montellier E, Boussouar F, Rousseaux S, et al (2013) Chromatin-to-nucleoprotamine transition is controlled by the histone H2B variant TH2B. Genes Dev 27:1680–1692. doi: 10.1101/gad.220095.113

Musacchio A (2015) The Molecular Biology of Spindle Assembly Checkpoint Signaling Dynamics. Curr Biol 25:R1002–R1018. doi: 10.1016/j.cub.2015.08.051

Nachman I, Regev A, Ramanathan S (2007) Dissecting Timing Variability in Yeast Meiosis. Cell 131:544–556. doi: 10.1016/J.CELL.2007.09.044

Nicklas RB, Koch CA (1969) Chromosome micromanipulation. 3. Spindle fiber tension and the reorientation of mal-oriented chromosomes. J Cell Biol 43:40–50

Oakberg EF (1956) Duration of spermatogenesis in the mouse and timing of stages of the cycle of the seminiferous epithelium. Am J Anat 99:507–516. doi: 10.1002/aja.1000990307

Odartchenko N, Cottier H, Feinendegen LE, Bond VP (1964) Evaluation of mitotic time in vivo, using tritiated thymidine as a cell marker: successive labeling with time of separate mitotic phases. Exp Cell Res 35:402–11

Page SL, Hawley RS (2004) The genetics and molecular biology of the synaptonemal complex. Annu Rev Cell Dev Biol 20:525–558. doi: 10.1146/annurev.cellbio.19.111301.155141

Pelletier R-M (2011) The blood-testis barrier: the junctional permeability, the proteins and the lipids. Prog Histochem Cytochem 46:49–127. doi: 10.1016/j.proghi.2011.05.001

Pelletier RM, Byers SW (1992) The blood-testis barrier and Sertoli cell junctions: structural considerations. Microsc Res Tech 20:3–33. doi: 10.1002/jemt.1070200104

Peters AH, Plug AW, van Vugt MJ, de Boer P (1997) A drying-down technique for the spreading of mammalian meiocytes from the male and female germline. Chromosome Res 5:66–8

Rieder CL, Salmon ED (1998) The vertebrate cell kinetochore and its roles during mitosis. Trends Cell Biol 8:310–8

Sun S-C, Kim N-H (2012) Spindle assembly checkpoint and its regulators in meiosis. Hum Reprod Update 18:60–72. doi: 10.1093/humupd/dmr044

van Beneden (1883) Recherches sur la maturation de l'oeuf et la fécondatlon. Ascaris megalocephala. Arch Biol 4: 265-640

van der Heijden GW, Dieker JW, Derijck AAHA, et al (2005) Asymmetry in histone H3 variants and lysine methylation between paternal and maternal chromatin of the early mouse zygote. Mech Dev 122:1008–22. doi: 10.1016/j.mod.2005.04.009

van der Laan R, Uringa E-J, Wassenaar E, et al (2004) Ubiquitin ligase Rad18Sc localizes to the XY body and to other chromosomal regions that are unpaired and transcriptionally silenced during male meiotic prophase. J Cell Sci 117:5023–33. doi: 10.1242/jcs.01368

Xiao X, Mruk DD, Cheng CY (2013) Intercellular adhesion molecules (ICAMs) and spermatogenesis. Hum Reprod Update 19:167–186. doi: 10.1093/humupd/dms049

SUPPLEMENTAL FIGURES

Fig. S1. Summary of the observation of cells which were in prometaphase stage already in the beginning of the recording. Two cells (C31 and C32) displayed a high increase of the red (C31) or green (C32) signal after 5h and 10 min and 7h 20 min of the recording (red cross). Clear chromatin condensation (black point), ring configuration of chromosomes (green ring)
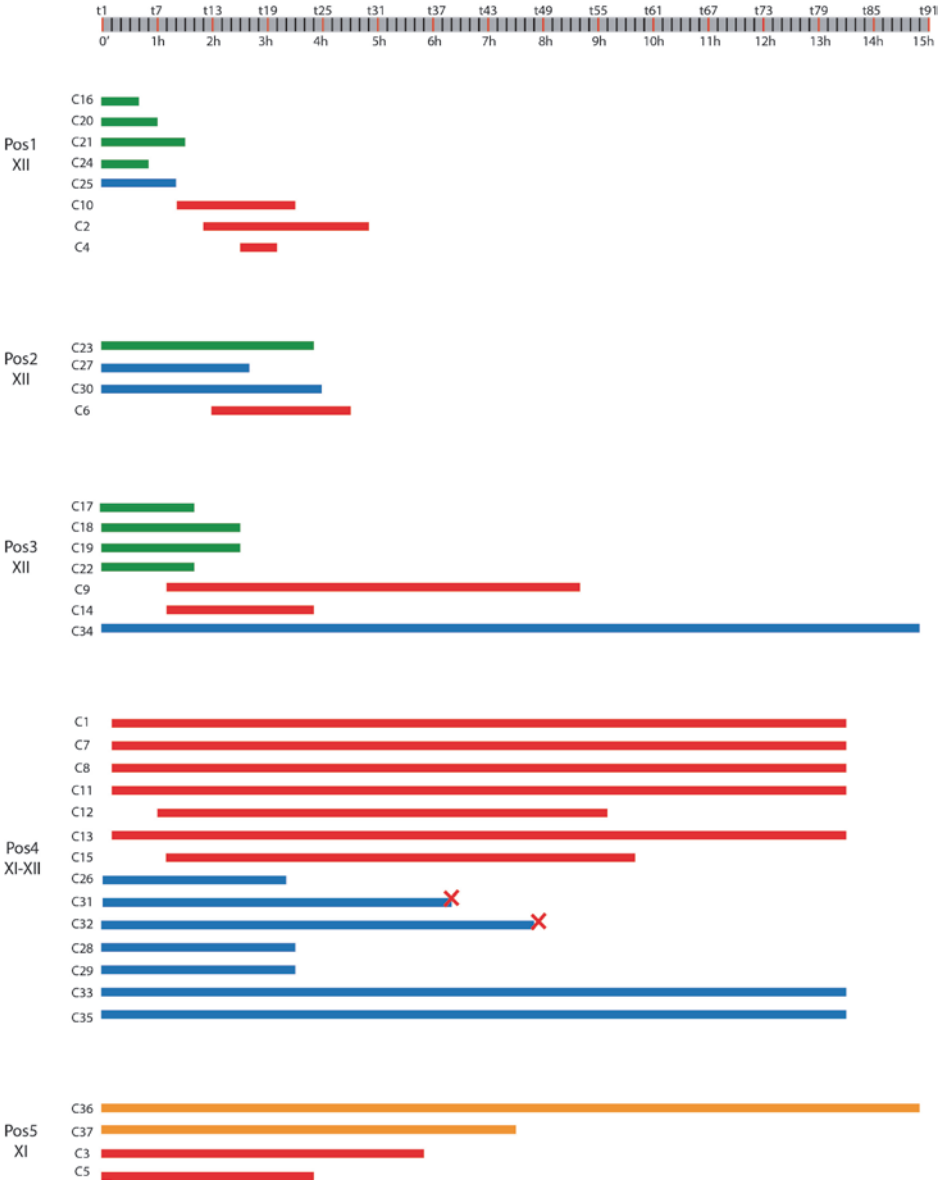
Fig. S2. Time during which the cells were recorded, per position. At the starting time points, cells were in diplotene (progressing up to metaphase, red bars; with metaphase-to-anaphase failure, orange bars) or (pro)metaphase (with or without progression to anaphase and secondary spermatocyte stage, green and blue bars, respectively). The "cross" indicates cells that died.

VIDEOS

Video 1. Metaphase-to-anaphase transition in mitosis (left) and meiosis (right). Starting time-point of division have been synchronized between the meiotic and the upper mitotic cells. Maximum projection (7 slices). 1 minute lapse, total recording 13 minutes. Arrows indicates the presence of a lagging chromosome/bivalent.

Video 2.Process of centromere biorientation before meiotic segregation (clear biorientation is achieved at t= 16 minutes). Maximum projection (7 slices). 1 minute lapse, total recording 20 minutes.

Video 3. Metaphase-to-anaphase transition and secondary spermatocyte formation during meiosis. Maximum projection (7 slices). 1 minute lapse, total recording 20 minutes. Arrows indicates the presence of lagging chromosome/bivalent.

Video 4. Time lapse imaging of the first five hours of position 1 (see Fig. S2). At t=1, cells are in pro(metaphase) stage (C16, C20, C21 and C25) or anaphase (C24). C16, C20, C21 and C24 progress to anaphase and secondary spermatocyte stage, while C25 remains in metaphase stage during the entire recording (see also Fig. 4, right side, and Fig. S1). A lateral flow of cells in the adluminal compartment can be observed. Cells that come into view as a result of this flow belong to stage XI (cells in diplotene stage appear at t= 9 (C10), t=12 (C2) and t=16 (C4), and progress up to prometaphase at t=17, t = 17 and t= 18, respectively) (see also Fig. 4, left side). Maximum projection (7 slices). 10 minutes lapse.

Video 5. Cell in the period of oscillation with small amplitude. A "chromatin unit" (probably a univalent) go inside and outside the metaphase plate multiple times during the recording (arrow). Maximum projection (13 slices). 1 minute lapse, total recording 56 minutes. Arrows indicates the presence of lagging chromosome/bivalent.

Videos can be found at: http://cluster15.erasmusmc.nl/enguitamarruedo/

(Username and password available upon request).
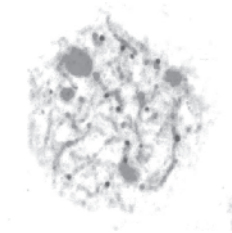
4A
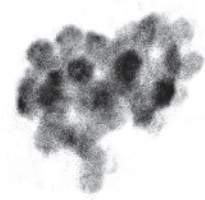
**Meiotic arrest occurs more frequently at metaphase
and is often incomplete in azoospermic men**

Submitted

Meiotic arrest occurs most frequently at metaphase and is often incomplete in azoospermic men

Andrea Enguita-Marruedo[1], Esther Sleddens-Linkels[1], Marja Ooms[1], Vera A. de Geus[1], Martina Wilke[2], Eric Blom[2], Gert R. Dohle[3], Leendert H.J. Looijenga[4,7], Wiggert van Cappellen[5], Esther B. Baart[6], and Willy M Baarends[1*]

1) Department of Developmental Biology

2) Department of Clinical genetics

3) Department of Urology

4) Department of Pathology

5) Department of Pathology/Erasmus Optical Imaging Centre

6) Department of Obstetrics and Gynaecology, Erasmus MC, University Medical Center Rotterdam, 7) Princess Maxima Center for Pediatrinc Oncology, Utrecht, The Netherlands.

*Corresponding author: w.baarends@erasmusmc.nl

Short title: Meiotic metaphase arrest in men

Key words: meiosis, meiotic checkpoint, XY body, infertility, metaphase arrest, meiotic arrest, spermatogenesis

4a

ABSTRACT

Study question:

Which meiotic checkpoints are activated in azoospermic males with spermatogenic impairments?

Summary answer:

By investigating testis biopsy material from selected patients with spermatogenic impairment, we most frequently observed partial or complete meiotic metaphase arrest, next to two novel arrest phenotypes, occurring just prior to, or shortly after meiotic division.

What is known already:

In mouse models for meiotic arrest, spermatogenesis has been described to arrest at either the pachytene stage of meiosis, due to a failure to complete chromosome pairing and/or meiotic DNA double-strand break repair, or at meiotic metaphase, due to failures in chromosome alignment. Meiotic arrest has been reported in 10-30% of azoospermic or severely oligospermic males, but the exact stage of arrest, and the underlying mechanisms remain unknown.

Study design, size, duration:

A retrospective observational study on surplus testis biopsy material (4% paraformaldehyde (PFA)-fixed and paraffin-embedded, (FFPE)) of 48 patients with severe spermatogenic impairment (Johnsen scores 3-6) and 13 controls with normal spermatogenesis (Johnsen score 10) collected between 2001 and 2013 were used for sectioning and subsequent immunofluorescent analyses.

Participants/materials, setting, methods:

Using an optimized combination of specific antibodies, we set up an immunofluorescent assay to assess meiotic entry, chromosome pairing, progression of DNA double-strand break (DSBs) repair, formation of meiotic metaphases, metaphase arrest, and spermatid formation in sections of FFPE testis biopsies. For selected patients, crossover frequency was also assessed in spermatocytes using the same method. Data collected from controls were used to set thresholds for normal values, and this allowed classification of arrest phenotypes in the patient group.

Main results and the role of chance:

Quantitative analyses of the results allowed definition of specific subgroups, characterized by different complete or incomplete meiotic arrests. Complete metaphase arrest, characterized by increased metaphase apoptosis and absence of spermatids, was observed most frequently (13 patients, 27.1%). In this subgroup, the 4 patients with the highest frequency of apoptotic metaphases also displayed a reduction in crossover number.

Incomplete metaphase arrest was observed in 8 patients (16.7%). The occurrence of (partial) metaphase arrest was interpreted as activation of the so-called Spindle Assembly Checkpoint. A subgroup of only 4 patients (8.3%) displayed a failure to complete the chromosome pairing process. Together with the absence of later cell types, this was interpreted as activation of the so-called pachytene checkpoint. Two new types of meiotic arrest were defined: premetaphase arrest, characterized by presence of pachytene spermatocytes but absence of meiotic metaphases, and postmetaphase arrest, whereby normal development was observed up to meiotic metaphase, but no spermatids were detected (7 and 6 patients, 14.6 and 12.5%, respectively).

Limitations, reasons for caution:

The number of control samples that were used to set thresholds is relatively small. When the obtained value for a specific parameter in the patient group is close to the defined threshold, classification of the patient is less reliable. Future studies that increase the number of controls could more precisely define these thresholds. If a staining result is negative, the possibility of fixation artefacts should be considered.

Wider implications of the findings:

Using a large patient group with the relatively rare phenotype of (partial) meiotic arrest, and a new approach that is applicable to surplus biopsy material, we have classified azoospermic patients based on the type of meiotic arrest. This classification provides insight into the mechanisms of spermatogenic arrest, and can be used as support tool to select candidate causative mutations in combination with exome sequencing. It also provides a first step towards development of a risk assessment tool to determine feasibility and safety of using testicular sperm or spermatids for assisted reproduction in individual cases.

INTRODUCTION

Spermatogenesis is a complex process involving mitotic amplification, followed by meiosis, and the differentiation of haploid spermatids into mature spermatozoa (spermiogenesis). The quality of the haploid (epi)genome of a male germ cell depends on the activity of checkpoint mechanisms. These should induce apoptosis of germ cells in which damage has been accumulated, or in which some developmental step was not properly completed.

Several specific checkpoints that operate during spermatogenesis have been described for mice, and all are active during meiosis (Roeder and Bailis 2000; Eaker et al. 2002; Barchi et al. 2005; Royo et al. 2010; MacQueen and Hochwagen 2011; Faisal and Kauppi 2016). Meiosis is at the heart of gametogenesis, and required to generate haploid cells from diploid precursors. Meiosis is inherently potentially damaging to the genome, because it involves the induction and repair of around 200 DNA double-strand breaks (DSBs) at the onset of meiotic prophase in mammals (Moens et al. 2002; Cole et al. 2012). Meiotic DSB formation is an essential process that allows homologous chromosomes to search for each other and form pairs (Baudat et al. 2000; Romanienko and Camerini-Otero 2000). Once this pairing has been achieved, homologous chromosomes become physically connected by the formation of a protein structure between them, the synaptonemal complex, in a process called synapsis. In males, the X and Y chromosome share homology only in a short area, the pseudo-autosomal region (PAR), and synapsis is restricted to this region. The presence of the asynapsed X and Y chromosome arms is associated with the formation of the XY body at pachytene, a transcriptionally silenced chromatin region that carries specific epigenetic marks (Turner et al. 2005; Baarends et al. 2005).

Proper XY body formation relies on completion of chromosome pairing and DSB repair on the autosomes (Homolka et al. 2007). Intriguingly, the so-called pachytene checkpoint, which eliminates spermatocytes in which chromosomes have failed to complete synapsis, is functionally coupled to failure to form the XY body in male mice (Royo et al. 2010). In the absence of proper transcriptional silencing of the sex chromosomes, the aberrant activation of X- and/or Y-linked genes triggers the apoptotic process (Royo et al. 2010). In addition, a second, DNA damage-dependent, checkpoint operates, somewhat later during pachytene (Pacheco et al. 2015; Marcet-Ortega et al. 2017). In mouse, it has been shown that targeted mutation of genes important for meiotic DSB formation, DSB repair, or chromosome pairing almost invariably results in apoptotic elimination of virtually all spermatocytes at mid pachytene (de Rooij and de Boer 2003; Barchi et al. 2005; Hamer et al. 2008; Burgoyne et al. 2009).

If repair and chromosome pairing occur normally, the next checkpoint comes into play, which assures the correct segregation of the chromosomes at the metaphase-to-anaphase transition. This is the so-called Spindle Assembly Checkpoint (SAC,) which functions in both mitosis and meiosis (Sun and Kim 2012; Musacchio 2015; Faisal and Kauppi 2016; Marston and Wassmann 2017). In mammalian cells the SAC is activated prior to each cell division, and delays anaphase onset until all chromosomes are properly aligned on the metaphase plate, and correct tension is established between two poles (created by the attached microtubules) (Musacchio 2015). In meiosis I, the organisation of chromosomes is essentially different from mitosis. Pairs of homologous chromosomes, connected by chiasmata (the visible manifestation of crossovers) need to be separated, and therefore, sister kinetochores from one chromosome attach to microtubules emanating from the same pole, and the two pairs of sister kinetochores from the homologous chromosome need to attach to opposite poles. When this situation is achieved for all chromosome pairs, the SAC should be inactivated. Then, sister chromatid cohesion along the chromosomal arms is released, and anaphase and the actual reductional division follow. The regulation of the mammalian meiotic SAC and its efficiency in case only a single chromosome pair remains unattached varies depending on sex and species. For instance, in male mouse meiosis, activation of the SAC in case of a single misaligned bivalent is extremely efficient (Vernet et al. 2011; Faisal and Kauppi 2016). In contrast, in both mouse and human female meiosis, the presence of univalent chromosomes may delay anaphase, but usually the division eventually continues, resulting in an aneuploid oocyte (Greaney et al. 2017; Marston and Wassmann 2017).

In normal fertile control human males, approximately 2-4% of sperm cells are aneuploid (Templado et al. 2013). The sex chromosomes and chromosome 21 are most prone to segregation errors, and also most frequently observed as univalents in meiotic metaphases. Similarly, in normal mice, around 1% of sperm cells has been estimated to be aneuploid (Lowe et al. 1996). For human male infertility patients that are diagnosed with nonobstructive azoospermia, aneuploidy frequencies are significantly higher (Tempest 2011). This might indicate that when spermatogenesis is impaired in men, the SAC cannot always efficiently act, resulting in formation of more aneuploid sperm. In contrast, removal of spermatocytes with univalents is extremely efficient in mice, in particular when concerning the sex chromosomes, since 50% failure of XY recombination did not lead to an increase in sperm with aneuploidy for the sex chromosomes, unless the checkpoint was impaired (Faisal and Kauppi 2017). Instead, an increase in metaphase I apoptosis was observed, indicative of SAC mediated arrest followed by programmed cell death. In infertile men, occurrence of meiotic arrest phenotypes has also been described, and estimations of the percentage of oligo- or azoospermic patients in which a meiotic arrest occurs vary

between 10 and 30%, mostly based on morphological assessment of germ cell types present in histological sections of testis biopsies (Martin-du Pan and Campana 1993; Foresta et al. 1995; Tesarik et al. 1998; North et al. 2004; Guichaoua et al. 2005; Topping et al. 2006; Sun et al. 2007; Hann et al. 2011; Weedin et al. 2011). It has been suggested for a long time that failure to repair meiotic DSBs or to form crossover could cause meiotic arrest in at least part of these patients (Hultén et al. 1970, 1974; Pearson et al. 1970; Templado et al. 1976, 1980; Thomson et al. 1979; Chaganti and German 1979; Mićić et al. 1982). In addition, several publications have performed detailed analyses of different meiotic parameters, such as progression of chromosome pairing and crossover formation(Vidal et al. 1982; Guichaoua et al. 2005; Codina-Pascual et al. 2005; Sciurano et al. 2006, 2012). More recently, RNA sequencing analyses have also been performed to characterize a small group of selected patients that displayed a failure to form XY bodies, and an association with misregulation of genes involved in the so-called "pachytene arrest" in mouse was reported (Jan et al. 2018). However, in general, arrest phenotypes in azoospermic or severely oligospermic males remain poorly characterized and very few genetic causes of nonobstructive azoospermia in men have been identified (Tüttelmann et al. 2018). The most relevant and most recently described gene for which mutations are clearly associated with a "maturation arrest" phenotype is the X-linked *TEX11* gene (Yatsenko et al. 2015). This gene encodes a protein that has been shown to be required for proper chromosome pairing as well as crossover formation in mouse (Yang et al. 2008). In carriers of numerical (sex) chromosome aberrations or chromosome translocations, different meiotic defects have also been described in association with maturation arrest and oligozoospermia or azoospermia (Faed et al. 1982; Rosenmann et al. 1985; Gabriel-Robez et al. 1986, 1987, 1988.; Batanian and Hulten 1987; Guichaoua et al. 1990; Johannisson et al. 1993; Solari and Rey Valzacchi 1997; Pigozzi et al. 2005; Li et al. 2017).

  Here we aimed to obtain more insight in the types, frequency, and completeness of meiotic arrest in patients with severe spermatogenic impairment. We developed an optimized set of validated protein markers to reliably identify cells at different stages of spermatogenesis by immunofluorescent staining of surplus paraffin-embedded testis biopsy samples. We used the phosphorylated form of the histone variant H2AX (γH2AX) that is a well-known marker of DSBs and of the XY body, to distinguish the stages of meiotic prophase (Mahadevaiah et al. 2001). Another histone modification, phosphorylation of Histone 3 at serine 10 (H3s10ph), marks mitotic and meiotic metaphase chromosomes (Song et al. 2011). We used an anti-acrosome antibody to detect the presence of spermatids (Moore et al. 1987). The use of this immunofluorescent approach allowed a novel and precise determination of cells at specific stages of spermatogenesis, permitting the classification of patients in different groups.

Additionally, we assessed the presence and number of crossover sites using an antibody directed against the protein MLH1. This protein is known to mark future crossover sites in pachytene spermatocytes (Barlow and Hultén 1998). Interestingly, we also identified γH2AX as a bona fide marker of apoptotic meiotic metaphases, and found that spermatogenesis most frequently arrests at meiotic metaphase in men with severe spermatogenic impairment, likely due to the activation of a spindle assembly checkpoint. Intriguingly, we also identified a relatively large group of patients in which cells arrested just prior to entry in meiotic metaphase stage or immediately following this stage.

This immunostaining protocol will be of help in establishing genotype-phenotype relationships in combination with exome or whole-genome sequencing approaches. In addition, the partial arrest phenotypes should be further analysed to determine a possible relationship with (epi)genetic disturbances of developed spermatids.

RESULTS

Immunofluorescent analyses of progression of spermatogenesis in paraffin-embedded testis biopsies

We analysed testis biopsies from 48 non-obstructive azoospermic patients with Johnsen scores (JS) S3-6 or a classification of disturbed spermatogenesis (16% of the total group of patients, see Materials and Methods). 15 patients with JS10 (normal spermatogenesis) served as controls. In order to evaluate progression through spermatogenesis, we optimized an immunofluorescent staining protocol for analysis of paraffin sections of both controls and patients. The most important adaptation involved addition of a proteinase K step, to increase epitope accession and reduce background. First, we assessed whether entry in meiotic prophase and subsequent progression up to meiotic metaphase were normal using specific antibodies against phosphorylated H2AX (γH2AX) and anti-phosphorylated H3 (H3Ser10ph). γH2AX served to detect meiotic DSBs (entry into meiosis) and XY body formation (which occurs at pachytene, when synapsis is complete). H3Ser10ph was used as a marker of metaphase chromosomes. When we analysed the staining patterns of the antibodies in our control samples, we observed that in early meiotic prophase cells, γH2AX signal was distributed in patches throughout the nucleus (Fig. 1A, meiotic entry). In pachytene nuclei, γH2AX signal became restricted to the chromatin of the XY pair (Fig. 1A, XY body). Using higher magnification, substages of meiotic prophase could be distinguished in more detail (Fig. 1B). During leptotene or early zygotene, γH2AX was distributed in patches covering the whole nucleus. In late zygotene, γH2AX signal appeared as a limited number of

foci or patches, and then accumulated only on the XY body in pachytene, whereby an elongated XY body shape was observed in early pachytene, and a rounded shape in mid- and late pachytene. Cells in metaphase stage are marked by H3Ser10ph (Fig. 1A, metaphases). Occasionally, metaphase chromosomes also displayed intense γH2AX signal along the condensed chromosomes. This staining covered the whole metaphase plate, and was therefore very different compared to the more focal γH2AX patches that can be observed in association with (meiotic) DSBs. It was a rare observation in controls, but very frequent in some of the patients, and thus possibly indicative of aberrant development. This type of pan-chromosomal γH2AX staining has been described as a hallmark of cells entering apoptosis (Solier and Pommier 2014). Therefore we considered these aberrant metaphases as having entered an apoptotic pathway (Fig. 1A, apoptotic metaphase). As H3ser10ph marks both meiotic and mitotic metaphases, we cannot a priori discriminate between them, but mitotic metaphases are mostly localized to the basal side of the tubule, whereas meiotic metaphases localized closer to the lumen.

To assess progression of spermiogenesis, an antibody that labelled the acrosome of the spermatids was used (Fig. 1A, spermatids), and different steps of spermatid differentiation could be distinguished (Fig. 1C). The acrosome signal appeared as a small sphere corresponding to the acrosome vesicle in type 1 spermatids, and spread in a moon crescent shape over the nucleus in type 2. In type 3, the nucleus was more elongated. Type 4 and 5 spermatids presented an elongated nucleus and a spread and V-shaped acrosome signal. Type 5 spermatids were approximately half the size of type 4, indicating that elongation but also condensation had taken place. In control samples, all these stages were always present.

We quantified meiotic entry, XY body formation, and (apoptotic) metaphases for the patients with JS 10 (normal spermatogenesis, controls) and the patients with Johnsen score 3-6. In addition, the presence of spermatids was scored, as well as the most advanced type of spermatid observed. Next, we set thresholds for each parameter, and interpreted the results in terms of the type of spermatogenic arrest, as outlined below.

▶ **Fig. 1. Progression of spermatogenesis in paraffin-embedded testis sections. A)** Immunostaining of γH2AX (green) (control, first two set of images), γH2AX (green) and H3S10ph (red) (control and patient displaying metaphase arrest, second two set of images) and acrosome (green) (control, last set of images). **B)** Meiotic prophase stages present in controls (late zygotene (LZ) nucleus is magnification of LZ indicated in (A)). Immunostaining of γH2AX (green). **C)** Types of spermatids in the control, according to the developmental level of the acrosome. Immunostaining of acrosome (green). Scale bar 10 μm.
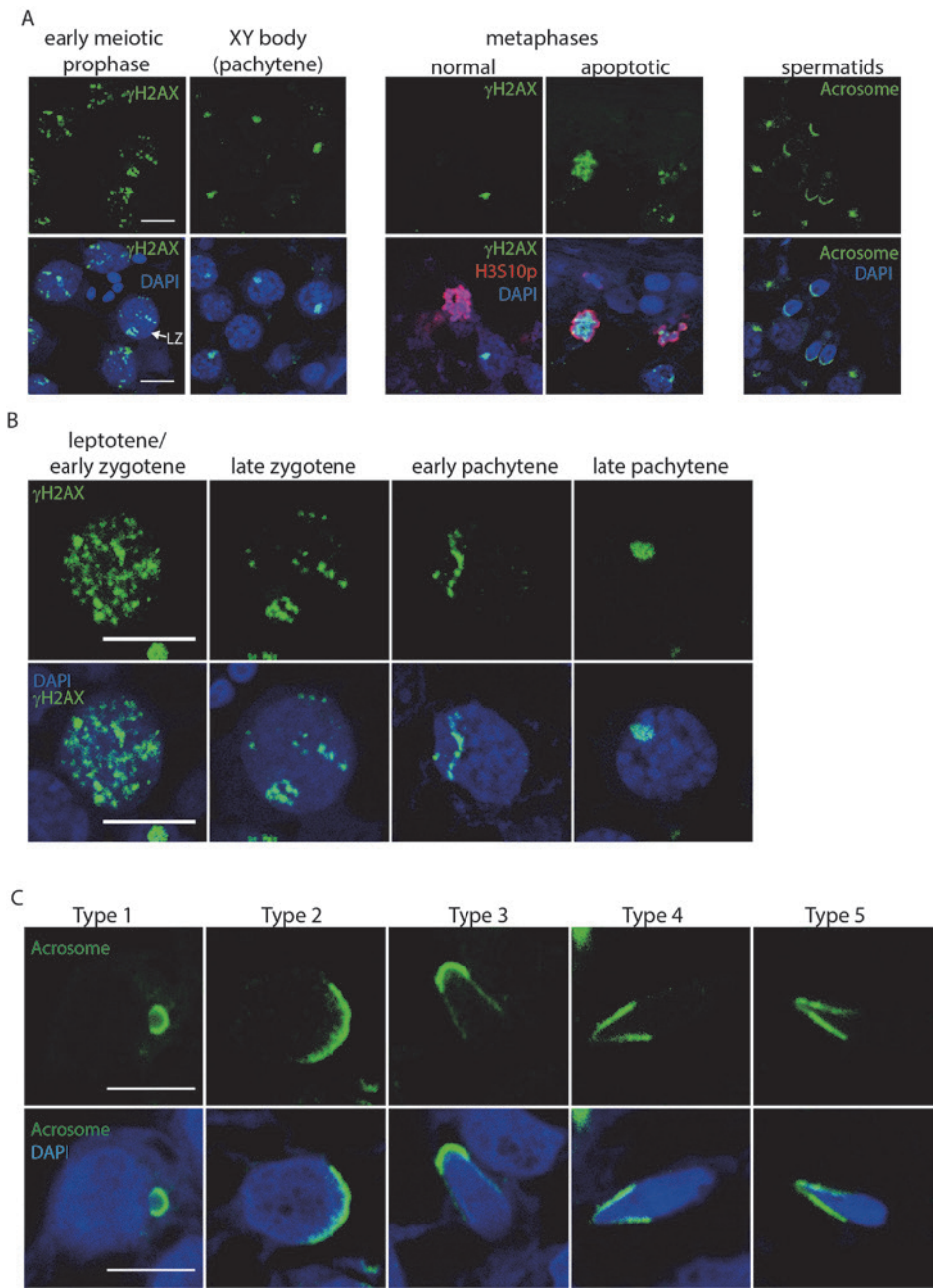
Meiotic entry

In order to analyse the capacity of spermatogonia to enter meiotic prophase, we calculated the percentage of round tubule sections containing early meiotic prophase cells (% EC+T) (Fig. 2A). Controls (n=13) showed a mean percentage of EC+T of 88.2 ± 18.6. We defined a threshold at 40% EC+T (based on the lowest control value (no outlier), see Materials and Methods) above which we considered meiotic entry frequency to be normal. 1 patient (P10) showed total absence of early cells (classified as Group I: Failure to enter meiosis, Table I), this was 1 of the 2 patients that carried an *AZFc* deletion. 2 patients (P4 and P18) showed a reduction in % EC+T (15.4 and 29.0 %) (Fig. 2A, light green dots). For the other 45 patients we observed a percentage of EC+T of 49.4 or higher.

XY body formation (activation of pachytene checkpoint)

Subsequently, we analysed the percentage of round tubule sections containing XY bodies (% XY +T) (Fig. 2B). In controls, 96.5 ± 4.5% of the counted tubules contained XY bodies. As expected, no tubules containing XY bodies were found in the patient with no meiotic entry (P10, dark green dot). From the patients whereby normal or reduced entry into meiotic prophase was observed, 4 displayed a complete lack of XY bodies in the testis biopsy. So in these patients, spermatocytes enter meiotic prophase, but fail to accomplish a normal pachytene configuration whereby the autosomal chromosome pairs display complete synapsis and the XY body is formed. These were classified as Group II: Failure to form the XY body (Table I). The rest of the patients showed a very wide range of %XY+T, whereby the percentage was below the normal threshold that was set at 80% (see Materials and Methods) for 29 patients, including the 2 patients for whom reduced meiotic entry was determined (light green dots in Fig. 2B, and Table I). To assess the efficiency of progression from early meiotic prophase up to pachytene (XY body present), independent of meiotic entry, we assessed the number of XY bodies per XY+T (Fig. 2C). More than 7.7 XY bodies per XY+T was set as a threshold for normal XY body formation. We observed a reduced number of XY bodies in XY+T for 21 patients, compared to the controls. In these patients, spermatocytes reach pachytene, but with reduced efficiency, indicating cell loss at some point between meiotic entry and pachytene.

Further analysis of meiotic prophase in the 4 patients with complete failure in XY body formation (Group II, Table I) revealed some differences in the phenotype (Fig. 3): P3 and P33 presented tubules with groups of early cells, as we also observed in control samples. The most advanced cell type present in these patients was leptotene/early zygotene, indicating a global failure to complete chromosome pairing (Fig. 3A). In contrast, P7 and P25 presented
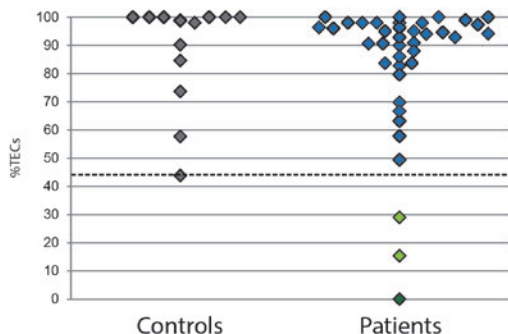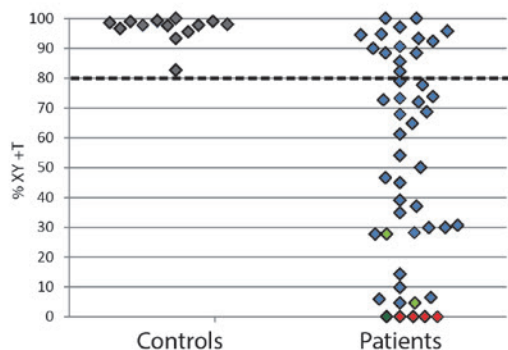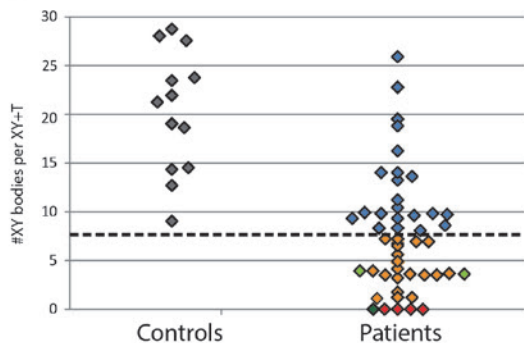
Figure 2. Assessment of meiotic entry and XY body formation A) Meiotic entry. Percentage of tubules that contain early cells. B and C) XY body formation. B) Percentage of tubules that contains XY body positive cells. C) Number of XY bodies per XY body positive tubule. Color code: grey (control), blue (patient, no further classification), dark green (patients displaying no meiotic entry), red (patients displaying no XY body formation), light green (patients displaying reduced meiotic entry and reduced XY body formation), orange (patients displaying reduced XY body formation). Dashed line: threshold.

4a

generally only one early cell per tubule and these cells were observed to reach late zygotene (Fig 3B). Thus, in these patients, fewer cells appeared to enter meiotic prophase, but these individual cells were then able to progress somewhat further in chromosome pairing compared to P3. Intriguingly, spermatocyte nuclei of P25 were half the size of the nuclei observed in the other 3 patient biopsies in this group. This could indicate a gross alteration in nuclear/chromatin structure in spermatocytes of this patient, but fixation artefacts cannot be excluded.

Capacity to reach metaphase I

Once cells achieve XY body formation, it is expected that they would be able to reach metaphase. Because of the overall rarity of metaphases, we decided to score the total number of metaphases per section, and then normalize to the total area evaluated (number of metaphases per mm^2). Metaphases were detected in all control and patient samples. Taking all the data together, we observed a clear positive correlation between the number of metaphases counted and the number of XY bodies per XY+T per control/patient (R^2 0.35, p value <0.0001, Fig. 4A). Based upon the control values, a threshold of 2.53 could be set below which we considered the capacity to reach metaphase as reduced. If no pachytene spermatocytes were observed within a biopsy, all observed metaphases are expected to be of mitotic origin. The normalized values of the metaphase counts obtained for this group of patients (failure to enter meiosis, and failure to form the XY body) were used to define a threshold of 1.83 metaphases/mm^2, below which we considered that the cells fail to reach the meiotic metaphase stage (assuming a normal frequency of mitotic metaphases in these cases). We observed a subgroup of 8 patients with a reduced number of XY bodies per XY+T, for which the number of metaphases fell below this threshold (Table 1). In only 1 of these, P46, we detected some spermatids (including type 5 spermatids). This indicates that there must be rare cells that reach metaphase I and complete the meiotic divisions. The other 7 patients completely lacked spermatids, indicating that in addition to inefficient progression through prophase, the cells of the patients in this group are incapable of reaching meiotic metaphase I. These 7 patients were classified as Group III: Failure to reach meiotic metaphase (Table I). In only 1 patient of this subgroup (P44), we frequently observed spermatocyte nuclei that displayed a ring-like γH2AX pattern following the edge of the nucleus or an intense global γH2AX staining (Fig. 4B, top), rarely seen in controls. These patterns have been reported as indicative for early and late apoptotic cells, respectively (Solier and Pommier 2014). Thus most likely the spermatocytes in this patient enter apoptosis at some point in the transition from pachytene to metaphase. For the other 6 patients in this group, it was not clear whether spermatocytes were lost through apoptosis,

nor was it clear at which substage most spermatocytes were lost, since all were also clearly less efficient in reaching pachytene (XY body formation was reduced).
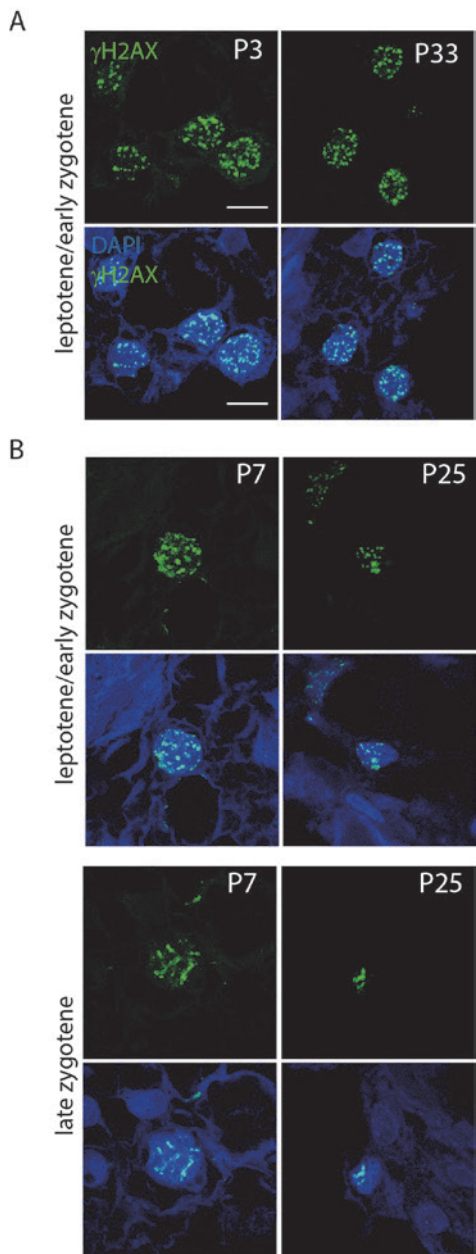
Fig. 3. XY body failure. A) and **B)** aberrations in the γH2AX pattern (green staining) in samples of patients displaying failure to form XY body. P3 and P33, both displayed clusters of cells in early zygotene. However, P7 and P25 reach a somewhat further advanced zygotene-like stage, but only few and single spermatocyte nuclei were observed. Scale bar 10 μm. Patient numbers are indicated on the images.

Presence of apoptotic metaphases (activation of the SAC)

If meiotic metaphases are detected in a biopsy, these might be normal, or aberrant and actually be arrested due to problems in for example alignment and bi-orientation of the bivalents or spindle formation. In contrast to mitotic cells, where metaphase arrest is usually transient, meiotic metaphase arrest due to for example lack of crossover formation is known to be permanent, and associated with apoptosis in mouse (Eaker et al. 2002). When spermatogenesis progresses normally, a small percentage of apoptotic meiotic metaphases would be expected. This assumption is based on the reported occasional lack of crossover formation (based on lack of detectable MLH1 foci or absence of chiasmata for single bivalents in a small percentage of normal human spermatocytes) (Codina-Pascual et al. 2006; Uroz and Templado 2012), that may trigger activation of the SAC followed by induction of apoptosis (Burgoyne et al. 2009). For human biopsies that contained meiotic metaphases, we determined the percentage of apoptotic metaphases, assuming that any increase in total metaphase apoptosis frequency would be mainly caused by an increase in the occurrence of meiotic apoptotic metaphases (these patients display normal meiotic entry, and are thus unlikely to experience increased mitotic metaphase apoptosis). The mean percentage of apoptotic metaphases in the control group was 4.6% ± 3.4 (Fig. 4C, and Table I), and a threshold was defined at 11.5 % apoptotic metaphases. For 21 patients the observed percentage of apoptotic metaphases was higher than the threshold, indicating frequent activation of the SAC, leading to apoptosis. Some of these patients also displayed a reduced number of XY bodies per XY+T, but no significant correlation between these two parameters was observed (R^2 0.00729, p value 0.6205). To determine whether the activation of the SAC resulted in complete metaphase I (or II) arrest, the presence of spermatids was analysed (Fig. 4D, and Table I). For 13 of the 21 patients that showed increased metaphase apoptosis, no spermatids were detected, indicating complete metaphase arrest. These patients were classified as Group IV: complete metaphase arrest (Table I). For 1 patient in this group (P9) we observed many nuclei with a pan-nuclear apoptotic γH2AX signal, similar to what was observed in P44 (Fig. 4B, middle image). This was observed in addition to the apoptotic metaphases. Since P9 also displayed a very high density of metaphases (7.54 metaphases/mm^2), this suggests that there is little cell loss of spermatocytes prior to meiotic metaphase, and that these cells die shortly after metaphase I, or directly after the meiotic division(s).

4a
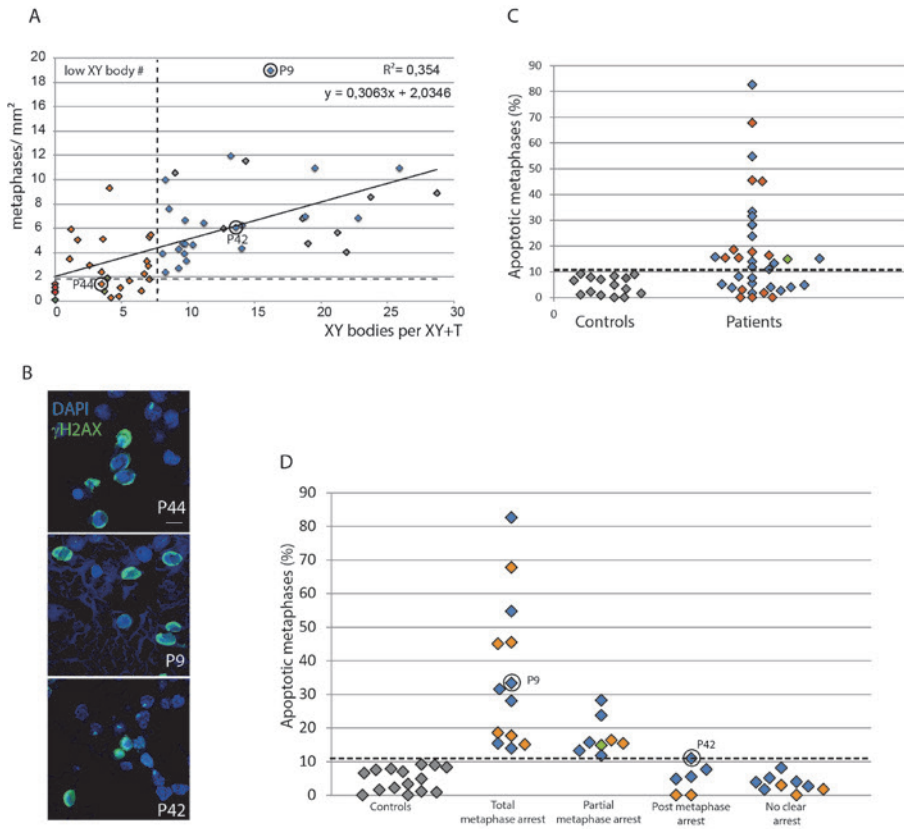
Fig. 4. Assessment of meiotic metaphase. A) Correlation between the number of XY bodies per XY+T, and the number of metaphases per mm^2. p value <0.0001. Color code: grey (controls), blue (patients, no further classification), dark green (patients, no meiotic entry), red (patients, no XY body formation), light green (patients, reduced meiotic entry and reduced XY body formation), orange (patients, reduced XY body formation). Dashed line: threshold. **B)** Representative images of pan-nuclear γH2AX staining in samples of P44 (Group III, failure to reach metaphase) and P9 (Group IV, complete metaphase arrest), and P42 (Group VI, postmetaphase arrest). **C)** Percentages of apoptotic metaphases. **D)** Further classification of patients depending on the presence/absence of spermatids. Scale bar 10 μm. Patient numbers are indicated on the images.

4 patients from Group IV displayed more specific aberrations in the γH2AX staining pattern during pachytene. Of these, P40 displayed persistent breaks in pachytene (in combination with partial failure to form the XY body) (Fig. 5A). For the three others, (P13,14 and 24) we often observed abnormal XY bodies or two (or more) γH2AX-positive XY body-like structures (Fig. 5B). For P13 ((46,XY,inv(1)(p21q32.1)), it seems reasonable to interpret the presence of an extra XY body-like γH2AX domain as the presence of γH2AX on an incompletely synapsed

bivalent of chromosome 1 (due to the inversion), in addition to a normal XY body. For P14 and P24, chromosomal aberrations may also be suspected, even if they were not detected in the karyotype analysis. Interestingly, in addition to P13, the other patient (P35) diagnosed with a structural genetic abnormality (46X,t(Y;19)(q12;q13.3)), was also included in this Group IV, but no XY body aberration was observed here.

Finally, the remaining 8 patients with a high percentage of apoptotic metaphases also contained spermatids in the biopsy, and these were classified as Group V: partial metaphase arrest (Table I). In total, 17 of the 48 analysed patients (35.4%) (Table I) displayed spermatids in their biopsy. However, we (occasionally) observed the most mature type 5 in only 3 out of these 17 patients. Interestingly, the most advanced spermatid types present in biopsies of Group V patients (partial metaphase arrest), were in general type 2 or 3, indicating that when the SAC is frequently activated, surviving spermatids are mostly incapable of completing spermatogenesis.

Absence of spermatids

Of the remaining 15 patients displaying normal values for all parameters analysed 6 were categorized as group VI: patients with postmetaphase arrest, since they lacked spermatids (Fig. 4D, Table I). For only 1 patient in this group we observed apoptotic nuclei (P42; Fig. 4B, bottom image), similar to those of P44 (Group III ; failure to reach metaphase) and P9 (Group IV; complete metaphase arrest). Since there was no clear evidence for activation of the metaphase checkpoint (10.9% apoptotic metaphases), we infer that these apoptotic cells correspond to secondary spermatocytes or very early spermatids. 9 patients did display spermatids in the biopsy, whereby all other assessed parameters normal. These were classified as group VII: patients with no clear meiotic arrest (Fig. 4D, Table I).

Classification of patients according to the type and degree of spermatogenic arrest

In total seven categories of patients were defined (Table I, Fig. 6). This classification is based on five of the parameters that we analysed: entry in meiosis, presence/absence of XY bodies, presence of meiotic metaphases, percentage of apoptotic metaphases and presence of spermatids. Partial failure to form the XY body did not have much discriminative value in relation to the type of meiotic arrest. Therefore, this condition was not taken into account in the classification system. In our set of 48 samples, failure to enter meiosis (category 1) was observed only once (2%, Fig. 5). Also, only 8.3% of the cases displayed complete activation of the pachytene checkpoint (failure to form the XY body), while 44 % displayed activation of the SAC, resulting in complete or partial metaphase arrest (27% and 17%, respectively, Fig.

6). In addition to the pachytene and metaphase checkpoint, two additional types of arrest were defined: pre-metaphase and post-metaphase arrest (15% and 13%, respectively). Finally, 19% of the patients' biopsies did not present a clear meiotic arrest.
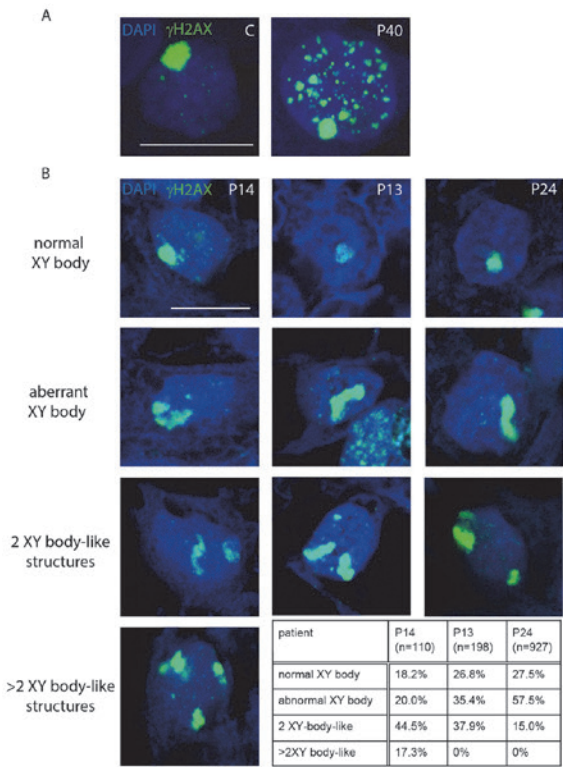
Fig. 5. Aberrations in pachytene spermatocytes. A) Control (C) pachytene nucleus, and pachytene nucleus of patient P40, displaying many persistent small patches of γH2AX staining, indicative of persistent meiotic DSBs. **B)** Pachytene nuclei from three patients with aberrant XY body-like structures:, P14, P13, and P24, all displaying varying aberrant XY body-like structures in the indicated percentages in the Table in the lower right corner. n indicates number of nuclei analysed. All three patients were diagnosed with complete metaphase arrest and reduced MLH1 foci number. P13 displayed a chromosomal abnormality (46, XY, inv(1)(p21q32.1)). Scale bars 10 µm. Patient numbers are indicated on the images.

patient	P14 (n=110)	P13 (n=198)	P24 (n=927)
normal XY body	18.2%	26.8%	27.5%
abnormal XY body	20.0%	35.4%	57.5%
2 XY-body-like	44.5%	37.9%	15.0%
>2XY body-like	17.3%	0%	0%

Complete metaphase arrest and crossover frequency

MLH1 is a mismatch repair protein which marks the future sites of cross-overs during the pachytene stage of meiosis I. Lack of crossover formation is a well-known trigger for metaphase checkpoint activation in mouse spermatocytes (Gorbsky 2015). To assess whether patients for whom we had observed complete metaphase arrest also showed a reduced crossover frequency, immunofluorescent analyses were performed. Antibodies against MLH1 and SYCP3 (marker of the chromosomal axes) were used (Fig. 7A). We counted the number of MLH1 foci of 5-6 nuclei from each of the 13 patients with complete metaphase arrest, and 7 randomly chosen controls. 2 patients were excluded from the analysis, since no staining for MLH1 and SYCP3 was obtained. In total 11 patients (56 nuclei)

and 7 controls (37 nuclei) were analysed. The number of detected MLH1 foci in control nuclei varied from 21 to 57 per spermatocyte (mean 40.8). For the patients we observed a range of 5 to 77 MLH1 foci per spermatocyte. The mean numbers of MLH1 foci in patients and controls are shown in Fig. 7B. More than 30 MLH1 foci per spermatocyte was set as a threshold for a normal average MLH1 foci number (see Materials and Methods).
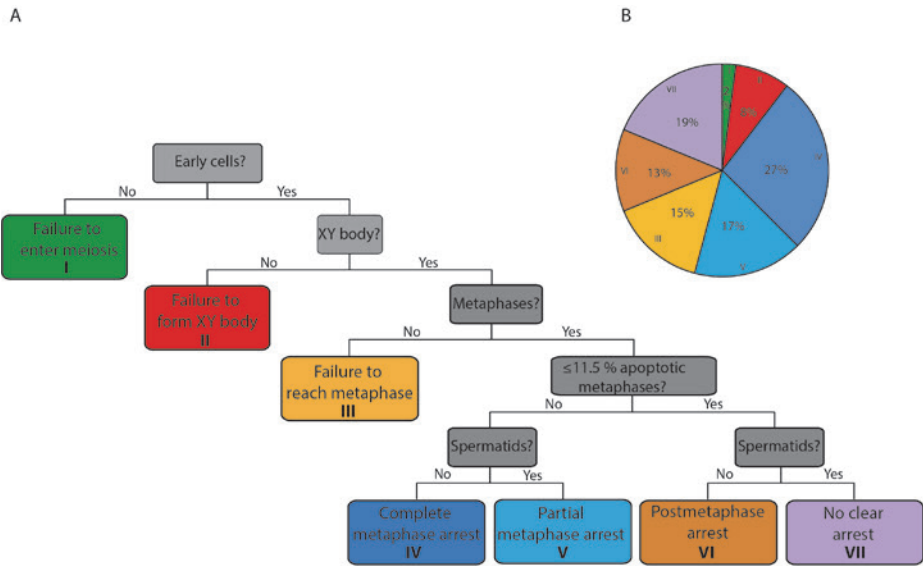
Fig. 6. Patient classification and frequency of different meiotic arrest types. A) decision tree for the classification of patients with severe spermatogenic impairment ,and **B),** pie diagram showing the percentages of testis biopsies belonging to each category.

4 patients were found to have a reduced number of MLH1 foci according to our definition. Interestingly, the three patients for whom we had observed more than 1 XY body-like structure (P24, P14 and P13) were included in this group (marked with a red circle). The variability in MLH1 foci among spermatocytes is shown in Fig. 7C. While all the nuclei from patients P12 and P24 were below the set threshold, MLH1 foci numbers in pachytene nuclei of the P14 and P13 biopsies were more variable. Analysis of the relation between the mean number of MLH1 foci and the percentage of apoptotic metaphases (Fig. 7D) showed that the four patients with a reduced number of MLH1 foci also displayed the highest percentage of apoptotic metaphases (45 to 82.5% apoptotic metaphases).

DISCUSSION

Here, we have optimized a classification system for testis biopsies of patients with spermatogenic impairment, according to their spermatogenic defect. We have used the current knowledge regarding parameters for activation of meiotic checkpoints in mouse spermatogenesis in an immunocytochemical approach. Different parameters were analysed in a quantitative manner, and five of these were found to be informative for classification of the patient biopsies: entry in meiosis, presence/absence of XY bodies, presence of meiotic metaphases, percentage of apoptotic metaphases and presence of spermatids. From these, the percentage of apoptotic metaphases was found to be the major discriminator to define cases with (complete) meiotic arrest. Thus, two immunostainings and relatively simple scoring methods have resulted in a fast classification method that can be further optimized for use in diagnosis of patients with severe spermatogenic impairment.

Uniform activation of known meiotic checkpoints indicates a genetic cause of spermatogenic arrest

This study, involving analyses of 48 azoospermic men with signs of spermatogenic arrest, shows that the metaphase checkpoint is more frequently uniformly activated than the pachytene checkpoint (27% (Group IV) and 8% (Group II) of the cases, respectively). Specific knockout of genes expected to exert meiotic functions in mice has most frequently resulted in pachytene checkpoint activation (de Rooij and de Boer 2003; Barchi et al. 2005). In such models, DSB formation, overall DSB repair, and/or chromosome pairing were severely affected. Therefore, such genes might be mutated in patients displaying failure to form XY bodies. Since we selected patients whose early meiotic cells display DSB formation (as indicated by the pan-nuclear γH2AX patches), we would expect mutations in genes related to DSB repair, or chromosome pairing. In a recent study of azoospermic men (Jan et al. 2018), nine cases categorized as displaying "pachytene arrest" were subdivided in class I (no XY body formation and no MLH1 foci) and class II (normal XY body formation and normal MLH1 foci).However, meiotic metaphase was not analysed. Since the class II patients in this study were described to display aberrations in expression of cell cycle genes, it could be worthwhile to assess if spermatocytes in these type II patients might also arrest at metaphase, instead of at prophase.

▶ **Fig. 7. Crossover formation in patients with metaphase arrest and controls**. **A)** Immunostaining of MLH1 (green) and SYCP3 (red) in a control sample. **B)** Mean number of MLH1 foci in controls (grey marks) and patients (orange, reduced formation of XY body; blue, normal XY body formation). **C)** Number of MLH1 foci per nucleus for each analysed patient. **D)** Mean number of MLH1 foci (Y axis), percentage of apoptotic metaphases (X axis). Circles indicate patients for whom pachytene nuclei frequently displayed more than 1 XY body-like structure, T indicates patients with known chromosomal aberration. Dashed line: Threshold.
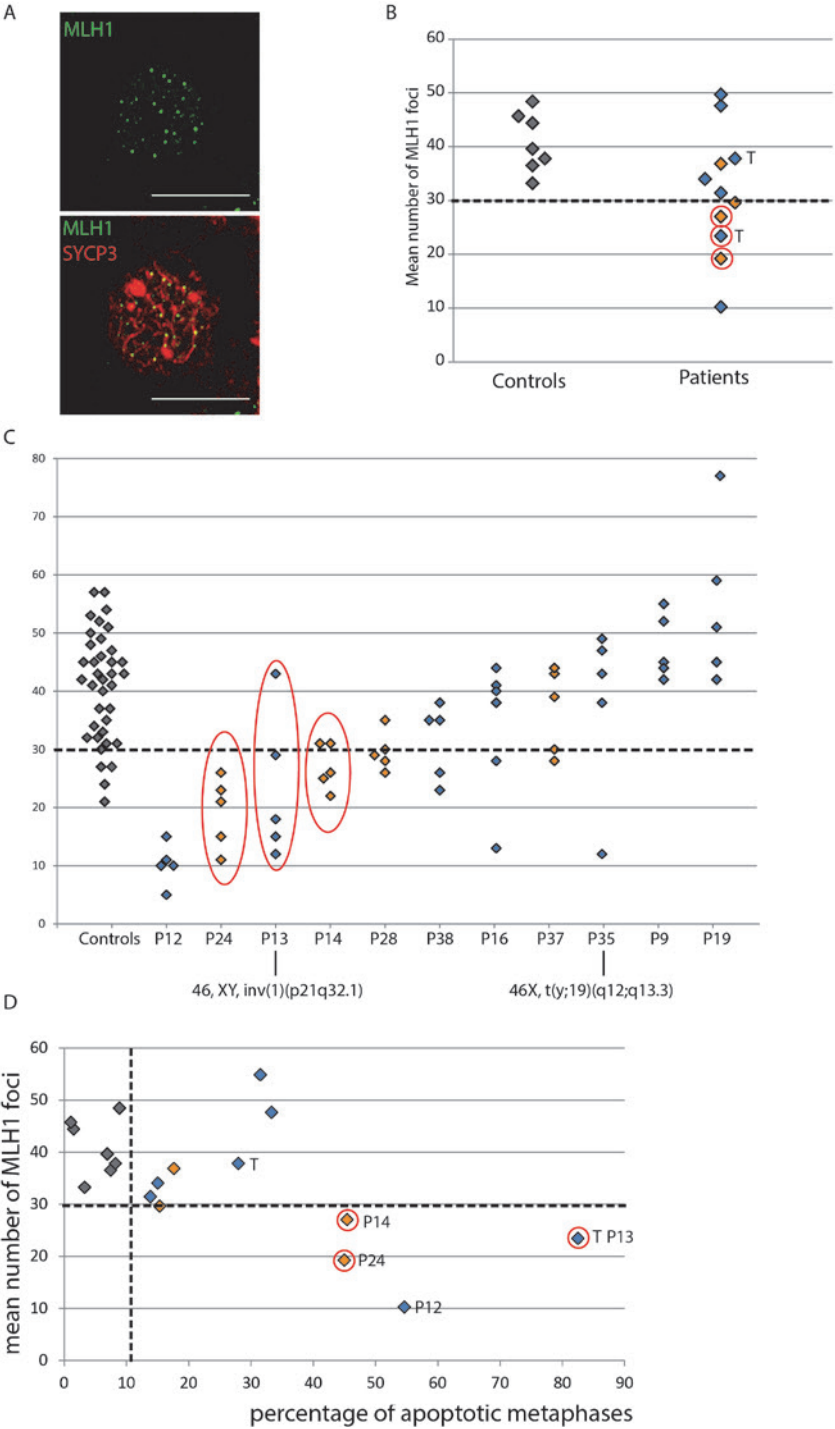
Category	ID	Johnsen score	% meiotic entry tubules	# XYbodies /XY+T	# metaphases /mm2	% apoptotic metaphases	% tubules with spermatids	maximal spermatid stage observed	mean # MLH1 foci	Genetic analyses
Control	C1	10	43.86	12.68	5.97	2.2	84	T5	n.a	n.a.
	C2	10	98.75	23.73	8.57	1.6		T5	44.4	n.a.
	C3	10	n.a.	n.a.	6.15	0.8	94	T5	n.a	n.a.
	C4	10	57.69	21.24	5.65	9.1	90	T5	n.a	n.a.
	C5	10	n.a.	n.a.	10.06	4.9	n.a.	T5	n.a	n.a.
	C6	10	84.62	28.72	8.87	0	n.a.	T5	n.a	n.a.
	C7	10	73.68	21.91	4.03	0	n.a.	T5	n.a	n.a.
	C8	10	90.2	18.62	6.80	1.1	n.a.	T5	45.7	n.a.
	C9	10	100	14.33	11.52	6.5	92	T5	n.a	n.a.
	C10	10	100	19.02	4.74	7.5	92	T5	36.5	n.a.
	C11	10	100	9.02	10.54	8.3	100	T5	37.8	n.a.
	C12	10	100	28.02	n.a.	3.3	n.a.	T5	33.2	n.a.
	C13	10	100	23.44	n.a.	7.8	93	T5	n.a	*CFTR* : 1717-1G->A/Q1476
	C14	10	98	27.53	n.a.	7.0	n.a.	T5	39.6	n.a.
	C15	10	100	14.50	n.a.	8.9	88	T5	48.4	n.a.
Group I: No entry	P10	5	0	0	0.86	n.a.	0	-	n.a	*AZFc* deletion
Group II:Failure to form XY body	P3	4-5	90	0	0.73	n.a.	0	-	n.a	n.a.
	P7	3-4	57.81	0	1.41	n.a.	0	-	n.a.	n.a.
	P25	3	100	0	0.10	n.a.	0	-	n.a.	x (*CFTR* n.a.)
	P33	3-4	96	0	1.13	n.a.	0	-	n.a.	n.a.
Group III: Failure to reach metaphase.	P4	3	15.38	3.7	0.81	n.a.	0	-	n.a.	x
	P30	3	100	6.5	0.86	n.a.	0	-	n.a.	n.a.
	P39	5-6	98	7.1	1.79	n.a.	0	-	n.a.	n.a.
	P41	3-4	100	5.6	1.69	n.a.	0	-	n.a	*CFTR* (R117H/7T)
	P44	1-4	98	3.5	1.41	n.a.	0	-	n.a.	x (*CFTR* n.a.)
	P45	3	98	4.2	0.28	n.a.	0	-	n.a.	n.a.
	P47	6	98	4.8	0.40	n.a.	0	-	n.a.	x (*CFTR* n.a.)
Group IV: Complete metaphase arrest	P9	5-6	98.97	16.2	19.00	33.3	0	-	47.6	x
	P12	4	94.12	8.6	7.64	54.7	0	-	10.2	x
	P13	5-6	94.64	13.2	11.95	82.5	0	-	23.4	46,XY,inv(1)(p21q32.1)
	P14	5	63.16	1.7	5.04	54.5	0	-	27	x (*CFTR* n.a.)
	P16	5-6	90.63	14.1	6.28	15.1	0	-	34	n.a.
	P17	3-4	82.76	4.1	9.30	67.7	0	-	n.d.	*AZFc* deletion
	P19	5	79.66	8.3	2.39	31.5	0	-	54.8	x
	P24	6	96.4	7.0	2.90	45.0	0	-	19.2	x
	P28	4	100	3.5	2.39	15.4	0	-	29.6	x
	P35	5	100	19.5	10.94	28.0	0	-	37.8	46,X,t(Y;19)(q12;q13.3)
	P37	3	100	1.1	3.45	17.6	0	-	36.8	x
	P38	2-5	88	10.4	4.64	13.9	0	-	31.4	x (*CFTR* n.a.)
	P40	5	100	1.2	5.92	18.5	0	-	n.d.	n.a.
Group V: Partial metaphase arrest	P2	5	90.91	9.7	3.93	23.7	20	T2	n.a.	n.a.
	P18	4	28.99	3.92	1.89	14.8	18	T3,rare T5	n.a.	x (*CFTR* n.a.)
	P20	6	49.44	8.07	3.93	11.8	40	T3	n.a.	x
	P21	3-5	95	9.9	3.33	28.2	38	T2, rare T3	n.a.	x (*CFTR* n.a.)
	P23	6	100	14	4.36	15.7	46	T2, rare T3	n.a.	n.a.
	P26	*	100	9.3	4.31	13.2	44	T3	n.a.	x
	P27	*	100	6.7	2.24	15.4	20	T3	n.a.	n.a.
	P36	6	100	7.1	5.27	16.3	4	T2	n.a.	n.a.
Group VI: Postmetaphase arrest	P22	*	100	9.3	2.75	5.5	0	-	n.a.	x (*CFTR* n.a.)
	P31	5	100	11.2	6.45	7.6	0	-	n.a.	n.a.
	P34	5	100	13.6	6.10	4.8	0	-	n.a.	x (*CFTR* n.a.)
	P42	6	100	18.8	6.96	10.9	0	-	n.a.	x
	P43	6	83.7	3.6	5.12	0	0	-	n.a.	x (*CFTR* n.a.)
	P48	4	100	2.6	2.95	0	0	-	n.a.	x (*CFTR* n.a.)
Group VII: No clear arrest	P1	3-4	66.67	6.9	3.30	0	8	T3	n.a.	x
	P5	5	69.81	9.61	4.76	3.9	42	T3, rare T4	n.a.	x
	P6	3-4	92.86	22.8	6.86	2.7	38	T2, rare T3	n.a.	n.a.
	P8	4-5	86	9.8	6.65	5.1	54	T5	n.a.	n.a.
	P11	5	96	9.8	4.71	8.1	28	T2	n.a.	n.a.
	P15	6	97.33	25.9	10.96	1.7	26	T2, rare T3	n.a.	n.a.
	P29	4	94	7.2	5.47	1.8	64	T3, rare T4	n.a.	n.a.
	P32	5	86	8.3	10.01	3.9	10	T3	n.a.	x (*CFTR* n.a.)
	P46	6	100	4.9	1.11	2.9	38	T5	n.a.	n.a.

4a

◀ **Table I. Summary of results for patients and controls.** *no Johnsen score available; n.a. , not analysed; n.d., not detected; -, no spermatids detected; x no genetic aberrations detected. Blue values, below threshold set for normal XY body formation or metaphase density (based on control values); Red values, all zero values, and values below the threshold set for reaching meiotic metaphase, and for normal number of MLH1 foci.

Metaphase arrest has been observed much less frequently than pachytene arrest in mouse models of infertility, and mainly when crossover formation was affected (Baker et al. 1996; Lipkin et al. 2002; Eaker et al. 2002). Based on these findings, a reduction in the number of crossovers has been predicted as cause of metaphase arrest in humans as well (Hultén et al. 1970, 1974; Pearson et al. 1970; Templado et al. 1976, 1980; Thomson et al. 1979; Chaganti and German 1979; Mićić et al. 1982). In mice, mutation of genes such as *Mlh1* (Edelmann et al. 1996; Baker et al. 1996) and *Rnf212* (Reynolds et al. 2013) almost completely abolish crossover formation, but do not affect overall chromosome pairing and DSB repair. A genetic mutation in either of these genes could be suspected for P12, since all analysed cells displayed a very low number of MLH1 foci and a very high percentage of apoptotic metaphases (54.7%), but a normal γH2AX pattern in pachytene was observed. Additionally, for two other patients (P17, diagnosed with *AZFc* deletion, and P40, for whom no chromosomal aberrations were reported), we failed to detect MLH1 foci. This may be due to a total failure of forming crossovers, or it could be due to a technical artefact. Both patients show reduced XY body formation but normal capacity to reach metaphase, so it would be expected that MLH1-positive pachytene spermatocytes would be detected if present. Interestingly, P40 presented persistent DSBs in pachytene. So for P40, it may be suggested that the lack of detectable crossover formation could be related to at least a partial failure to complete DSB repair. P17 was diagnosed with an *AZFc* deletion. Azoospermic patients with *AZFc* deletions have variable phenotypes (ranging from Sertoli cell only (SCO) to oligozoospermia) whereby genetic background and the size of the deletion are known modifiers (Krausz and Casamonti 2017). Interestingly, in two separate studies of spermatocytes from patients carrying *AZF*c deletions, increased apoptosis of pachytene cells was sometimes observed, but the γH2AX staining pattern was normal (Geoffroy-Siraudin et al. 2007; Streichemberger et al. 2012). In the only other patient diagnosed with an *AZFc* deletion in our patient group (P10, failure to enter meiotic prophase) no spermatocytes were detected, so crossover formation was not analysed.

Mutation of *Shoc1* (Guiraldelli et al. 2018)*,* or of the X-linked *Tex11* gene in mouse (Yang et al. 2008) leads to a somewhat more subtle and variable reduction in the number of crossovers (~19% for *Shoc1* and ~30% for *Tex11*), compared to what is observed in *Mlh1* knockout males, but also leads to complete metaphase arrest. In addition, these mice display defects in chromosome pairing and, in the case of TEX11 deficiency, part of the

spermatocytes undergo apoptosis in response to the pachytene checkpoint. Interestingly, mutations in *TEX11* have been reported in a small percentage of men diagnosed with a meiotic arrest phenotype (Yatsenko et al. 2015; Yang et al. 2015). Two of the four patients with reduced MLH1 foci number displayed a phenotype that was similar to that of *Tex11* knockout mice: a reduction in XY body number, aberrant γH2AX patterns (multiple XY body-like structures) in pachytene, and metaphase arrest (P24 and P14, no genetic aberrations). Thus for these two patients *TEX11* would be good candidate gene to screen for causative mutations.

P13, one of the two patients with a structural chromosomal aberration (46,XY,inv(1)(p21q32.1)) also displayed a low MLH1 foci number. This result indicates that the presence of a translocation bivalent might affect recombination on the other chromosomes as has been previously described (Douet-Guilbert et al. 2005; Li et al. 2017). However, this phenomenon is variable, also in our analyses since P35 (46X,t(Y;19)(q12;q13.3) displayed normal MLH1 foci numbers and a normal However, this phenomenon is variable, also in our analyses since P

Interestingly, the four patients with the strongest reduction in MLH1 foci number, displayed the highest percentage of apoptotic metaphases (more than 40%). This confirms that reduction in the number of crossovers is a potent activator of metaphase arrest, most likely via activation of the SAC, due to the fact that univalent chromosomes cannot be properly aligned. Still, the majority of the patients displaying complete metaphase arrest (7 out of 11 patients for whom MLH1 staining could be obtained) did not present a clear reduction in the number of crossovers. This group of patients displayed a lower percentage of apoptotic metaphases (< 35%) when compared to the ones that showed clear reduction of MLH1 foci number. Also, no alterations in the γH2AX pattern of pachytene nuclei from these patient were observed (although five of them displayed reduced frequency of XY body formation). It might be suggested that in these cases alterations in other proteins involved in the metaphase-anaphase transition cause the observed arrest. In addition, mild reduction in crossover frequency (for example, lack of the obligate crossover in the PAR), which would not be detected in an average counting, could still trigger metaphase arrest in some of the patients.

Premetaphase and postmetaphase arrest: novel checkpoints or necrosis?

In 15% of the testis biopsies we observed XY bodies but neither metaphases nor spermatids (Group III), indicating loss of spermatocytes cells before they reach metaphase I (premetaphase arrest) Interestingly, a similar phenotype has been previously described for

two different knockout mouse models. Mice lacking cyclin A1 do not reveal obvious defects in meiotic prophase prior to late diplotene, when their development arrests (Nickerson et al. 2007). Similarly, for mice lacking *Rpl10l*, a testis-specific retrogene present in all eutherians, spermatocyte arrest just before the transition to metaphase I was also observed (Jiang et al. 2017). Thus, also in mice, arrest between pachytene and metaphase I has been described, but whether this involves activation of a specific checkpoint, or a collapse of the developmental potential of the cells is not known. Our patients in Group III also displayed reduced XY body formation, indicating clear problems to reach pachytene in addition to a failure to reach metaphase.

We also identified a group of patients (13%) for whom absence of spermatids was the only clear abnormality observed (post-metaphase arrest, Group VI). Similar to the premetaphase arrest, post-metaphase arrest could involve activation of a specific checkpoint, or a global dysregulation of gene expression, followed by some form of cell death within a short period between the first meiotic division and early spermatid stages. Early spermatid arrest occurs in mice in which the expression of the transcription factor CREMtau, the testis-specific variant of CREM, has been disrupted (Nantel and Sassone-Corsi 1996). If spermatids are not present at all, malfunction of the gene *ZFY* could also be suspected as a cause of the failure to develop further than the meiotic divisions. In mice, *Zfy1* and *Zfy2* promote completion of meiosis II (Vernet et al. 2014). In men, there is a single *ZFY* gene, which is more similar to the mouse *Zfy1* gene (Decarpentrie et al. 2012). It is an interesting possibility that mutations in this gene might result in a post-metaphase arrest in men.

Only one sample in each of the Group III and VI pre- and postmetaphase arrest patients displayed cells with global aberrant γH2AX staining (Fig. 3C), indicating that for these patients, nuclei might indeed be eliminated by apoptosis before (pre-metaphase arrest) or after metaphase (post-metaphase arrest). Since no such apoptotic nuclei were observed in the rest of the samples, activation of an apoptotic pathway not involving pan-nuclear γH2AX formation (like necroptosis or necrosis) may explain the rapid loss of cells in those patients. In addition, or alternatively, malfunctioning cells may detach from the Sertoli cells followed by sloughing into the lumen, as was previously reported for mouse round spermatids in certain mouse models (Yan 2009).

Partial activation of known meiotic checkpoints and no clear arrest: clinical implications

Azoospermic patients may conceive through ART involving TESE followed by ICSI. In addition, recent publications indicate that also round spermatid injection (ROSI) could be successfully performed in such cases (Tanaka et al. 2015). For our JS3-6 patients, spermatids were detected in 36% of the cases and for almost half of this group (17% of the total), a

partial metaphase arrest was observed. In some cases, this was associated with partial failure to form the XY body, indicating severe meiotic problems, resulting in partial activation of one or both known meiotic checkpoints. The surviving spermatids appear incapable of completing spermatogenesis, because no spermatids later than step 2 or 3 were detected. At present, we do not know whether these spermatids have properly passed the checkpoint, or escaped from the checkpoint.

No activation of the metaphase checkpoint was observed for the patients categorized as "no clear arrest". However, 5 out of 9 patients of this group displayed only T2-T3 spermatids, indicating disturbed spermiogenesis. The other four patients displayed presence of T4-T5 spermatids and thus possibly also mature spermatozoa, but in general only in a few tubules. At present we cannot point to any possible specific cause of the deficient spermiogenesis in patients categorized as "no clear arrest" (also no genetic analysis were performed in the majority of these cases). Environmental or developmental disturbances are not excluded.

In summary, we have developed and optimized an immunocytochemical approach to classify testis biopsies of patients with severe spermatogenic impairment, according to their meiotic defect. Uniform activation of meiotic checkpoints suggests a genetic cause of spermatogenic arrest. Therefore, our technique can be used as a tool to preselect patients for sequencing (search for infertility genes). If partial activation of meiotic checkpoints is observed, further research is recommended to determine if the surviving spermatids have increased frequencies of (epi)genetic aberrations (risk assessment), before performing ICSI or ROSI.

MATERIALS AND METHODS

Patient inclusion and genetic and pathological results

Surplus testicular biopsy material, fixed in 4% paraformaldehyde and embedded in paraffin, was collected from a group of 462 patients. The testis biopsies were obtained to perform morphological assessment and testicular sperm extraction, because the patient was azoospermic, or severely oligospermic, or because testicular cancer was suspected, in the period between 2001 and 2013. Patients for whom some form of malignancy was reported in the analyses of the biopsy were excluded. Informative remarks regarding progression of spermatogenesis were available for testis biopsies of 313 patients, including the Johnsen score (JS, (Johnsen 1970)) routinely determined in the Pathology laboratory. From these, 24% displayed a JS lower than 3, 16% had JS 3-6 (these were all analysed, if surplus material was still available), 27% JS 7-8, and 13% JS 9-10 (almost normal spermatogenesis, most likely suffering from obstructive azoospermia). Forty-nine patients with JS 3-6 were selected as

well as 4 patients, where no JS was assigned but for whom spermatogenic arrest, or disturbed spermatogenesis was described (see Table I for available information). From this group, enough surplus material to perform our analyses was available for a total of 48 patients. In addition, 15 patients with JS 10 were randomly chosen and used as controls. In total, 30 of the selected patients had also been analysed for *AZF* deletions, common *CFTR* mutations, and karyotyping was performed as described (Dohle et al., 2002). Aberrations were found in 5 of them: one displayed a pericentric inversion in chromosome 1, (P13; 46,XY,inv(1)(p21q32.1)), another a balanced translocation between the long arm of the Y-chromosome and the long arm of chromosome 19 (P35; 46,X,t(Y;19)(q12;q13.3)), two *AZFc (DAZ)* deletions (P10 and P17) were detected and a heterozygote carrier of a *CFTR* mutation (P41 (R117H/7T)). From the group of the controls, one had been analysed for genetic aberrations, and this patient (C13) carried two *CFTR* mutations: 1717-1G->A and Q1476X, most likely explaining the obstructive azoospermia in this patient.

Ethical approval

The use of surplus tissue samples remaining after diagnosis was approved by the local institutional ethics committee of the Erasmus MC Rotterdam (METC 02.981). This included the permission to use the secondary tissue without further consent. Samples were used according to the "Code for Proper Secondary Use of Human Tissue in The Netherlands" developed by the Dutch Federation of Medical Scientific Societies (FMWV,http://www.federa.org/), version 2002, update 2011). This is a retrospective study based on surplus material that was anonymized, prohibiting tracing back to the patient.

Fluorescent immunohistochemistry

Testis biopsies were sectioned (section thickness, 6 μm), and placed on a drop of dH2O on slides (Starfrost).After stretching the sections on a heating plate at 39°C, the water was removed and the slides were dried overnight at 37ºC in an incubator. Subsequently, the slides were placed at 60°C in an oven for 1 hour to melt the paraffin. Then, the slides were dewaxed and rehydrated as follows: 3 x 5 minutes xylene, 3 x 5 minutes 100% ethanol and 3 x 5 minutes phosphate buffered saline (PBS). The slides were then incubated for 15 minutes in Proteinase K in PBS (1μg/ml). This was followed by washing steps with demineralized H2O (dH2O; 4 x 2 minutes) and an incubation with terminal deoxynucleotidyl transferase (TdT) buffer (0.1M Na-cacodylate, pH 6.8, 1.0 mM CoCl, 0.1 mM DTT) for 30 minutes in a humid chamber. Subsequently, the slides were washed 3 x 5 minutes with TB buffer (300mM NaCl, 30mM tri-sodiumcitrate-dihydrate in dH2O) and 3 x 5 minutes with dH$_2$O. Thereafter, an epitope retrieval step was performed with sodium citrate buffer pH6 (1mM Tri-Sodium

citrate (dihydrate)) in a microwave at maximum power (1 x10 minutes, 2 times x 5 minutes, refilling the evaporated water after each microwave step). The slides were cooled down to room temperature in the sodium citrate buffer for approximately one hour, after which they were washed with PBS (3 x 5 minutes). Blocking was performed by incubating the sections in 10% normal goat serum and 5% bovine serum albumin (BSA) diluted in PBS, in a humid chamber for 30 minutes at room temperature. We used dual fluorescent staining, but performed sequential immunostaining rounds for each primary antibody and its associated secondary, fluorescent-tagged antibody, in order to reduce the risk of secondary antibody cross reaction. Thus, in the first round, the first primary antibody (diluted in 5% BSA/PBS) was added to the sections and the slides were incubated in a humid chamber at 4 °C overnight. The second day, the slides were first kept at room temperature for one hour and then washed 3 x 5 minutes with PBS. Subsequently, the first secondary antibody (diluted in PBS) was added and the slides were incubated for 1.5 hour in a humid chamber at room temperature. The slides were subsequently washed 3 x 5 minutes in PBS and then incubated with the second primary antibody in 5% BSA/PBS overnight, for a second round of immunostaining. The third day, we performed the steps for detection of the second secondary antibody. Finally, slides were washed 3 x 5 minutes in PBS, and mounted using Prolong Gold Antifade reagent with DAPI.

Antibodies

The following primary antibodies were used: rabbit polyclonal anti-SYCP3 (Lammers et al. 1994) at 1:10000, mouse monoclonal anti-MLH1 (cat. 551091, BD Pharmigen) at 1:25, mouse polyclonal anti-γH2AX at 1:10000 (Millipore,05-636), rabbit polyclonal anti-H3Ser10ph at 1:1000 (06-570, Millipore), and mouse acrosome-specific antibody at 1:100 (Moore et al. 1987). For secondary antibodies, we used goat anti-rabbit alexa 488 IgG, and goat anti-mouse alexa 546 IgG (Invitrogen), both at 1:500 dilution.

Quantitative and qualitative analyses of fluorescent immunostainings of human testis biopsy sections

Qualitative analyses of spermatid development were performed on samples stained with anti-acrosome-specific antibody. Detailed qualitative analyses of meiotic progression in selected patient samples were performed on samples immunostained with anti-SYCP3 and anti-γH2AX, or antiH3S10ph and anti-γH2AX. For these purposes, confocal images were taken using a Zeiss LSM700 confocal, equipped with a digital camera (Axiocam MRm Rev.3 1388X1040 monochrome camera for epi-fluorescence). Quantitative analysis of meiotic entry, XY body formation and number of metaphases per sample were performed at 200x or

1000x magnification on a Axioplan 2; Carl Zeiss fluorescence microscope, on samples stained with anti-γH2AX and anti-H3ser10ph. For meiotic entry and XY body formation, only round tubules were scored (defined as tubules whereby the longest and shortest diameter differed less than two-fold). A minimum of 50 random round tubules was evaluated per patient. The number of tubules that contained at least one early cell was counted to determine the percentage of early cell positive tubules (200x magnification, EC+T). The same analysis was performed for the XY body, to determine the percentage of XY body positive tubules (XY+T). In addition, the number of XY bodies per tubule was assessed at 1000x magnification. To obtain the percentage of apoptotic metaphases, all metaphases in a section were scored (63x oil immersion Plan-Apochromat objective, Zeiss LSM700 confocal microscope) and classified as apoptotic if they were also clearly positive for γH2AX immunosignal (signal of similar intensity as observed for the XY body). In addition, the number of metaphases was normalized to the area analysed (metaphases/mm^2).

Quantitative analysis of fluorescent MLH1 immunostaining of human testis biopsy sections

Samples of controls and patients included in the category "metaphase arrest" were stained for MLH1 and SYCP3, and analysed using confocal microscopy (63x oil immersion Plan-Apochromat objective). MLH1 signal appeared as small foci along the SYCP3 axis of the spermatocytes. For counting MLH1 foci, Z-stacks from five or six different spermatocytes showing SYCP3 and MLH1 fluorescence, were made per sample (5x zoom). These Z-stacks were merged into 2D images (maximum projection). The number of MLH1 foci was counted using the "Find Maxima" function of the Image J software (FIJI, (Schindelin et al. 2012)). The noise tolerance was set manually.

Statistics/Threshold calculations

To determine the normal range of values for each parameter in the control group, thresholds were calculated using the mean ± 2 SD (95% confidence interval). If the lowest/highest value of the control group was not inside this confidence interval, a Grubb's test was performed to determine if it was an outlier. In case it was not an outlier, this value was used as threshold.

Values obtained for the patients were then analysed. If a patient value for a certain parameter was inside the correspondent confidence interval it was considered "normal". Values outside the confidence interval (below the lower limit or above the upper limit) were considered reduced or increased, respectively (e.g. reduced XY body formation). In all cases,

absence of more advanced stages indicated cell arrest at or around the latest stage observed.

ACKNOWLEDGEMENTS

FUNDING

CONFLICT OF INTEREST

The authors declare to have no conflict of interest in relation to this work.

4a

REFERENCES

Baarends WM, Wassenaar E, van der Laan R, et al (2005) Silencing of Unpaired Chromatin and Histone H2A Ubiquitination in Mammalian Meiosis. Mol Cell Biol 25:1041–1053. doi: 10.1128/MCB.25.3.1041-1053.2005

Baker SM, Plug AW, Prolla TA, et al (1996) Involvement of mouse Mlh1 in DNA mismatch repair and meiotic crossing over. Nat Genet 13:336–42. doi: 10.1038/ng0796-336

Barchi M, Mahadevaiah S, Di Giacomo M, et al (2005) Surveillance of different recombination defects in mouse spermatocytes yields distinct responses despite elimination at an identical developmental stage. Mol Cell Biol 25:7203–15. doi: 10.1128/MCB.25.16.7203-7215.2005

Barlow AL, Hultén MA (1998) Crossing over analysis at pachytene in man. Eur J Hum Genet 6:350–8. doi: 10.1038/sj.ejhg.5200200

Batanian J, Hulten MA (1987) Electron microscopic investigations of synaptonemal complexes in an infertile human male carrier of a pericentric inversion inv(1)(p32q42). Regular loop formation but defective synapsis including a possible interchromosomal effect. Hum Genet 76:81–9

Baudat F, Manova K, Yuen JP, et al (2000) Chromosome synapsis defects and sexually dimorphic meiotic progression in mice lacking Spo11. Mol Cell 6:989–98

Burgoyne PS, Mahadevaiah SK, Turner JMA (2009) The consequences of asynapsis for mammalian meiosis. Nat Rev Genet 10:207–16. doi: 10.1038/nrg2505

Chaganti RS, German J (1979) Human male infertility, probably genetically determined, due to defective meiosis and spermatogenic arrest. Am J Hum Genet 31:634–41

Codina-Pascual M, Campillo M, Kraus J, et al (2006) Crossover frequency and synaptonemal complex length: their variability and effects on human male meiosis. MHR Basic Sci Reprod Med 12:123–133. doi: 10.1093/molehr/gal007

Codina-Pascual M, Oliver-Bonet M, Navarro J, et al (2005) Synapsis and meiotic recombination analyses: MLH1 focus in the XY pair as an indicator. Hum Reprod 20:2133–9. doi: 10.1093/humrep/dei023

Cole F, Kauppi L, Lange J, et al (2012) Homeostatic control of recombination is implemented progressively in mouse meiosis. Nat Cell Biol 14:424–30. doi: 10.1038/ncb2451

de Rooij DG, de Boer P (2003) Specific arrests of spermatogenesis in genetically modified and mutant mice. Cytogenet Genome Res 103:267–76. doi: 10.1159/000076812

Decarpentrie F, Vernet N, Mahadevaiah SK, et al (2012) Human and mouse ZFY genes produce a conserved testis-specific transcript encoding a zinc finger protein with a short acidic domain and modified transactivation potential. Hum Mol Genet 21:2631–45. doi: 10.1093/hmg/dds088

Douet-Guilbert N, Bris M-JL, Amice V, et al (2005) Interchromosomal effect in sperm of males with translocations: report of 6 cases and review of the literature. Int J Androl 28:372–9. doi: 10.1111/j.1365-2605.2005.00571.x

Eaker S, Cobb J, Pyle A, Handel MA (2002) Meiotic prophase abnormalities and metaphase cell death in MLH1-deficient mouse spermatocytes: insights into regulation of spermatogenic progress. Dev Biol 249:85–95

Edelmann W, Cohen PE, Kane M, et al (1996) Meiotic Pachytene Arrest in MLH1-Deficient Mice. Cell 85:1125–1134. doi: 10.1016/S0092-8674(00)81312-4

Faed MJ, Lamont MA, Baxby K (1982) Cytogenetic and histological studies of testicular biopsies from subfertile men with chromosome anomaly. J Med Genet 19:49–56

Faisal I, Kauppi L (2016) Sex chromosome recombination failure, apoptosis, and fertility in male mice. Chromosoma 125:227–35. doi: 10.1007/s00412-015-0542-9

Faisal I, Kauppi L (2017) Reduced MAD2 levels dampen the apoptotic response to non-exchange sex chromosomes and lead to sperm aneuploidy. Development 144:1988–1996. doi: 10.1242/dev.149492

Foresta C, Ferlin A, Bettella A, et al (1995) Diagnostic and clinical features in azoospermia. Clin Endocrinol (Oxf) 43:537–43

Gabriel-Robez O, Ratomponirina C, Cranz C, et al Robertsonian heterozygosity and male sterility. Andrologia 20:463–6

Gabriel-Robez O, Ratomponirina C, Croquette M, et al Reproductive failure and pericentric inversion in man. Andrologia 19:662–9

Gabriel-Robez O, Ratomponirina C, Dutrillaux B, et al (1986) Meiotic association between the XY chromosomes and the autosomal quadrivalent of a reciprocal translocation in two infertile men, 46,XY,t(19;22) and 46,XY,t(17;21). Cytogenet Cell Genet 43:154–60. doi: 10.1159/000132314

Geoffroy-Siraudin C, Aknin-Seiffer I, Metzler-Guillemain C, et al (2007) Meiotic abnormalities in patients bearing complete AZFc deletion of Y chromosome. Hum Reprod 22:1567–1572. doi: 10.1093/humrep/dem045

Gorbsky GJ (2015) The spindle checkpoint and chromosome segregation in meiosis. FEBS J 282:2471–87. doi: 10.1111/febs.13166

Greaney J, Wei Z, Homer H (2017) Regulation of chromosome segregation in oocytes and the cellular basis for female meiotic errors. Hum Reprod Update 24:135–161. doi: 10.1093/humupd/dmx035

Guichaoua MR, Perrin J, Metzler-Guillemain C, et al (2005) Meiotic anomalies in infertile men with severe spermatogenic defects. Hum Reprod 20:1897–1902. doi: 10.1093/humrep/deh868

Guichaoua MR, Quack B, Speed RM, et al (1990) Infertility in human males with autosomal translocations: meiotic study of a 14;22 Robertsonian translocation. Hum Genet 86:162–6

Guiraldelli MF, Felberg A, Almeida LP, et al (2018) SHOC1 is a ERCC4-(HhH)2-like protein, integral to the formation of crossover recombination intermediates during mammalian meiosis. PLoS Genet 14:e1007381. doi: 10.1371/journal.pgen.1007381

Hamer G, Novak I, Kouznetsova A, Höög C (2008) Disruption of pairing and synapsis of chromosomes causes stage-specific apoptosis of male meiotic cells. Theriogenology 69:333–9. doi: 10.1016/j.theriogenology.2007.09.029

Hann MC, Lau PE, Tempest HG (2011) Meiotic recombination and male infertility: from basic science to clinical reality? Asian J Androl 13:212–8. doi: 10.1038/aja.2011.1

Homolka D, Ivanek R, Capkova J, et al (2007) Chromosomal rearrangement interferes with meiotic X chromosome inactivation. Genome Res 17:1431–1437. doi: 10.1101/gr.6520107

Hultén M, Eliasson R, Tillinger KG (1970) Low chiasma count and other meiotic irregularities in two infertile 46, XY men with spermatogenic arrest. Hereditas 65:285–90

Hultén M, Solari AJ, Skakkebaek NE (1974) Abnormal synaptonemal complex in an oligochiasmatic man with spermatogenic arrest. Hereditas 78:105–16

Jan SZ, Jongejan A, Korver CM, et al (2018) Distinct prophase arrest mechanisms in human male meiosis. Development 145:dev160614. doi: 10.1242/dev.160614

Jiang L, Li T, Zhang X, et al (2017) RPL10L Is Required for Male Meiotic Division by Compensating for RPL10 during Meiotic Sex Chromosome Inactivation in Mice. Curr Biol 27:1498–1505.e6. doi: 10.1016/j.cub.2017.04.017

Johannisson R, Schwinger E, Wolff HH, et al (1993) The effect of 13;14 Robertsonian translocations on germ-cell differentiation in infertile males. Cytogenet Cell Genet 63:151–5. doi: 10.1159/000133524

Johnsen SG (1970) Testicular biopsy score count--a method for registration of

4a

spermatogenesis in human testes: normal values and results in 335 hypogonadal males. Hormones 1:2–25

Krausz C, Casamonti E (2017) Spermatogenic failure and the Y chromosome. Hum Genet 136:637–655. doi: 10.1007/s00439-017-1793-8

Lammers JH, Offenberg HH, van Aalderen M, et al (1994) The gene encoding a major component of the lateral elements of synaptonemal complexes of the rat is related to X-linked lymphocyte-regulated genes. Mol Cell Biol 14:1137–46

Li G, Iqbal F, Wang L, et al (2017) Meiotic defects and decreased expression of genes located around the chromosomal breakpoint in the testis of a patient with a novel 46,X,t(Y;1)(p11.3;p31) translocation. Int J Mol Med 40:367–377. doi: 10.3892/ijmm.2017.3029

Lipkin SM, Moens PB, Wang V, et al (2002) Meiotic arrest and aneuploidy in MLH3-deficient mice. Nat Genet 31:385–90. doi: 10.1038/ng931

Lowe X, O'Hogan S, Moore D, et al (1996) Aneuploid epididymal sperm detected in chromosomally normal and Robertsonian translocation-bearing mice using a new three-chromosome FISH method. Chromosoma 105:204–10

MacQueen AJ, Hochwagen A (2011) Checkpoint mechanisms: the puppet masters of meiotic prophase. Trends Cell Biol 21:393–400. doi: 10.1016/j.tcb.2011.03.004

Mahadevaiah SK, Turner JM, Baudat F, et al (2001) Recombinational DNA double-strand breaks in mice precede synapsis. Nat Genet 27:271–6. doi: 10.1038/85830

Marcet-Ortega M, Pacheco S, Martínez-Marchal A, et al (2017) p53 and TAp63 participate in the recombination-dependent pachytene arrest in mouse spermatocytes. PLoS Genet 13:e1006845. doi: 10.1371/journal.pgen.1006845

Marston AL, Wassmann K (2017) Multiple Duties for Spindle Assembly Checkpoint Kinases in Meiosis. Front cell Dev Biol 5:109. doi: 10.3389/fcell.2017.00109

Martin-du Pan RC, Campana A (1993) Physiopathology of spermatogenic arrest. Fertil Steril 60:937–46

Mićić M, Mićić S, Diklić V (1982) Low chiasma frequency as an aetiological factor in male infertility. Clin Genet 22:266–9

Moens PB, Kolas NK, Tarsounas M, et al (2002) The time course and chromosomal localization of recombination-related proteins at meiosis in the mouse are compatible with models that can resolve the early DNA-DNA interactions without reciprocal recombination. J Cell Sci 115:1611–22

Moore HDM, Smith CA, Hartman TD, Bye AP (1987) Visualization and characterization of the acrosome reaction of human spermatozoa by immunolocalization with monoclonal antibody. Gamete Res 17:245–259. doi: 10.1002/mrd.1120170308

Musacchio A (2015) The Molecular Biology of Spindle Assembly Checkpoint Signaling Dynamics. Curr Biol 25:R1002–R1018. doi: 10.1016/j.cub.2015.08.051

Nantel F, Sassone-Corsi P (1996) CREM: a transcriptional master switch during the spermatogenesis differentiation program. Front Biosci 1:d266-9

Nickerson HD, Joshi A, Wolgemuth DJ (2007) Cyclin A1-deficient mice lack histone H3 serine 10 phosphorylation and exhibit altered aurora B dynamics in late prophase of male meiosis. Dev Biol 306:725–35. doi: 10.1016/j.ydbio.2007.04.009

North M-O, Lellei I, Erdei E, et al (2004) Meiotic studies of infertile men in case of non-obstructive azoospermia with normal karyotype and no microdeleted Y-chromosome precise the clinical couple management. Ann Genet 47:113–23. doi: 10.1016/j.anngen.2003.10.003

Pacheco S, Marcet-Ortega M, Lange J, et al (2015) The ATM signaling cascade promotes

recombination-dependent pachytene arrest in mouse spermatocytes. PLoS Genet 11:e1005017. doi: 10.1371/journal.pgen.1005017

Pearson PL, Ellis JD, Evans HJ (1970) A gross reduction in chiasma formation during meiotic prophase and a defective DNA repair mechanism associated with a case of human male infertility. Cytogenetics 9:460–7

Pigozzi MI, Sciurano RB, Solari AJ (2005) Changes in crossover distribution along a quadrivalent in a man carrier of a reciprocal translocation t(11;14). Biocell 29:195–203

Pinho MJ, Neves R, Costa P, et al (2005) Unique t(Y;1)(q12;q12) reciprocal translocation with loss of the heterochromatic region of chromosome 1 in a male with azoospermia due to meiotic arrest: a case report. Hum Reprod 20:689–96. doi: 10.1093/humrep/deh653

Reynolds A, Qiao H, Yang Y, et al (2013) RNF212 is a dosage-sensitive regulator of crossing-over during mammalian meiosis. Nat Genet 45:269–78. doi: 10.1038/ng.2541

Roeder GS, Bailis JM (2000) The pachytene checkpoint. Trends Genet 16:395–403

Romanienko PJ, Camerini-Otero RD (2000) The mouse Spo11 gene is required for meiotic chromosome synapsis. Mol Cell 6:975–87

Rosenmann A, Wahrman J, Richler C, et al (1985) Meiotic association between the XY chromosomes and unpaired autosomal elements as a cause of human male sterility. Cytogenet Cell Genet 39:19–29. doi: 10.1159/000132098

Royo H, Polikiewicz G, Mahadevaiah SK, et al (2010) Evidence that meiotic sex chromosome inactivation is essential for male fertility. Curr Biol 20:2117–23. doi: 10.1016/j.cub.2010.11.010

Schindelin J, Arganda-Carreras I, Frise E, et al (2012) Fiji: an open-source platform for biological-image analysis. Nat Methods 9:676–82. doi: 10.1038/nmeth.2019

Sciurano RB, Rahn MI, Pigozzi MI, et al (2006) An azoospermic man with a double-strand DNA break-processing deficiency in the spermatocyte nuclei: case report. Hum Reprod 21:1194–203. doi: 10.1093/humrep/dei479

Sciurano RB, Rahn MI, Rey-Valzacchi G, et al (2012) The role of asynapsis in human spermatocyte failure. Int J Androl 35:541–9. doi: 10.1111/j.1365-2605.2011.01221.x

Solari AJ, Rey Valzacchi G (1997) The prevalence of a YY synaptonemal complex over XY synapsis in an XYY man with exclusive XYY spermatocytes. Chromosome Res 5:467–74

Solier S, Pommier Y (2014) The nuclear γ-H2AX apoptotic ring: implications for cancers and autoimmune diseases. Cell Mol Life Sci 71:2289–97. doi: 10.1007/s00018-013-1555-2

Song N, Liu J, An S, et al (2011) Immunohistochemical Analysis of Histone H3 Modifications in Germ Cells during Mouse Spermatogenesis. ACTA Histochem Cytochem 44:183–190. doi: 10.1267/ahc.11027

Streichemberger E, Perrin J, Saias-Magnan J, et al (2012) Case report of apoptosis in testis of four AZFc-deleted patients: increased DNA fragmentation during meiosis, but decreased apoptotic markers in post-meiotic germ cells. Hum Reprod 27:1939–1945. doi: 10.1093/humrep/des128

Sun F, Turek P, Greene C, et al (2007) Abnormal progression through meiosis in men with nonobstructive azoospermia. Fertil Steril 87:565–71. doi: 10.1016/j.fertnstert.2006.07.1531

Sun S-C, Kim N-H (2012) Spindle assembly checkpoint and its regulators in meiosis. Hum Reprod Update 18:60–72. doi: 10.1093/humupd/dmr044

Tanaka A, Nagayoshi M, Takemoto Y, et al (2015) Fourteen babies born after round spermatid injection into human oocytes. Proc Natl Acad Sci U S A 112:14629–34. doi: 10.1073/pnas.1517466112

Tempest HG (2011) Meiotic recombination errors, the origin of sperm aneuploidy and

4a

clinical recommendations. Syst Biol Reprod Med 57:93–101. doi: 10.3109/19396368.2010.504879

Templado C, Marina S, Coll MD, Egozcue J (1980) Meiotic studies in human semen. Report of 180 cases. Hum Genet 53:335–9

Templado C, Marina S, Egozcue J (1976) Three cases of low chiasma frequency associated with infertility in man. Andrologia 8:285–9

Templado C, Uroz L, Estop A (2013) New insights on the origin and relevance of aneuploidy in human spermatozoa. Mol Hum Reprod 19:634–43. doi: 10.1093/molehr/gat039

Tesarik J, Greco E, Cohen-Bacrie P, Mendoza C (1998) Germ cell apoptosis in men with complete and incomplete spermiogenesis failure. Mol Hum Reprod 4:757–62

Thomson E, Fletcher J, Chandley AC, Kucerová M (1979) Meiotic and radiation studies in four oligochiasmatic men. J Med Genet 16:270–7

Topping D, Brown P, Judis L, et al (2006) Synaptic defects at meiosis I and non-obstructive azoospermia. Hum Reprod 21:3171–7. doi: 10.1093/humrep/del281

Turner JMA, Mahadevaiah SK, Fernandez-Capetillo O, et al (2005) Silencing of unsynapsed meiotic chromosomes in the mouse. Nat Genet 37:41–47. doi: 10.1038/ng1484

Tüttelmann F, Ruckert C, Röpke A (2018) Disorders of spermatogenesis: Perspectives for novel genetic diagnostics after 20 years of unchanged routine. Medizinische Genet Mitteilungsblatt des Berufsverbandes Medizinische Genet eV 30:12–20. doi: 10.1007/s11825-018-0181-7

Uroz L, Templado C (2012) Meiotic non-disjunction mechanisms in human fertile males. Hum Reprod 27:1518–24. doi: 10.1093/humrep/des051

Vernet N, Mahadevaiah SK, Ojarikre OA, et al (2011) The Y-encoded gene zfy2 acts to remove cells with unpaired chromosomes at the first meiotic metaphase in male mice. Curr Biol 21:787–93. doi: 10.1016/j.cub.2011.03.057

Vernet N, Mahadevaiah SK, Yamauchi Y, et al (2014) Mouse Y-linked Zfy1 and Zfy2 are expressed during the male-specific interphase between meiosis I and meiosis II and promote the 2nd meiotic division. PLoS Genet 10:e1004444. doi: 10.1371/journal.pgen.1004444

Vidal F, Templado C, Navarro J, et al (1982) Meiotic and synaptonemal complex studies in 45 subfertile males. Hum Genet 60:301–4

Weedin JW, Bennett RC, Fenig DM, et al (2011) Early versus late maturation arrest: reproductive outcomes of testicular failure. J Urol 186:621–6. doi: 10.1016/j.juro.2011.03.156

Yan W (2009) Male infertility caused by spermiogenic defects: lessons from gene knockouts. Mol Cell Endocrinol 306:24–32. doi: 10.1016/j.mce.2009.03.003

Yang F, Gell K, van der Heijden GW, et al (2008) Meiotic failure in male mice lacking an X-linked factor. Genes Dev 22:682–91. doi: 10.1101/gad.1613608

Yang F, Silber S, Leu NA, et al (2015) TEX11 is mutated in infertile men with azoospermia and regulates genome-wide recombination rates in mouse. EMBO Mol Med 7:1198–210. doi: 10.15252/emmm.201404967

Yatsenko AN, Georgiadis AP, Röpke A, et al (2015) X-linked TEX11 mutations, meiotic arrest, and azoospermia in infertile men. N Engl J Med 372:2097–107. doi: 10.1056/NEJMoa1406192
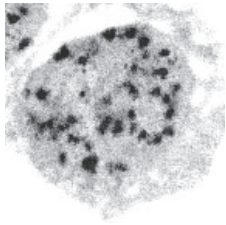
4B
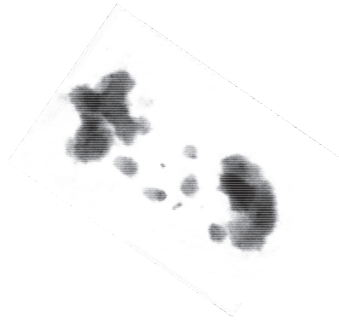
Sequencing of a "mouse azoospermia" gene panel in azoospermic men: identification of *RNF212* and *STAG3* mutations as novel genetic causes of meiotic arrest

Human Reproduction. "In press"

Sequencing of a "mouse azoospermia" gene panel in azoospermic men: identification of *RNF212* and *STAG3* mutations as novel genetic causes of meiotic arrest.

A. Riera-Escamilla[1], A. Enguita-Marruedo[2], D. Moreno-Mendoza[1], C. Chianese[3], E. Sleddens-Linkels[2] E. Contini[4], M. Benelli[5], A. Natali[6], GM. Colpi[7], E. Ruiz-Castañé[1], M. Maggi[3], WM. Baarends[2*] and C. Krausz[1,3*]

1) Andrology Department, Fundació Puigvert, Universitat Autònoma de Barcelona, Instituto de Investigaciones Biomédicas Sant Pau (IIB-Sant Pau), 08025 Barcelona, Catalonia, Spain.

2) Department of Developmental Biology, Erasmus MC University Medical Centre, 3015GD Rotterdam, The Netherlands.

3) Department of Experimental and Clinical Biomedical Sciences "Mario Serio", Centre of Excellence DeNothe, University of Florence, 50139, Florence, Italy

4) Department of Experimental and Clinical Medicine, Center of Research and Innovation of Myeloproliferative neoplasms (CRIMM), AOU Careggi, University of Florence, 50139, Florence, Italy.

5) Bioinformatics Unit, Hospital of Prato, 59100, Prato, Italy

6) Department of Urology, Careggi Hospital, University of Florence, 50139, Florence, Italy.

7) Department of Andrology and IVF, San Carlo Clinic, Paderno-Dugnano/Milano, 20037, Italy.

*Corresponding author: Csilla Krausz. c.krausz@dfc.unifi.it; Willy M. Baarends w.baarends@erasmusmc.nl

Short title: Mutations in *RNF212* and *STAG3* cause meiotic arrest in men

Keywords: genetics, male infertility, azoospermia, spermatogenesis, gene mutations

4b

ABSTRACT

Study question:

What is the diagnostic potential of Next Generation Sequencing based on a "mouse azoospermia" gene panel in human non-obstructive azoospermia (NOA)?

Summary answer:

The diagnostic performance of sequencing a gene panel based on genes associated with mouse azoospermia was relatively successful in idiopathic NOA patients and allowed the discovery of two novel genes involved in NOA due to meiotic arrest.

What is known already:

Non-obstructive azoospermia (NOA) is a largely heterogeneous clinical entity, which includes different histological pictures. In a large proportion of NOA the etiology remains unknown (idiopathic NOA) and yet unknown genetic factors are likely to play be involved.. The mouse is the most broadly used mammalian model for studying human disease because of its usefulness for genetic manipulation, and genetic and physiological similarities to man. Mouse azoospermia models are available in the Mouse Genome Informatics database (MGI: http://www.informatics.jax.org/)

Study design, size, duration:

1st step: design of a "mouse azoospermia" gene panel through the consultation of MGI; 2nd step: NGS analysis of 175 genes in a group of highly selected NOA patients (n=33); 3rd step: Characterization of the discovered gene defects in human testis tissue: meiotic studies by using surplus testicular biopsy material from the carriers of *RNF212* and *STAG3* pathogenic variants; 4th step: *RNF212* and *STAG3* expression analysis in a collection of testis biopsies.

Participants/materials, setting, methods:

From a total of 1300 infertile patients 33 idiopathic NOA patients were analysed in this study: 31 unrelated and 2 brothers from a consanguineous family. The testis histology of the 31 unrelated NOA patients was as follows: 20 Sertoli Cell Only Syndrome, 11 spermatogenic arrest (6 spermatogonial arrest and 5 spermatocytic arrest). The 2 brothers were affected by spermatocytic arrest. DNA extracted from blood was used for NGS on Illumina NextSeq500 platform. Generated sequence data was filtered for rare and potentially pathogenic variants. Functional studies in surplus testicular tissue from the carriers included the investigation of meiotic entry, XY body formation and metaphases by performing fluorescent immunohistochemical stainings and immunocytochemistry. mRNA expression analysis through RT-qPCR of *RNF212* and *STAG3* was carried out in a collection of testis biopsies with different histology.

Main results and the role of chance:

Our approach was relatively successful leading to the genetic diagnosis in one sporadic NOA patient and in two NOA brothers. This relatively high diagnostic performance is likely to be related to the stringent patients selection criteria i.e all known causes of azoospermia were excluded and to the relatively high number of patients with rare testis histology (spermatocytic arrest). In fact, all three mutation carriers presented meiotic arrest leading to the genetic diagnosis in 3/7 cases with this specific testicular phenotype. For the first time we report biallelic variants in *STAG3* in one sporadic patient, and a homozygous *RNF212* variant in the two brothers as the genetic cause of NOA. Meiotic studies allowed the detection of the functional consequences of the mutations and provided information on the role of STAG3 and RNF212 in human male meiosis.

Limitations, reasons for caution:

All genes, with the exception of 5/175, included in the panel cause azoospermia in mice only in the homozygous or hemyzygous status. Consequently, apart from the 5 known dominant genes, heterozygous variants (except compound heterozygosity) in the remaining genes were not taken into consideration as causes of NOA. We identified the genetic cause in approximately half of the patients with spermatocytic arrest. The low number of analyzed patients can be considered as a limitation, but it is a very rare testis phenotype. Due to the low frequency of this specific phenotype among infertile men, our finding may be considered of low clinical impact. However, at an individual level it does have relevance for prognostic purposes prior testicular sperm extraction.

Wider implications of the findings:

Our study represents an additional step towards elucidating the genetic basis of early spermatogenic failure, since we discovered two new genes involved in human male meiotic arrest. We propose the inclusion of *RNF212* and *STAG3* in a future male infertility diagnostic gene panel. Based on the associated testis phenotype, the identification of pathogenic mutations in these genes confers also a negative predictive value for testicular sperm retrieval. Our meiotic studies provide novel insights into the role of these proteins in human male meiosis. Mutations in *STAG3* were first described as a cause of female infertility (POI) and ovarian cancer, and *Rnf212* knockout in mouse leads to male and female infertility. Hence, our results stimulate further research on shared genetic factors causing infertility in both sexes and indicate that genetic counselling should involve not only male but also female relatives of NOA patients.

Study funding/competing interest(s):

INTRODUCTION

Male infertility is a multifactorial heterogeneous pathological condition affecting approximately 7% of men. For approximately 40% of these cases, the etiology remains unknown and these are considered as "idiopathic". The severest form of male infertility is non-obstructive azoospermia (NOA), which occurs in approximately 1% of all men of reproductive age (Tournaye et al. 2016). It has been predicted that more than 2000 genes are involved in spermatogenesis (Mueller et al. 2008) and men affected by azoospermia are at the highest risk of being carriers of genetic anomalies(Krausz and Riera-Escamilla 2018). In fact, 15% of NOA patients carry karyotype anomalies, and Y chromosome microdeletions (AZF deletions) are found in 8-10%. Concerning monogenic causes, massive parallel sequencing approaches have been relatively successful in identifying new candidate genetic factors, especially in patients from consanguineous families. (For review see Krausz *et al.*, 2018). The majority of these studies applied the discovery-oriented approach and used the availability of the knockout (KO) mouse reproductive phenotype for a given gene as crucial criteria for prioritization of the detected variants. The mouse is one of the most broadly used mammalian models for studying human disease because of genetic and physiological similarities between the two species (Perlman 2016). In 2011, a study reported that more than 400 genes had so far been identified to be essential for male fertility in mice (Jamsai and O'Bryan 2011). Alterations in these genes lead to a large range of defects during spermatogenesis (premeiotic, meiotic or postmeiotic stages) and/or alterations at post-testicular maturation and fertilization stages (Jamsai and O'Bryan 2011). The Mouse Genomic Informatics website (http://www.informatics.jax.org/) provides a public database containing integrated genetic, genomic, and biological data from more than 60 thousand mutant alleles with phenotype annotation (http://www.informatics.jax.org/). Among these >60.000 annotations, 1083 lead to disturbances in male reproductive phenotype (from azoospermia to terato/asthenozoospermia). The aim of our study was to evaluate the frequency of mutations in genes reported in the MGI database in relationship with azoospermia, in a cohort of highly selected idiopathic NOA patients.

RESULTS

Gene panel

By extrapolating data from the MGI browser we generated a gene panel that includes 175 human genes (Genes are annotated in table SIV). Briefly, 297 allelic compositions with

different genetic backgrounds leading to azoospermia in mouse were deposited in the Mammalian Phenotype Browser. Among them, 254 involve single gene alterations while in 42 more than one gene is altered. These 254 compositions imply a total of 189 different mouse genes which cause azoospermia in mutants. For 14/189 of these genes no ortholog exists in human, consequently we obtained a list of 175 human genes. Among these genes, the large majority (170/175) cause azoospermia in mouse only in homozygosis. All coding exons and splicing sites of the 175 genes (168 autosomal and 7 X-linked) were sequenced as described in Materials and Methods.

Variants identified

In the highly selected group of the 31 unrelated azoospermic patients we indentified a total of 74 low frequency (MAF<0.05), and predicted as pathogenic variants (see table SV) in 49 genes in 28 patients. 72 variants belonging to 48 genes were found in heterozygosis in 27 patients and were discarded as potential cause of azoospermia for the following reasons: i) heterozygous mouse mutants do not show azoospermia; ii) 13/49 genes have previously been reported to be associated with recessive diseases with proven paternal transmission (in OMIM), implying that the heterozygous genotype in human is not associated to azoospermia; iii) 5/49 genes cause human dominant diseases (OMIM) with diseases which were not observed in our patients, implying a lack of in vivo pathogenic effect of the observed variant. One patient (07-002) carried two variants in *STAG3* (compound heterozygosis) and was subjected to further analyses.

Patient 07-002 affected by complete bilateral meiotic arrest carries two loss of function variants in *STAG3*: a frameshift insertion (NM_001282718:c.1759dupG) and a splicing variant (NM_001282716:c.2394+1G>A). The frameshift variant generates a premature stop gain in the 597th amino acid leading to a protein lacking the entire armadillo (ARM)-type domain, which is predicted to be involved with DNA and protein interactions. This variant was previously reported in the gnomAD database with a MAF= 0.000004073. Concerning the splicing variant, it is a novel variant located in a canonical position (+1) in the splice donor site of exon 23 which is indispensable for normal splicing. The fertile brother DNA sample was available for testing by Sanger sequencing, and this analysis showed that he was a heterozygous carrier for the frameshift mutation but not for the splicing variant (Fig. 1A).

Concerning the two azoospermic brothers from the consanguineous family, we have focused on shared variants and identified: i) a variant in *RNF212* (NM_001131034.3:c.111dupT) in homozygosis; ii) three heterozygous low-frequency and

predicted as pathogenic variants in 3 additional candidate genes (see table SV). The *RNF212* frameshift variant is located inside the Zinc Finger domain and the insertion of the nucleotide leads to a premature stop gain in Lysine 38. The variant was previously described in the gnomAD database with a MAF=0.00006582. The father and mother DNA sample were available for testing by Sanger sequencing and analyses of their DNA showed that both parents are heterozygous carriers (Fig. 2A)

Testis expression analysis

In order to get more insight into the type of testicular cells expressing *RNF212* and STAG3, we performed a quantitative RT-qPCR analysis. This analysis shows a high *RNF212* and *STAG3* mRNA expression in germ cells with the highest expression in biopsies showing spermatogonial and spermatocytic arrest. These findings suggest that, principally, early spermatogenic germ cells such as spermatogonias and spermatocytes express these genes (Fig. S1)

Meiotic studies

Analysis of meiotic entry and XY body formation

For this part of the analysis, paraffin-embedded testis biopsies were immunostained using two specific antibodies, as described in Material and Methods. Anti-phosphorylated H2AX (γH2AX), was used to mark meiotic DSBs and XY body formation (Mahadevaiah et al. 2001). This staining served to assess progression of DSB repair as well as progression of chromosome pairing, since a clear XY body appears only when all autosomal pairs have fully synapsed. In addition, we used an antibody that detects phosphorylated H3 (H3Ser10ph), a general marker of metaphase chromosomes (Song et al. 2011). According to our previously defined thresholds (submitted manuscript) normal meiotic entry corresponds to ≥ 40% early cell positive tubules (EC+T).

▶ **Fig. 1. Investigation on the patient carrying the *STAG3* variants. A)** The pedigree structure shows the segregation of the STAG3 variants (c.1759dupG and c.2394+1G>**A).** The numbers inside the rhombus correspond to the number of children that has each familiar. **B)** Histological sections (Heamatoxilin-stained) of testis biopsy from control (left) and *STAG3* mutation (right) patients. Control sample shows all stages of spermatogenesis, including spermatogonia (spg), spermatocytes (spc) and condensed spermatids (spt). No spermatids are detected in the biopsy of the patient, bit many spermatocytes can be observed. **C)** Immunofluorescent detection of Histone H3 serine 10 phosphorylation (H3S10p, red, marker of M-phase), gH2AX (green, marker of DSBs and XY body), and DAPI (blue, DNA). In the control sample, a group of meiotic metaphases and anaphases is present, as well as several pachytene spermatocytes displaying a gH2AX -positive XY body. In the patient with the *STAG3* mutation, few metaphases were observed, mostly localised in the periphery, and likely representing mitoses of spermatogonia. No XY bodies were detected, indicating that cells fail to reach pachytene. Most spermatocytes displayed an aberrant pattern whereby many gH2AX -positive patches covered the nuclei.
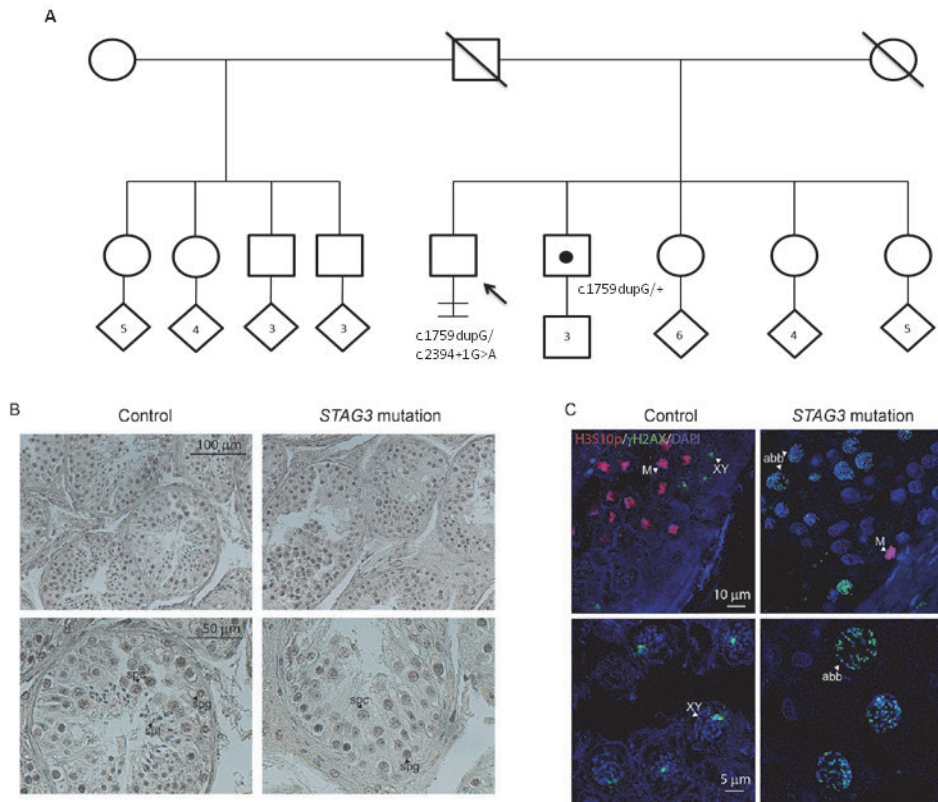
-Patient 07-002 carrying the *STAG3* mutations: in this patient with spermatocytic arrest (Fig. 1B), meiotic entry appeared to occur with normal frequency, based on the presence of many nuclei that displayed small patches of γH2AX. However, this staining was brighter compared to what we observed in the control. No XY bodies were observed. Together these results indicate persistence of meiotic DSBs and a failure to complete chromosome pairing (Fig. 1C)

-Brothers carrying the *RNF212* mutation: normal meiotic entry was observed for both patients (97.8 and 86.5% EC+T, brother 1 and 2, respectively) (Fig. 2B). Also, 100% and 98.1 % of the tubules of brother 1 and 2 displayed cells that contained XY bodies (in controls, 96.5 ± 4.5% of the counted tubules contained XY bodies), and both displayed normal XY body formation (11.2 and 10.8 for brother 1 and 2, respectively; threshold ≥ 7.7 XY bodies per XY+T (Fig 2B, XY body). See material and methods for calculation of thresholds. Additionally, the γH2AX pattern of the pachytene spermatocytes was analysed in detail for both brothers (Fig. 2C). For this, anti-SYCP3 was used to mark chromosome axes in combination with anti-γH2AX on paraffin-embedded testis biopsies of brother 1, and on spermatocyte spreads of
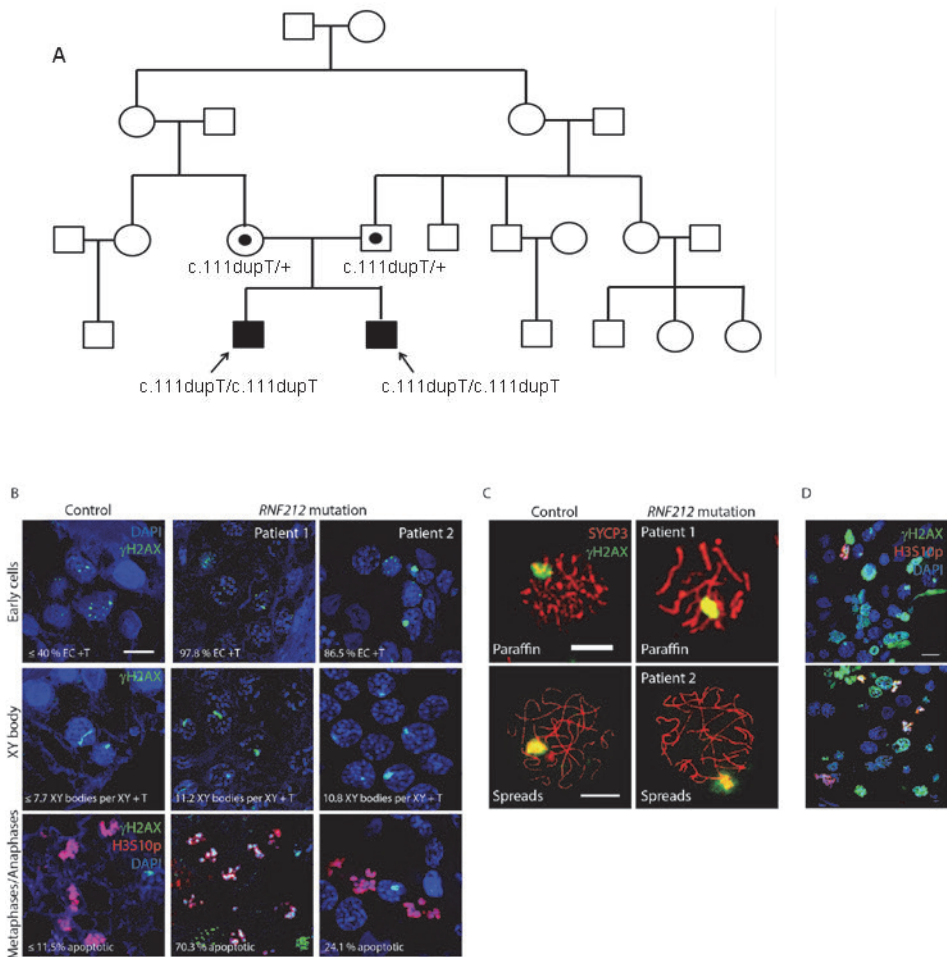
Figure 2. Investigation on the two brothers carrying the RNF212 variant. A) The pedigree structure shows the segregation of the RNF212:c.111dupT variant. **B)** Progression of meiotic prophase (early meiosis, XY body formation and metaphase/anaphase) in paraffin-embedded testis sections of control 1, Brother 1 and 2. Immunostaining of H3Ser10ph (red) and γH2AX (red). Chromatin is stained with DAPI (blue). Thresholds for the percentage of early cell positive tubules (% EC+T), average number of XY bodies per XY body positive tubule (XY bodies per XY+T) and percentage of apoptotic metaphases, are displayed in the controls' images. The values of these parameters are displayed for the patients in the correspondent images. **C)** Pachytene nuclei of control 1 and brother 1 (paraffin-embedded testis biopsies) and control 2 and brother 2 (spermatocyte spreads). Immunostaining of SYCP3 (red) and γH2AX (red). **D)** Aberrant intense global γH2AX staining in tubules of brother 2. Immunostaining of H3Ser10ph (red) and γH2AX (red) on paraffin-embedded testis biopsies. Scale bar represent 10 μm.

brother 2 (more optimal for analyses of chromosome patterns). A normal γH2AX pattern and normal chromosome synapsis was observed for both patients.

Analysis of metaphases:

In order to determine if the spermatocytes were able to complete development up to the meiotic divisions, we quantified the number of metaphases using H3S10ph as marker, and also assessed the percentage of apoptotic metaphases, using pan-chromosomal γH2AX staining in combination with a signal for H3S10ph as indicator. A threshold of 11.5 % apoptotic metaphases was previously defined for the normal situation (submitted manuscript).

-Patient 07-002 carrying the *STAG3* variants: only 2.09 metaphases/mm^2 were observed (47 metaphases/22.46 mm^2 sections). In the control sample, we counted 6.99 metaphases/mm2 (149/21.33 mm^2 sections). The average in the larger control cohort (11 obstructive azoospermia patients) that we investigated separately (submitted manuscript) was 7.54 ± 2.50, leading to a threshold of 2.53 below which we consider the number of metaphases to be below normal. In addition, we also established an upper threshold of 1.9 metaphases/mm^2 based on 5 patients for which we also failed to detect XY bodies in combination with absence of spermatids (manuscript submitted). Together this indicates that the spermatocytes are lost before they reach meiotic metaphase I.

-Brothers carrying the *RNF212* variant: both patients displayed a percentage of apoptotic metaphases higher than the threshold, but this percentage was much higher for brother 1 (70.3%) than for brother 2 (24.07%) (Figure 2B, metaphases/anaphases). Only in brother 2 we also frequently observed tubules in which the majority of the nuclei (all stages) displayed aberrant intense global γH2AX staining (Figure 2D). This suggests massive apoptosis of the nuclei inside certain tubules

Assessment of the presence of spermatids in the brothers carrying the RNF212 variant

To assess progression of spermiogenesis in paraffin-embedded testis sections, we used an anti-acrosome antibody to detect the presence of spermatids (Florke-Gerloff et al. 1983). No specific staining was obtained for the sections of brother 1. We also searched for the DAPI pattern that is characteristic of spermatids, and none were detected for this patient. For brother 2, presence of elongated/condensed spermatids was assessed in spreads, using anti-protamine 1 antibody (figure S2A). No spermatids were found. To also analyse the possible presence of early round spermatids, we used Crest (marker for the centromeres) staining, in combination with the DAPI pattern (figure S2A). In the control, round spermatids displayed a characteristic DAPI-intense chromocenter, where some Crest signals are

included. In contrast to previous stages (figure S2A, Crest in pachytene), Crest foci displayed irregular shapes (frequently elongated) and different sizes. This type of nuclei was not found in brother 2, indicating that round spermatids were also absent. Therefore, and despite the different apoptotic responses observed for the two brothers, both were categorized as displaying complete metaphase arrest

Reduced Crossover (CO) frequency and presence of univalents in brothers carrying the RNF212 variant

We analyzed CO formation in both brothers, using the well known marker MLH1. Although we obtained specific MLH1 foci in our control sample that was paraformaldehyde-fixed, only A DAPI-like unspecific staining was obtained for brother 1, indicating that anti-MLH1 did not work on Bouins'-fixed paraffin-embedded testis biopsies. For brother 2, specific SYCP3 staining but no clear MLH1 staining was obtained when using paraffin-embedded testis sections. MLH1 foci were also absent when spermatocyte spreads were used for immunocytochemistry (Fig. S2A). This suggests complete absence of crossovers.

Absence of crossovers results in the formation of univalents. To determine if they were present, a minimum of 20 metaphase/anaphase nuclei (H3Ser10ph-positive) were analyzed (n = 21, 22 and 21 in paraffin sections from brother 1, 2 and control 1, respectively) (Fig. S2B and C). Cells were categorized as metaphase when displaying only one set of chromatin, or anaphase when displaying two (Fig. S2B). Only metaphases were observed for the control. For brother 2, most H3S10-positive cells were also at metaphase stage. In contrast, mainly anaphases were found for brother 1 (Fig. S2C). For the patients we sometimes observed metaphases consisting of several chromatin entities dispersed through the cell, or a few chromosomes appeared separated from the main metaphase plate (the latter was also rarely observed in the control). These entities, which probably correspond to univalents, were also observed between the two poles in anaphases in brother 1 (Fig. S2B, anaphase of brother 1, arrowheads). In total, 2/21 (9.5%), 16/21 (76.2%) and 10/22 (45.5%) nuclei displayed clear separated chromatin entities (possible univalents) in control, brother 1 and brother 2, respectively. This result shows that crossover formation is reduced in both brothers.

Analysis of TEX11 expression and localization in brothers carrying the RNF212 variant

We analyzed the localization of TEX11 (together with the chromosomal axes marker SYCP3) in human spermatocyte spread preparations (Fig. S3A). To this end, we tested two commercially available antibodies (Sigma and Abcam), one of which (Abcam) was previously described to detect TEX11 in human mainly in spermatids of paraffin sections (Yatsenko et al. 2015). On human spread nuclei TEX11 foci were only observed with the Abcam antibody and

4b

appeared on synapsed axes from zygotene till pachytene in the control. This is similar to what has been described for mouse (Yang et al. 2008). The same pattern was observed for brother 2 (Fig. S3A). No apparent reduction in the number of TEX11 foci was observed in brother 2 compared to the control. For both patients and a control we also performed DAB (3,3'-diaminobenzidine) immunohistochemistry (Fig. S3B) for TEX11 on paraffin sections. TEX11 staining was observed in the nuclei of the spermatocytes, in the control and in both patients.

DISCUSSION

The introduction of high-throughput sequencing has exponentially improved diagnostic and research yields in relation to both rare and common complex diseases. In the field of Andrology, exome analysis has been relatively successful especially for descendants of consanguineous families and familial cases of infertility (recently reviewed by Krausz et al. 2018). In this study we aimed to assess the diagnostic potential of a gene panel designed on the basis of available mouse models. We have chosen this approach because all genes included in the panel are strong candidates for spermatogenic failure in human. The availability of the mouse model for these genes made the interpretation of the obtained results straight forwarded. In fact, functional studies, including mouse KO, are prerequisites to attributing a disease-causing role to a newly discovered gene. Hence, to we designed a gene panel that includes all monogenic models of mouse azoospermia and we sequenced the human orthologues in a cohort of 31 unrelated azoospermic patients and 2 azoospermic brothers from a consanguineous family. We identified a total of 74 low frequency and predicted as pathogenic variants in 49 genes in the group of 31 unrelated NOA patients and 4 shared variants in the two brothers.

Our major finding in the cohort of 31 unrelated NOA patients is the identification of a novel gene for male infertility, *STAG3*. We describe a patient (07-002) with compound heterozygous variants in this gene. The two variants are predicted to disturb significantly the protein. The frameshift insertion causes a premature stop gain in the 597th amino acid (normal STAG3 length: 1225 amino acids) while the splicing variant located in a canonical position (+1) of the splice donor site of 23rd exon (*STAG3* has 34 exons) is predicted to affect splicing by DANN, GERP, MutationTaster and the Human Splicing Finder (http://www.umd.be/HSF3/). *STAG3* encodes a meiosis specific component of the cohesin complex which is necessary for: i) the correct formation of chromosome axis; ii) the cohesion of sister chromatids after DNA replication iii) DNA DSB repair during meiosis (Garcia-Cruz et al. 2010; Fukuda et al. 2014; Winters et al. 2014; Hopkins et al. 2014; Llano et al. 2014; Ward et al. 2016; Nambiar and

Smith 2018). Various mutations (frameshift, splicing and missense) have been already reported in *STAG3* as a cause of Premature Ovarian Insufficiency (Caburet et al. 2014; Le Quesne Stabej et al. 2016; Colombo et al. 2017; He et al. 2018; Franca et al. 2018). In 4 out of 5 familial POI cases the mutations were in homozygosis since the carriers were from consanguineous families (Caburet et al. 2014; Le Quesne Stabej et al. 2016; Colombo et al. 2017; He et al. 2018). The first woman with POI carrying compound heterozygous variants in this gene was reported recently by Franca *et* al. (2018). *STAG3* is a strong candidate for male infertility because male mice lacking *Stag3* display a severe meiotic arrest phenotype (Llano et al. 2014) and in the MGI database mice, both male and female, are reported to be infertile due to azoospermia and absence of oocytes respectively. Our observation of lack of XY body formation, persistent γH2AX foci and failure to reach meiotic metaphase are consistent with the STAG3-deficient mouse phenotype. The use of remnant testis biopsy material for the immunofluorescent assessment of meiotic progression provides patient-relevant information since it allowed us to determine that in man, similar to mouse, STAG3 is required for proper meiotic chromosome pairing. Hence, it should be considered that if rare spermatids that may form in the testis of this patient would be found, they would most likely be genetically abnormal, and the patient should be informed of this likely risk.

Here, for the first time in the literature we report causative mutations in *STAG3* in human azoospermia which is clearly associated with a negative predictive value for testicular sperm retrieval.

Concerning the familiar case we identified a homozygous pathogenic variant in *RNF212* (NM_001131034.3:c.111dupT) shared by the two brothers. The truncating mutation is located inside the Zinc Finger domain and creates a new stop gain in the 38th amino acid (total RNF212 protein length is 297 amino acids). The protein encoded by *RNF212* is a RING-family E3-ligase required for chiasmata formation and assembly of crossover-specific recombination complexes (Reynolds et al. 2013; Qiao et al. 2014, 2018; Rao et al. 2017). Studies on mouse models show that the RNF212 protein functions to couple chromosome synapsis to the formation of crossover-specific recombination complexes (Reynolds et al. 2013). *Rnf212* mutation in mice causes sterility in both sexes and in particular *Rnf212* knockout mice are sterile due to the loss of spermatocytes at post–anaphase stage (Reynolds et al. 2013). Consistently, when TESE was attempted for the two brothers TESE, 90% of the tubules suffered spermatogenic arrest at the spermatocytic level. In addition, our immunofluorescent analyses of both brothers showed that spermatocytes reached pachytene, but underwent apoptosis during the first meiotic division (metaphase or anaphase). In addition, univalents were frequently observed. In *Rnf212*^{-/-} mice, crossing over

is diminished by ≥ 90%, as expected (Reynolds et al. 2013). We observed that 76.2 and 45.5% metaphase/anaphase cells contain possible univalent for patient 1 and 2, respectively. Although we could not detect MLH1 foci, the appropriate metaphase alignment of at least some bivalents, suggests that some crossovers still form in our *RNF212* patients. A reduction in the number of crossovers and metaphase arrest has also been observed in male mice upon deletion of the X-linked *Tex11* (Yang et al. 2008)*.* TEX11 is thought to be stabilized by RNF212, and the number of TEX11 foci is markedly lower (around 6 times less foci) upon deletion of *Rnf212* in male mice (Reynolds et al. 2013). Nevertheless, our analysis suggests that TEX11 foci formation is not affected by the *RNF212* mutation in our patients. So, although we have shown here that the meiotic localization and expression pattern of TEX11 is similar in mouse and man, in contrast to what was previously observed (Yatsenko et al. 2015), our data suggests that the functional interaction between RNF212 and TEX11 may be somewhat different in man compared to mouse.

In conclusion, by using a hypothesis-driven approach, which consisted in the sequencing of the 175 genes, we obtained a genetic diagnosis in one sporadic NOA patient and in two NOA brothers. Ours is the first study reporting biallelic variants in *STAG3* in one sporadic patient and a homozygous *RNF212* variant in the two brothers as the genetic cause of NOA. All three mutation carriers presented meiotic arrest leading to the genetic diagnosis in 3/7 cases with this specific testicular phenotype. Our study represents an additional step towards elucidating the genetic basis of early spermatogenic failure, since we report two new genes involved in human male meiotic arrest. We propose the inclusion of *RNF212* and *STAG3* in a future male infertility diagnostic gene panel. Meiotic studies allowed the detection of the functional consequences of the mutations and provided information on the role of STAG3 and RNF212 in human male meiosis.

More than half of the 175 sequenced genes are reported to affect also female reproduction in mice (among them *Rnf212 and Stag3*) and *STAG3* mutations were first described as a cause of female infertility (POI) and ovarian cancer. Hence, our results stimulate further research on shared genetic factors causing both POI and NOA. The diagnosis of such genetic factors implies that genetic counselling for NOA has relevance not only to the male family members and male descendants but also to female relatives.

MATERIAL AND METHODS

Subjects

From a total of 1300 infertile men attending the Fundacio Puigvert in Barcelona (Catalonia, Spain) and tested for Y chromosome microdeletions, we have selected those

affected by idiopathic NOA. 33 subjects gave informed consent for the present study and were enrolled. Two infertile brothers with consanguineous parents referred to the University Hospital of Careggi in Florence (Italy). These patients were selected according to the following inclusion criteria: i) azoospermia due to either spermatogenic arrest (at spermatogonial or spermatocytic level) or Sertoli Cell Only Syndrome (type I and II); ii) normal karyotype; iii) absence of Y-chromosome microdeletions and *TEX11* mutations; iv) absence of all known causes of azoospermia. Peripheral blood samples from the patients were collected for subsequent DNA extraction and genetic analyses. The testicular phenotype of the 31 unrelated patients was as follows: 20 Sertoli Cell Only Syndrome (17 type I and 3 type II), 11 spermatogenic arrest (6 spermatogonial arrest and 5 speramatocytic arrest). Regarding the two brothers, both showed bilateral spermatocytic arrest. Clinical characteristics of the patients are reported in table I. All recruited subjects signed an informed consent, upon approval by the local ethical committee.

Gene panel design

A list of genes with potential role in azoospermia was generated by reviewing data deposited in the MGI - Mouse Genome informatics (http://www.informatics.jax.org/) database. Briefly, we searched with the keyword "Azoospermia" in the Mammalian Phenotype Browser of the MGI and selected those mutants which involve a single gene i.e the phenotype is due to the alteration of one distinct gene. Subsequently, we searched for the human orthologs of the mouse genes by consulting the following databases: MGI and the DIOPT - DRSC Integrative Ortholog Prediction Tool (https://www.flyrnai.org/cgi-in/DRSC_orthologs.pl)

Gene panel sequencing

DNA libraries indexed with oligonucleotides compatible with Illumina's sequencing chemistry were prepared and captured using the NimbleGen SeqCap EZ Choice Library (Roche) following the manufacturer's protocol. Only the coding regions and the flanking sequences (±50 nucleotides) were included for the enrichment and library preparation. The enriched libraries were quantified with Qubit (Life technologies) and Bioanalyzer 2100 (Agilent technologies) The sequencing was performed on a NextSeq500 instrument (Illumina) to generate 2x150nt long sequences with an average coverage depth of 300X. Quality of reads was checked through FastQC (http://www.bioinformatics.babraham.ac.uk/projects/fastqc/). Reads were analyzed with an Illumina pipeline based on Burrows-Wheeler Aligner (BWA) for sequence alignment on GRCh37 (hg19) reference, on Broad Institute GATK for genotyping and on ANNOVAR for variant annotation.

Variants filtering

For the 31 unrelated azoospermic patients (sporadic cases), a standard variant filtering was applied to all samples. Briefly, we selected missense variants, stop gains/losses, frameshift insertions/deletions, and filtered out common polymorphisms (≥ 5% in the general population) after consulting the dbSNP 138, the 1000G (http://www.1000genomes.org) and the genome aggregation database gnomAD (http://gnomad-old.broadinstitute.org/). The obtained data was further filtered according to their potentially damaging effect depending on the type of variant. For SNVs, the prediction of pathogenicity was based on a series of prediction tools, such as SIFT, Polyphen2_HDIV, Polyphen2_HVAR, Mutation Taster, Mutation Assessor. An in-house index of pathogenicity (IP) was created as a score calculated on the basis of the five prediction tools employed, each providing a value ranging from 0 (null probability of being a deleterious variant) to 1 (full probability of being a deleterious variant). Not all prediction tools were always available; therefore a ratio was calculated between the summary score of pathogenicity and the number of prediction tools available for a given variant. Hence, we established an arbitrary threshold of IP>0.6, which means that the majority (not necessary all) of the interrogated tools gave a "pathogenic" score (See table SI). We also considered as "possibly pathogenic" all low frequency frameshift variants and indels within non repeated regions. Pathogenicity of the prioritized variants was also manually checked using Varsome (https://varsome.com/). Then the Integrative Genomics Viewer (IGV) was employed to exclude possible false positive calls and finally, the prioritized variants were validated by Sanger sequencing.

For the two brothers from a consanguineous family, after the abovementioned filtering we applied the recessive model approach for further analysis. So we filtered for rare and predicted as "pathogenic" variants in hemizygous or homozygous state that were shared by the two siblings.

Variant Validation with Sanger Sequencing

To confirm the candidate variants identified in the *RNF212* and *STAG3* genes we performed Sanger sequencing. Standard PCR was performed in a 10 μl reaction volume using the PCR Master Mix, 2x (Promega, Madison, WI, USA) and using the following protocol: 5-minute initial denaturation step at 94˚C; 35 cycles of 1-minute denaturation at 94˚C, 1-minute annealing at 60˚C, 1-minute extension at 72˚C; and final 5-minute extension at 72˚C. Presence of amplification products was verified through electrophoresis on a 2% agarose gel. PCR products purification was performed by using ExoSAP-IT (Affymetrix, Santa Clara, CA, USA) in a 6 μl reaction volume, through a 15-minutes initial incubation at 37°C followed by a second 15-minutes initial incubation at 80°C. Sequencing reaction was performed using the

The BigDye® Terminator v3.1 Cycle Sequencing Kit (Lifetechnologies, Foster City, CA, USA) in a 10 µl reaction volume using the following protocol: 1-minute initial denaturation step at 96˚C; 25 cycles of 10-second denaturation at 96 °C, 5-second annealing at 50°C, and 4-minute extension at 60°C. Capillary electrophoresis was performed on 4-capillary 3130 Genetic Analyzer (Applied Biosystems, Carlsbad, CA, USA). we performed direct sequencing of the region of interest (ABI 3130 Genetic Aanalyzer). Primers are reported in table SII.

Quantitative RT-PCR.

Quantitative RT-PCR (qRT-PCR) analysis was performed to evaluate *RNF212* and *STAG3* expression in biopsy samples of different types of adult testis histology collected in our laboratory. The extraction was performed through a combination of two commercially available kits, the TRI Reagent (Sigma-Aldrich, St. Louis, MO, USA) and the AllPrep DNA/RNA kit (Sigma-Aldrich, St. Louis, MO, USA), according to the manufacturer's instructions. cDNA synthesis was carried out using the High-Capacity cDNA Reverse Transcription Kit (Lifetechnologies, Foster City, CA, USA). qRT-PCR was performed using the TaqMan® Universal PCR Master Mix (Lifetechnologies, Foster City, CA, USA) with the following standard thermal cycler conditions: 40 cycles at 95 °C for 30 seconds and 60 °C for 1 min. We characterized at molecular level two samples with Sertoli cell-only syndrome (SCOS), two samples with spermatogonial arrest, two samples with spermatocytic arrest, and one sample with obstructive azoospermia (conserved spermatogenesis at the histological examination). This molecular characterization consisted in the expression analysis of four genes known to be expressed in different stages of spermatogenesis: *DAZ* (spermatogonia/early spermatocytes), *CDY1* (Spermatids), *BRDT* (pachytene spermatocytes/round and elongating spermatids) and *PRM2* (spermatids/mature spermatozoa). The housekeeping reference gene was *GAPDH.* Employed commercially assays are detailed in Table SIII. qRT-PCR runs were performed on a StepOne™ System (Applied biosystems, Carlsbad, CA, USA). Experiments were run in triplicates.

Meiotic studies:

Surplus testicular biopsy material was fixed in Bouins' fixative (brother 1) or 4% paraformaldehyde in PBS (brother 2, and from one control (control 1) who suffered obstructive azoospermia, and displayed a Johnsen score (JS) (Johnsen 1970) of 10 (normal spermatogenesis, presence of all cell types). For the carrier of the *STAG3* mutation (07-002) and a control sample (Control 3), the surplus testicular biopsy material was fixed in Bouins. In addition, surplus testicular biopsy material was processed to make nuclear spreads as described below from brother 2 and from a control (control 2, from fresh material). Nuclear spreads of control 2 displayed all spermatogenic cell types. By using multiple fluorescent

immunohistochemical stainings we analysed meiotic entry, metaphase formation (including assessment of univalent presence), formation of the XY body (the silenced chromatin area in male pachytene spermatocytes that contains the XY chromosome pair), apoptosis and spermatid formation. Moreover, crossover (CO) frequency was determined using immunocytochemistry (using an antibody targeting the CO-marker MLH1) for brother 2 and control 2. Finally since TEX11 is thought to be stabilized by RNF212 in mice, we also measured TEX11 expression in these patients using immunohistochemistry.

Fluorescent immunohistochemistry

Testis biopsies, embedded in paraffin, were sectioned (section thickness, 6 um), and placed on a drop of dH2O on coated slides (Starfrost). After stretching them on a heating plate at 39 ºC, the water was removed and the slides were dried overnight at 37 ºC in an incubator. Subsequently, the slides were placed at 60ºC in an oven for 1 hour to melt the paraffin. Then, the slides were dewaxed and rehydrated as follows: 3 x 5 minutes xylene, 3 x 5 minutes 100% ethanol and 3 x 5 minutes phosphate buffered saline (PBS). The slides were then incubated for 15 minutes in Proteinase K in PBS (1ug/ml). This was followed by washing steps with demineralized H2O (dH2O; 4 x 2 minutes) and an incubation with terminal deoxynucleotidyl transferase (TdT) buffer (0.1M Na-cacodylate, pH 6.8,1.0 mM CoCl,0.1 mM DTT) for 30 minutes in a humid chamber. Subsequently, the slides were washed 3 x 5 minutes with TB buffer (300mM NaCl, 30mMtri-sodiumcitrate-dihydrate in dH2O) and 3 x 5 minutes with dH2O. Thereafter, an epitope retrieval step was performed with sodium citrate buffer pH6 (1mM Tri-Sodium citrate (dihydrate)) in a microwave at maximum power (1 x10 minutes, 2 times x 5 minutes, refilling the evaporated water after each microwave step). The slides were cooled down to room temperature in the sodium citrate buffer for approximately one hour, after which they were washed with PBS (3 x 5 minutes). Blocking was performed by incubating the sections in 10% normal goat serum and 5% bovine serum albumin (BSA) diluted in PBS, in a humid chamber for 30 minutes at room temperature. We used dual fluorescent staining, but with sequential incubation of the primary antibodies, as well as sequential detection, in order to reduce the risk of unspecific staining. The first primary antibody (diluted in 5% BSA/PBS) was then added to the sections and the slides were incubated in a humid chamber at 4 ºC overnight. The second day, the slides were first kept at room temperature for one hour and then washed 3 x 5 minutes with PBS. Subsequently, the first secondary antibody (diluted in PBS) was added and the slides were incubated for 1.5 hour in a humid chamber at room temperature. The slides were subsequently washed 3 x 5 minutes in PBS and incubated with the second primary antibody in 5% BSA/PBS overnight. The third day, we repeated the same steps for the detection of the

second secondary antibody. Finally, slides were washed 3 x 5 minutes in PBS, and mounted using Prolong Gold Antifade reagent with DAPI.

Fluorescent immunocytochemistry

Nuclear spreads of spermatocytes were prepared from testis biopsies, following the protocol described by Peters et al., 1997. The steps of decapsulation of the tunica albuginea and placement of the cell suspension in hypobuffer solution were not performed for frozen testis biopsies (brother 2). Spread preparations of both control and patients were stored at −80C. Thawed slides were washed in PBS (3×10 min), and non-specific sites were blocked with 0.5% w/v BSA and 0.5% w/v milk powder in PBS. Primary antibodies were diluted in 10% w/v BSA in PBS, and incubations were performed overnight at room temperature in a humid chamber. Subsequently, slides were washed (3×10 min) in PBS, blocked in 10% v/v normal goat serum (Sigma) in blocking buffer (supernatant of 5% w/v milk powder in PBS centrifuged at 14,000 rpm for 10 min), and incubated with secondary antibodies in 10% normal goat serum in blocking buffer at room temperature for 2 hours. Finally, slides were washed (3×10 min) in PBS and embedded in Prolong Gold with DAPI (Invitrogen). Stripping of the slides was performed following the protocol described by van de Werken et al., 2013.

Antibodies

The following primary antibodies were used: mouse monoclonal anti-SYCP3 (ABCAM:ab97672) at 1:200, rabbit polyclonal anti-SYCP3 (Lammers et al. 1994) at 1:750, goat polyclonal SYCP3 at 1:100 (R&D systems), mouse monoclonal anti-MLH1 (cat. 551091, BD Pharmigen) at 1:25, mouse polyclonal anti- γH2AX at 1:750 (Millipore,05-636), mouse acrosome-specific antibody (Moore et al. 1987), rabbit polyclonal anti-TEX11 (Sigma: HPA002950), goat polyclonal anti-TEX11 (Abcam: 99461), human anti-centromere antibody (ACA) (Crest) at 1:1000 (human centromere antiserum, Fitzgerald Industries), rabbit polyclonal anti-TP2 at 1:1000 (Alfonso and Kistler 1993), mouse monoclonal anti-protamine 1 at 1:500 (MAb-001, Briar Patch), rabbit polyclonal anti-MSH4 (ABCAM: ab58666). For secondary antibodies, we used a goat anti-rabbit alexa 488 IgG, goat anti-mouse alexa 488 and goat anti-mouse alexa 546 IgG (Invitrogen), all at 1:500 dilution.

Calculation of thresholds:

Based on a large cohort of patients and controls we calculated thresholds for meiotic entry, meiotic metaphase, and activation apoptosis during meiotic metaphase (manuscript to be submitted). In brief, we used the mean ± 2 SD (95% confidence interval). If the lowest/highest value of the control group was not inside this confidence interval, a Grubb's test was performed to determine if it was an outlier. In case it was not an outlier, this value was used as threshold.

ACKNOWLEDGEMENTS

FUNDING

CONFLICT OF INTEREST

The authors declare no conflict of interest.

PATIENT CONSENT

All participants signed an informed consent.

ETHICS APPROVAL

The local Ethical Committee of the Fundació Puigvert and of the University Hospital of Careggi approved the study.

Patient code	Testicular histology	Sperm retrieval after TESE	FSH (IU/L)	LH (IU/L)	Testosterone (nmol/L)	Right Testicular volume (cc)	Left Testicular volume (cc)
13-403	SCOS type I	No	42.9	17	10.6	7	7
09-195	SCOS type II	Yes	18	n.a	n.a	10	12
08-457	SCOS type I	No	6.19	3.09	20.8	12	12
16-394	Incomplete SpermatoGonial Arrest	Yes	16.8	6.96	20.5	15	13
12-201	Incomplete SpermatoCytic Arrest	Yes	12.1	4.67	8.6	10	10
13-603	SCOS type I	No	16	12.42	11.2	12	13
11-381	SCOS type I	No	11.7	4.74	19.24	10	12
07-478	SCOS type I	No	23	9	9.4	12	12
15-546	SCOS type I	No	21.8	7.5	19.7	12	10
15-547	SCOS type I	No	13.72	7.61	15.5	10	12
15-368	SCOS type I	No	24.8	6.3	10	11	10
09-464	SCOS type I	No	20.3	n.a	10.2	10	9
11-536	Incomplete SpermatoGonial Arrest	Yes	20	n.a	n.a	15	15
11-272	SpermatoCytic Arrest	No	7.16	n.a	16	22	22
11-456	SCOS type II	No	18	9.7	14.81	12	12
14-313	SCOS type I	No	12.7	4.16	29.7	12	13
15-572	Incomplete SpermatoGonial Arrest	Yes	3.21	6.24	21.8	25	25
15-192	SCOS type I	No	19.1	10.3	25.9	11	13
07-002	SpermatoCytic Arrest	No	4.1	2.8	15.6	15	15
15-302	SCOS type I	No	22.3	5.27	24.89	12	12
15-539	SCOS type I	No	26.9	8.4	13.62	9	8
15-654	SCOS type I	No	18.1	17.22	17.2	10	10
13-400	SCOS type II	Yes	6.11	n.a	n.a	18	18
07-099	SCOS type I	No	6.8	2.87	n.a	13	12
16-531	Incomplete SpermatoGonial Arrest	No	4.78	2.67	18.9	15	20
04-179	SpermatoCytic Arrest	No	20	5.9	23.9	10	12
16-639	Incomplete SpermatoGonial Arrest	No	14.66	9.85	23.4	20	18
16-702	SpermatoCytic Arrest	No	5	6.33	21.1	18	18
10-440	SCOS type I	No	25.34	18.03	10	10	4
10-499	Incomplete SpermatoGonial Arrest	Yes	4.36	2.93	20.67	20	20
16-606	SCOS type I	No	22.52	n.a	n.a	10	10
A1053	SpermatoCytic Arrest	No*	2.72	5.4	11	18	18
A1535	SpermatoCytic Arrest	No	3.62	1.77	8.3	12	12

* microTESE allowed the retrieval of few spermatids; n.a: not available

**Table I:** Clinical characteristics of the selected azoospermic patients

REFERENCES

Alfonso PJ, Kistler WS (1993) Immunohistochemical localization of spermatid nuclear transition protein 2 in the testes of rats and mice. Biol Reprod 48:522–9

Caburet S, Arboleda VA, Llano E, et al (2014) Mutant cohesin in premature ovarian failure. N Engl J Med 370:943–949. doi: 10.1056/NEJMoa1309635

Colombo R, Pontoglio A, Bini M (2017) A STAG3 missense mutation in two sisters with primary ovarian insufficiency. Eur. J. Obstet. Gynecol. Reprod. Biol. 216:269–271

Florke-Gerloff S, Topfer-Petersen E, Muller-Esterl W, et al (1983) Acrosin and the acrosome in human spermatogenesis. Hum Genet 65:61–67

Franca MM, Nishi MY, Funari MFA, et al (2018) Two rare loss-of-function variants in the STAG3 gene leading to primary ovarian insufficiency. Eur J Med Genet. doi: 10.1016/j.ejmg.2018.07.008

Fukuda T, Fukuda N, Agostinho A, et al (2014) STAG3-mediated stabilization of REC8 cohesin complexes promotes chromosome synapsis during meiosis. EMBO J 33:1243–1255. doi: 10.1002/embj.201387329

Garcia-Cruz R, Brieno MA, Roig I, et al (2010) Dynamics of cohesin proteins REC8, STAG3, SMC1 beta and SMC3 are consistent with a role in sister chromatid cohesion during meiosis in human oocytes. Hum Reprod 25:2316–2327. doi: 10.1093/humrep/deq180

He W-B, Banerjee S, Meng L-L, et al (2018) Whole-exome sequencing identifies a homozygous donor splice-site mutation in STAG3 that causes primary ovarian insufficiency. Clin Genet 93:340–344. doi: 10.1111/cge.13034

Hopkins J, Hwang G, Jacob J, et al (2014) Meiosis-specific cohesin component, Stag3 is essential for maintaining centromere chromatid cohesion, and required for DNA repair and synapsis between homologous chromosomes. PLoS Genet 10:e1004413. doi: 10.1371/journal.pgen.1004413

Jamsai D, O'Bryan MK (2011) Mouse models in male fertility research. Asian J Androl 13:139–151. doi: 10.1038/aja.2010.101

Johnsen SG (1970) Testicular biopsy score count--a method for registration of spermatogenesis in human testes: normal values and results in 335 hypogonadal males. Hormones 1:2–25

Krausz C, Cioppi F, Riera-Escamilla A (2018) Testing for genetic contributions to infertility: potential clinical impact. Expert Rev Mol Diagn 18:331–346. doi: 10.1080/14737159.2018.1453358

Krausz C, Riera-Escamilla A (2018) Genetics of male infertility. Nat Rev Urol 15:369–384. doi: 10.1038/s41585-018-0003-3

Lammers JH, Offenberg HH, van Aalderen M, et al (1994) The gene encoding a major component of the lateral elements of synaptonemal complexes of the rat is related to X-linked lymphocyte-regulated genes. Mol Cell Biol 14:1137–46

Le Quesne Stabej P, Williams HJ, James C, et al (2016) STAG3 truncating variant as the cause of primary ovarian insufficiency. Eur J Hum Genet 24:135–138. doi: 10.1038/ejhg.2015.107

Llano E, Gomez-H L, Garcia-Tunon I, et al (2014) STAG3 is a strong candidate gene for male infertility. Hum Mol Genet 23:3421–3431. doi: 10.1093/hmg/ddu051

Mahadevaiah SK, Turner JM, Baudat F, et al (2001) Recombinational DNA double-strand breaks in mice precede synapsis. Nat Genet 27:271–6. doi: 10.1038/85830

Moore HDM, Smith CA, Hartman TD, Bye AP (1987) Visualization and characterization of the acrosome reaction of human spermatozoa by immunolocalization with monoclonal antibody. Gamete Res 17:245–259. doi: 10.1002/mrd.1120170308

Mueller JL, Mahadevaiah SK, Park PJ, et al (2008) The mouse X chromosome is enriched for multicopy testis genes showing postmeiotic expression. Nat Genet 40:794–799. doi: 10.1038/ng.126

Nambiar M, Smith GR (2018) Pericentromere-Specific Cohesin Complex Prevents Meiotic Pericentric DNA Double-Strand Breaks and Lethal Crossovers. Mol Cell 71:540–553.e4. doi: 10.1016/j.molcel.2018.06.035

Perlman RL (2016) Mouse models of human disease: An evolutionary perspective. Evol Med

public Heal 2016:170–176. doi: 10.1093/emph/eow014

Peters AH, Plug AW, van Vugt MJ, de Boer P (1997) A drying-down technique for the spreading of mammalian meiocytes from the male and female germline. Chromosome Res 5:66–8

Qiao H, Prasada Rao HBD, Yang Y, et al (2014) Antagonistic roles of ubiquitin ligase HEI10 and SUMO ligase RNF212 regulate meiotic recombination. Nat Genet 46:194–9. doi: 10.1038/ng.2858

Qiao H, Rao HBDP, Yun Y, et al (2018) Impeding DNA Break Repair Enables Oocyte Quality Control. Mol Cell 72:211–221.e3. doi: 10.1016/j.molcel.2018.08.031

Rao HBDP, Qiao H, Bhatt SK, et al (2017) A SUMO-ubiquitin relay recruits proteasomes to chromosome axes to regulate meiotic recombination. Science 355:403–407. doi: 10.1126/science.aaf6407

Reynolds A, Qiao H, Yang Y, et al (2013) RNF212 is a dosage-sensitive regulator of crossing-over during mammalian meiosis. Nat Genet 45:269–78. doi: 10.1038/ng.2541

Song N, Liu J, An S, et al (2011) Immunohistochemical Analysis of Histone H3 Modifications in Germ Cells during Mouse Spermatogenesis. ACTA Histochem Cytochem 44:183–190. doi: 10.1267/ahc.11027

Tournaye H, Krausz C, Oates RD (2016) Novel concepts in the aetiology of male reproductive impairment. lancet Diabetes Endocrinol. doi: 10.1016/S2213-8587(16)30040-7

van de Werken C, Jahr H, Avo Santos M, et al (2013) A universal method for sequential immunofluorescent analysis of chromatin and chromatin-associated proteins on chromosome spreads. Chromosome Res 21:475–89. doi: 10.1007/s10577-013-9373-9

Ward A, Hopkins J, Mckay M, et al (2016) Genetic Interactions Between the Meiosis-Specific Cohesin Components, STAG3, REC8, and RAD21L. G3 (Bethesda) 6:1713–1724. doi: 10.1534/g3.116.029462

Winters T, McNicoll F, Jessberger R (2014) Meiotic cohesin STAG3 is required for chromosome axis formation and sister chromatid cohesion. EMBO J 33:1256–1270. doi: 10.1002/embj.201387330

Yang F, Gell K, van der Heijden GW, et al (2008) Meiotic failure in male mice lacking an X-linked factor. Genes Dev 22:682–91. doi: 10.1101/gad.1613608

Yatsenko AN, Georgiadis AP, Röpke A, et al (2015) X-linked TEX11 mutations, meiotic arrest, and azoospermia in infertile men. N Engl J Med 372:2097–107. doi: 10.1056/NEJMoa1406192

4b

SUPPLEMENTAL FIGURES
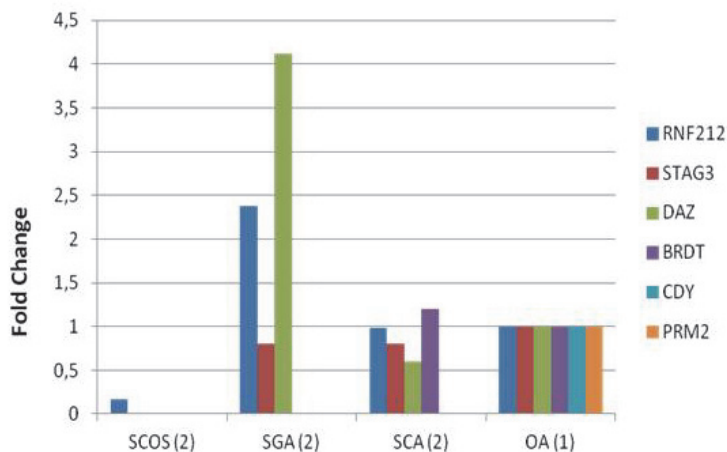
Fig. S1. Expression evaluation of the *RNF212 and STAG3* genes in adult testis biopsies. Quantitative RT-PCR (qRT-PCR) analysis was performed to evaluate *RNF212 and STAG3* expression in biopsy samples of different types of adult testis histologies: i) two SCOS (Sertoli Cell-Only Syndrome); ii) two SGA: maturation arrest at the spermatogonial level; iii) two SCA: maturation arrest at the spermatocytic level. One sample with obstructive azoospermia (OA) was used as internal control. Samples were first characterized by testing for four spermatogenic markers expressed at different stages of spermatogenesis: *PRM2* (spermatids/mature spermatozoa); *CDY1* (spermatids); *BRDT* (pachytene spermatocytes/round and elongating spermatids) and *DAZ* (spermatogonia/early spermatocytes).

▶ **Fig. S2. Assessment of the presence of spermatids and univalents in the brothers carrying the *RNF212* variant. A)** Spread preparations of control 2 and brother 2. Immunostaining of SYCP3 (red) and MLH1 (green), or SYCP3 (red) and Crest (green) (spermatocytes). Immunostaining of Crest (green), or protamine-1 (green) (spermatids). Chromatin is stained with DAPI (blue). Both round and elongating spermatids are absent in brother 2. Scale bar 10 μm. **B)** Metaphase and anaphase nuclei (maximum projection) of control 1 and both patients. Immunostaining of H3Ser10ph (red). Chromatin is stained with DAPI (blue). Arrowheads indicate lagging chromosomes. Scale bar 10 μm. **C)** Analysis of metaphases/anaphase nuclei (H3Ser10ph-positive) (n = 21, 22 and 21 in paraffin sections from brother 1, 2 and control 1, respectively). Cells were categorized as metaphase or anaphase, and these as normal or abnormal (because of the presence of possible univalents or other aberrations).

A
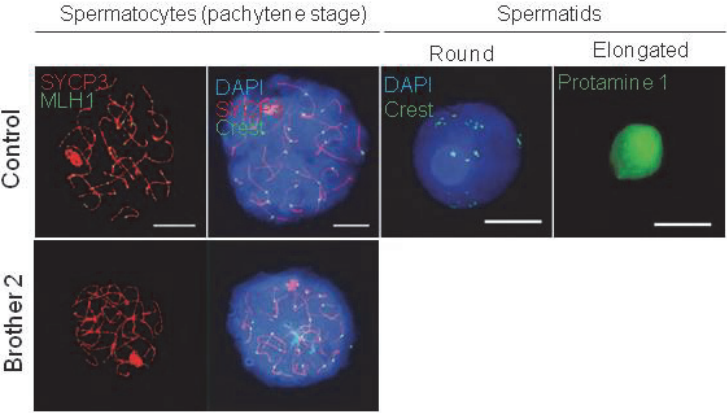
B
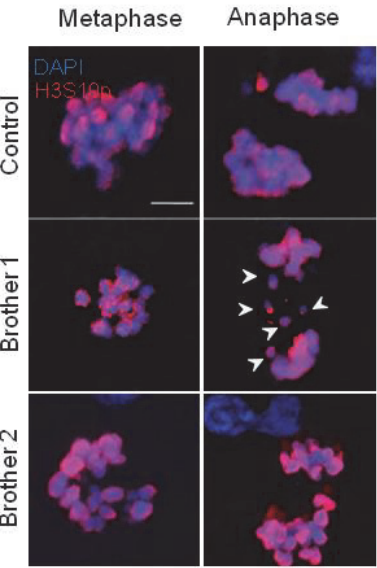
C

	Control	Brother1	Brother2
Total cells	21	21	22
METAPHASES	21	12	19
Normal	19	3	8
Abnormal	2	9	11
Possibly univalents	2	9	9
ANAPHASES	0	9	3
Normal	0	2	1
Abnormal	0	7	2
Possibly univalents	0	7	1
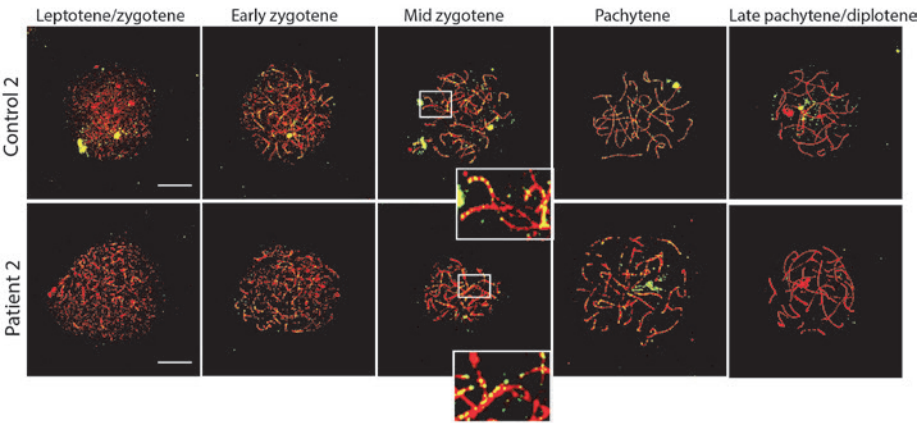
4b
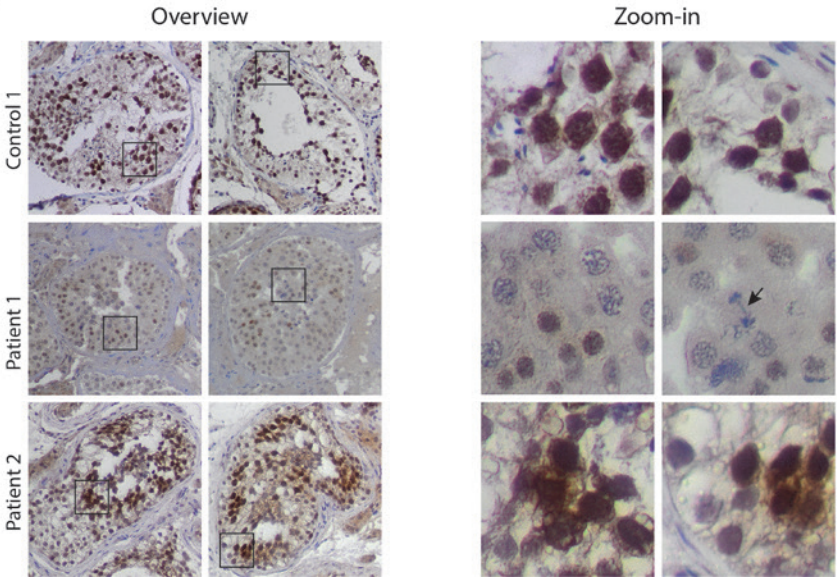
Fig. S3. Analysis of TEX11 expression and localization in testis biopsies from the two brothers carrying the *RNF212* pathogenic variant. A) Progression of meiotic prophase I in spermatocyte spreads of control 2 and brother 2. Immunostaining of SYCP3 (red) and TEX11 (green). Enlarged regions (indicated by white boxes) are displayed in mid zygotene stage of both control and brother 2. B) DAB (3,3'-diaminobenzidine) immunohistochemistry for TEX11 on paraffin sections of control 1 and both patients. Enlarged regions (indicated by black boxes) are shown on the right. Arrow indicates a chromosome bridge between the two separating groups of anaphase chromosomes of patient 1. Scale bar 10 μm.

SUPPLEMENTAL TABLES

Table SI. Algorithms employed to calculate the index of pathogenicity for variant prioritization**.**

Algorithm	Prediction	Meaning	Numeric value (u)
SIFT	T	tolerated	0
	D	damaging	1
Polyphen	B	Benign	0
	P	probably damaging	0.5
	D	damaging	1
Mutation Assessor	N	neutral	0
	L	low	0.25
	M	medium	0.5
	H	high	1
Mutation Taster	P	polymorphism	0
	D	damaging	1

Index of pathogenicity (IP) was calculated according to the following formula:

$$\frac{\left(\sum_{r=1}^{n} u_r \right)}{k}$$

Where **k**= number of available prediction tools.

Table SII. Primers employed for *RNF212 and STAG3* mutational screening by Sanger sequencing

Variant	FW primer (5'-3')	Rev primer (5'-3')	Size (bp)
RNF212:c.112_113insT	CAGCCTCATCCTGTCAGAACAT	AACGGAGCAAAGTGACTGAA	319
STAG3:c.1759dupG	AGAGTGTCCTCCTCCCATCC	AGCTCTTCAAGCTCCTGCTG	270
STAG3:exon23:c.2394+1G>A	GCTGTCGAGTTTGAGGGACA	GACAAAAGCCTGTAGGGGGA	227

.

Table SIII. Commercially available TaqMan gene expression assays used in this study for the analysis of testis biopsies.

Gene	Function	Assay ID
STAG3	Target gene	Hs00429370_m1
RNF212	Target gene	Hs00857304_m1
DAZ	Spermatogonia/early spermatocytes biomarker	Hs00414014_m1
BRDT	Pachytene spermatocytes/round and elongating spermatids	Hs00976114_m1
CDY1	Spermatids biomarker	Hs00371514_m1
PRM2	Spermatids/mature spermatozoa biomarker	Hs04187294_g1
GAPDH	Reference housekeeping gene	Hs0275891_g1

Supplementary table IV: List of genes included in the "mouse azoospermia" gene panel sequenced in 33 iNOA patients

Gene symbol	Chromosome	Karyotype band
ACVR2A	2	q22.3
ADRM1	20	q13.33
AFF4	5	q31.1
AGPS	2	q31.2
AGTPBP1	9	q21.33
AK7	14	q32.2
AKAP9	7	q21.2
APAF1	12	q23.1
AR	X	q12
ATM	11	q22.3
BAX	19	q13.33
BCL2L2	14	q11.2
BOLL	2	q33.1
BRCA1	17	q21.31
BRCA2	13	q13.1
BRDT	1	p22.1
BSG	19	p13.3
BTBD18	11	q12.1
C11orf80	11	q13.2
C14orf39	14	q23.1

CCDC42	17	p13.1
CCNB1IP1	14	q11.2
CDK2	12	q13.2
CDK4	12	q14.1
CEP63	3	q22.2
CIB1	15	q26.1
CKS2	9	q22.2
CLCN2	3	q27.1
CLDN11	3	q26.2
CLPP	19	p13.3
CNBD2	20	q11.23
CUL4A	13	q34
DHH	12	q13.12
DMC1	22	q13.1
DMRTC2	19	q13.2
DNMT3A	2	p23.3
DNMT3L	21	q22.3
EHD1	11	q13.1
EHMT2	6	p21.33
EIF2S3	X	p22.11
EIF4G3	1	p36.12
ETV5	3	q27.2
FADS2	11	q12.2
FANCF	11	p14.3
FANCM	14	q21.2
FKBP6	7	q11.23
FOXP3	X	p11.23
GAL3ST1	22	q12.2
GJA1	6	q22.31
GNPAT	1	q42.2
GOLGA3	12	q24.33
GTF2A1	14	q31.1
HCN2	19	p13.3
HMGA1	6	p21.31
HMGA2	12	q14.3
HORMAD1	1	q21.3
HORMAD2	22	q12.2
HOXA10	7	p15.2
HOXA11	7	p15.2
HSF2	6	q22.31
HSP90AA1	14	q32.31
HSPBP1	19	q13.42
IKBKG	X	q28
INSL6	9	p24.1
IP6K1	3	p21.31

4b

IQCG	3	q29
KCNJ6	21	q22.13
KISS1	1	q32.1
KISS1R	19	p13.3
KIT	4	q12
KITLG	12	q21.32
KL	13	q13.1
LHB	19	q13.33
LHX3	9	q34.3
LIPE	19	q13.2
LMNA	1	q22
LMTK2	7	q21.3
MAD2L2	1	p36.22
MAP2	2	q34
MCM8	20	p12.3
MCMDC2	8	q13.1
MEI1	22	q13.2
MEI4	6	q14.1
MEIG1	10	p13
MEIOB	16	p13.3
MEIOC	17	q21,31
MGAT2	14	q21.3
MLH1	3	p22.2
MLH3	14	q24.3
MORC1	3	q13.13
MORC2	22	q12.2
MOV10L1	22	q13.33
MSH4	1	p31.1
MSH5	6	p21.33
MYBL1	8	q13.1
NANOS2	19	q13.32
NANOS3	19	p13.12
NHLH2	1	p13.1
NKAPL	6	p22.1
NME5	5	q31.2
NUP210L	1	q21.3
NUPR1	16	p11.2
P2RX1	17	p13.2
PAFAH1B1	17	p13.3
PANK2	20	p13
PATZ1	22	q12.2
PIN1	19	p13.2
PIWIL1	12	q24.33
PIWIL2	8	p21.3
PLD6	17	p11.2

POC1A	3	p21.2
POLG	15	q26.1
PPP1CC	12	q24.11
PRDM1	6	q21
PRDM9	5	p14.2
PROKR2	20	p12.3
PSMC3IP	17	q21.2
RAD21L1	20	p13
RANBP1	22	q11.21
RANBP9	6	p23
RBM5	3	p21.31
REC8	14	q12
RNF17	13	q12.12
RNF212	4	p16.3
RNF8	6	p21.2
RXFP1	4	q32.1
RXFP2	13	q13.1
SAFB	19	p13.3
SBF1	22	q13.33
SCMH1	1	p34.2
SCML2	X	p22.13
SETX	9	q34.13
SIAH1	16	q12.1
SIX5	19	q13.32
SLC12A2	5	q23.3
SLC19A2	1	q24.2
SLC4A2	7	q36.1
SLX4	16	p13.3
SMC1B	22	q13.31
SOX30	5	q33.3
SPATA22	17	p13.2
SPO11	20	q13.31
STAG3	7	q22.1
STRA8	7	q33
STX2	12	q24.33
SUN1	7	p22.3
SYCE1	10	q26.3
SYCE3	22	q13.33
SYCP1	1	p13.2
SYCP2	20	q13.33
SYCP3	12	q23.2
TASP1	20	p12.1
TAZ	X	q28
TBPL1	6	q23.2
TDRD1	10	q25.3

4b

TDRD12	19	q13.11
TDRD6	6	p12.3
TDRD9	14	q32.33
TDRKH	1	q21.3
TERB1	16	q22.1
TEX19	17	q25.3
THEG	19	p13.3
TMEM203	9	q34.3
TOPAZ1	3	p21.31
TPST2	22	q12.1
TSC22D3	X	q22.3
TTC26	7	q34
UBE2W	8	q21.11
UTP14C	13	q14.3
VRK1	14	q32.2
WT1	11	p13
YBX2	17	p13.1
YTHDC2	5	q22.2
ZBTB16	11	q23.2
ZC3HC1	7	q32.2

Supplementary table V. Selected variants (low frequency and predicted as pathogenic) identified in the 33 iNOA patients

Patient code	Gene	Variant description	Type of variant	Patient genotype	Mouse genotype	OMIM disease associated (Inheritance)*	Reason to discard pathogenicity (in case of AD reported in OMIM)
04-179	*CLCN2*	NM_001171088:c.1802_1803insCCG p.R601delinsRR	nonframeshift insertion	het	hom	Hyperaldosteronism familial, type II (AD) / Leukoencephalopathy with ataxia (AR)	Familial hyperaldosteronism not present in the patient
	UBE2W	NM_018299:c.530-2Adel	splicing	het	hom	No disease associated	-
	HSPBP1	NM_001297600:c.C751T:p.R251C	missense	het	hom	No disease associated	-
	GAL3ST1	NM_004861:c.G1004A:p.R335H	missense	het	hom	No disease associated	-
07-002	*EIF4G3*	NM_001198801:c.2193+2T>C	splicing	het	hom	No disease associated	-
	IQCG	NM_001134435:c.T224C:p.L75P	missense	het	hom	No disease associated	-
	AKAP9	NM_005751:c.C2473T:p.L825F	missense	het	hom	Long QT syndrome-11 (AD)	Patient is not affected by Long QT syndrome
	STAG3	NM_001282718:c.1759dupG:p.A586fs	frameshift insertion	het	hom	Premature ovarian failure 8 (AR)	-
	STAG3	NM_001282718:c.2220+1G>A	splicing	het	hom	Premature ovarian failure 8 (AR)	-
	UTP14C	NM_021645:c.C1070A:p.P357H	missense	het	hom	No disease associated	-
07-099	*PROKR2*	NM_144773:c.T518G:p.L173R	missense	het	hom	Hypogonadotropic hypogonadism 3 with or without anosmia (AD)	Mutation found in two controls without hypogonadism (Magdalena Avbelj Stefanija et al. 2012). Moreover, homozygous truncating mutations described in men (Abreu et al. 2008)

4b

07-478	DHH	NM_021044:c.C217G:p.R73G	missense	het	hom	46XYY sex reversal 7 (AR)	.
08-457	SBF1	NM_002972:c.G2216A:p.R739H	missense	het	hom	Charcot-Marie-Tooth disease, type 4B3 (AR)	.
07-095	NME5	NM_003551:c.G149A:p.S50N	missense	het	hom	No disease associated	.
	MLH3	NM_001040108:c.G1870C:p.E624Q	missense	het	hom	Colorectal cancer, hereditary nonpolyposis, type 7 (no data)	.
	P2RX1	NM_002558:c.G286A:p.G96R	missense	het	hom	No disease associated	.
	ADRM1	NM_001281437:c.G47A:p.R16Q	missense	het	hom	No disease associated	.
09-464	YTHDC2	NM_022828:c.G2639A:p.R880H	missense	het	hom	No disease associated	.
10-440	ETV5	NM_004454:c.A1043G:p.K348R	missense	het	hom	No disease associated	.
	DMRTC2	NM_001040283:c.1101_1102insTAG AAA:p.S367delinsSX	stopgain	het	hom	No disease associated	.
10-499	UBE2W	NM_018299:c.530-2Adel	splicing	het	hom	No disease associated	.
11-272	HORMAD1	NM_001199829:c.A1129T:p.R377W	missense	het	hom	No disease associated	.
	YTHDC2	NM_022828:c.1689-2A>T	splicing	het	hom	No disease associated	.
	AK7	NM_152327:c.150_161delp.50_54del	nonframeshift deletion	het	hom	Spermatogenic failure 27 (AR)	.
	BSG	NM_198591:c.C505T:p.R169W	missense	het	hom	No disease associated	.
11-381	SYCP1	NM_001282542:c.C2503T:p.P835S	missense	het	hom	No disease associated	.
	UBE2W	NM_018299:c.530-2Adel	splicing	het	hom	No disease associated	.
	ATM	NM_000051:c.C3161G:p.P1054R	missense	het	hom	Ataxia-telangiectasia (AR)	.
	GOLGA3	NM_001172557:c.A1139G:p.N380S	missense	het	hom	No disease associated	.
	DNMT3L	NM_013369:c.C811T:p.R271W	missense	het	hom	No disease associated	.
11-456	MSH5	NM_002441:c.C1051G:p.R351G	missense	het	hom	Premature ovarian failure 13 (AR)	.
	STX2	NM_001980:c.T94G:p.F32V	missense	het	hom	No disease associated	.
	ADRM1	NM_001281437:c.1059_1060insGAC ACGAAG:p.G353delinsGDTK	nonframeshift insertion	het	hom	No disease associated	.

11-536	KITLG	NM_003994:c.G544T:p.D182Y	missense	het	hom	Deafness, autosomal dominant 69, unilateral or asymmetric (AD) / Hyperpigmentation with or without hypopigmentation(AD)	Patient is not deaf and/or hyperpigmented
	FANCM	NM_001308133:c.G2242T:p.E748X	stopgain	het	hom	Premature ovarian failure 15 (AR) /Spermatogenic failure 28 (AR)	
	PROKR2	NM_144773:c.C403T:p.R135C	missense	het	hom	Hypogonadotropic hypogonadism 3 with or without anosmia (AD)	Mutation found in two controls without hypogonadism (Magdalena Avbelj Stefanija et al. 2012). Moreover, homozygous truncating mutations described in men (Abreu et al. 2008)
12-201	LMTK2	NM_014916:c.A3967G:p.S1323G	missense	het	hom	No disease associated	-
	UTP14C	NM_021645:c.T326A:p.V109D	missense	het	hom	No disease associated	-
	CUL4A	NM_001008895:c.C2186T:p.P729L	missense	het	hom	No disease associated	-
13-400	TDRD6	NM_001010870:c.G2765A:p.C922Y	missense	het	hom	No disease associated	-
	POLG	NM_001126131:c.C1760T:p.P587L	missense	het	hom	Mitochondrial DNA depletion syndrome 4A - Alpers type (AR) / Mitochondrial DNA depletion syndrome 4B-MNGIE type (AR) /Mitochondrial recessive ataxia syndrome - includes SANDO and SCAE (AR) /Progressive external ophthalmoplegia, autosomal recessive 1 (AR) /Progressive external ophthalmoplegia, autosomal dominant 1 (AD)	Patient is not affected for any of the POLG-linked disease reported in OMIM. In addition, same compund heterozygous mutations described in a healthy father (Da Pozzo et al.

4b

Sample	Gene	cDNA change	Variant type	het	hom	Disease associated	Comment
	POLG	NM_001126131:c.752T>p.T251I	missense	het	hom	Mitochondrial DNA depletion syndrome 4A - Alpers type (AR) / Mitochondrial DNA depletion syndrome 4B-MNGIE type (AR) /Mitochondrial recessive ataxia syndrome - includes SANDO and SCAE (AR) /Progressive external ophthalmoplegia, autosomal recessive 1 (AR) /Progressive external ophthalmoplegia, autosomal dominant 1 (AD)	2016)
13-403	AKAP9	NM_005751:c.C7796T:p.S2599L	missense	het	hom	Long QT syndrome-11 (AD)	Patient is not affected by Long QT syndrome
	BRCA2	NM_000059:c.G223C:p.A75P	missense	het	hom	Fanconi anemia, complementation group D1 (AR) / Wilms tumor (AD)	Patient is not affected by Wilms tumor
	VRK1	NM_003384:c.C466A:p.Q156K	missense	het	hom	Pontocerebellar hypoplasia type 1A (AR)	-
	POLG	NM_001126131:c.C1837T:p.H613Y	missense	het	hom	Mitochondrial DNA depletion syndrome 4A - Alpers type (AR) / Mitochondrial DNA depletion syndrome 4B-MNGIE type (AR) /Mitochondrial recessive ataxia syndrome - includes SANDO and SCAE (AR) /Progressive external ophthalmoplegia, autosomal recessive 1 (AR) /Progressive external ophthalmoplegia, autosomal dominant 1 (AD)	Patient is not affected for any of the POLG-linked diseases reported in OMIM
	ADRM1	NM_001281437:c.1059_1060insGACACGAAG:p.G353delinsGDTK	nonframeshift insertion	het	hom	No disease associated	-
13-603	THEG	NM_199202:c.C505T:p.R169C	missense	het	hom	No disease associated	-
	TPST2	NM_001008566:c.G458A:p.R153H	missense	het	hom	No disease associated	-
13-413	EHMT2	NM_001289413:c.C344T:p.S115F	missense	het	hom	No disease associated	-
	UBE2W	NM_018299:c.530-2Adel	splicing	het	hom	No disease associated	-

4b

| Sample	Gene	Variant	Type			Disease association	Notes
15-302	MOV10L1	NM_001164106:c.G454A:p.E152K	missense	het	hom	No disease associated	-
	UBE2W	NM_018299:c.530-2Adel	splicing	het	hom	No disease associated	-
15-368	MAP2	NM_002374:c.T2664A:p.N888K	missense	het	hom	No disease associated	-
	POC1A	NM_001161580:c.C498A:p.D166E	missense	het	hom	Short stature, onychodysplasia, facial dysmorphism, and hypotrichosis (AR)	-
	TDRD6	NM_001010870:c.2112_2114del:p.704_705del	nonframeshift deletion	het	hom	No disease associated	-
	UBE2W	NM_018299:c.530-2Adel	splicing	het	hom	No disease associated	-
	GOLGA3	NM_001172557:c.A1139G:p.N380S	missense	het	hom	No disease associated	-
	HSPBP1	NM_001297600:c.G617C:p.G206A	missense	het	hom	No disease associated	-
15-546	UBE2W	NM_018299:c.530-2Adel	splicing	het	hom	No disease associated	-
	NANOS2	NM_001029861:c.G208A:p.G70R	missense	het	hom	No disease associated	-
15-547	UBE2W	NM_018299:c.530-2Adel	splicing	het	hom	No disease associated	-
	TDRD9	NM_153046:c.G3514A:p.V1172I	missense	het	hom	Spermatogenic failure 30 (AR)	-
15-572	FANCM	NM_001308133:c.2505_2508del:p.I835fs	frameshift deletion	het	hom	Premature ovarian failure 15 (AR) /Spermatogenic failure 28 (AR)	-
	POLG	NM_001126131:c.G3287A:p.R1096H	missense	het	hom	Mitochondrial DNA depletion syndrome 4A - Alpers type (AR) / Mitochondrial DNA depletion syndrome 4B-MNGIE type (AR) / Mitochondrial recessive ataxia syndrome - includes SANDO and SCAE (AR) / Progressive external ophthalmoplegia, autosomal recessive 1 (AR) /Progressive external ophthalmoplegia, autosomal dominant 1 (AD)	Patient is not affected for any of the POLG-linked diseases reported in OMIM
15-654	MOV10L1	NM_001164106:c.G163T:p.A55S	missense	het	hom	No disease associated	-
	RXFP1	NM_001253727:c.G172A:p.D58N	missense	het	hom	No disease associated	-
	MLH3	NM_001040108:c.G1870C	missense	het	hom	Colorectal cancer, hereditary nonpolyposis, type 7 (n.d)	-

	Gene	Transcript / variant	Mutation	het	hom	Disease association	Notes
	TDRD9	NM_153046:c.T3833G:p.F1278C	missense	het	hom	Spermatogenic failure 30 (AR)	.
16-394	DNMT3A	NM_022552:c.A89C:p.E30A	missense	het	hom	Tatton-Brown-Rahman syndrome (AD)	Patient is not affected by Tatton-Brown-Rahman syndrome
16-531	SLC19A2	NM_006996:c.A998G:p.N333S	missense	het	hom	Thiamine-responsive megaloblastic anemia syndrome (AR)	.
16-606	RNF17	NM_001184993:c.983_985del:p.328_329del	nonframeshift deletion	het	hom	No disease associated	.
16-639	POLG	NM_001126131:c.150_158del:p.50_53del	nonframeshift deletion	het	hom	Mitochondrial DNA depletion syndrome 4A - Alpers type (AR) / Mitochondrial DNA depletion syndrome 4B-MNGIE type (AR) /Mitochondrial recessive ataxia syndrome - includes SANDO and SCAE (AR) /Progressive external ophthalmoplegia, autosomal recessive 1 (AR) /Progressive external ophthalmoplegia, autosomal dominant 1 (AD)	Patient is not affected for any of the POLG-linked diseases reported in OMIM
	HORMAD2	NM_152510:c.C298T:p.R100C	missense	het	hom	No disease associated	.
A1335 and A1053 (borthers)	RNF212	NM_001131034.3:c.111dupT	Frameshift insertion	hom	hom	No disease associated	.
	EHD1	NM_001282445:c.545-4C>G	splicing	het	hom	No disease associated	.
	HCN2	NM_001194:c.182+3G>A	splicing	het	hom	No disease associated	.
	TASP1	NM_017714:c.404-4insTT	splicing	het	hom	No disease associated	.

5
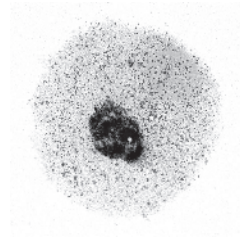
Role of the ATP-dependent nucleosome remodeler CHD5 during postmeiotic chromatin remodeling in mouse spermatogenesis

Work in progress

Role of the ATP-dependent nucleosome remodeler CHD5 during postmeiotic chromatin remodeling in mouse spermatogenesis

Andrea Enguita-Marruedo[1], Igor Macinkovic[3], Esther Sleddens[1], Wiggert A. Van Cappellen[2], Esther Hoogerwerf[1], Marek Bartkuhn[4], Elisabeth Klaus[1], Alexander Brehm[3], and Willy M. Baarends[1]

1) Department of Developmental Biology, Erasmus MC, Rotterdam, The Netherlands.

 2) Department of Pathology/Erasmus Optical Imaging Centre, Erasmus MC, Rotterdam, The Netherlands.

3) Institute of Molecular Biology and Tumour Research, Philipps University Marburg, Germany

4) Institute for Genetics, Justus-Liebig-University Giessen, Heinrich-Buff-Ring 58-62, 35392 Giessen, Germany

5

ABSTRACT

  Members of the chromatin-helicase-DNA (CHD) family play an important role in chromatin regulation during development and differentiation. Family members CHD3, CHD4 and CHD5 can all act as remodelling subunits of the Nucleosome Remodeling and Deacetylation (NuRD) complex in the brain. During spermatogenesis, CHD3 and 4 are expressed in spermatocytes, whereas CHD5 is expressed in postmeiotic spermatids, and required for fertility. Here, we have asked whether CHD family members may function as part of the NuRD remodeling complex in developing male germ cells, as described for somatic cells, and set up a technique to follow chromatin remodeling in elongating spermatids. Using an immunocytochemical approach, and an antibody recognising both CHD3 and CHD4, we observed only partial overlap of its signal with that of specific NuRD complex components in spermatocytes, and no clear colocalisation. In spermatids, containing either an X or a Y sex chromosome, the Y-chromosomal focal spot that is highly enriched for CHD5 did accumulate NuRD components as well as the chromatin marks MacroH2.1 and H3K27me3, but lacked H3.1 and H3K9me3, in both wild-type and $Chd5^{-/-}$ mice. We observed no change in transcription levels of Y chromosomal single-copy and multicopy genes in $Chd5$ knockout spermatids. Interestingly, the known NuRD complex components RbAp46&48 and HDAC1 remained present on the Y chromosome in $Chd5^{-/-}$ spermatids, suggesting that the deacetylase module of the NuRD complex may still be active. Using an antibody that binds to selected socalled G4 quadruplex DNA structures and denatured DNA, we observed that it specifically marked all chromatin of elongating spermatids, and that this signal was strongly decreased upon loss of CHD5. These results indicate that despite its enrichment on part of the Y chromosome, CHD5 most likely performs a global function in chromatin structure regulation during spermatid nuclear elongation. We have used transgenic expression of GFP-tagged H2B, in combination with an mCherry (red fluorescent)-tagged spermatocyte-stage marker (SYCP3), to measure the loss of H2B- GFP in elongating spermatids in vivo in wild-type and $Chd5^{-/-}$ mice. Further studies using this approach will help us to understand the possible role of CHD5 in regulating the dynamics of the histone-to-protamine transition.

INTRODUCTION

In eukaryotic cells, genomic DNA is packaged into chromatin and compartmentalized in the nucleus. However, DNA must be accessible for critical cellular processes such as transcription, replication, recombination, and repair. DNA accessibility is facilitated by histone modifying enzymes and ATP-dependent nucleosome remodelers. ATP-dependent chromatin remodelers are classified into 4 distinct families: SWI/SNF (switch/ sucrose-non-fermenting), ISWI (imitation switch), CHD (chromodomain-helicase-DNA binding) and INO80 (inositol requiring 80). All share a conserved core SNF2-like ATPase domain that belongs to the superfamily 2 (SF2) of DEAD/H-box helicases (Tyagi et al. 2016). The CHD family comprises 9 proteins that are characterized by the presence of 2 tandem chromodomains at the N terminal region, which were first characterized in Drosophila HP1 and Polycomb proteins (Paro and Hogness 1991; Tyagi et al. 2016). The chromodomains in these two proteins contribute to binding to histone methylated marks, H3K9me3 and H3K27me3, respectively (Brehm et al. 2004). The CHD family is divided into 3 subfamilies, each of them characterized by the presence of a specific set of domains. The proteins of subfamily 2 (CHD3, CHD4 and CHD5) share a similar domain structure that includes a pair of tandem PHD fingers at the N-terminal region (Bergs et al. 2014; Tyagi et al. 2016). In vitro, PHD fingers of both CHD4 and CHD5 can bind to histone H3 tails (Musselman et al. 2009; Oliver et al. 2012; Paul et al. 2013). CHD5 also possesses a SANT domain, which is a feature of subfamily 3 (CHD6-CHD9), resulting in some discrepancy in the classification of CHD5. SANT domains interact primarily with unmodified histone tails and are unique histone-interaction modules that couple histone binding to enzyme catalysis (de la Cruz et al. 2005; Marfella and Imbalzano 2007). Remarkably, CHD5 possesses also a 182 amino acid stretch within the C-terminal region (aa 1556 to 1740) that is unique to CHD5 (Bergs et al. 2014).

While CHD3 and CHD4 are expressed in many cell types, the expression of CHD5 is mostly restricted to the brain and testis (Zhuang et al. 2014). In the brain, CHD3, CHD4, and CHD5 are subunits of the Nucleosome Remodeling and Deacetylation (NuRD) complex, where the switch among the three remodelers in the complex is essential for mouse cortical development (Nitarska et al. 2016). In the testis, the three remodelers could also be part of such a complex. Since they show complementary expression during spermatogenesis (Bergs et al. 2014), the NuRD complex may also switch between CHD3/4 (our antibody does not discriminate between the two variants) and CHD5 during spermatogenesis. While CHD3/4 is expressed in spermatogonia and spermatocytes, CHD5 is expressed in nuclei of step 5-8 round spermatids (Bergs et al. 2014). CHD5 accumulates to some extent in the chromocenter, and most clearly in a spot within or at the edge of the chromocenter,

adjacent to the area that encompasses the Y chromosome (Bergs et al. 2014). Previous studies have described that CHD5 deficient mice are subfertile or sterile due to defective spermatid maturation and sperm chromatin compaction, associated with an increased fraction of sperm with abnormal morphology (Li and Mills 2014; Zhuang et al. 2014; Li et al. 2014)

Here, we aimed to assess if CHD family members function as part of the NuRD complex in developing male germ cells. Additionally, using $Chd5^{-/-}$ mice, we aimed to unravel the specific role of CHD5 in round spermatids. The data indicate that some of the CHD3/4 and CHD5 functions may indeed require NuRD complex activity. In addition, the data are consistent with a global function of CHD5 in chromatin structure regulation in developing spermatids, despite its enrichment on part of the Y chromosome. In order to analyse the possible effect of the lack of CHD5 during the histone-to-protamine transition in condensing spermatids, we have used our established procedure for live cell analyses in testicular tubules, and set up a method to compare the loss of H2B-GFP during the histone-to-protamine transition between wild-type and $Chd5^{-/-}$ mice, which are carrying the transgenes H2B-GFP and Cherry-SYCP3. This new tool will help us to understand the role of CHD5 in late round spermatids, and how this relates to the histone-to-protamine transition.

RESULTS

Localization of the NuRD complex components in spermatocytes

We first analyzed the localization of CHD3/4 and two known NuRD complex components, RbAp46&48, and HDAC1 (Torchy et al. 2015), in nuclear spread preparations of wild-type spermatocytes. As previously described (Bergs et al. 2014), CHD3/4 was enriched on the XY body in pachytene spermatocytes. The XY body encompasses the silenced chromatin of the X and Y chromosome in pachytene spermatocytes. Within this domain, CHD3/4 was mainly enriched on the pseudoautosomal region (PAR, the short region of homology between the X and Y chromosome) in early pachytene and also on the X centromere in mid and late pachytene ((Bergs et al. 2014) and Fig. 1A,B, enlargements in early, mid and late pachytene). In diplotene, CHD3/4 enrichment was observed on all centromeric heterochromatin (Fig.1 B enlargement in diplotene), and became more evenly distributed on the XY body (Fig.1 A, enlargement in diplotene).
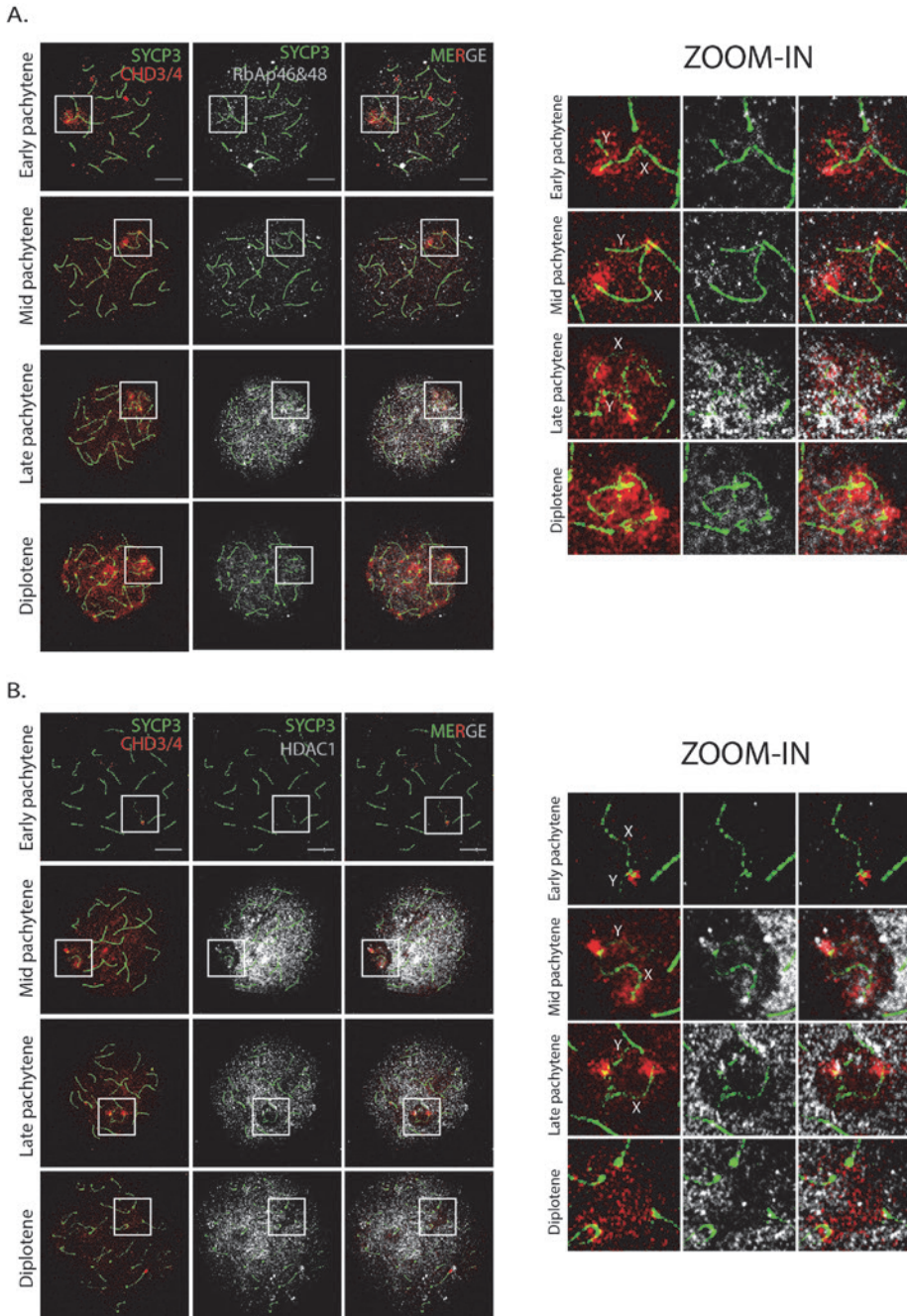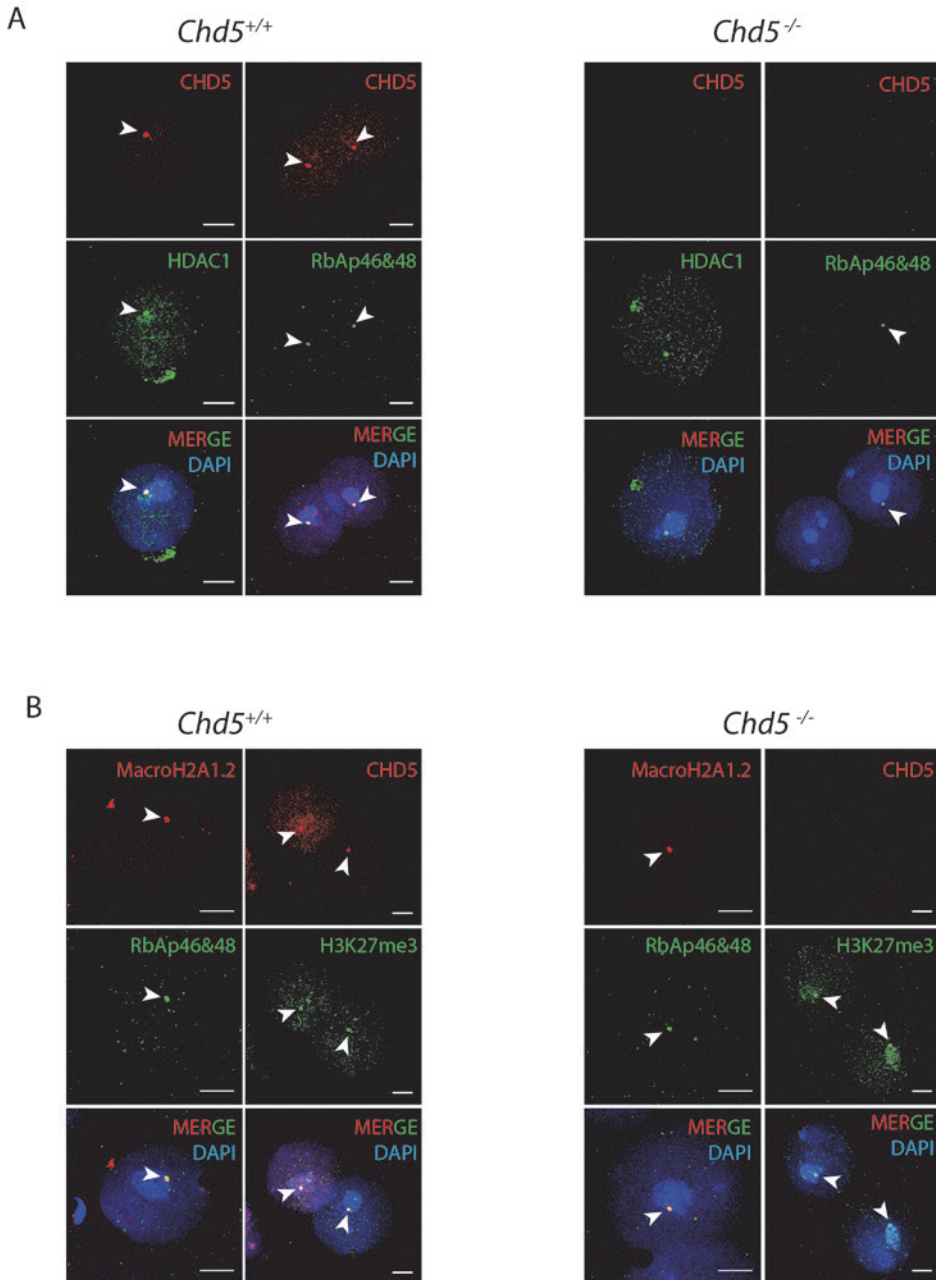
Fig. 1. Localization of the NuRD complex components in spermatocytes. **A)** Immunostaining of SYCP3 (green), CHD3/4 (red) and RbAp46&48 (white). **B)** Immunostaining of SYCP3 (green), CHD3/4 (red) and HDAC1 (white). Scale bar 10 μm.

RbAp46&48 displayed a more uniform distribution in the nucleus, with increased expression in late pachytene (Fig. 1A). The signal partially overlapped with that of CHD3/4, but did not appear enriched in CHD4-positive regions. HDAC1 signal was not detectable in early pachytene (Fig.1B, early pachytene). In mid and late pachytene, HDAC1 was present in the nucleus but strongly reduced in the XY body, in contrast to the CHD3/4 enrichment here (Fig.1B, mid and late pachytene). However, HDAC1 was present in the PAR and the X centromere, where it overlapped but hardly colocalized with CHD3/4 (Fig. 1B, enlargements in mid and late pachytene). In diplotene, HDAC1 was depleted from the centromeric heterochromatin, where CHD3/4 was enriched (Fig. 1B, enlargements in diplotene).

CHD5 colocalizes with NuRD complex components in spermatids, but is not required for their association with chromatin.

In round spermatids, the expression of CHD3/4 is switched off, while CHD5 is expressed in the late stages (Bergs et al. 2014). In wild type spermatids, CHD5 accumulates to some extent in the chromocenter (the region containing the centromeres of all chromosomes), but also, and most clearly, in a spot within or at the edge of the chromocenter, adjacent to the area that encompasses the Y chromosome (Bergs et al. 2014) (Fig. 2, left panel). In order to determine if CHD5 could also function as part of the NuRD complex, we compared the localization of CHD5 and the proteins HDAC1 and RbAp46&48 in nuclear spread preparations of wild-type, $Chd5^{+/-}$ and $Chd5^{-/-}$ mice. We observed that in the wild-type and $Chd5^{+/-}$ situation, HDAC1 and RbAp46&48 frequently colocalized with CHD5 in the same focal spot in round spermatids (Fig. 2, left panel. Only $Chd5^{+/+}$ is shown, $Chd5^{+/-}$ displayed a similar pattern). In $Chd5^{-/-}$, the focal spots of HDAC1 and RbAp46&48 were still observed. We next quantified the type of staining patterns observed in at least 120 round spermatids per mouse (2 wild-type, 2 $Chd5^{+/-}$ and 2 $Chd5^{-/-}$ mice) (Table 1A). In all genotypes, more than 50% of the round spermatids lacked a spot of CHD5 as well as the other analysed proteins, and these nuclei most likely correspond either to spermatids carrying a X chromosome or to the very early spermatids that do not express CHD5 yet. In the remaining spermatids, CHD5 and HDAC1/RbAp46&48 mostly colocalized (63-95% of colocalization), in both $Chd5^{+/+}$ and $Chd5^{+/-}$ mice. In $Chd5^{-/-}$ mice, the focal spot of HDAC1 or RbAp46&48 was still observed, which indicates that CHD5 is not required for their localisation.

Fig. 2. Localization of NuRD complex components and histone marks in a Y-chromosomal focal spot in spermatids. **A)** Immunostaining of CHD5 (red) and HDAC1 or RbAp46&48 (green) in *Chd5*^{+/+} and *Chd5*^{-/-} spermatids (left and right panel, respectively). **B)** Immunostaining of MacroH2A1.1 or CHD5 (red) and RbAp46&48 and H3K27me3 in *Chd5*^{+/+} and *Chd5*^{-/-} spermatids (left and right panel, respectively). Arrowheads indicate the Y-chromosomal focal spot. Scale bar 10 μm.

A

RbAp46&48		Total	Round spermatids						
			Total with focal spot (CHD5 and/or RbAp46&48)		CHD5 spot	RbAP46&48 spot	Colocalization		
Genotype	Mice		n	%	(n)	(n)	n	%
Chd5+/+	Ms1	207	90	43.5	89	58	57	63.3
	Ms2	193	51	26.4	48	51	48	94.1
Chd5+/-	Ms3	369	146	39.6	130	146	130	89.0
	Ms4	325	90	27.7	82	90	82	91.1
Chd5-/-	Ms5	134	35	26.1	0	35	0	0
	Ms6	132	41	31.1	0	41	0	0

HDAC1		Total	Round spermatids						
			Total with focal spot (CHD5 and/or HDAC1)		CHD5 spot	HDAC1 spot (n)	Colocalization		
Genotype	Mice		n	%	(n)		n	%
Chd5+/+	Ms1	161	45	28.0	39	41	38	84.4
	Ms2	126	27	21.4	20	27	20	74.1
Chd5+/-	Ms3	318	76	23.9	71	76	71	93.4
	Ms4	366	93	25.4	88	91	88	94.6
Chd5-/-	Ms5	143	27	18.9	0	27	0	0
	Ms6	126	23	18.3	0	23	0	0

B

H3K27me3		Total	Round spermatids						
			Total with focal spot (CHD5 and/or H3K27me3)		CHD5 spot	H3K27m3 spot	Colocalization		
Genotype	Mice		n	%	(n)	(n)	n	%
Chd5+/+	Ms1	160	44	27.5	39	39	39	88.6
	Ms2	152	42	27.6	26	42	26	61.9
Chd5-/-	Ms5	146	27	18.5	0	27	0	0
	Ms6	147	30	20.4	0	30	0	0

Table 1. Quantifications of round spermatids containing a NuRD complex components/H3K27me3 Y-chromosomal focal spot. **A)** Presence and colocalization of CHD5 and RbAp46&48 (upper table) or CHD5 and HDAC1 (lower table) at the Y-chromosomal focal spot in $Chd5^{+/+}$, $Chd5^{+/-}$ and $Chd5^{-/-}$ spermatids. **B)** Presence and colocalization of CHD5 and H3K27me3 at the Y-chromosomal focal spot in $Chd5^{+/+}$ and $Chd5^{-/-}$ spermatids. N = minimum of 120 round spermatids per mice, 2 mice per quantification. Each mouse was coded with a number, meaning that the same number correspond to the same mouse. The level of colocalization was obtained by dividing the number of spermatids in which CHD5 and the correspond protein colocalized by the total number of spermatids with a focal spot. Unpaired t-test showed stadistical difference (p value < 0.05) only when comparing the percentage of spermatids with CHD5 and/or H3K27me3 focal spot of $Chd5^{+/+}$ and $Chd5^{-/-}$ mice (p-value = 0.01),

CHD5 colocalizes with MacroH2.1 and H3K27me3 in round spermatids

MacroH2A1.2, a histone variant involved in transcriptional repression (Gamble et al. 2010), also localizes at the focal spot in the chromocenter of spermatids that contain the Y chromosome (Turner et al. 2001; Bergs et al. 2014)(Fig. 2B, left panel)**.** Colocalization with CHD5 is observed in approximately 50% of the macroH2A.1-positive spermatids (Bergs et al. 2014), suggesting that macroH2A.1 localizes at the spot before CHD5. As expected, we observed that MacroH2A.1 also colocalizes with the component of the NuRD complex RbAp46&48 at the focal spot, both in wild-type and $Chd5^{-/-}$ spermatids (Fig. 2B). MacroH2A signal has been reported to overlap with the histone modification H3K27me3 (trimethylation of lysine 27 on histone H3), which frequently marks facultative heterochromatin regions (Gamble et al. 2010; Biterge and Schneider 2014). Since the NuRD complex has been shown to stimulate H3K27 trimethylation at specific target genes (Reynolds et al. 2012; Hayashi et

al. 2016), we decided to analyze the localization of this histone modification in $Chd5^{+/+}$ and $Chd5^{-/-}$ spermatids. We observed that H3K27me3 was also present at the Y-chromosomal focal spot , both in spermatids of wild-type and of $Chd5^{-/-}$ mice (Fig. 2B). We next quantified the staining pattern in at least 120 round spermatids per mouse (2 wild-type, and 2 $Chd5^{-/-}$ mice) (Table 1B). Similar to the results obtained for HDAC1 and RbAp46&48, we observed a high frequency of colocalization of CHD5 with H3K27me3 (62 and 89% colocalization, mouse 1 and 2, respectively). Although its presence in round spermatids was slightly reduced (p-value <0.05), the focal spot of H3K27me3 remained present in the absence of the remodeler.

The CHD5-enriched Y chromosomal region corresponds to a weak-staining DAPI area which is depleted of H3.1 and H3K9me3

During meiotic prophase, the X and Y chromosome undergo a unique overall nucleosome replacement, whereby H3.1 is replaced by the replication-independent H3.3 (van der Heijden et al. 2007). As expected based on the Y-chromosomal localisation of CHD5, the CHD5-MacroH2.1 spot was also depleted of H3.1 (Figure 3). In addition, we noted that the CHD5-enriched region corresponds to a weak DAPI-staining area. A typical mark of constitutive heterochromatin is the trimethylation of histone H3 on lysine 9 (H3K9me3) (Saksouk et al. 2015), and this PTM is also enriched on the chromocenter of wild type spermatids (Govin et al. 2007). To obtain more insight in the type of chromatin that accumulates CHD5, we analysed the H3K9me3 pattern in combination with the HDAC1 signal. We observed that H3K9me3 indeed localized at the chromocenter, but was depleted from the HDAC1 (CHD5) spot in both wild-type and $Chd5^{-/-}$ spermatids. Taken together, we can conclude that the Y chromosomal region that accumulates CHD5 (in the NuRD complex), MacroH2.1 and H3K27me3, but lacks H3.1 and H3K9me3, carries a very peculiar chromatin signature that appears not to depend on the presence of CHD5.

CHD5 does not regulate transcription of Y chromosomal genes

Given the enrichment of CHD5 on part of the Y chromosome, we wondered if its absence might affect transcription of specific Y-chromosomal genes that reside in the CHD5-enriched chromatin. In general, overall transcription of Y chromosomal genes is repressed during meiotic prophase, but following the meiotic division, specific genes, and in particular X-linked multi-copy genes, have been shown to be (re)activated (Hendriksen et al. 1995; Odorisio et al. 1996; Touré et al. 2005; Turner et al. 2006; Namekawa et al. 2006; Moretti et al. 2016). A previous transcriptomic study of purified round spermatids from wild type and $Chd5^{-/-}$ mice showed only limited effects of CHD5 loss on global transcription levels in round spermatids, and no mention of dysregulation of Y chromosomal genes (Li et al. 2014).
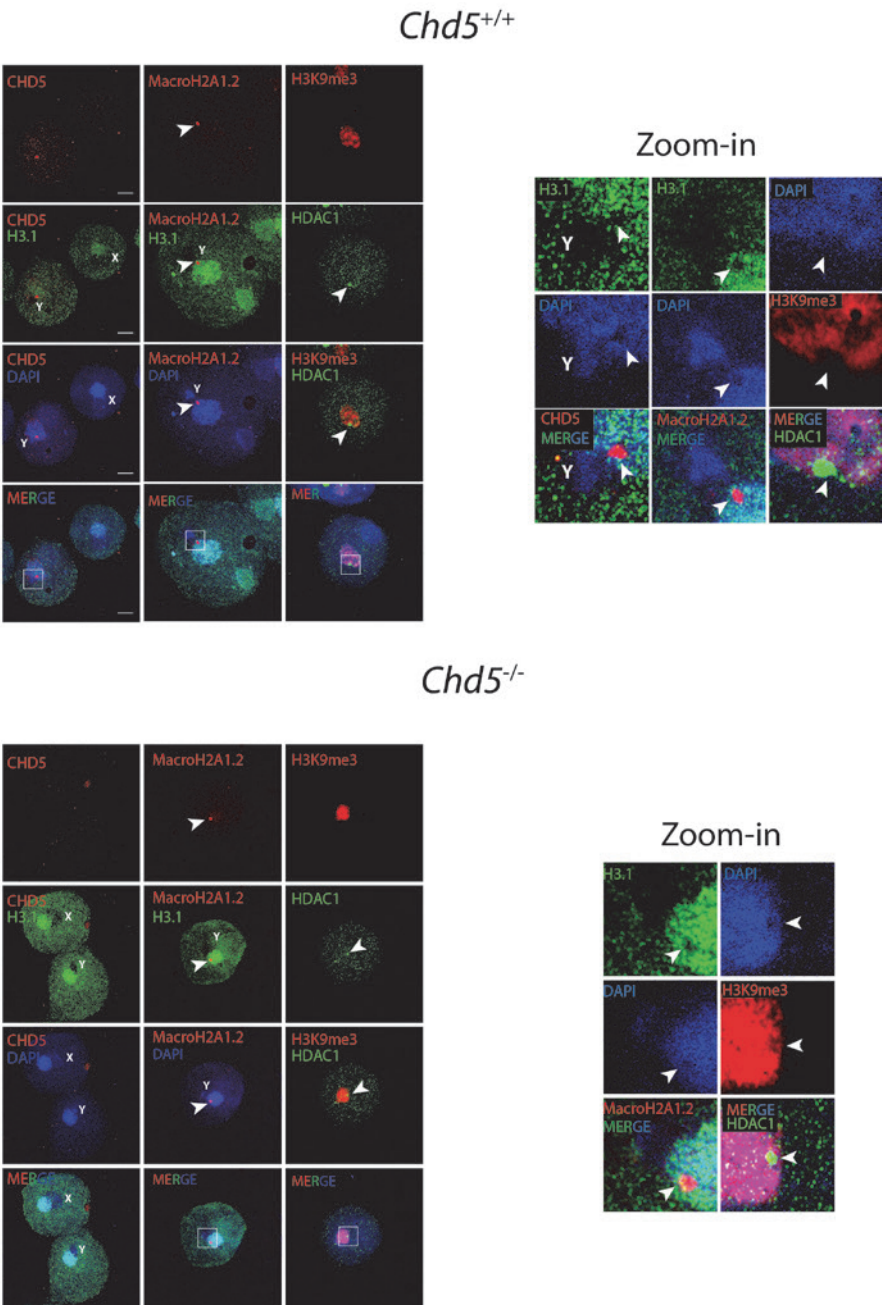
Fig. 3. Chromatin remodeling in round spermatids of *Chd5*$^{+/+}$ and *Chd5*$^{-/-}$ mice. Immunostaining of CHD5, MacroH2A1.2 or H3K9me3 (red) and H3.1 or HDAC1 (green) in *Chd5*$^{+/+}$ and *Chd5* $^{-/-}$ spermatids (upper and lower panel, respectively). Arrowheads indicate the Y-chromosomal focal spot. Scale bar 10 μm

We re-analysed the publicly available data to assess if any Y chromosomal genes were differentially expressed, but none were found (Supplemental table 1) to be differentially expressed in a significant manner. However, the Y chromosome is enriched for multi-copy genes that may escape detection in such transcriptomic analyses due to annotation problems. Since the intense CHD5 focal spot was observed in association with the Y chromosome, we hypothesized that this may be due to the presence of multiple binding sites in a region containing repeated genes. Thus, we selected Y chromosomal genes based on a high multicopy number (Soh et al. 2014) (Fig. S1B), and analysed their expression. Additionally, we included the single copy Y chromosomal genes *Rbmy, Uba1y and Zfy2*, in the analysis as controls (not changed in the transcriptomic analyses). RT-qPCR was performed on cDNA, synthesised from mRNA which was isolated from purified wild-type and knockout spermatid fractions (n=2 mice). As autosomal control genes, we selected *Ctag2, Mgat4e* and *Ddr1,* which have been reported to be stable, downregulated and upregulated in *Chd5$^{-/-}$* mice, respectively (Li et al. 2014). RT-qPCR analysis showed a similar tendency for these genes (Fig. S1A), and we also verified that the majority of the analysed Y chromosomal genes displayed increased expression in spermatids compared to spermatocytes (Fig. S1B). Except for *Uba1y*, no clear differences were observed between the gene expression levels of the selected Y chromosomal genes between wild-type and *Chd5$^{-/-}$* mice (Fig. 4).
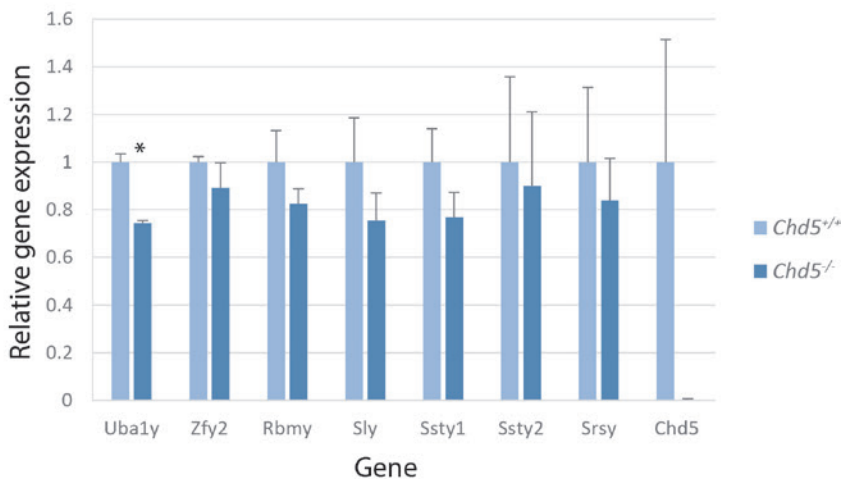

Fig. 4. Gene expression of Y chromosomal genes in *Chd5$^{+/+}$* and *Chd5$^{-/-}$* spermatids (mean ± SD). Results of CHD5 expression were also included. Gene expression levels were normalised to the housekeeping gene B-actin and further normalised to the wild-type. N= 2 wild-type mice. Significant values (p-value < 0.05) are indicated with an asterisk.

Formation of G-quadruplex DNA and/or denatured DNA accompanies spermatid elongation and is reduced in the absence of CHD5

Single-stranded guanine (G)-rich DNA can form stable secondary structures called G-quadruplex (G4) DNA (Maizels and Gray 2013) . In theory, G4 DNA can arise anywhere in the genome where sufficiently long stretches of single-stranded G-rich DNA are exposed during replication, transcription or recombination (Maizels and Gray 2013; Henderson et al. 2014). Previously, the monoclonal antibody 1H6 was raised against (T4G4)2 intermolecular guanine quadruplex (G4) DNA structures(Henderson et al. 2014; Hoffmann et al. 2016). Recently, the specificity of this antibody has been nuanced, and the authors proposed that that 1H6 binds with high affinity to adjacent T's that are restricted in their movement in selected G4 structures and denatured DNA (Kazemier et al. 2017). The analysis of the staining pattern of this antibody in wild-type nuclear spread preparations showed a strong increase in signal appearing in elongating spermatids, with little if any staining at earlier stages (Fig. 5A). In early elongating spermatids, a strong staining could be observed in the chromocenter, while a dimmer signal was obtained in the rest of the nucleus. In later elongating spermatids, 1H6 signal was only visible at the chromocenter, and this signal disappeared completely in condensing spermatids. A similar pattern but with a clearly lower intensity of the signal was observed for $Chd5^{-/-}$ mice, and an intermediate signal level was detected in the $Chd5^{+/-}$ genotype. Quantification of the mean intensity/pixel and the total amount of 1H6 signal in the three genotypes confirmed this finding (n = minimum of 15 nuclei per mouse, 2 mice per genotype ($Chd5^{+/+}$, $Chd5^{+/-}$ and $Chd5^{-/-}$)) (Fig. 5B, arbitrary units). Quantification of the DAPI signal is shown as control, and remained stable in the three genotypes. We do not know the precise DNA conformation the antibody recognizes in this case, but it must be a conformation that is present only during chromatin remodeling (performed by ATP-dependent remodelers), and thus associated with the histone-to-protamine transition.

Analyses of the dynamics of the histone-to-protamine transition: set-up of a live cell imaging approach

The results from the H16 antibody staining are consistent with the hypothesis that CHD5 is involved in the regulation of chromatin remodeling during spermatid nuclear elongation. In fact, it might be suggested that changes in the dynamics of remodeling might reduce the formation of specific DNA structures recognized by the H16 antibody. To investigate this further, we decided to analyse the histone-to-protamine transition in living cells, to be able to assess the duration of the process in wild type and $Chd5$ knockout spermatids.
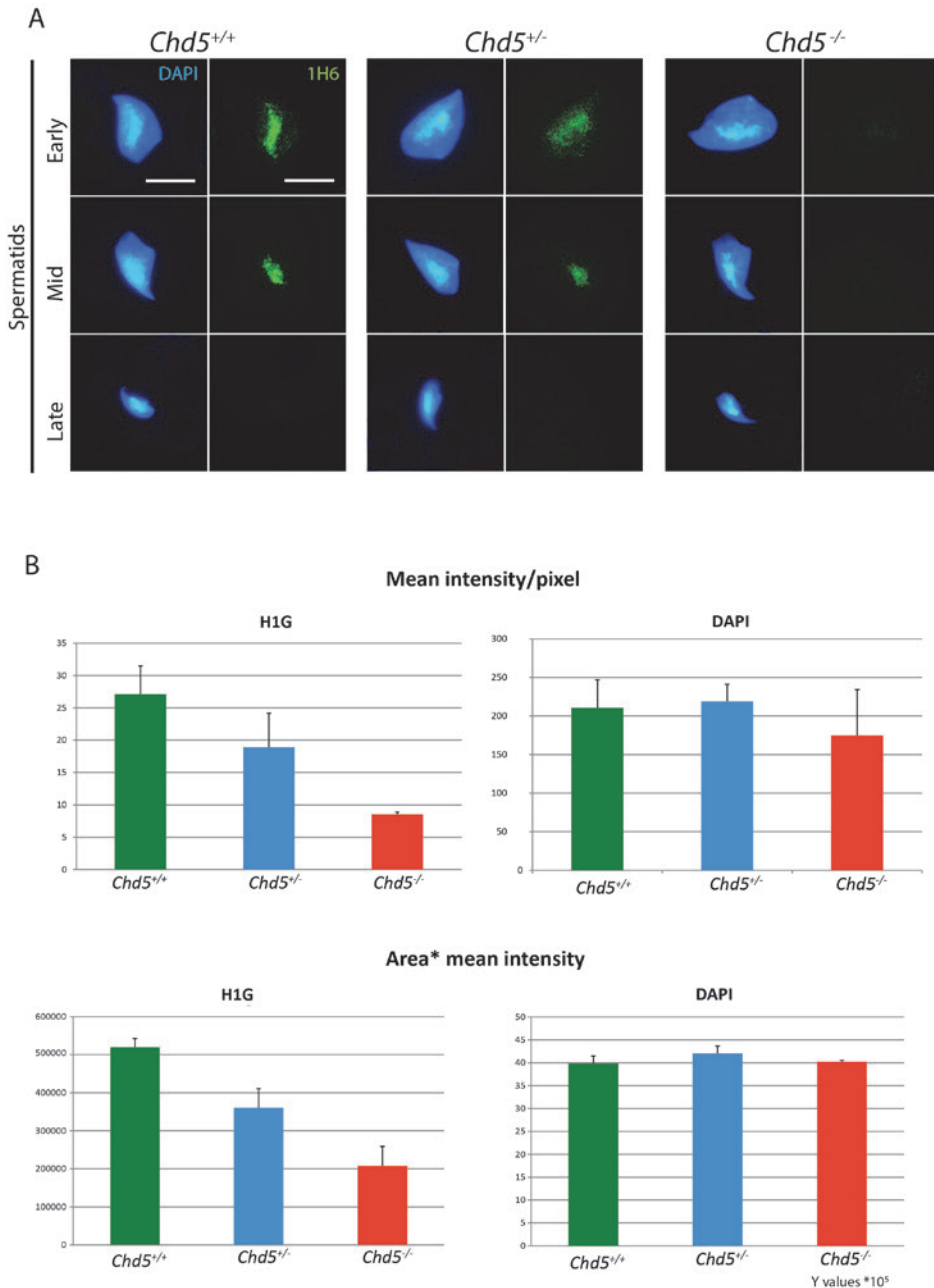
Fig. 5. Formation of G-quadrulex DNA and/or denatured DNA in spermatids. **A)** Immunostaining of 1H6 (G-quadrulex DNA and/or denatured DNA marker) in *Chd5*^{+/+}, *Chd5*^{+/-} and *Chd5*^{-/-} elongating spermatids. Scale bar 10 μm. **B)** Quantification of the mean intensity/pixel (± SD) (Arbitrary units, AU) and the total amount of 1H6 and DAPI signal in *Chd5*^{+/+}, *Chd5*^{+/-} and *Chd5*^{-/-} elongating spermatids (±SD) (n = minimum of 15 nuclei per mouse, 2 mice per genotype.)

Previously, we have set up a system to study spermatogenesis in living mouse cells (Enguita-Marruedo et al. 2018) wild-type and $Chd5^{-/-}$ mice expressing fluorescent-tagged SYCP3 (mCherry-SYCP3 (CSYCP)), and GFP-tagged histone H2B (H2B-GFP, transgenic construct see materials and methods). We cultured the seminiferous tubules in a gelatinous protein mixture (basement membrane extract, BME) to maintain the three-dimensional structure (see Material and Methods for more details). Inside the tubules, different types of cells could be distinguished based on their localization and on the CSYCP and H2B-GFP patterns (Fig. 6A). We could classify each location in one of the 12 stages defined for mice (Oakberg 1956), according to the combination of cells that was present. Spermatogonia and very early primary spermatocytes are situated closer to the basal membrane of the tubule (Fig. 6A, spg). They displayed the highest signal of H2B-GFP in comparison to later stages and no CSYCP signal. Primary spermatocytes displayed H2B-GFP (lower level compared to earlier cell types) and CSYCP (chromosome axes and centromeres) signal (Fig. 6A, spc). We observed loss of a large fraction of H2B-GFP at meiotic entry, which may be caused by nucleosomal reorganization that is known to occur early in spermatogenesis, when a large fraction of the canonical histones is replaced by (testis-specific) variants. One of these is the testis-specific H2B isoform, TH2B (Montellier et al. 2013). The layer closest to the lumen contained round and elongating spermatids, whose H2B-GFP signal was even lower than in previous stages, and decreased more and more when comparing earlier and later spermatid stages (Fig. 6A, enlargements). Round and early elongating spermatids displayed higher H2B-GFP signal in the chromocenter compared to the rest of the nuclei. Very early round spermatids still displayed some CSYCP signal, which was freely diffusing in the nucleoplasm.

For the first comparison of one wild-type and one $Chd5^{-/-}$ mouse, two separate experiments were performed (using the same settings for both, see materials and methods). In total, 9-10 locations were selected per experiment. An interval of 10 min was chosen for these time-lapse recordings, in order to prevent problems of bleaching and cell damage during the long experiment. Cells were segmented into Sertoli cells, spermatogonia, spermatocytes and spermatids, based on the presence/absence of CSYCP and the level of H2B-GFP signal (see Materials and Methods). Because the segmentation was not always optimal, some of the spermatogonial signal was sometimes attributed to the spermatids. This resulted in a high level of "contamination", in particular in the locations where the H2B-GFP signal in spermatids was very low. To solve this problem, we selected a rectangular box in the middle of the tubule where the spermatids were located. In this way, the contamination coming from the basal cells of the tubule (spermatogonia and early spermatocytes) was removed. Inside the rectangle, the already segmented Sertoli cells, spermatogonia and spermatocytes were removed. The leftover signal was then measured as spermatid signal. In both wild-type

and *Chd5*^{-/-} mice, a significant decrease in the level of H2B-GFP signal appeared to occur between stages VIII and X (Fig. 6B. The whole sequence is shown in Fig. S2 and S3), and no clear differences were observed.

DISCUSSION

CHD3/4 may function in a complex that is different from the canonical NuRD complex in the testis

In spermatocytes, we have observed only a partial colocalization of CHD3/4 and the other NuRD complex components HDAC1 and RbAp46&48, suggesting that a canonical NuRD complex is not always formed. In accordance with our observations, recent studies reported that CHD4 is a peripheral component of the NuRD complex (Zhang et al. 2016; Low et al. 2016), and not central as it has been traditionally presented (Torchy et al. 2015). Due to the peripherical location, CHD4 could easily disengage from the complex to carry out independent functions. In the absence of CHD4, a stable NuRD-type complex would still be formed, termed the nucleosome deacetylase complex (NuDe), which possesses a robust deacetylase activity (Zhang et al. 2016; Low et al. 2016).

HDAC1 was depleted from the XY body in pachytene, as well as from the centromeric heterochromatin in diplotene. In these areas, CHD3/4 could be acting alone. For example, a NuRD-independent role of CHD4 during the DNA damage response and during cell cycle progression has been suggested (O'Shaughnessy and Hendrich 2013). Alternatively, it might be suggested that HDAC2, and not HDAC1, forms part of the NuRD complex in the HDAC1-depeleted locations. Generally, HDAC1 and HDAC2 have redundant functions, and both can coexist in the same complex. However, their relative contribution to the NuRD complex may sometimes be cell-specific (Kelly and Cowley 2013), and one of the variants could be preferentially incorporated. Additionally, in a few significant exceptions (early embryogenesis and brain development) HDAC1 and HDAC2 perform different functions (Kelly and Cowley 2013). Finally, CHD3/4 could be interacting with another remodeler complex. An interaction between CHD4 (not included in the NuRD complex) and Polycomb has been reported to be essential during astroglial differentiation (Sparmann et al. 2013). It is notable that the Polycomb complex can also contain RbpA46&48, which is present together with CHD4 in these areas of the spermatocytes. It is possible that CHD4-Polycomb interactions could also have a role in the spermatocyte nucleus. HDAC1 and RbAp46&48, but not CHD3/4, displayed overall colocalisation in the nucleus in mid and late pachytene (excluding XY body) and in diplotene (excluding the centromeric heterochromatin).
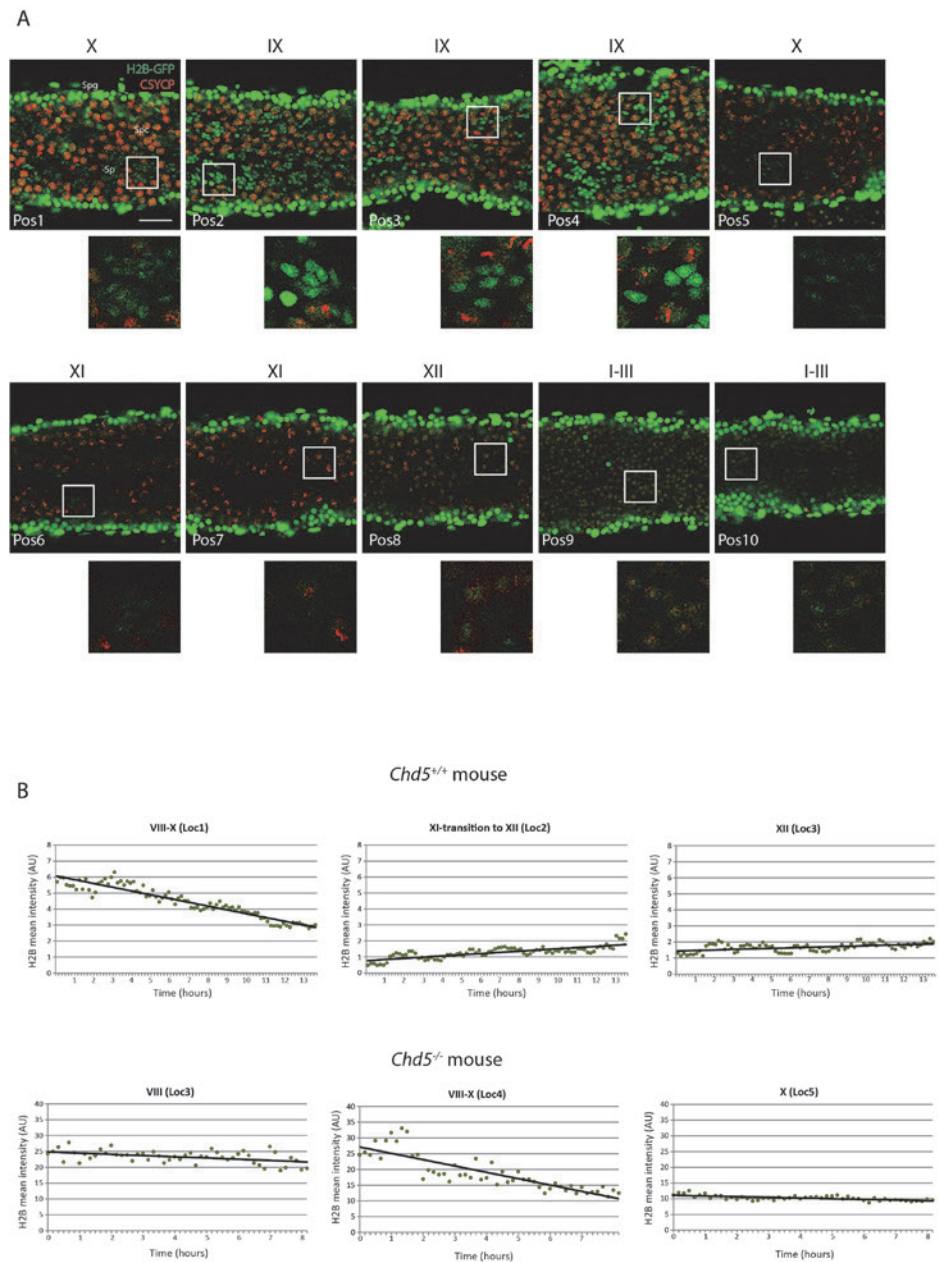
Fig. 6. Progression of spermatogenesis. **A)** Stages of the cycle of the seminiferous epithelium in mice expressing mCherry-tagged SYCP3 and GFP-tagged histone H2B. Enlargments show the different spermatid type of each position. Scale bar 50 μm. **B)** Mean intensity of H2B-GFP signal in spermatids of three sequential positions of *Chd5*^{+/+} and *Chd5*^{-/-} mice.

In these areas, the deacetylase complex NuDe might be formed. Alternatively, a Sin3 histone deacetylase (HDAC) complex, which contains RbAp46&48 and HDAC1/2, but not CHD4, could also be formed (Adams et al. 2018). Specifically, the isoform Sin3A associates preferentially with HDAC1 (over HDAC2), and is essential for maintenance of germ cell viability in male mice (Pellegrino et al. 2012; Adams et al. 2018).

Taking together, these results suggest that the specific features of the PAR and X centromere requires the formation of a canonical NuRD complex, while other areas could have different requirements. In some areas, CHD3/4 may function alone or in a complex that is different from the canonical NuRD complex. In other locations where CHD3/4 is absent, a NuDe complex, or a Sin3 complex, could assemble.

CHD5 may function as part of the NuRD complex in round spermatids to regulate a specific region on the Y chromosome.

In round spermatids, CDH5 colocalizes with both NuRD complex components RbAp46&48 and HDAC1 in an intense focal spot near the chromocenter, adjacent to the area that encompasses the Y chromosome. This may indicate that CHD5 is part of a NuRD complex in this area. However, the loss of CHD5 did not affect the focal spots of either RbAp46&48 or HDAC1. As proposed for CHD3/4, the nucleosome deacetylase complex NuDe, may still be formed in this situation. This could also occur in the rest of the nucleus, where HDAC1 and RbAp46&48 signal remained when CHD5 is absent. The NuDe complex possess a strong deacetylase activity (Low et al. 2016), so we could expect a reduction in the acetylation levels in $Chd5^{-/-}$ spermatids. In accordance with this notion, Li et al. 2014 reported reduced H4 hyperacetylation levels in $Chd5^{-/-}$ spermatids. Alternatively, both a NuRD and a Sin3 complex could be naturally present in these areas. In the absence of CHD5 (and of a canonical NuRD complex), RbAp46&48 and HDAC1 signals would belong exclusively to the Sin3 complex.

The Y chromosomal region that accumulates CHD5 corresponds to a facultative heterochromatin area

The specific accumulation of MacroH2A and H3K27me3 on the CHD5-enriched Y-chromosomal focal spot, combined with the exclusion of H3K9me3 from this area indicate that this region behaves as a facultative heterochromatic area. The NuRD complex has been shown to stimulate H3K27 trimethylation (Reynolds et al. 2012; Hayashi et al. 2016),by deacetylating H3K27ac that becomes a substrate for the Polycomb complex, which methylates it forming H3K27me3 (Reynolds et al. 2012; Hayashi et al. 2016). Alternatively, CHD5 might be required to remove H3.1/H3.2 from the chromatin structure, making the

chromatin relatively H3.3-rich. H3K27me3 will be preferentially added to histone H3.3, and the chromatin region involved would be repressed (Reynolds et al. 2012; Hayashi et al. 2016). However, lack of CHD5 did not result in the disappearance of the H3K27me3 spot or changes in the H3.1 signal, rendering this scenario unlikely. It appears more probable that the NuRD-type complex without CHD5 still stimulates H3K27 trimethylation, or that H3K27 trimethylation occurs independent of the activity of the NuRD complex at this location. Taken together with the analyses of gene expression, we conclude that the Y chromosomal region that accumulates CHD5 (in the NuRD complex), MacroH2.1 and H3K27me3, but lacks H3.1 and H3K9me3 carries a very peculiar chromatin signature, whereby CHD5 is not required for regulation of gene expression in this region.

Alterations in chromatin remodeling occur in the absence of CHD5, and these alterations can be further studied in vivo

The 1H6 antibody has been reported to bind to adjacent T's that are restricted in their movement in selected G4 structures and denatured DNA (Kazemier et al. 2017). We have observed that 1H6 signal appeared only in elongating spermatids, and that the intensity of the signal was reduced in $Chd5^{+/-}$, and even more drastically in $Chd5^{-/-}$ mice. It is clear that the structure that the antibody recognizes appears during chromatin remodeling, and that is affected when CHD5 expression is reduced ($Chd5^{+/-}$) or absent ($Chd5^{-/-}$). One possibility is that the helicase activity of a remodeler like CHD5 might result in some melting of the DNA while histones are removed, allowing the transient formation of G4 quadruplex DNA or denatured DNA. In $Chd5^{+/-}$ and $Chd5^{-/-}$ mice, the process may be slowed down, or occur through a different pathway, resulting in reduced G4 quadruplex staining.

In order to study the alterations in chromatin remodelling that occurs in the absence of CHD5, we have adapted our previously reported method for live cell analyses during spermatogenesis (Enguita-Marruedo et al. 2018) to study the loss of H2B-GFP from spermatids as they replace the histones by transition proteins. We have performed the first experiments to compare histone removal between wild-type and $Chd5^{-/-}$ mice. In both genotypes, a significant decrease in the level of H2B-GFP signal appeared to occur between stages VIII and X, suggesting no alterations in the initial steps of the histone-to-protamine transition when CHD5 is absent. However, further analyses need to be performed to confirm this observation.

In summary, we have used an immunocytochemical approach to zoom in on the role of the chromatin-helicase-DNA (CHD) members CHD3/4 and 5 during spermatogenesis. In spermatocytes, we have observed that CHD3/4 only partially overlap with NuRD complex

components in spermatocytes, suggesting that the formation of a canonical NuRD complex only occurs in specific locations. Absence of CHD5 did not cause the disappearance of other NuRD complex components or histone marks from the Y-chromosomal focal spot, but causes the overall reduction of H16 staining (marking G4 quadruplex DNA structures and denatured DNA). This suggests that despite its enrichment on part of the Y chromosome, CHD5 most likely performs a global function in chromatin structure regulation during spermatid nuclear elongation. Finally, we developed a system to measure the loss of H2B-GFP in $Chd5^{+/+}$ and $Chd5^{-/-}$ spermatids in vivo. Although the first experiments did not show clear differences between the $Chd5^{+/+}$ and $Chd5^{-/-}$ chromatin remodeling dynamics, further optimization of the system would help to better analyse possible alterations occurring during the histone-to-protamine transition in $Chd5^{-/-}$ mice.

MATERIALS AND METHODS

Ethics statement

All animal experiments were approved by the local animal experiments committee DEC Consult and animals were maintained under supervision of the Animal Welfare Officer.

Mice

$Chd5^{-/-}$ mice were previously described (Zhuang et al. 2014) an crossed with H2B-GFP/CSYCP mice (described in chapter "live imaging"). Mice containing both transgenes and the $Chd5$ deletion were identified by PCR on tail tip or toe tip. We used the forward primer 5'CACCATCGTGGAACAGTACG3' for CSYCP, 5'GGCCACAAGTTCAGCGTGTC3' for H2B-GFP, and 5'CCTGGCTGGTTGCTGAATCTA 3' for CHD5 (both wild-type and knockout allele). We used the reverse primers 5'GGGAGGTGTGGGAGGTTTT3' for CSYCP, 5'ATGCGGTTCACCAGGTGTC3' for H2B-GFP, and 5'CCTTCCACTTGATCAGGTAA 3' and 5'GCCAAAGATAACCCTGAATG 3'for CHD5 (wild type and knockout, respectively). PCR was carried out using standard protocols and the following conditions for CSYCP: Initial hold at for 5 minutes at 94°C, followed by 35 cycles of 94°C for 45 seconds,54°C for 1 minute, 72°C for 1 minute, and finally 72°C for 10 minutes. This generated a fragment of 947bp, specific for the presence of the transgene. For H2B-GFP the conditions were: initial hold at for 5 minutes at 94°C, followed by 35 cycles of 94°C for 30 seconds, 60°C for 1 minute, 72°C for 1 minute, and finally 72°C for 10 minutes. This generates a fragment of 300 bp. For CHD5 the conditions were: initial hold for 5 minutes at 95oC, followed by 35 cycles of 95 $^{\circ}$C (30 seconds), 55 $^{\circ}$C (30 seconds) and 72 $^{\circ}$C (45 seconds), 72°C for 45 seconds, 72°C for 10 minutes, and finally kept at 10°C. This generates two

fragments of 580 bp and 1300 bp for the wild-type allele, and one fragment of 321 bp for the knockout allele.

Immunocytochemistry

Spread nuclei of spermatocytes were prepared from isolated gonads as described by Peters et al., 1997, and stored at -80C. Thawed slides were washed in PBS (3×10 min), and non-specific sites were blocked with 0.5% w/v BSA and 0.5% w/v milk powder in PBS. Primary antibodies were diluted in 10% w/v BSA in PBS, and incubations were performed overnight at room temperature in a humid chamber. Subsequently, slides were washed (3×10 min) in PBS, blocked in 10% v/v normal goat serum (Sigma) in blocking buffer (supernatant of 5% w/v milk powder in PBS centrifuged at 14,000 rpm for 10 min), and incubated with secondary antibodies in 10% normal goat serum in blocking buffer at room temperature for 2 hours. Finally, slides were washed (3×10 min) in PBS and embedded in Prolong Gold with DAPI (Invitrogen).

Primary antibodies: rabbit polyclonal anti-CHD5 (M-182) (sc-68389, Santa Cruz) at 1:200, rabbit polyclonal anti- CHD3/4 (Mi(H-242)) (sc-11378, Santa Cruz) at 1:50, mouse monoclonal anti-SYCP3 (ABCAM:ab97672) at 1:200, rabbit polyclonal anti-SYCP3 (Lammers et al. 1994) at 1:10000, goat anti-SYCP3 (R&D systems) at 1:100, mouse polyclonal anti-H3.1/3.2 (van der Heijden et al. 2005) at 1:5000, rabbit anti-H3K9me3 at 1:100 (ab8898-100, abcam), rabbit polyclonal anti-macroH2A1.2 (Upstate) at 1:100, mouse monoclonal anti-RbAp46&48 at 1:100 (MA1-23277, Thermo Fisher), mouse monoclonal anti-HDAC1 (WH0003065M2, Sigma-Aldrich) at 1:100, rabbit monoclonal anti-RNA polymerase II (E1Z3G, Cell signalling), at 1:100, mouse monoclonal anti-H3K27me3 (ab6002, Abcam) at 1:100, mouse monoclonal antibody 1H6 (Henderson et al. 2014; Hoffmann et al. 2016; Kazemier et al. 2017) at 1:1000. For secondary antibodies, we used a goat anti-rabbit alexa 488 IgG, goat anti-mouse alexa 488, goat anti-rabbit 546 IgG, donkey anti-goat alexa 488, donkey anti-rabbit alexa 546, donkey anti-mouse alexa 633 IgG, all at 1:500 dilution.

Confocal images were taken using a Zeiss LSM700 confocal.

Analysis of publicly available RNA-seq data

We downloaded publicly available RNA-seq data of round spermatids carrying a mutated allele for Chd5 gene either homozygously or heterozygously along with data from wildtype spermatids (Short read archive accession numbers SRX503594, SRX503618 and SRX503619). SRA archive files were extracted to Fastq format using SRA-toolkit (https://www.ncbi.nlm.nih.gov/books/NBK158900/). After quality control using fastqc available at http://www.bioinformatics.babraham.ac.uk/projects/fastqc/ no further quality

trimming or adaptor removal was performed. Paired-end reads were aligned using TopHat v2.1.1 (Trapnell et al. 2009) against the UCSC version of the mouse mm10 genome downloaded from Illumina's iGenome repository (http://support.illumina.com/sequencing/sequencing_software/igenome.html). For differential gene expression analysis, extraction of read counts per gene was done using featureCounts (Liao et al. 2014) with the UCSC genes defining GTF file from the Illumina iGenome repository. Normalization of read counts and identification of differentially expressed genes was subsequently done DESeq (Anders and Huber 2010) version 1 comparing the homozygous Chd5 mutant and wildtype spermatids using default settings.

Quantitative (q)PCR

qPCR was performed using qPCR SYBR Green Mix and cDNA and analysed by the CFX Biorad manager. The thermocycling conditions for the qPCR reaction consisted of the following: initial denaturation for 3 minutes at 95 °C, denaturation for 30 seconds at 95 °C + annealing for 30 seconds at 58 °C + extension for 45 seconds at 72 °C for 40 cycles, final denaturation for 1 minute at 95 °C, final annealing for 1 minute at 45 °C and final extension for 50 seconds at 95 °C. At least two independent experiments were performed and all experiments were performed in duplicate. The data was normalised using the housekeeping gene *Actb* as a reference. Normalisation was done using the ΔΔCt method. Relative gene expression levels were further calculated using the wild-type data as reference. Primers for *Actb, Chd5, Rbmy, Sly, Ssty1, Ssty2, Srsy, Uba1y* and *Zfy2* were designed using Primer3 in such a way that they would span at least one intron/exon boundary (Supplemental table 2). This was to avoid possible DNA contamination from the results. The primer set for *Chd5* was designed from exon 11 till 12, because exon 12 and 13 are deleted in the knockout mouse (Zhuang et al. 2014).

Unpaired t-test were performed on the results of the RT-qPCR's.

Isolation of testis tubules for culture

Adult mouse testes from transgenic wild-type and *Chd5*^{-/-} mice carrying the H2B-GFP/CSYCP transgene were isolated and dissected following a previously described protocol (van der Laan et al. 2004) with some modifications. Decapsulated testes were immersed in 20 ml Dulbecco's phosphate buffered saline (Invitrogen, Carlsbad, CA, USA) containing 1.1 mM Ca^{2+}, 0.52 mM $Mg2^+$, 6mM DL-lactic acid and 5.6 mM glucose (PBS[+]), in the presence of collagenase (1μg/μl; type 1 Worthington) and hyaluronidase (0.5 μg/μl; H3884 Sigma) in a 50 ml falcon tube. The testes were then incubated in a waterbath at 33C and shaken at 90 cycles/min, amplitude of 20 mm, for 5 minutes. The incubation was stopped when the

enzymatic digestion had resulted in dissociation of the interstitial tissue and disengagement of testis tubules. Tubules were separated from interstitial cells by washing in PBS$^+$ twice. Next, tubules were placed in a 30 mm BSA-coated Petri dish, where the tubules were separated from each other using dissection tweezers (Nr. 5). We staged the tubules using the transillumination technique (Kotaja, Kimmins et al. 2004). We cut small tubules fragments (of about 1 cm), taking care that the spermiation point (transition VIII-IX stage) was situated in the middle, so the tubules contain both round and elongating spermatids. The small tubule fragments were carefully transferred to a 15 mm BSA-coated Petri dish. Please note that testicular myoid cells, the main component of the outer layer of the seminiferous tubules, were present in the fragments used during the experiments, indicating that this method keeps the tubule wall intact. After collecting a pool of fragments, we used dissection tweezers (Nr. 5) to place 4-5 of these fragments into a 50 μl drop containing 1:4 v/v (RPMI + 10% KRS culture medium)/ Cultrex® Basement Membrane Extract (BME), type 2; Trevigen pipetted onto a 24 mm laminin-coated cover slip in each live cell chamber. The chambers with the tubules were centrifuged 5 minutes at 500 rpm and 4°C. Next, the chambers were incubated for 30 minutes at 33°C to allow the BME to jellify. Finally, 2 ml of RPMI + 10% KRS culture medium was added.

Time lapse microscopy

For the time lapse imaging, we used a Leica SP5 confocal microscope. Chamber and objective (HCX PL APO CS 40 x 1.25 NA, oil immersion) were kept a 33 ^{o}C and 5% CO$_2$. Red fluorescent images were obtained with a 594 nm laser and detection through a 600-680 nm band pass filter. Green fluorescent images were obtained after excitation with a 488-nm laser and a 500-550nm band pass filter. In total, 9-10 locations were selected per experiment. For each position, a stack of 31 (wild-type) and 63 (*Chd5$^{-/-}$*) slices of 1 μm was made, from the basal membrane till the middle part of the tubule. The time lapse between images was 10 minutes.

Segmentation of the different cells and resulting measurements of both the green and the red signal was performed in ImageJ. Further Analysis of the resulting measurements was performed in R. All code used for the analysis can be found under supplemental material (S4).

REFERENCES

Adams GE, Chandru A, Cowley SM (2018) Co-repressor, co-activator and general transcription factor: the many faces of the Sin3 histone deacetylase (HDAC) complex. Biochem J 475:3921–3932. doi: 10.1042/BCJ20170314

Anders S, Huber W (2010) Differential expression analysis for sequence count data. Genome Biol 11:R106. doi: 10.1186/gb-2010-11-10-r106

Bergs JW, Neuendorff N, van der Heijden G, et al (2014) Differential expression and sex chromosome association of CHD3/4 and CHD5 during spermatogenesis. PLoS One 9:e98203. doi: 10.1371/journal.pone.0098203

Biterge B, Schneider R (2014) Histone variants: key players of chromatin. Cell Tissue Res 356:457–466. doi: 10.1007/s00441-014-1862-4

Brehm A, Tufteland KR, Aasland R, Becker PB (2004) The many colours of chromodomains. Bioessays 26:133–40. doi: 10.1002/bies.10392

de la Cruz X, Lois S, Sánchez-Molina S, Martínez-Balbás MA (2005) Do protein motifs read the histone code? Bioessays 27:164–75. doi: 10.1002/bies.20176

Enguita-Marruedo A, Van Cappellen WA, Hoogerbrugge JW, et al (2018) Live cell analyses of synaptonemal complex dynamics and chromosome movements in cultured mouse testis tubules and embryonic ovaries. Chromosoma. doi: 10.1007/s00412-018-0668-7

Gamble MJ, Frizzell KM, Yang C, et al (2010) The histone variant macroH2A1 marks repressed autosomal chromatin, but protects a subset of its target genes from silencing. Genes Dev 24:21–32. doi: 10.1101/gad.1876110

Govin J, Escoffier E, Rousseaux S, et al (2007) Pericentric heterochromatin reprogramming by new histone variants during mouse spermiogenesis. J Cell Biol 176:283–94. doi: 10.1083/jcb.200604141

Hayashi M, Maehara K, Harada A, et al (2016) Chd5 Regulates MuERV-L/MERVL Expression in Mouse Embryonic Stem Cells Via H3K27me3 Modification and Histone H3.1/H3.2. J Cell Biochem 117:780–792. doi: 10.1002/jcb.25368

Henderson A, Wu Y, Huang YC, et al (2014) Detection of G-quadruplex DNA in mammalian cells. Nucleic Acids Res 42:860–869. doi: 10.1093/nar/gkt957

Hendriksen PJ, Hoogerbrugge JW, Themmen AP, et al (1995) Postmeiotic transcription of X and Y chromosomal genes during spermatogenesis in the mouse. Dev Biol 170:730–3. doi: 10.1006/dbio.1995.1252

Hoffmann RF, Moshkin YM, Mouton S, et al (2016) Guanine quadruplex structures localize to heterochromatin. Nucleic Acids Res 44:152–63. doi: 10.1093/nar/gkv900

Kazemier HG, Paeschke K, Lansdorp PM (2017) Guanine quadruplex monoclonal antibody 1H6 cross-reacts with restrained thymidine-rich single stranded DNA. Nucleic Acids Res 45:5913–5919. doi: 10.1093/nar/gkx245

Kelly RDW, Cowley SM (2013) The physiological roles of histone deacetylase (HDAC) 1 and 2: complex co-stars with multiple leading parts. Biochem Soc Trans 41:741–749. doi: 10.1042/BST20130010

Lammers JH, Offenberg HH, van Aalderen M, et al (1994) The gene encoding a major component of the lateral elements of synaptonemal complexes of the rat is related to X-linked lymphocyte-regulated genes. Mol Cell Biol 14:1137–46

Li W, Mills AA (2014) Packing for the journey: CHD5 remodels the genome. Cell Cycle 13:1833–4. doi: 10.4161/cc.29378

Li W, Wu J, Kim S-Y, et al (2014) Chd5 orchestrates chromatin remodelling during sperm development. Nat Commun 5:3812. doi: 10.1038/ncomms4812

Liao Y, Smyth GK, Shi W (2014) featureCounts: an efficient general purpose program for assigning sequence reads to genomic features. Bioinformatics 30:923–930. doi: 10.1093/bioinformatics/btt656

Low JKK, Webb SR, Silva APG, et al (2016) CHD4 Is a Peripheral Component of the Nucleosome Remodeling and Deacetylase Complex. J Biol Chem 291:15853–15866. doi: 10.1074/jbc.M115.707018

Maizels N, Gray LT (2013) The G4 genome. PLoS Genet 9:e1003468. doi: 10.1371/journal.pgen.1003468

5

Marfella CGA, Imbalzano AN (2007) The Chd family of chromatin remodelers. Mutat Res 618:30–40. doi: 10.1016/j.mrfmmm.2006.07.012

Montellier E, Boussouar F, Rousseaux S, et al (2013) Chromatin-to-nucleoprotamine transition is controlled by the histone H2B variant TH2B. Genes Dev 27:1680–1692. doi: 10.1101/gad.220095.113

Moretti C, Vaiman D, Tores F, Cocquet J (2016) Expression and epigenomic landscape of the sex chromosomes in mouse post-meiotic male germ cells. Epigenetics Chromatin 9:47. doi: 10.1186/s13072-016-0099-8

Musselman CA, Mansfield RE, Garske AL, et al (2009) Binding of the CHD4 PHD2 finger to histone H3 is modulated by covalent modifications. Biochem J 423:179–87. doi: 10.1042/BJ20090870

Namekawa SH, Park PJ, Zhang L-F, et al (2006) Postmeiotic Sex Chromatin in the Male Germline of Mice. Curr Biol 16:660–667. doi: 10.1016/j.cub.2006.01.066

Nitarska J, Smith JG, Sherlock WT, et al (2016) A Functional Switch of NuRD Chromatin Remodeling Complex Subunits Regulates Mouse Cortical Development. Cell Rep 17:1683–1698. doi: 10.1016/j.celrep.2016.10.022

O'Shaughnessy A, Hendrich B (2013) CHD4 in the DNA-damage response and cell cycle progression: not so NuRDy now. Biochem Soc Trans 41:777–82. doi: 10.1042/BST20130027

Oakberg EF (1956) Duration of spermatogenesis in the mouse and timing of stages of the cycle of the seminiferous epithelium. Am J Anat 99:507–516. doi: 10.1002/aja.1000990307

Odorisio T, Mahadevaiah SK, McCarrey JR, Burgoyne PS (1996) Transcriptional analysis of the candidate spermatogenesis gene Ube1y and of the closely related Ube1x shows that they are coexpressed in spermatogonia and spermatids but are repressed in pachytene spermatocytes. Dev Biol 180:336–43. doi: 10.1006/dbio.1996.0305

Oliver SS, Musselman CA, Srinivasan R, et al (2012) Multivalent Recognition of Histone Tails by the PHD Fingers of CHD5. Biochemistry 51:6534–6544. doi: 10.1021/bi3006972

Paro R, Hogness DS (1991) The Polycomb protein shares a homologous domain with a heterochromatin-associated protein of Drosophila. Proc Natl Acad Sci 88:263–267. doi: 10.1073/pnas.88.1.263

Paul S, Kuo A, Schalch T, et al (2013) Chd5 requires PHD-mediated histone 3 binding for tumor suppression. Cell Rep 3:92–102. doi: 10.1016/j.celrep.2012.12.009

Pellegrino J, Castrillon DH, David G (2012) Chromatin associated Sin3A is essential for male germ cell lineage in the mouse. Dev Biol 369:349–355. doi: 10.1016/J.YDBIO.2012.07.006

Reynolds N, Salmon-Divon M, Dvinge H, et al (2012) NuRD-mediated deacetylation of H3K27 facilitates recruitment of Polycomb Repressive Complex 2 to direct gene repression. EMBO J 31:593–605. doi: 10.1038/emboj.2011.431

Saksouk N, Simboeck E, Déjardin J (2015) Constitutive heterochromatin formation and transcription in mammals. Epigenetics Chromatin 8:3. doi: 10.1186/1756-8935-8-3

Soh YQS, Alföldi J, Pyntikova T, et al (2014) Sequencing the mouse Y chromosome reveals convergent gene acquisition and amplification on both sex chromosomes. Cell 159:800–13. doi: 10.1016/j.cell.2014.09.052

Sparmann A, Xie Y, Verhoeven E, et al (2013) The chromodomain helicase Chd4 is required for Polycomb-mediated inhibition of astroglial differentiation. EMBO J 32:1598–612. doi: 10.1038/emboj.2013.93

Torchy MP, Hamiche A, Klaholz BP (2015) Structure and function insights into the NuRD chromatin remodeling complex. Cell Mol Life Sci 72:2491–507. doi: 10.1007/s00018-015-1880-8

Touré A, Clemente EJ, Ellis P, et al (2005) Identification of novel Y chromosome encoded transcripts by testis transcriptome analysis of mice with deletions of the Y chromosome long arm. Genome Biol 6:R102. doi: 10.1186/gb-2005-6-12-r102

Trapnell C, Pachter L, Salzberg SL (2009) TopHat: discovering splice junctions with RNA-Seq. Bioinformatics 25:1105–11. doi: 10.1093/bioinformatics/btp120

Turner JM, Burgoyne PS, Singh PB (2001) M31 and macroH2A1.2 colocalise at the pseudoautosomal region during mouse meiosis. J Cell Sci 114:3367–75

Turner JMA, Mahadevaiah SK, Ellis PJI, et al (2006) Pachytene asynapsis drives meiotic sex chromosome inactivation and leads to substantial postmeiotic repression in spermatids. Dev Cell 10:521–9. doi: 10.1016/j.devcel.2006.02.009

Tyagi M, Imam N, Verma K, Patel AK (2016) Chromatin remodelers: We are the drivers!! Nucleus 7:388–404. doi: 10.1080/19491034.2016.1211217

van der Heijden GW, Derijck AAHA, Pósfai E, et al (2007) Chromosome-wide nucleosome replacement and H3.3 incorporation during mammalian meiotic sex chromosome inactivation. Nat Genet 39:251–8. doi: 10.1038/ng1949

van der Heijden GW, Dieker JW, Derijck AAHA, et al (2005) Asymmetry in histone H3 variants and lysine methylation between paternal and maternal chromatin of the early mouse zygote. Mech Dev 122:1008–22. doi: 10.1016/j.mod.2005.04.009

van der Laan R, Uringa E-J, Wassenaar E, et al (2004) Ubiquitin ligase Rad18Sc localizes to the XY body and to other chromosomal regions that are unpaired and transcriptionally silenced during male meiotic prophase. J Cell Sci 117:5023–33. doi: 10.1242/jcs.01368

Zhang W, Aubert A, Gomez de Segura JM, et al (2016) The Nucleosome Remodeling and Deacetylase Complex NuRD Is Built from Preformed Catalytically Active Sub-modules. J Mol Biol 428:2931–42. doi: 10.1016/j.jmb.2016.04.025

Zhuang T, Hess RA, Kolla V, et al (2014) CHD5 is required for spermiogenesis and chromatin condensation. Mech Dev 131:35–46. doi: 10.1016/j.mod.2013.10.005

5

SUPPLEMENTAL FIGURES

A

B

Y-Gene	Copy Number
Rbmy	35
Sly	126
Ssty1	85
Ssty2	221
Srsy	197
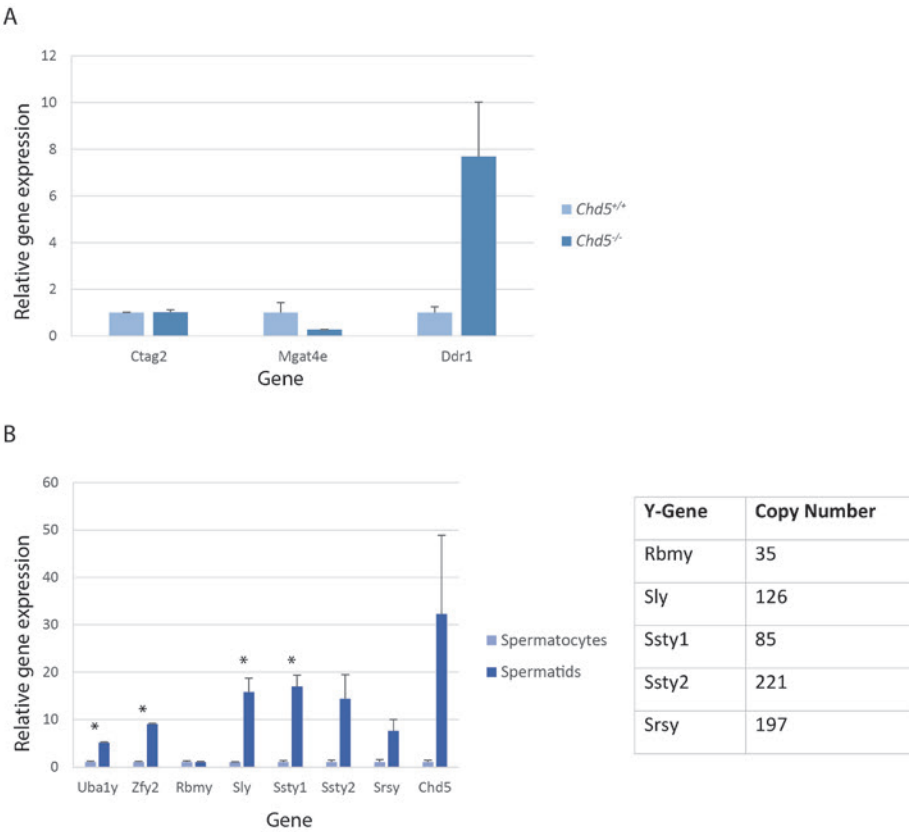
Fig. S1. Gene expression levels in *Chd5$^{+/+}$* and *Chd5$^{-/-}$* spermatocytes and spermatids (mean ± SD). **A)** Autosomal genes Ctag2, Mgat4e and Ddr1, which were previously reported to be stable, downregulated and upregulated in *Chd5$^{-/-}$* spermatids, respectively (Li et al. 2014). Gene expression levels were normalised to the housekeeping gene B-actin and further normalised to the wild-type. N= 2 *Chd5$^{+/+}$* and 2 *Chd5$^{-/-}$* mice. **B)** Y chromosomal genes and *Chd5* gene expression in wild type spermatocytes and spermatids. Gene expression levels were normalised against the housekeeping gene B-actin and further normalised against the spermatocytes. N= 2 wild-type mice. Significant values (p-value < 0.05) are indicated with an asterisk.
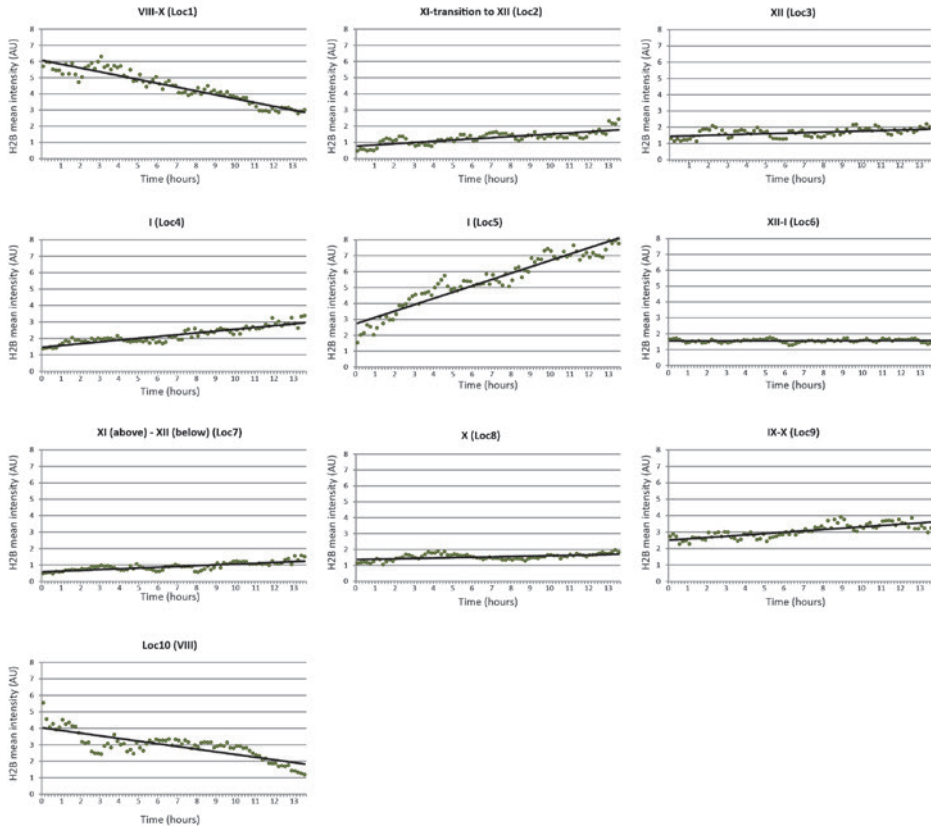
Fig. S2. Mean intensity of H2B-GFP signal in spermatids of *Chd5*^{+/+} mice.
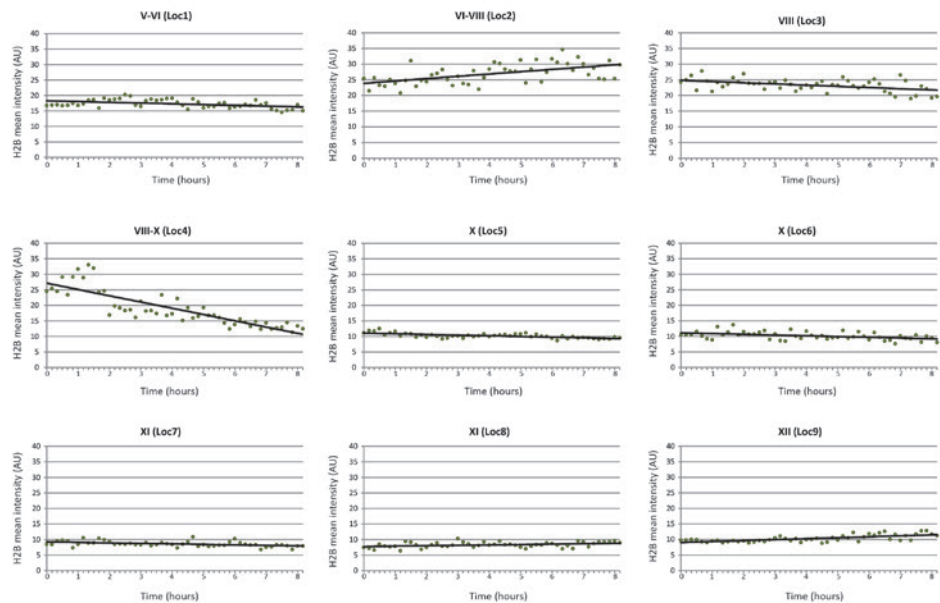
Fig. S3. Mean intensity of H2B-GFP signal in spermatids of *Chd5*$^{-/-}$ mice.

Fig. S4. Code for segmentation of the different cell types.

.ijm and .R FILES can be found at: http://cluster15.erasmusmc.nl/enguitamarruedo/

(Username and password available upon request).

SUPPLEMENTAL TABLES

Table S1. In silico analysis of the RNA sequencing results obtained by (Li et al. 2014), performed on round spermatids isolated from *Chd5*^{+/+}, *Chd5* ^{+/-} and *Chd5*^{-/-} mice. "KO vs WT" worksheet contains the complete analysis, "Y chromosomal genes" worksheet contains the results of the Y chromosomal genes and some of the genes represented in Fig. 8b in (Li et al. 2014).

Data can be found at: http://cluster15.erasmusmc.nl/enguitamarruedo/

(Username and password available upon request).

Gene	Forward Primer	Reverse Primer
Chd5	CTACGCCAAGATGGAGGAAC	ACTGGTCGTAGGGCAGGTC
Actb	ACTGGGACGACATGGAGAAG	GGGGTGTTGAAGGTCTCAAA
Rbmy	GGAGGCCTCAACATAAAGACC	GCGTCGGAAAGTAAGGAAAG
Sly	CAAAGGCAGCAACCAGAAAT	TCTTCATTGAATTTCTGTACATCCA
Ssty1	GCAGAGCGGTACAACACAAA	ATCCTTCATGATTGGCACCT
Ssty2	GGCTCTGAGGACAACTGGAG	CAGAGGGGTCTCTGGAATGA
Srsy	ACACTCATCATCACCGCAAG	GCCCATAGGATAGGCACAAA
Uba1y	AATGGCATTGGTCCCATAGA	CTTGACTGACAATGCCTCCA
Zfy2	GAGCATGAGCAACAGATGGA	GTCAAGGCCACCAGATTCAT
Ctag2	CAAATATCCAGCAGCAGCAA	TGGGATGTTTCTCACCACAA
Mgat4e	TGTCACAGGCAGGACAGAAG	TTTTCCTCAGGGATTTGCAG
Ddr1	GCGATCTGAACCAGTTCCTC	CCACGTGTAACAGCATAGGG

Table S2. Primers used for RT-qPCR.

&

Summary

Samenvatting

Abbreviation list

Curriculum vitae

PhD Portfolio

Acknowledgements

SUMMARY

In species with sexual reproduction, the generation of a new organism occurs by fusion of the maternal and the paternal gamete (single chromosome set, 1n). Upon fertilization, the combination of the two haploid genomes reconstitutes a diploid genome (2n). Formation of gametes occurs during spermatogenesis in males, and oogenesis in females. The work presented in this thesis aimed at a better understanding of dynamic aspects of chromosome pairing, chromosome separation, and chromosome remodeling during mammalian gametogenesis, mainly focusing on spermatogenesis. Spermatogenesis can be divided in three stages: mitotic amplification of the diploid progenitor cell, meiosis and spermiogenesis. Haploidization of gametes occurs during meiosis, which is achieved via the first and second meiotic divisions. Completion of the first meiotic division leads to the formation of two haploid daughter cells (secondary spermatocytes). From each secondary spermatocyte, two haploid spermatids are formed during the second meiotic division. Thus, each primary spermatocyte gives rise to four haploid spermatids. Each meiotic division can be divided in the stages: prophase, metaphase, anaphase and telophase. During the first meiotic prophase, a series of exclusive meiotic chromosome events takes place: pairing (alignment of the homologous chromosomes), synapsis (formation of proteinaceous structure between the homologous chromosomes, the synaptonemal complex (SC)), and recombination (DNA exchange between the homologous chromosomes, which results in the formation of crossovers). During these processes, actual movements of the chromosomes inside the nucleus are required. Additionally, at least two checkpoints operate during the first meiotic division in mice: the pachytene checkpoint and the Spindle Assembly Checkpoint (SAC). The pachytene checkpoint, which eliminates spermatocytes in which chromosomes have failed to complete synapsis, is functionally coupled to failure to form the XY body (region where the large non-homologous regions of the X and Y chromosomes that remain unsynapsed become silenced). The SAC delays anaphase onset until all chromosomes are properly aligned on the metaphase plate. Once meiosis is complete, the resulting spermatids enter spermiogenesis, the last step, involving a dramatic reduction in the size of the nucleus, and tail formation, finally giving rise to mature spermatozoa.

Following a general introduction in **Chapter 1**, we describe the setup of a system to study mouse gametogenesis in living cells, in their natural environment (inside the seminiferous tubule or the ovary) in **Chapters 2** and **3**. In **Chapter 2**, we aimed to study chromosome dynamics during the first meiotic prophase. For this, we generated transgenic mice expressing fluorescent tagged SYCP3-cherry. SYCP3 is one of the main components of the lateral elements of the SC. We described two types of movements that occur during the

&

entire first meiotic prophase: rotation of the nucleus itself and movement of the SC inside the nucleus. These movements could assist chromosome pairing, prevent or eliminate topological entanglements, or have a role in homologous recombination. In early stages, formation of the bouquet structure (when telomeres cluster together in the nuclear periphery) is thought to reduce the complexity of the homology search process required for pairing and synapsis. We have observed synchronized bouquet configuration in living cysts of two or three zygotene oocyte nuclei, which presented cycles of telomere clustering and dissolution. Some events of reclustering may occur when not all the chromosomes were properly synapsed, or may help to solve chromosome entanglements. In diplotene spermatocytes, desynapsis was found to proceed in a discontinuous manner, whereby even brief chromosome re-associations events (re-synapsis) were observed. Finally, analyses of the tagged protein exchange rate within the SC was analysed in pachytene spermatocytes by FRAP experiments. The results showed a final recovery of 40%, which may suggest that both endogenous and tagged-SYCP3 can exchange. Later stages of the first meiotic division were analysed in **Chapter 3**, using transgenic mice expressing mCherry-tagged SYCP3 in combination with GFP-tagged histone H2B (to visualize chromatin). We observed that progression from one stage to the other seems to depend on signals coming from the syncytium, but also from each individual cell. The latter was particularly evident during the metaphase-to-anaphase transitions, when cells displayed individual timing of transitions from one stage to the other, most likely governed by activation of the SAC, delaying the onset of anaphase until all chromosomes are correctly aligned. Additionally, we have also observed that the prometaphase stage can last extremely long (more than 12 hours), suggesting that male meiotic metaphase I chromosomes require an extremely lengthy period to satisfy the SAC. Once satisfied, metaphase-to-anaphase transitions were rapid (<10 minutes), and formation of secondary spermatocyte occurred, whereby the two daughter nuclei behaved synchronously.

In addition to the value of using mouse models to study gametogeneis in vivo, microscopic evaluation of spermatogenic and oogenic processes in fixed tissues is still an essential tool to analyse human material. For example, in the analysis of male infertility, fixed material is often the only available source for examination of the phenotype of the disorder. In **Chapter 4A**, we have used paraffin-embedded testis biopsy samples of 48 patients with Non-Obstructive Azoospermia (NOA) and developed an immunofluorescent approach that allowed us to classify them according to their type of spermatogenic arrest. Interestingly, we showed that complete metaphase arrest was the most frequently observed (27% of the patients), compared to other complete arrests. Reduction of the number of crossovers was identified as a potent activator of this arrest, most likely via activation of the SAC. Uniform

activation of meiotic checkpoints suggests a genetic cause of spermatogenic arrest. Therefore, our technique can be used as a tool to preselect patients for sequencing (search for infertility genes). Intriguingly, a partial metaphase arrest (presence of spermatids) was observed for 17% of the patients. Further research is recommended to determine if the surviving spermatids have increased frequencies of (epi)genetic aberrations, before performing in vitro fertilisation techniques using testicular sperm. In **Chapter 4B**, we used the data available from the MGI database to select genes that lead to disturbances in mouse male reproduction, and their human homologs were analyzed in a group of 33 NOA patients using Next Generation Sequencing. Our major findings were the identification of a novel gene for male infertility, *STAG3*, and the identification of a homozygous mutation in the gene *RNF212* shared by two brothers coming from a consanguineous family. Using the protocol described in **Chapter 4A**, we established a failure to form the XY body in the patient carrying two different *STAG3* mutations (compound heterozygosity). The two patients carrying a homozygous *RNF212* mutation displayed metaphase arrest and presence of univalents, as expected since crossover formation is enormously reduced in $Rnf212^{-/-}$ mice compared to controls.

Both meiosis and spermiogenesis require drastic chromatin changes. Members of the chromatin-helicase-DNA (CHD) family CHD3 and CHD4 are expressed in spermatocytes, whereas CHD5 is expressed in postmeiotic spermatids, and required for male fertility. In the brain, these proteins form part of the Nucleosome Remodeling and Deacetylation (NuRD) complex. In **Chapter 5**, we have analysed if the CHD proteins form similar complexes in male germ cells. Using an immunocytochemical approach, we observed only partial overlap of the signal of CHD3/4 and that of specific NuRD complex components in spermatocytes, suggesting that the formation of a canonical NuRD complex does not always occur. In spermatids, the Y-chromosomal focal spot that was highly enriched for CHD5 also accumulated specific chromatin marks, as well as specific NuRD components, in both wild-type and $Chd5^{-/-}$ mice, suggesting that a complex without CHD5 may still be formed. Based on mRNA expression analyses (re-analyzed in silico data of a previous transcriptomic study of purified round spermatids from wild type and $Chd5^{-/-}$ mice and RT-QPCR experiments) we established that none of the known Y chromosomal genes were differentially expressed in the absence of the remodeler. Using an antibody that binds to specific quadruplex DNA structures and denatured DNA, we observed that it marked all chromatin of elongating spermatids, and that this signal was strongly decreased upon loss of CHD5. These results indicate that despite its enrichment on part of the Y chromosome, CHD5 most likely performs a global function in chromatin structure regulation during spermatid nuclear elongation. Finally, using transgenic mice expressing GFP-tagged H2B and mCherry-SYCP3,

&

we developed a system to measure the loss of H2B- GFP in elongating spermatids in vivo in wild-type and $Chd5^{-/-}$ mice, but we did not observe clear differences between the $Chd5^{+/+}$ and $Chd5^{-/-}$ chromatin remodeling dynamics.

Taken together, we have worked on the development of new tools for the study of mouse gametogenesis in vivo, and this has provided new insights in the dynamics of the first meiotic division, and in the process of histone-to-protamine transition during spermiogenesis. Additionally, we have also focused on human male infertility, and developed an immunofluorescent method to specify the type of spermatogenic impairment in NOA patients, when only fixed material is available. Using this approach, the observed meiotic arrest type can be coupled to genes known to be involved in the affected process, and the number of candidate fertility genes can be restricted based on known functions of genes in which DNA mutations are observed upon for example, exome sequencing. In this way, we expect that it will be of great use to identify causative mutations of fertility genes in patients. Further implications of these findings, as well as suggestions for optimization of the current methods, were discussed in detail in **Chapter 6**.

SAMENVATTING

Bijna alle schimmels, planten en dieren maken gebruik van seksuele voortplanting. Een nieuw organisme ontstaat dan door de fusie van een mannelijke en een vrouwelijke voortplantingscel, waarbij ieder van deze cellen dan één exemplaar van ieder chromosoom (de dragers van de erfelijke eigenschappen) bij zich draagt (één haploïde set chromosomen, 1n). Als deze twee cellen bij de bevruchting versmelten, ontstaat er weer een diploïde cel (twee sets chromosomen, 2n), waaruit dan een nieuw organisme kan ontstaan die eigenschappen van vader en moeder bij zich draagt. De voortplantingscellen of gameten bij zoogdieren ontstaan tijdens spermatogenese bij de man en de oögenese bij de vrouw. Het in dit proefschrift beschreven onderzoek had als doel om dynamische aspecten van de paring van chromosomen, het scheiden van de chromosomen, en het reorganiseren van de structuur van chromosomen tijdens de gametogenese beter te begrijpen. Daarbij werd voornamelijk de spermatogenese bestudeerd. Spermatogenese bestaat uit drie deelprocessen: de mitotische vermenigvuldiging van diploïde voorlopercellen, gevolgd door de meiose en uiteindelijk de spermiogenese waarbij de rijpe zaadcel zich vormt. Haploïdizatie vindt plaats tijdens de meiose, die uit twee celdelingen bestaat. De eerste meiotische deling leidt tot de vorming van twee haploïde dochtercellen; de secundaire spermatocyten. Uit iedere secundaire spermatocyt ontstaan na de tweede meiotische deling dan weer twee spermatiden. Zo worden uit iedere diploïde primaire spermatocyt vier haploïde spermatiden gevormd. Elk van de twee meiotische delingen bestaat uit de substadia profase, metafase, anafase en telofase. Tijdens de eerste meiotische profase vindt een aantal zeer speciale chromosomale gebeurtenissen plaats: paring (homologe chromosomen rangschikken zich naast elkaar), synapsis (homologe chromosomen worden middels een specifieke eiwitstructuur (het synaptonemale complex, SC) aan elkaar gebonden) en DNA recombinatie (uitwisseling van DNA tussen homologe chromosomen, waarbij zogenoemde crossovers gevormd worden). Tijdens deze processen is het noodzakelijk dat de chromosomen zich op een georganiseerde manier in de kern bewegen. Om te zorgen dat al deze processen op een correcte manier verlopen zijn er zogenoemde "*checkpoints*" actief. Dit zijn speciale controlemechanismen. Het pachyteen checkpoint elimineert spermatocyten die er niet in zijn geslaagd hun chromosomen op de juiste wijze te paren waardoor het SC zich niet correct heeft gevormd. Dit checkpoint is gekoppeld aan het feit dat in het geval van foute chromosoomparing ook een hele speciale organisatie van de geslachtschromosomen (het X en het Y chromosoom) niet plaats zal vinden, dit wordt het falen van de *XY-body* vorming genoemd. De XY-body omvat de X en Y chromosomen in een spermatocyt. Deze twee chromosomen paren alleen in het zogenoemde pseudoautosomale deel, waar de DNA volgorde op de verder zeer verschillende chromosomen nog

overeenkomt. De rest van deze twee chromosomen blijft altijd ongepaard, en dit is gekoppeld aan het tijdelijk uitschakelen van bijna alle genen op X en Y. Het pachyteen checkpoint is actief als één of meerdere chromosoomparingen in de spermatocyt fout gaat, dan worden de X- en Y-chromosomale genen niet goed uitgeschakeld, en gaat de cel dood. Een tweede checkpoint heet het *spindle assembly checkpoint* (SAC). Dit checkpoint zorgt ervoor dat de overgang van metafase naar anafase niet kan plaatsvinden voordat alle chromosoomparen correct gerangschikt zijn in het midden van de cel (de metafaseplaat), waarbij de gepaarde chromosomen zodanig verbonden zijn met spoeldraden dat ze naar tegenover elkaar liggende polen van de cel getrokken worden. Dit checkpoint is ook actief tijdens mitose en tijdens de tweede meiotische deling, dan controleert het of de splitsing van chromosomen in twee chromatiden zodanig plaatsvindt dat er van ieder chromosoom één chromatide in iedere dochtercel terechtkomt. Als de twee meiotische delingen zich correct hebben voltrokken starten de gevormde spermatiden met de spermiogenese, waarbij de grootte van de kern vele malen kleiner wordt gemaakt, en zich een flagel vormt, uiteindelijk resulterend in een rijpe zaadcel.

   Na de algemene inleiding in **Hoofdstuk 1** beschrijven we in de **Hoofdstukken 2** en **3** hoe we een techniek hebben opgezet waarbij we gametogenese in levende cellen van de muis in vitro kunnen bestuderen, terwijl deze cellen zich in hun min of meer natuurlijke omgeving bevinden (spermatocyten en oocyten in respectievelijk de testisbuisjes en embryonale ovaria). Het doel van het onderzoek beschreven in **Hoofdstuk 2** was het bestuderen van de dynamiek van de chromosomen tijdens de profase van de eerste meiotische deling. Hiervoor hebben we een transgeen muismodel gemaakt die een fluorescent gemarkeerde component van het SC (SYCP3) in de spermatocyten en oocyten produceren. SYCP3 is een belangrijke component van de laterale elementen die onderdeel zijn van het SC. De laterale elementen vormen langs de assen van ieder chromosoom. We namen twee types beweging waar: rotatie van de kernen en bewegingen van de SC structuren binnenin de kernen. Beide bewegingen kunnen van belang zijn bij het bewerkstelligen van correcte chromosoomparing, bij het ontwarren van chromosomen, of bij het DNA recombinatieproces. Aan het begin van de profase is duidelijk een clustering van de chromosoomuiteinden (telomeren) in de buurt van de kernmembraan te zien (dit wordt het boeketstadium genoemd, naar een boeket bloemen waarbij de uiteinden ook opeengepakt zijn). Deze clustering wordt geacht de chromosoomparing te faciliteren doordat het zorgt voor verminderde complexiteit van the chromosoomstructuren. Wij namen waar dat de clustering van chromosomen in zygoteen oocyten die met hun cytoplasma met elkaar verbonden waren gesynchroniseerd plaatsvond. Hierbij waren cyclische clustering en verspreidingsbewegingen zichtbaar. De herclusteringen zouden samen kunnen hangen met situaties waarbij nog niet alle chromosomen gepaard

zijn, of kunnen optreden wanneer chromosomen zodanig "in de war" zitten dat de paring niet goed kan plaatsvinden. In spermatocyten, in het diploteenstadium, zagen we dat het desynapsen van chromosomen af en toe haperde en dat er soms zelfs weer even een resynapsis plaatsvond. Door te kijken naar het vervangen van eiwitten waarvan het fluorescente signaal definitief uitgeschakeld werd met een sterke laserstraal, door eiwitten met nog wel actieve fluorescentie (*Fluorescence Recovery After Photobleaching*, FRAP) werd inzicht gekregen in de mate waarin het fluorescent gemarkeerde SYCP3 langdurig gebonden is aan het DNA of chromatine. Het bleek dat 40% van de eiwitten binnen korte tijd vervangen werden, waarbij mogelijk ook uitwisseling met het endogene, niet gemarkeerde SYCP3 eiwit plaatsvindt. In **Hoofdstuk 3** richtten we ons op de laatste fasen van de eerste meiotische deling, hierbij gebruikten we muizen die naast het met rode fluorescentie gemarkeerde SCP3 eiwit ook een histon (H2B) gekoppeld aan het groen fluorescente eiwit (GFP) tot expressie brengen. Dit maakte het mogelijk om ook het chromatine (DNA met daar aan gebonden eiwitten) goed zichtbaar te maken. Het bleek dat de overgang van de ene fase in de andere soms gedicteerd leek te worden door een signaal dat meerdere cellen in een zogenoemd syncytium (cellen met cytoplasmabruggen met elkaar verbonden) tegelijk aanstuurde, en soms ook op individueel celniveau gereguleerd kom worden. Met name de metafase-naar-anafase transitie werd in iedere cel afzonderlijk ingezet, waarschijnlijk gereguleerd door het SAC, waardoor de overgang naar anafase wordt geremd totdat alle chromosomen correct georiënteerd zijn. Het was opvallen dat het prometafase stadium erg lang duurde (meer dan 12 uur). Dit wijst erop dat in meiotische cellen veel tijd nodig is om alle chromosomen correct te organiseren op de metafaseplaat. Als de uiteindelijke overgang naar anafase werd ingezet, voltrok dit proces zich erg snel (binnen 10 minuten), de hieruit gevormde secundaire spermatocyten gedroegen zich synchroon.

  Muismodellen kunnen goed gebruikt worden om processen te bestuderen in levende cellen die op weg zijn om zaad- of eicel te worden. Het is echter ook heel belangrijk om goede technieken te hebben voor de analyse van gefixeerde cellen en weefsels, omdat materiaal van menselijke oorsprong (bijvoorbeeld testis-biopsieën van mannen die onvruchtbaar zijn) meestal alleen als zodanig beschikbaar is. In **Hoofdstuk 4A** hebben we coupes gebruikt die gesneden waren van gefixeerde testis-biopsieën die in paraffine waren ingebed. We hebben vervolgens een fluorescente immunohistochemisch kleuringsprotocol ontwikkeld om restmateriaal van 48 patiënten met niet-obstructieve azoöspermie (NOA) te analyseren met als doel om vast te stellen welk aspect van de spermatogenese geblokkeerd was. Bij een verbazingwekkend hoog percentage van deze patiënten (27%) vonden we dat de spermatogenese blokkeerde tijdens de meiotische metafase. In een deel van deze patiënten correleerde dit met een verlaagde crossover frequentie, waarbij we concludeerden dat de

aanwezigheid van één of meerdere chromosoomparen zonder crossover in deze patiënten het SAC blijvend activeerden, uiteindelijk leidend tot celdood. Wanneer bij een patiënt een heel uniforme meiotische blokkade wordt geconstateerd is het waarschijnlijk dat er een genetisch defect ten grondslag ligt aan het geobserveerde defect. Het in **Hoofdstuk 4A** ontwikkelde protocol kan gebruikt worden om patiënten met eenzelfde type meiotisch arrest te selecteren, en (nieuwe) fertiliteitsgenen te identificeren. In een ander deel van de patiënten (17%) vonden we dat slechts een deel van de spermatocyten een blokkade in metafase ondervond, en andere cellen zich wel tot spermatiden ontwikkelden. Het is aan te raden om in deze gevallen te onderzoeken in hoeverre deze spermatiden een verhoogde frequentie hebben van (epi)genetische afwijkingen voordat overgegaan wordt tot geassisteerde voortplanting met testiculair zaad bij dit type patiënt. In **Hoofdstuk 4B** hebben we gegevens uit de *Mouse Genome Informatics* (MGI) databank gebruikt om een lijst te maken van genen die betrokken zijn bij spermatogenese in de muis. De homologe genen bij de mens zijn vervolgens geanalyseerd in een groep van 33 NOA patiënten met behulp van *next generation sequencing* (NGI). Hierbij werd een nieuw fertiliteitsgen bij de mens geïdentificeerd: *STAG3*. Daarnaast werd een homozygote mutatie gevonden in het *RNF212* gen in twee broers uit een familie waarbij sprake was van consanguiniteit. Gebruikmakend van het protocol beschreven in **Hoofdstuk 4A** konden we vaststellen dat de patiënt met 2 verschillende *STAG3* mutaties (samengesteld heterozygoot) een defect vertoonde in XY body vorming. De patiënten met de *RNF212* mutatie vertoonden een meiotisch metafase arrest. Daarnaast waren er vaak univalenten bij de gevonden meiotische metafases en anafases. Dit beeld is in overeenstemming met wat bekend is over het fenotype van muizen zonder RNF212 eiwit; daarbij is het aantal crossovers sterk verminderd in vergelijking met controles.

Grote veranderingen in chromatine structuur treden op tijdens zowel meiose als tijdens spermiogenese. Een groep van gerelateerde eiwitten die chromatine kunnen remodeleren is de *chromatin-helicase-DNA* (CHD) familie van eiwitten. CHD3 en CHD4 zijn twee leden van deze familie die aanwezig zijn in spermatocyten, terwijl een ander lid, CHD5, specifiek tot expressie komt in spermatiden. Van CHD5 is bekend dat het essentieel is voor de vruchtbaarheid bij mannelijke muizen. In de hersenen zijn CHD3, CHD4 en CHD5 ook aanwezig en daar kunnen zij onderdeel uitmaken van een functioneel complex genaamd *Nucleosome Remodeling and Deacetylation* (NuRD) complex . In **Hoofdstuk 5** hebben we onderzocht of de aanwezige CHD eiwitten in spermatocyten en spermatiden vergelijkbare complexen vormen. Met immunohistochemische technieken zagen we dat componenten van het NuRD complex slechts gedeeltelijk colocaliseerden met de CHD eiwitten. Dit resultaat wijst er op dat de CHD eiwitten in spermatocyten en spermatiden misschien ook activiteiten hebben die onafhankelijk zijn van het NuRD complex. CHD5 is verrijkt aanwezig

op een klein deel van het Y chromosoom in spermatiden. We hebben vastgesteld dat dit gebied ook verrijkt is voor componenten van het NuRD complex in associatie met bepaalde histonmodificaties. Deze specifieke chromatine-signatuur was nog steeds aanwezig in de *Chd5* knockout spermatiden. Dit resultaat geeft aan dat een deel van het NuRD complex in afwezigheid van CHD5 nog steeds wordt gevormd. Op basis van mRNA expressie analyse (*in silico* data en experimenteel vergaard) konden we ook vaststellen dat de afwezigheid van CHD5 geen effect heeft op de expressie van bekende Y chromosomale genen. We vonden echter wel een effect op de structuur van het chromatine, dit werd zichtbaar doordat een eiwit (antilichaam) dat zich specifiek bind aan bepaalde DNA structuren aanwezig in de hele kern minder gebonden werd aan het chromatine van spermatiden wanneer één of beide kopieën van het *Chd5* gen gemuteerd waren. Dit resultaat wijst op een meer globale rol van CHD5 in de regulatie van het chromatine in spermatiden, ondanks de opeenhoping van CHD5 op een deel van het Y chromosoom. Om dit verder te onderzoeken hebben we een techniek opgezet om de verwijdering van histonen van het DNA tijdens de kerncondensatie in spermatiden te kunnen meten. Hierbij hebben we gebruik gemaakt van de transgene muizen zoals beschreven in **Hoofdstuk 3**, en de hoeveelheid aanwezig H2B gekoppeld aan GFP gebruikt als maat voor de hoeveelheid histonen in de kernen. De resultaten die tot dusverre beschikbaar zijn lieten geen duidelijke verandering zien in het proces van histon verwijdering in *Chd5* knockout spermatiden in vergelijking met dit proces in de controles.

De nieuwe technieken voor de analyse van levende cellen die in dit proefschrift worden beschreven hebben nieuw inzicht verschaft in dynamische aspecten van de eerste meiotische deling, en het proces van de vervanging van histonen door protamines tijdens de kerncondensatie in spermatiden. Daarnaast hebben we ons ook gericht op mannelijke infertiliteit, en een fluorescent immuunkleuringsprotocol opgezet om het stadium waarop spermatocytontwikkeling gestoord raakt vast te kunnen stellen in gefixeerd testisbiopsiemateriaal. Met behulp van deze aanpak zullen onderzoekers in staat zijn om het geobserveerde type meiotische blokkade te koppelen aan wat bekend is omtrent genen die betrokken zijn bij het aangedane proces. Vervolgens zal deze kennis dan helpen om bij genoomanalyses vast te stellen welk van de geobserveerde DNA mutaties het meest waarschijnlijk is als oorzaak van de infertiliteit. De verdere implicaties van de resultaten van het in dit proefschrift beschreven onderzoek en suggesties voor verdere optimalisatie van protocollen zijn beschreven in **Hoofdstuk 6**.

&

LIST OF ABBREVIATIONS

aa	amino acid
AD	adrenomedullin
AEs	axial elements
ART	assisted reproductive technology
BME	basement membrane extract
BSA	bovine serum albumin
BTB	blood-testis barrier
CHD	chromatin-helicase-DNA
CO	crossover
CSYCP	N-terminal fluorescent-tagged SYCP3 (mCherry-SYCP3)
DAB	3,3'-diaminobenzidine
DAPI	4', 6-Diamidino-2-Phenylindole
dHJ	double Holliday junction
D loop	displacement loop
DNA	deoxyribonucleic acid
DSB	DNA double-stranded break
E	embryonic day
EC+T	tubule sections containing early meiotic prophase cells
EpiLCs	primordial germ cells-like cells derived from epiblast like cells
FFPE	paraformaldehyde fixed and paraffin-embedded
FRAP	fluorescent recovery after photobleaching
G4	guanine quadruplex
GFP	green fluorescent protein
γH2AX	phosphorylated histone H2AX
GVB	germinal vesicle
HDAC	histone deacetylase
H2B-GFP	GFP-tagged histone H2B
HR	homologous recombination
H3K9me3	trimethylation of histone H3 on lysine 9
H3K27me3	trimethylation of lysine 27 on histone H3
H3s10ph	phosphorylation of Histone 3 at serine 10
ICSI	intracytoplasmic sperm injection
IGV	Integrative Genomics Viewer
IP	index of pathogenicity
IVF	in vitro fertilization

&

JS	Johnsen score
Kb	Kilobase
KO	knockout
KRS	knockout serum replacement
LEs	lateral elements
LSFM	light sheet–based fluorescence microscopy
Mb	megabase
MEIOB	meiosis specific with OB domains
MF	microfluidics
MGI	Mouse Genome Informatics database
mH2A	MacroH2A
MI	metaphase I
MSCI	meiotic sex chromosome inactivation
MSH	Mut S Homolog
MSUC	meiotic silencing of unsynapsed chromatin
NCO	non-crossover
NEBD	nuclear envelope breakdown
NOA	non-obstructive azoospermia
NuDe	nucleosome deacetylase
NuRD	Nucleosome Remodeling and Deacetylation
OMIM	Online Mendelian Inheritance in Man database
PAR	pseudoautosomal region
PBS	phosphate buffered saline
PFA	paraformaldehyde
PGC	primordial germ cell
PGCLC	primordial germ cell-like cells
POI	premature ovarian insufficiency
PRM	Protamine
PTM	post-translational modification
RNA	ribonucleic acid
RNA pol	RNA polymerase
RPA	Replication Protein A
RPMs	telomere-led rapid prophase movements
qRT-PCR	quantitative reverse transcription polymerase chain reaction
SAC	spindle assembly checkpoint
ROSI	round spermatid injection

SC	synaptonemal complex
SCO	Sertoli cell only
SCOS	Sertoli cell Only syndrome
SDSA	synthesis-dependent strand annealing
SIM	structured illumination microscopy
SPATA22	spermatogenesis associated 22
ssDNA	single stranded DNA
SYCPC	C-terminal fluorescent-tagged SYCP3 (SYCP3-mCherry)
TdT	terminal deoxynucleotidyl transferase
TESE	testicular sperm extraction
TF	transverse filament
TH2B	testis-specific H2B histone
TMC	testicular peritubular myoid cells
TP	transition protein
WT	wild type
Xp	short arm of the X chromosome
Xq	long arm of the X chromosome
XY+T	tubule sections containing XY bodies
Yp	short arm of the Y chromosome
Yq	long arm of the Y chromosome

&

CURRICULUM VITAE

Name:	Andrea Enguita-Marruedo
Date of birth :	October 19th 1989
Place of Birth :	Madrid
e-mail address **:**	a.enguitamarruedo@erasmusmc.nl

Education

Oct 2013- June 2019   PhD in Reproduction and Development
Erasmus University Medical Center, Rotterdam, The Netherlands

Sept 2012- Sept 2013   MSc in Genetics and Cell Biology. Cum laude granted
Autonomous University of Madrid, Spain

Sept 2007- June 2012   Bachelor in Biology. Cum laude granted
Autonomous University of Madrid.

Research experience

Oct 2013- June 2019   PhD in Reproduction and Development. Erasmus MC, Rotterdam
Dynamics of mouse and human gametogenesis

2016 and 2015
(15 days and 1 month)   Secondment at Institute of Molecular Biology and Tumor Research,
Marburg, Germany
Molecular techniques

Sept 2011- Sept 2013   Department of Biology, Autonomous University of Madrid, Spain.
DNA repair at the different stages of the first meiotic prophase

July 2012-Sept 2012   Cicerone Scholarship at National Centre of Cardiovascular Investigation
Madrid, Spain

June 2011-Sept 2011   Internship at MD Anderson International hospital's Cytogenetics Laboratory, Madrid, Spain Conventional
Conventional Cytogenetics and Molecular Techniques

PHD PORTFOLIO

Summary of PhD training and teaching

Name PhD student: Andrea Enguita-Marruedo Erasmus MC Department: Developmental Biology Research school: Medical Genetics Centre (MGC)	PhD period: October 2013-June 2019 Promotor : Joost Gribnau Supervisor(s): Willy M. Baarends, Wiggert A. van Cappellen

1. PhD training

● **Courses**	**Year**
Biochemistry and Biophysics Course	2013
OIC course "Introduction to Confocal Microscopy"	2013
Cell and Developmental Biology course	2014
Epigenetic Regulation in Health and Disease	2014
Genetics	2014
OIC course "Functional Imaging and Super Resolution"	2014
Safety working in the laboratory	2014
Research Integrity	2015
Biostatistical Methods I: Basic Principles (CC02A)	2017
● **Seminars and workshops**	
Winter School of the Collaborative Research Centre TRR81, Kleinwalsertal (oral presentations)	2014, 2015
2nd Reprotrain Workshop, Marburg, Germany (oral presentation)	2014
21st MGC Workshop, Münster, Germany	2014
The Microscopic Image Analysis: From Theory to Practice	2014
The Photoshop and Illustrator CS6 Workshop for PhD-students and other researchers	2014
Reprotrain workshop "Biomedical Application and Transfer of Knowledge Opportunities" Barcelona, Spain	2015
● **(Inter)nationals conferences**	
EMBO Meiosis conference (poster presentation)	2015
REPROTRAIN "Frontiers in Male Infertility Research" (oral presentation)	2015
1st Meionet meeting, Poblet, Spain (oral presentation)	2016
Students and Postdocs Meiosis meeting, Montpellier, France (oral presentation)	2016
14th Dutch Chromatin meeting , Leiden	2016
2nd Meionet meeting, Miraflores de la Sierra, Madrid, Spain (oral presentation)	2017
4th Symposium "Chromatin changes in differentiation and malignancies", Egmond aan Zee, The Netherlands (poster presentation)	2017

2. Teaching

Teaching assistant (spread preparations), 2nd Reprotrain Workshop Marburg, Germany	2014
Teaching assistant in "VO Vroege embryo's, klonen en transgenese"	2017
Assesing "Evolution and Development" posters (2nd year Nanobiology students)	2016,2017, 2018